Universitat de Girona

MILLING STABILITY IMPROVEMENT THROUGH NOVEL PREDICTION AND SUPPRESSION TECHNIQUES

Alexander Iglesias Ramos

MILLING STABILITY IMPROVEMENT THROUGH NOVEL PREDICTION AND SUPPRESSION TECHNIQUES

Alexander Iglesias Ramos

Universitat de Girona

MILLING STABILITY IMPROVEMENT THROUGH NOVEL PREDICTION AND SUPPRESSION TECHNIQUES

A THESIS SUBMITTED IN PARTIAL FULFILLMENT OF THE REQUIREMENTS FOR THE DEGREE OF
DOCTOR OF PHILOSOPHY FROM THE UNIVERSITAT DE GIRONA

by
Alexander Iglesias Ramos

supervisors
Joaquim de Ciurana i Gay
Jokin Muñoa Gorostidi
Zoltan Dombovari

2015

Doctors Joaquim de Ciurana, Professor in the Mechanical Engineering and Construction department of the University of Girona, Jokin Muñoa, head of the Dynamics and Control department at IK4-Ideko and Zoltán Dombóvári, Assistant Professor in the department of Applied Mechanics at the Faculty of Mechanical Engineering of the Budapest University of Technology and Economics,

CERTIFY that:

This work, entitled "MILLING STABILITY IMPROVEMENT THROUGH NOVEL PREDICTION AND SUPPRESSION TECHNIQUES", presented by Alexander Iglesias for the PhD degree, was carried out under our direction and fulfills all the requirements for a PhD degree.

Jokin Muñoa Gorostidi   Joaquim de Ciurana i Gay   Zoltán Dombóvári

Girona, 17th December 2015

Acknowledgements

Plasmatrix. Several topics researched in these projects had a close connection with the subject of this Thesis.

Out of the office, I really appreciate the support of my family, especially my mother, who helped me with the household chores on the busiest days.

Finally, I would like to remark the great support received by my three Thesis Directors: Quim de Ciurana, major contributor to speed up the pace of this work, for his wise advices and continuous monitoring of the process, preventing me from deviating from the real objectives; Zoltan Dombovari, for his enormous dedication, wise support in the most complex mathematical concepts of this Thesis and the vast number of high quality pictures he has provided; and Jokin Muñoa, the main ideologue of this Thesis, for his great skills to lead this Thesis to a good end and his farsighted vision of today's chatter problems and possible ways to increase the knowledge on it and further understand and control the problem.

Preface

Although the rapid evolution of science and technology have brought up many new groundbreaking manufacturing processes in the recent years, such as laser technology or rapid manufacturing, milling process still remains as one of the most popular processes in the manufacturing industry.

Globalization of the market is pushing the manufacturing sector into a tougher competition day by day, demanding the best possible performance from every player in the sector. Milling process is also subject to this pressure, with increasing requirements in terms of productivity and quality. The competitiveness of the companies depends on their adaptability to these higher demands and constantly changing scenario by means of the continuous research and technology development to differentiate from the competitors. This technology race has boosted milling process capabilities to a large extent, bringing the process limits to levels that were unthinkable just a few years ago.

On the other hand, current high speed machining trends imply the use of lighter machines which show a much better dynamic behavior while, at the same time, a large percentage of the rigidity is lost. In the same way, accuracy needs lead to a reduction of friction in every machine interface, especially in the guiding systems of the machine. This point is also positive from an accuracy and energetic point of view, but it reduces drastically the damping of the machine.

All these factors, higher material removal rate together with a reduction of machine's stiffness and damping, have brought chatter vibrations to the spotlight, as probably the main milling process limitation in the XXI century. Apart from being the main process limitation, they are also one of the most harmful problems in general machining and a hard problem to solve. Although chatter has been subject of much research work in the last years, there is still a great improvement potential in the field, due to its complex nature.

The overarching goal of this Thesis is to go one step further in milling instability prediction and avoidance, including new concepts and methods in current prediction models and developing smart and flexible solutions for chatter suppression.

The Thesis is organized in 4 Parts and 13 Chapters.

Part 1 deals with the introduction, critical study of the state of the art and proposed advances beyond the current state of the art, that is, the objectives of the Thesis. It is composed of Chapters 1, 2 and 3.

Chapter 1 presents the underlying background and the personal motivation that drive this work.

Chapter 2 reviews the state of the art regarding chatter prediction. Current stability model range is described and the frequency model is thoroughly detailed. A number of research studies, which claim possible inaccuracy sources of the stability models are listed, and experimental characterization techniques, which could handle these errors, are also described. Current chatter detection and suppression state of the art is also included.

Chapter 3 summarizes the main conclusions from the state of the art analysis and sets the objectives to pursue during the development of the Thesis.

Part 2 addresses the milling stability prediction improvements carried out during this work. It is composed of Chapters 4, 5, 6, 7 and 8.

Chapter 4 sets the starting point of this research, with a description of a process planning methodology based on an adapted model for heavy roughing operations. In this work, the inaccuracies described in Chapter 2 are reflected.

Chapter 5 presents a series of analytical formulae to calculate both Hopf and flip type lobes and their characteristic points for one dominant mode systems. Several hints on flip type lobe shapes as a function of the degree of discontinuity of the cutting process are drawn.

Chapter 6 presents a new combined analytical model for stability calculation in milling processes. This model is based on the classical zeroth order approximation (ZOA) method, with the addition of the flip type lobe family calculated with the same concept as the Hopf lobe, thus maintaining the speed and improving the accuracy of the original method.

Chapter 7 describes an inverse methodology to obtain the stability lobes out of experimental cutting tests. The dynamic parameters of the system are then inversely calculated from the fitted stability lobes.

Chapter 8 presents a new methodology to obtain the frequency response function (FRF) of a machine system using the cutting force itself as the input force excitation. The obtained FRF is defined in the frequency range of interest, keeping similar boundary conditions to the real cutting process, which therefore results in a more accurate dynamic parameter extraction.

Part 3 presents three groundbreaking chatter suppression techniques based on different approaches that outperform in a great extent all known solutions. It is composed of Chapters 9, 10 and 11.

Chapter 9 proposes an automatic process parameter tuning through an algorithm fed with the acoustic monitoring signal of the cutting process. The system is contactless and wireless; therefore, it does not invade machine's workspace and provides an automatic, flexible and cheap solution against chatter onset.

Chapter 10 presents a variable stiffness self-tunable mass damper concept. This semi-active solution works as a standard tuned mass damper, with the important breakthrough of its self-tuning capability over a wide frequency range.

Chapter 11 presents an active damping strategy through the own drives of the machine tool. The milling process is monitored through an accelerometer and the signal is introduced in the machine control as an additional acceleration feedback loop. This technique greatly outperforms current active damping related solutions, due to its comparatively easiness of integration and low investment needed.

Part 4 is composed of Chapters 12 and 13.

Chapter 12 shows conclusions and outlook.

Finally, Chapter 13 lists all references in this Thesis.

Public Dissemination of Research Results

Science Citation Index (SCI) Journals

Barnada, F., Teixidor, D., Iglesias, A., Quintana, G., & Ciurana, J. (2015). Wireless device for on-line chatter identification and process parameters correction in milling processes. *Robotics and Computer Integrated Manufacturing*, submitted.

Iglesias, A., Munoa, J., & Ciurana, J. (2014). Optimisation of face milling operations with structural chatter using a stability model based process planning methodology. *The International Journal of Advanced Manufacturing Technology*, 70(1-4), 559-571.

Iglesias, A., Munoa, J., Ciurana, J., & Dombovari, Z. (2015). Analytical expressions for chatter analysis in milling operations with one dominant mode. *Journal of Sound and Vibration*, submitted.

Iglesias, A., Munoa, J., Ciurana, J., & Dombovari, Z. (2015). Analytical model for interrupted milling: ZOA method enhancement including double period instability. *International Journal of Machine Tools and Manufacture*, submitted.

Iglesias, A., Munoa, J., Ciurana, J., & Dombovari, Z. (2015). Analytical stability model for interrupted milling processes. *International Journal of Advanced Manufacturing Technology*, submitted.

Munoa, J., Beudaert, X., Erkorkmaz, K., Iglesias, A., Barrios, A., & Zatarain, M. (2015). Active suppression of structural chatter vibrations using machine drives and accelerometers. *CIRP Annals-Manufacturing Technology*, 64, 385-388.

Munoa, J., Iglesias, A., Olarra, A., Dombovari, Z., & Zatarain, M. (2016). Rough milling chatter suppression by self-tunable variable stiffness tuned mass damper, *CIRP Annals-Manufacturing Technology*, submitted.

International Conferences

Aguirre, G., Iglesias, A., Munoa, J., & Astarloa, A. (2014). Real milling force based dynamic parameter extraction method. *Proceedings of ISMA*, Leuven, Belgium.

Iglesias, A., Munoa, J., Ramírez, C., Ciurana, J., & Dombovari, Z. (2016). FRF Estimation through Sweep Milling Force Excitation (SMFE). *7th HPC 2016 – CIRP Conference on High Performance Cutting*, submitted.

Kilic, Z. M., Iglesias, A., Munoa, J., & Altintas, Y. (2010). Investigation of tool wear on the stability of milling process using an inverse method. *CIRP 2nd International Conference on Process Machine Interactions*, Vancouver, Canada.

Munoa, J., Dombovari, Z., Iglesias, A., & Stepan, G. (2015). Tuneable mass dampers with variable stiffness for chatter suppression. *International Conference on Virtual Machining Process Technology*, Vancouver, Canada.

Technical Papers

Iglesias, A. (2015). Vibraciones: un enemigo vencible. *IMHE : Información de máquinas-herramienta, equipos y accesorios*, 414, 48-54.

Iglesias, A., & Landa, J. (2013). Más productividad para el cielo: estrategia para mejorar de la productividad en piezas del sector aeronáutico mediante uniones amortiguadas. *IMHE: Información de máquinas-herramienta, equipos y accesorios*, 401, 42-44.

List of Acronyms

AE	Approximate entropy
ANN	Artificial neural network
AMB	Active magnetic bearing
AMRC	Advanced Manufacturing Research Centre
ARMA	Autoregressive moving average
ARMAX	Autoregressive moving average exogenous
CAM	Computer aided manufacturing
CER	Coarse grained entropy rate
CFDD	Curve-fitting in the frequency domain decomposition
CIRP	International Academy for Production Engineering
CNC	Computer numerical control
CRAC	Chatter recognition and control system
CS0	General coordinate system
CS1	Process coordinate system
CSSV	Continuous spindle speed variation
DDE	Delayed differential equation
DHT	Discrete Harley transform
DMS	Design and manufacturing solutions
DVA	Dynamic vibration absorber
FDD	Frequency domain decomposition
EFDD	Enhanced frequency domain decomposition
FFT	Fast Fourier transform
FHT	Fast Harley transform
FRF	Frequency response function
HMM	Hidden Markov models
IBR	Index-base reasoning
IDFT	Inverse discrete Fourier transform

LSCE	Least square complex exponential
MaxMRR	Maximum material removal rate
MCF	Maximum component frequency
MD	Mass damper
MRR	Material removal rate
MRSSV	Multi-level random spindle speed variation
NIST	National Institute of Standards and Technology
NURBS	Non-uniform rational B-Spline
OMA	Operational modal analysis
SD	Semi-discretization
SDOF	Single degree of freedom
SLD	Stability lobe diagram
SMFE	Sweep milling force excitation
SSI	Stochastic subspace identification
SSSV	Sinusoidal spindle speed variation
SVD	Singular value decomposition
SVM	Support vector machine
TPF	Tooth passing frequency
TMD	Tuned mass damper
UBC	University of British Columbia
VSTMD	Variable stiffness tunable mass damper
ZOA	Zeroth order approximation

List of Symbols

a	[mm]	Depth of cut
a_1	[mm/s^2]	Acceleration at the location of the accelerometer
a_2	[mm/s^2]	Acceleration at the tool tip
a_e	[mm]	Width of cut
a_f	[mm]	Depth of cut according to flip limit
a_H	[mm]	Depth of cut according to Hopf limit
a_{lim}	[mm]	Limit depth of cut
a_{max}	[mm]	Maximum depth f cut
c_1	[Ns/mm]	Damping of the main mode
c_{cr}	[Ns/mm]	Critical damping
d	[1]	Immersion ratio
dz	[mm]	Differential disk thickness
dF_{tj}	[N]	Differential tangential force per tooth j
dF_{rj}	[N]	Differential radial force per tooth j
dF_{aj}	[N]	Differential axial force per tooth j
f	[1]	Frequency ratio
f_1	[N]	Measured impact hammer force applied at the ram tip
f_2	[N]	Cutting force at the tool tip
f_c	[Hz]	Chatter frequency
f_{DH}	[Hz]	Optimum tuning frequency by Den Hartog
f_n	[Hz]	Natural frequency
$f_{opt,n}$	[Hz]	Optimum tuning frequency by Sims with $\beta_0>0$
$f_{opt,p}$	[Hz]	Optimum tuning frequency by Sims with $\beta_0<0$
f_r	[1]	Regenerative term
f_z	[mm/Z]	Feed per tooth
$g(\phi_j)$	[1]	Screen function
h_d	[mm]	Dynamic chip thickness

h_{d0}	[mm]	Dynamic chip thickness at previous tooth period
h_{d1}	[mm]	Dynamic chip thickness at present tooth period
h_s	[mm]	Static chip thickness
h	[mm] – [1]	Total chip thickness – No. of harmonics modulating chatter frequency
j	[1]	Tool teeth/flute
k	[N/mm]	Modal stiffness
k_1	[N/mm]	Modal stiffness of the main mode
l	[1]	Number of waves generated between each tooth. Number of lobe
m	[kg]	Modal mass – Number of flip lobe
m_1	[kg]	Modal mass of the main mode
m_2	[kg]	Mass of the tuned mass damper
m_a	[kg]	Static mass of the machine
m_b	[kg]	Moving mass
n_i	[1]	Number of integration steps in SMFE method
r_υ	[1]	Ratio between harmonics 1 and 0 of the directional factor
t	[s]	Variable time
u	[1]	Principal modal direction in bidirectional system
v	[1]	Perpendicular mode direction in bidirectional system
v_r	[mm/s]	Additional velocity command injected into the velocity control loop
C_i	[N/m]	Dynamic coefficient proportional to velocity
D	[mm]	Tool diameter
F_{tj}	[N]	Tangential cutting force per tooth
G	[N/mm]	Real part of the frequency response function
G_{FF}	[N^2]	Power spectrum of the force
G_{rF}	[mm/N]	Cross spectrum between the vibration amplitude and the force
H	[N/mm]	Imaginary part of the frequency response function
K	[s]	Vibration damping controller relating a_1 and v_r
K_a	[1]	Relative axial cutting force coefficient
K_{ae}	[N/mm]	Axial edge coefficient
K_d	[1]	Gain adjustment
K_f	[N/mm^2]	Static coefficient
K_{hpf}	[1]	High-pass filter
K_{lead}	[1]	Lead filter
K_{lpf}	[N/mm^2]	Low-pass filter

K_p	[Ns]	Velocity loop gain
K_r	[1]	Relative radial cutting force coefficient
K_{re}	[N/mm]	Radial edge coefficient
K_{res}	[1]	Resonance filter
K_t	[N/mm^2]	Tangential cutting force coefficient
K_{te}	[N/mm]	Tangential edge coefficient
K_v	[1/s]	Position loop gain
L	[Ns/mm]	Loop transfer function
M	[1]	Magnifying function
N	[rpm]	Spindle speed
N_a	[1]	Number of averages
N_i	[rpm]	Spindle speed at integration step i
N_{start}	[rpm]	Starting scanning speed
N_{end}	[rpm]	Ending scanning speed
P	[W]	Cutting power
P_{max}	[W]	Maximum cutting power
R	[1]	Variance ratio
S	[mm]	Length of the cutting edge
S_f	[1]	Sensitivity function
T	[s]	Tooth passing period
T_c	[Nm]	Cutting torque
$T_{c,max}$	[Nm]	Maximum cutting torque
T_f	[1]	Complementary sensitivity function
V_B	[μm]	Flank wear width
V_c	[m/min]	Cutting speed
Z	[1]	Number of teeth
$\{n\}$	[1]	Chip thickness direction vector
$\{p\}$	[1]	Modal vector of the tool
$\{p(j\omega)\}$	[mm]	Non-stationary solution of the vibration
$\{p_t(j\omega)\}$	[mm]	Non-stationary solution of the tool vibration
$\{p_w(j\omega)\}$	[mm]	Non-stationary solution of the workpiece vibration
$\{q\}$	[1]	Modal vector on the ram tip
$\{r(j\omega)\}$	[mm]	Vibration amplitude
$\{r_p(j\omega)\}$	[mm]	Stationary solution of the vibration

$\{r_t(j\omega)\}$	[mm]	Tool vibration amplitude
$\{r_w(j\omega)\}$	[mm]	Workpiece vibration amplitude
$\{F\}$	[N]	Cutting force (x, y, z)
$\{F_t(j\omega)\}$	[N]	Cutting force on the tool
$\{F_w(j\omega)\}$	[N]	Cutting force on the workpiece
$\{K\}$	[1]	Cutting coefficient vector
$\{K_e\}$	[N/mm]	Edge coefficient vector
$\{P\}$	[N]	Increment of cutting force in modal coordinates
$[A(t)]$	[1]	Directional factor matrix in Cartesian coordinates
$[B(t)]$	[1]	Directional factor matrix in modal coordinates
$[B_m]$	[1]	mth harmonic of the directional factor matrix in modal coordinates
$[C]$	[Ns/mm]	Damping matrix
$[K]$	[N/mm]	Stiffness matrix
$[M]$	Kg	Mass matrix
$[Q_1]$	[1]	$\{t, r, a\}$ to $\{x, y, z\}$ coordinate system rotation matrix
$[Q_2]$	[1]	CS1 to CS0 rotation matrix
$[Q_3]$	[1]	Modal to Cartesian coordinate system rotation matrix
$[Q_i]$	[1]	Modal vector
α	[rad]	Azimuthal rotation angle from modal to Cartesian coordinates
α_e	[rad]	Intrinsic rotation angle
α_{eq}	[1]	Equivalent directional factor for a differential disk
α_m	[1]	Integrated mth harmonic of the directional factor matrix
α_i	[N]	Dynamic coefficient proportional to acceleration
α_{xy}	[1]	Directional factor relating vibration in y with force in x
β	[rad]	Polar rotation angle from modal to Cartesian coordinates
β_{eq}	[1]	Equivalent directional factor in modal coordinates
β_m	[1]	Integrated mth harmonic of the directional factor matrix in modal coordinates
γ^2_{rF}	[1]	Coherence function
ε	[rad]	Phase shift between previous and current surface
ε_f	[rad]	Phase shift between previous and current surface (flip type instability)
ε_H	[rad]	Phase shift between previous and current surface (Hopf type instability)
η	[mm]	Radial distance from Cartesian to modal coordinates
η_p	[mm]	Stationary solution of the vibration in modal coordinates
$\eta(t)$	[mm]	Vibration amplitude in modal coordinates

θ_e	[rad]	Nutation angle
κ	[rad]	Lead angle
λ	[1]	Dimensionless chatter frequency
λ_f	[1]	Dimensionless flip chatter frequency
μ	[1]	Mass ratio
ν	[1]	Tooth passing frequency / natural frequency
ξ	[1]	Damping ratio
σ	[1]	Cutting stiffness over dynamic stiffness ratio
σ_s	[1]	Variance in the low frequency range
σ_n	[1]	Variance in the high frequency range
τ	[s]	Regenerative delay
υ	[1]	Damping ratio relative to c_{cr}
ϕ_{ex}	[rad]	Cutting exit angle
ϕ_j	[rad]	Immersion angle of tooth j
ϕ_{st}	[rad]	Cutting start angle
ϕ_{total}	[rad]	Total angle rotated during a sweep in SMFE method
χ	[rad]	Phase shift of the eigenvalue
ψ	[rad]	Phase of $[\Phi(j\omega)]$
ψ_e	[rad]	Precession angle
ω_c	[rad/s]	Chatter frequency
$\omega_{c,f}$	[rad/s]	Chatter frequency according to flip limit
$\omega_{c,H}$	[rad/s]	Chatter frequency according to Hopf limit
ω_g	[rad/s]	Rotation frequency of the cutting spindle
ω_i	[rad/s]	Angular speed at integration step i
ω_n	[rad/s]	Natural frequency
ω_{start}	[rad/s]	Starting scanning frequency
ω_{end}	[rad/s]	Ending scanning frequency
Λ	[1]	Eigenvalue
Λ_I	[1]	Imaginary part of the eigenvalue
Λ_R	[1]	Real part of the eigenvalue
Ω	[rad/s]	Tooth passing frequency
$\{\eta\}$	[mm]	Non-stationary solution of the vibration in modal coordinates
$[\alpha]$	[1]	Integrated directional factor matrix
$[\varphi]$	[1]	Singular vectors unitary matrix

$[\Pi]$	$[1]$	Singular value matrix
$[\Phi(j\omega)]$	$[N/mm]$	Relative frequency response function
$[\Phi_t(j\omega)]$	$[N/mm]$	Frequency response function of the tool
$[\Phi_w(j\omega)]$	$[N/mm]$	Frequency response function of the workpiece
$[\psi]$	$[N/mm]$	Oriented frequency response Function

Contents

Part IV: Conclusions

Sumari

El chatter és avui en dia un dels principals problemes en els processos de fresat. Per predir i evitar la seva aparició es disposa de models teòrics per al càlcul dels lòbuls d'estabilitat. No obstant això, les prediccions realitzades amb els models d'estabilitat de fresat no són robustes, presentant casos en què les desviacions entre la predicció i la realitat són importants.

Les causes d'aquestes desviacions són variades i poden ser degudes a la suma de múltiples efectes. A la vista dels estudis previs realitzats, els principals errors es troben en l'omissió de lòbuls de doble període (lòbuls flip) i errors en la determinació experimental dels paràmetres dinàmics del sistema mitjançant mètodes tradicionals. Aquesta Tesi aborda aquests dos problemes principals en la predicció, aportant nous coneixements sobre el chatter de doble període i desenvolupant una nova metodologia per a un càlcul més precís de la resposta dinàmica del sistema.

No obstant això, una predicció precisa de les condicions que donen lloc a un procés de fresat estable no garanteix l'aprofitament òptim de la màquina per maximitzar la productivitat, tal com s'exigeix en l'entorn productiu actual. Per això, es proposen tres noves tècniques per a l'eliminació de chatter en aquells casos en què, el procés de mecanitzat dissenyat estigui sota el perillós influx del chatter.

Resumen

El chatter es uno de los principales problemas en los procesos de fresado de hoy en día. Para predecir y evitar su aparición se dispone de modelos teóricos para el cálculo de los lóbulos de estabilidad. Sin embargo, las predicciones realizadas con los modelos de estabilidad de fresado no son robustas, presentándose casos en los que las desviaciones entre la predicción y la realidad son importantes.

Las causas de estas desviaciones son variadas y pueden deberse a la suma de múltiples efectos. A la vista de los estudios previos realizados, los principales errores se encuentran en la omisión de lóbulos de doble periodo (lóbulos flip) y errores en la determinación experimental de los parámetros dinámicos del sistema mediante métodos experimentales tradicionales. Esta Tesis aborda estos dos problemas principales en la predicción, aportando nuevos conocimientos sobre el chatter de doble periodo y desarrollando una nueva metodología para un cálculo más preciso de la respuesta dinámica del sistema.

No obstante, una predicción precisa de las condiciones que dan lugar a un proceso de fresado estable no garantiza el aprovechamiento óptimo de la máquina para maximizar la productividad, tal y como exige el entorno productivo actual. Por ello, se proponen tres novedosas técnicas para la estabilización del proceso en aquellos casos en los que el proceso de mecanizado diseñado esté bajo el peligroso influjo del chatter.

Abstract

Chatter is one of the major problems in today's milling processes. Theoretical models to calculate stability lobes are used to predict and avoid chatter onset. However, current predictions are not accurate enough and significant deviations between predicted and experimentally observed stability limits have been reported.

The causes for these deviations are diverse and can be the result of the sum of multiple effects. According to previous works, main errors in stability prediction are related to lack of knowledge about double period instability (flip lobes) and inappropriate determination of dynamic parameters through standard experimental characterization techniques. This Thesis deals with these two problems that affect accurate chatter prediction, contributing with new knowledge and calculation methods for double period type lobes and developing a new methodology for a more accurate dynamic response identification.

Nevertheless, an accurate chatter stability prediction does not necessarily imply an optimum use of the machine to maximize productivity, as it is required in current production environments. For this reason, three novel process stabilization techniques are proposed for those cases in which the designed machining process is subject to chatter vibrations.

Laburpena

Chatter-a arazo nagusienetako bat da egungo fresatze prozesuetan. Bere agerraldia aurreikusteko eta eragozteko modelo teorikoen bitartez kalkulatutako egonkortasun lobuluak erabiltzen dira. Hala ere, fresatze egonkortasuna kalkulatzeko modelo horien iragarpenak sendoak ez direla frogatu da hainbat kasutan, aurreikusitako eta gero esperimentalki egiaztatutako emaitzen artean desbideratze nabarmenak aurkituz.

Desbideratze horien arrazoiak anitzak dira eta efektu bat baino gehiagoren ondorio izan daitezke. Aurretik egindako ikerketen arabera, errore nagusiak periodo bikoitzeko ezegonkortasuna (flip lobuluak) kontutan ez hartzeagatik eta sistemaren parametro dinamikoak esperimentalki lortzeko prozesuan izaten diren kondizio ezegokiengatik gertatzen omen dira. Tesi honetan fresatze egonkortasuna kalkulatzeko orduan agertzen diren bi arazo nagusi hauek jorratzen dira. Modu honetan, periodo bikoitzeko chatter-aren inguruko ezagutza handitu da eta erantzun dinamikoaren kalkuluaren zehaztasuna hobetzeko metodo berri bat garatu da.

Hala eta guztiz ere, fresatze prozesurako baldintza egonkorrak iragartzeak ez du makinari etekin maximoa ateratzea bermatzen, egungo ekoizpen sistemak eskatzen duen moduan, produktibitatea optimizatzeko helburuarekin. Hori dela eta, chatter-aren eraginaren menpeko mozketa prozesuak egonkortzeko hiru teknika berri aurkezten dira.

Part I
Definition of Objectives

In the present Part, a brief introduction of the subject and the reasons that motivated this work are presented (Chapter 1), a review of the state of the art in the field is done (Chapter 2) and a critical analysis of the state of the art and the objectives to pursue in this Thesis are described (Chapter 3).

Chapter 1

Introduction

Chapter 1 explains the background and the motivation towards the subject of this Thesis.

1.1 BACKGROUND

Chatter continues to be nowadays one of the most harmful and most difficult problems to avoid in any kind of machining process. Therefore, the development of accurate chatter prediction models and efficient chatter avoidance tools is of paramount importance for the manufacturing industry.

Although stability lobes have been successfully used in many industrial machining process optimizations, currently they lack for enough reliability to apply them intensively in the manufacturing industry.

In milling processes, the source of model inaccuracies are usually attributed to omission of specific types of destabilization, nonlinearities of the process or dynamic parameter identification errors. Several authors have emphasized this fact in different research works.

Davies et al. (2000) experimentally demonstrated the existence of double period instability (flip lobes) in highly interrupted milling processes. The omission of these lobes could result in a severe failure of stability prediction in specific cases.

Improved models to calculate flip lobes in a fast and accurate way is crucial. This kind of instability calculation procedure is already solved, but the effective integration in current fast stability models is not done and the detailed effects are not fully understood yet.

Brecher and Esser (2007) consider geometry and cutting parameters as reliable information but claim a high level of uncertainty in the compliance of the machine tool and the stiffness of the process. Sims et al. (2010) explained through a fuzzy algorithm how a relatively small uncertainty of the input parameters of the stability models could affect the stability limit to a great extent.

In order to overcome these problems, alternative experimental methods can provide more accurate input data. Experimental methods rely on empirical data which are later used as inputs in the stability model. They provide in-process information and can account for process nonlinearities if they are conducted under conditions close to the real case. The alternative experimental methods could improve significantly model input data quality and therefore enhance chatter prediction model reliability.

Increasing global competitiveness is forcing manufacturing companies to increase their productivity at maximum levels. For this reason, when chatter cannot be predicted or when it cannot be avoided, mitigation or suppression solutions are being increasingly used. These solutions are usually implemented when the stability problem has already arisen and they are customized to solve a very specific problem, thus, it can be useless when similar problems appear along machine tool life or when the machining operation is changed. Moreover, today's solutions are very costly and not easily integrable in current manufacturing environments.

The development of cheap, wide actuation range and easily integrable solutions would pose a significant advance for the manufacturing sector.

1.2   MOTIVATION

In the last years, several research works have been conducted in the Dynamics and Control Research Line at IK4-Ideko in order to stay in world's cutting edge of milling stability modeling and improvement.

The Theses carried out by Munoa (2007) and Bediaga (2009) in the field of frequency domain and time domain stability models respectively, together with the later development of the semi-discretization model, has provided IK4-Ideko with the most important simulation models for milling process.

On the other hand, the continuous spindle speed variation (CSSV) technique to suppress chatter (Bediaga, 2000) and the active damping through inertial actuators (Mancisidor, 2014), have provided useful tools for chatter mitigation in cutting processes.

This Thesis follows the ongoing machining stability prediction and suppression work in the Dynamics and Control research line at IK4-Ideko. This knowledge has given rise to many publications by IK4-Ideko in the field of modeling (Zatarain et al., 2004; Munoa et al., 2009; Zatarain et al., 2010; Dombovari et al., 2011b; Munoa et al., 2013a) and chatter suppression through different methods (Munoa et al., 2010; Munoa et al., 2013b; Mancisidor et al., 2015). Moreover, the developed frequency domain milling models have been integrated in an internal software package called IKMILL, which is especially dedicated for milling stability analysis in the whole workspace of the machine.

The University of Girona, with the work developed at the Technological Innovation of the Production Systems research line, has also become an active research institution in milling chatter in the last years, specifically regarding experimental inverse methods (Quintana et al., 2008; Quintana, 2010).

In order to continue and enhance these previous works, the collaboration between IK4-Ideko and the University of Girona brings up a high potential partnership that forebodes a fruitful and successful research work. IK4-Ideko will collaborate with its expertise in milling stability prediction models, simulation tools and mitigation techniques while, on the other hand, the University of Girona will contribute with its knowledge about inverse experimental testing and chatter detection methods.

Although a big global effort has been done to increase the knowledge about chatter, with so important research groups as the University of British Columbia in Vancouver, headed by the Professor Yusuf Altintas, or the University of Budapest, with Gabor Stépán at the front, there is still much to investigate in the field.

In model verification tests carried out by the Dynamics and Control research line at IK4-Ideko, important mismatches have been found between theoretical stability prediction and measured machine behavior in some cases. Whereas there are some

milling cases in which the stability models provide a reasonably good correlation, there are others where it does not. Although several factors have been pointed out as a reason to explain the observed deviations, according to IK4-Ideko's expertise there are two main reasons that could be the most significant and those that bring the largest deviations around the predicted stability. As it will be stated in Chapter 2, these reasons have also been identified by other international researchers.

First, the omission of double period stability lobes could lead to important errors in the prediction of interrupted milling processes. Moreover, those methods that are already considering this type of instability are not optimized and usually extend simulation time far beyond.

The other important source of errors is the inaccuracies of the dynamic parameter extraction of the system (Brecher and Esser, 2007). There is a consensus among the research community about the need for improved methods for dynamic parameter identification.

IK4-Ideko's main customers are machine tool builders and, among them, milling machine or milling center manufacturers is a key group. It would be of great interest for them to integrate the milling stability model in the CNC, communicating the stability model with the CAM. As unstable operations would be automatically identified, intelligent chatter avoidance techniques could be developed to actively control chatter and improve cutting performance.

The achievement of the objectives of this Thesis will improve stability prediction reliability and chatter onset control and it will pose a step forward towards the industrialization of the investigated solutions. The attainment of the industrialization of chatter prediction and suppression solutions in a reliable way would be a huge leap for the machine tool industry.

Finally, the author's personal interest is related to the everyday work at IK4-Ideko. One of the author's main activities is the coordination of the Collaboration Plan between IK4-Ideko and SORALUCE, a milling machine tool builder and referent customer of IK4-Ideko, who has been developing innovation projects with IK4-Ideko for 25 years, renewing the Collaboration Plan year by year. From some years ago, one of the big challenges in this Collaboration Plan has been the investigation of process stability and especially the relation of machine architecture with process stability, that is, the cutting capability of the machine tool. Each of the new machine prototypes from SORALUCE are modeled through finite element models and the experimental correlation is performed after the new prototype is built. Moreover, experimental tests are conducted

in order to determine the cutting capability in the whole workspace of the machine. The missing link in this process is to relate the cutting capability to the machine dynamic properties and lately, to the machine structure. If this link was established, SORALUCE would gain a determinant competitive advantage to stay ahead of the competition and IK4-Ideko will accomplish a key methodology for milling process understanding.

On the other hand, the most complex after-sales services for SORALUCE are related to customers who find chatter as a limitation in their productive process. SORALUCE's objective is to develop chatter suppression techniques useful to handle this kind of problems and also to integrate them in the machine standard equipment, in order to anticipate to the problem and reinforce the brand image.

Chapter 2

State of the art

Chapter 2 reviews the fundamentals of machine tool vibrations, focusing on chatter vibration characteristics. The stability prediction models developed and the main breakthroughs made in the last century are described, with a special focus on the frequency domain model. New force characterization techniques and dynamic parameter extraction method by means of experimental methods are discussed. Finally, current chatter detection and suppression techniques are reviewed.

2.1 MACHINE TOOL VIBRATIONS

2.1.1 Classification

Vibrations are probably the most harmful and complex problem existing in machining processes. Machine tools are mechanical structures that vibrate as a result of the forces generated during the machining process. Many efforts have been made in vibration origin and mechanism study in machine tools.

Metal cutting processes can entail three different types of mechanical vibrations:

Free vibrations

Free vibrations occur when the mechanical system is displaced from its equilibrium and then is allowed to vibrate freely. In metal removal operations, free vibrations appear, for example, at the acceleration or deceleration of the moving masses of the machine tool and at the entrance or exit of the tool in the workpiece.

Forced vibrations

Forced vibrations appear due to external harmonic excitations associated, for example, with unbalanced shafts or by the periodical hitting of the tool's teeth on the workpiece.

Free and forced vibrations can be avoided, reduced or eliminated when the cause of vibration is identified. Engineers have developed and can implement several different widely known methodologies to mitigate and reduce their occurrence.

Self-excited vibrations

Self-excited vibrations are produced due to a dynamic instability generated by the cutting process itself. When the destabilization of the process occurs, the vibration level grows quickly until a limit cycle is reached. This type of vibration is called chatter.

Chatter brings the system to instability and is the most harmful and the least controllable type of vibration. This phenomenon is described in more detail in the following section.

2.1.2   Chatter vibrations in cutting

Chatter vibrations in cutting can occur basically when the "cutting process stiffness" is higher than machine's dynamic stiffness (Merritt, 1965). There are four main factors which determine the appearance of chatter: cutting conditions, workpiece material properties, tool geometry and the dynamics of machine tool system and workpiece.

Chatter has several negative effects, interrelated among them according to Figure 2.1, such as:
- Poor surface quality.
- Part rejection.
- Increased tool replacement needs.
- Excessive tool wear or tool breakage.
- Excessive noise.
- Machine tool components damage.

- Reduced material removal rate (MRR).
- More frequent maintenance needs.
- Waste of materials.
- Waste of energy.
- Environmental drawbacks.
- Increased production time.
- Increased production costs.
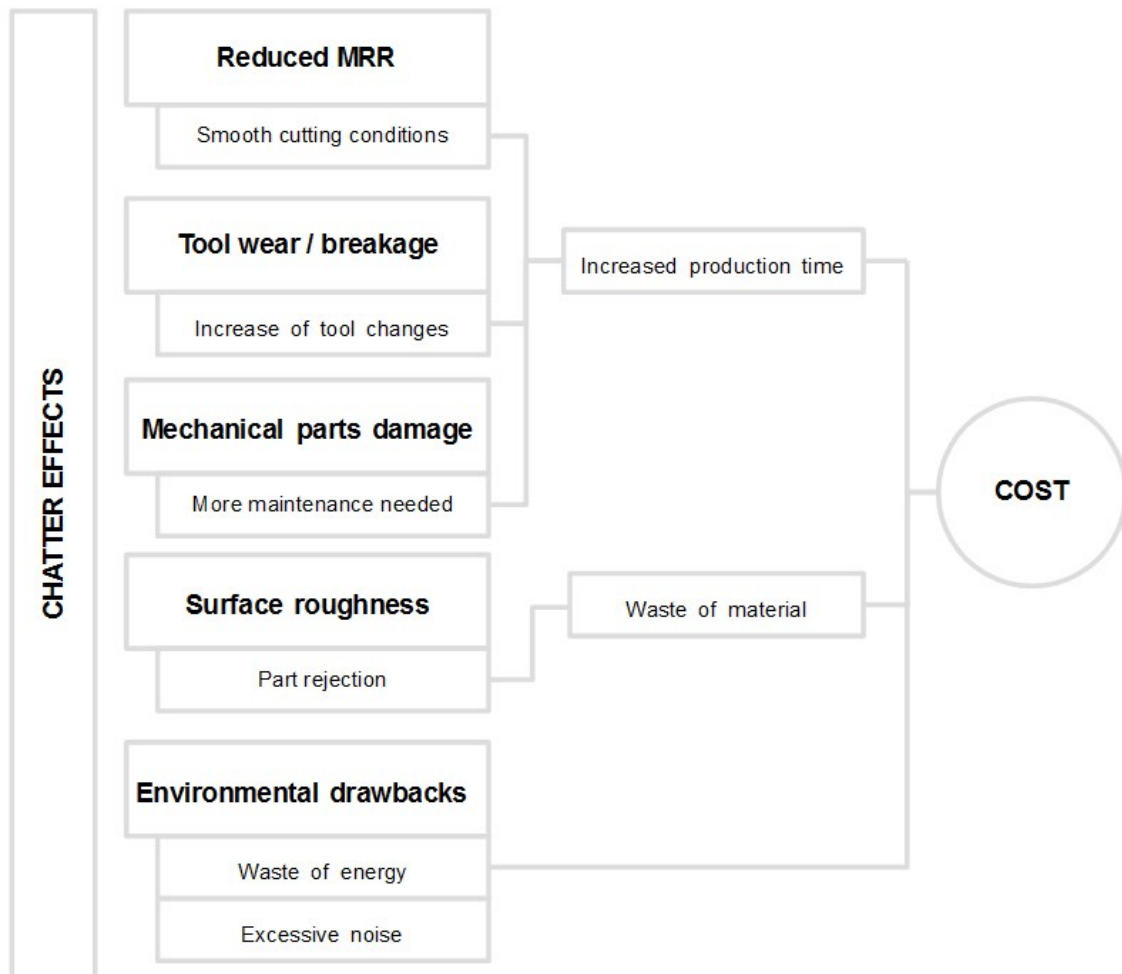
Figure 2.1: Chatter effects.

Although the regenerative effect was described more than 50 years ago (Tlusty and Polacek, 1957; Tobias and Fishwick, 1958), its prediction and control methods are still subject of research nowadays. Stability prediction models including, for instance, process damping effect, part behavior, changes on structure and variations on system dynamics along the tool path are being investigated by the research community (Quintana and Ciurana, 2011).

In spite of the fact that machine's design has become a more meticulous process in the last years, machine tool designers and manufacturers do not usually take measures to prevent chatter from the design stage and it is a common situation to come up with chatter problems when the first manufacturing tests are carried out in the machine.

The recent developments in material technology allow increasing the cutting conditions and consequently the chip load as well. This higher capacity together with the increase in new generation machine's rated power makes the stable cutting more demanding. On the other hand, cost competition and energetic efficiency wills result in more adjusted machine component design, lighter structures, which usually involves weaker and more prone to chatter machines building as well.

Moreover, rising needs in terms of accuracy have brought along a reduction of machining stability due to the low friction guiding systems required to fulfill these accuracy requirements. These new guiding systems are weakly damped structures. Highly damped structures are obviously against the overall accuracy but they also have a "good" side regarding chatter vibrations, since machining stability is directly proportional to the amount of damping of the machine.

A good example of this is the machining performance of a centerless grinding machine (Figure 2.2 and Figure 2.3). The stability increases when changing the guiding system of the regulating wheel from linear rolling bearings to friction guideways, since damping is rather higher in the last case.
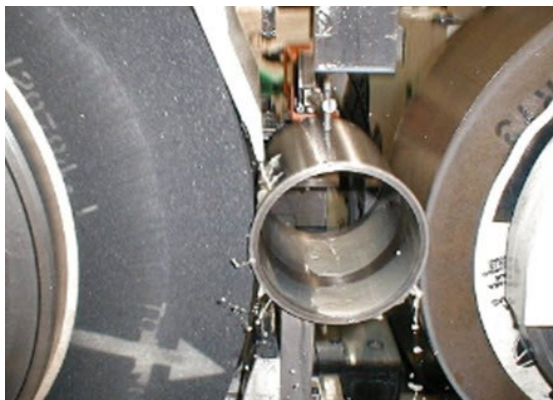
Figure 2.2: Centerless grinding process.
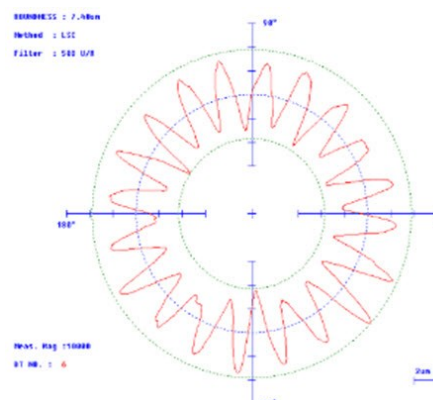
Figure 2.3: Roundness measurement in chattering centerless grinding process.

To make chatter removal even more challenging, manufactured parts have also become lighter and less stiff, in order to minimize costs or fuel consumption decrease in transports, for example. This fact also hampers cutting stability.

Chatter is a common problem when machining slender workpieces, thin walled structures or highly flexible parts (Figure 2.4).

Figure 2.4: Typical operations in which chatter may occur.

Therefore, and due to current machine design and use trends, chatter has become a more usual problem than in past decades, when machines were usually oversized, had slower primary and secondary cutting motions and, consequently, had a higher "chatter-resistance". Therefore, the new 21st century machine concept brings chatter to the front line of machining problems and makes crucial the development of new tools to predict, detect and avoid chatter.

Chatter mechanisms

There are different mechanisms that provoke chatter. Some of these types of chatter where described by Wiercigroch and Budak (2001).

- **Static instability** appears mainly when turning or boring tools are used. The cutting tool is crushed on the machined surface giving rise to a deformation that changes the effective rake angle of the tool. This effect produces a sudden increase of chip thickness and cutting forces.

- **Dynamic instability due to negative damping** occurs when the process gives rise to a negative damping that exceeds the damping of the system. Although this is not a usual case, there are some circumstances under which this effect may appear: the rubbing between the flank wear of the tool and the workpiece, the modification of the rake or relief angles and the increasing decreasing cutting force characteristic of some materials.

- **Mode coupling chatter** occurs when two perpendicular modes in the cutting plane are excited. The cutting edge describes an elliptic trajectory and when it penetrates the workpiece, the cutting forces oppose to it; however, when it gets out, the cutting forces coincide with the vibration speed, thus adding energy to the system. If the added energy is greater than the dissipated energy, the process becomes unstable.

- **Regenerative chatter** is the most common form of self-excited vibration. Initially, cutting forces excite system modes giving way to a wavy surface. When next tooth attacks this wavy surface, it describes a new wavy pattern over the new surface. Depending on the phase difference between the wavy surface left by the previous tooth and the wave left by the current tooth, the resulting vibration will grow or not, depending on the damping of the system. If this process is repeated with the successive teeth passing by, a regenerative effect will be produced and the vibration will amplify till it reaches a limit cycle.

In Figure 2.5a schematic view of the regenerative mechanism is shown. In Figure 2.5a there is no phase shift between the existing wavy surface and the current tool trajectory, therefore, the chip thickness remains constant and the process stable. In Figure 2.5b and Figure 2.5c there is a delay, which results in a variable chip thickness and consequently, a growing vibration. In the worst case scenario, where the stability is minimum, the phase "delay" is $\pi/2$ or $3\pi/2$.
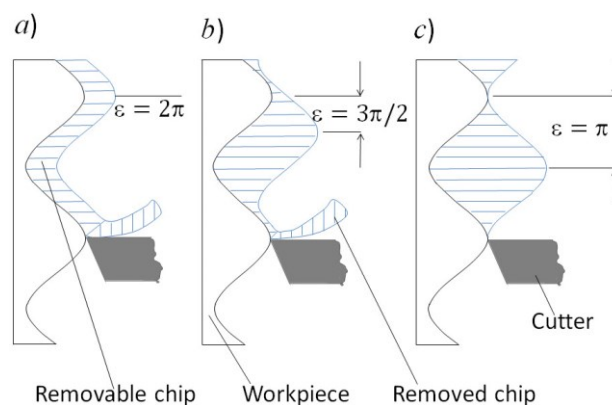
Figure 2.5: Regeneration mechanism.

2.1.3 Stability lobe diagrams

Stability lobe diagrams (SLD) are charts where the border between a stable and an unstable cut is represented. This border establishes the depth of cut over which the chatter phenomenon will occur, as a function of the rotating speed. The shape of the stability border is lobular (Figure 2.6) and presents sweet spots, rotating speeds at which a maximum material removal rate is achievable. The stability lobes are a high value tool for the process engineer, since it helps to determine the optimum cutting conditions for a specific operation.
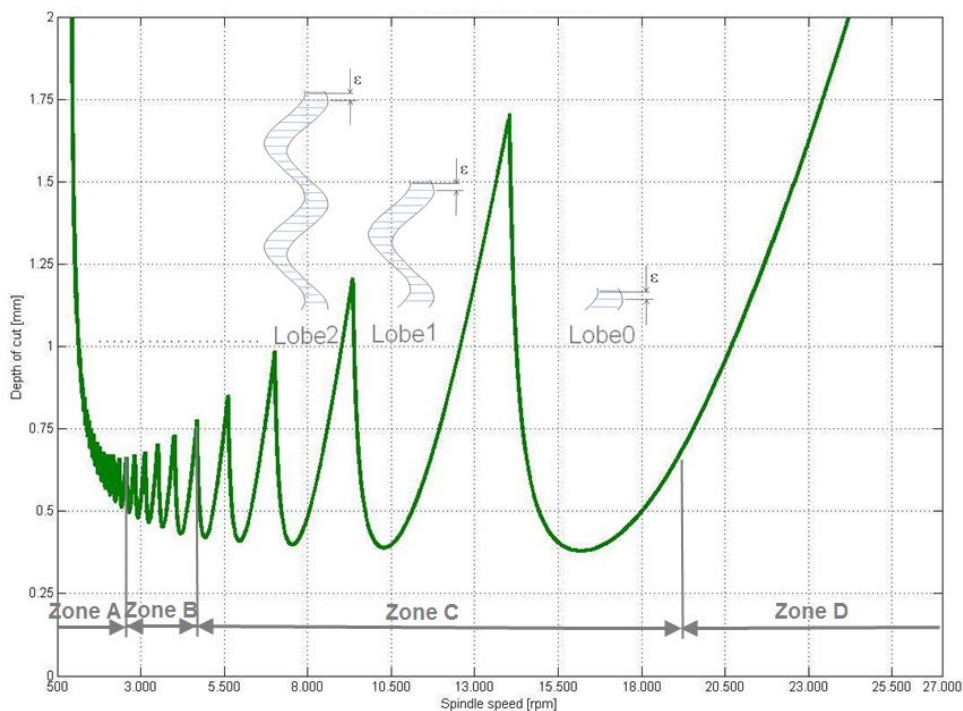
Figure 2.6: Stability lobe zones.

Each vibration mode of the system creates a family of lobes. Each of these groups of lobes affects a specific cutting range (zones B and C in Figure 2.6), depending on the frequency of the mode ω_n. Out of this range, the cutting process is gradually no longer affected by the mode as the rotation speed *N* is increased or decreased.

The lobe number (l) indicates the number of "complete waves" per revolution. In the specific case of a turning or a grinding process it would mean the number of marks left on the machined surface in each revolution. Theoretically this value can be obtained through the following relation:

$$l + \frac{\varepsilon}{2\pi} = \frac{60 f_c}{NZ}.$$

(2.1-1)

For a practical use, when the number of lobe l in a specific process has to be determined, the term ($\varepsilon/2\pi$) can be neglected.

The lower lobes are located on the right hand side of the lobe diagram. As the lobe number increases, the spacing between lobes gets smaller and the lobes appear further to the left.

The stability lobes can be divided in four different areas:

Zone A (l >10):

Here the ratio between the chatter frequency and the tooth passing frequency is very high $\omega_c >> \Omega$, that is, the number of lobe limiting the cutting process is high. At this cutting speed, limit axial depth of cut is very high due to process damping effects.

Zone B (5< l <10):

This is the medium speed zone, where the chatter frequency is slightly higher than the tooth passing frequency $\omega_c > \Omega$. The process damping effect almost disappears and the cutting capability is low, since lobes are very close together.

Zone C (0.5< l <5):

In this zone the chatter frequency is of the same order as the tooth passing frequency $\omega_c \approx \Omega$. Lobes are more spaced, giving way to the appearance of sweet spots. The right tuning of the speed in this zone is critical in order to obtain the best performance of the system.

Zone D (l <0.5):

In this zone the chatter frequency is lower than the tooth passing frequency $\omega_c < \Omega$. It is usually the ultra-high speed region and not always achievable due to the mechanical limitations of the machine. The main characteristic of this zone is that stability increases with speed.

2.2 STABILITY MODELS

2.2.1 Chronology

First research works on chatter date from the beginning of the 20th century, when Taylor (1907) described chatter as the "most obscure and delicate of all problems facing the machinist".

Arnold (1946) was the first one who tried to explain the causes of chatter, considering it occurred due to the negative damping of the process. However, this theory was contradicted by Tlusty and Polacek (1957, 1963) and Tobias and Fishwick (1958), who published papers claiming regenerative effect and mode coupling as main causes of chatter vibrations. As a solution, they suggested the use of stability charts (lobe diagrams) in order to obtain the depth of cut at which the process becomes unstable, as a function of the spindle speed. Later, Merit (1965) presented the problem as a feedback loop, clarifying the understanding of the problem. However, most of theoretical and experimental works were focused on continuous cutting processes, like turning.

The stability analysis in milling processes is more complicated due to the discontinuous nature of the process and its intrinsic nonlinearities. Cutting forces are originated by the simultaneous cutting of several flutes and they vary their magnitude and direction, since the combined rotation and feed speed of the cutting tool make the mill flutes enter and exit the workpiece periodically.

First attempts in dynamic modeling of the milling process were conducted by Sridhar et al. (1968), Koenigsberger and Tlusty (1970) and Opitz and Bernardi (1970). Sridhar developed a stability theory for a milling process based on the numerical integration of the milling equations for one revolution of the tool. The milling model was composed by a system of linear differential-difference equations, which are referred later as linear delayed differential equations.

In milling, cutting force and chip thickness directions vary with time and so do the directional coefficients as well (Figure 2.7). Koenigsberger and Tlusty (1970) solved this problem calculating the geometrical mean value of the cutting arc and projecting the directional coefficients according to this direction. On the other hand, Opitz and Bernardi (1970) improved the frequency model accuracy by calculating the mean directional factor as an average of its value along the whole arc covering the radial immersion area. They also claimed that chatter's origin was the regenerative effect in most cases, playing down the importance of mode coupling effect. Weck (1984) used the same approach as Opitz and Bernardi (1970) for a three-dimensional force model

and he remarked the importance of including the cross frequency response functions for a proper dynamic characterization of the machine.
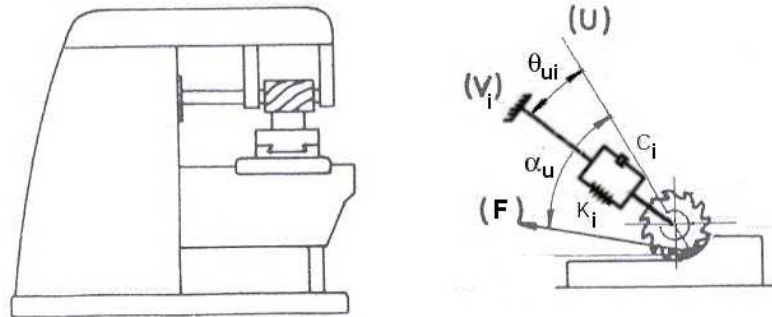
Figure 2.7: One-dimensional regeneration model. Directional factors (Koenigsberger and Tlusty, 1970).

For many years these basic approaches were used. The technique of calculating a mean directional coefficient and projecting the dynamics over it were defined by Altintas and Weck (2004) as single degree of freedom methods. These frequency domain models are often inaccurate and, therefore, they were relegated by initial value time domain models at the beginning of the 80s.

Initial value time domain simulations are capable of accounting for nonlinear effects of the process, such as the loss of contact between cutting edge and workpiece due to high vibration level (Tlusty and Ismail, 1981), the change of the cutting force coefficients as the chip thickness changes and process damping. In the last quarter of the 20th century, several works related to milling initial value time domain simulation were carried out (Tlusty and Ismail, 1981; Altintas and Spence, 1991; Montgomery and Altintas, 1991). This simulation gives detailed information of the milling process but the stability limit calculation is not straightforward.

It was after the work by Minis and Yanushevsky (1993) when the frequency domain analytical solution came back to the spotlight. These researchers improved the method by Sridhar et al. (1968) applying Floquet's theory and Fourier analysis to a two-dimensional milling model. Although this model relies on the numerical evaluation of the stability limits, it gives a deeper insight for a better understanding of the model.

Budak (1994) and Altintas and Budak (1995) presented an alternative general method for chatter analysis in the frequency domain. At the same time, they obtained an approach to the solution by using a Fourier series development of the Cartesian directional coefficient matrix and solved the system by considering the zeroth order term only (zeroth order approximation, ZOA). The proposed model is therefore single

frequency and two-dimensional and is capable of giving a good approximation to the solution in most milling cases with little computation time. The result converges to the same solution as Minis' numerical algorithm. This work is today the basic reference for chatter limit determination in milling processes.

The model by Altintas and Budak (1995) was applied for stability analysis of different kind of mills, such as cylindrical mills, ball end mills and inserted cutters (Altintas and Lee, 1996; Engin and Altintas, 2001a; Engin and Altintas, 2001b).

The two-dimensional milling model by Altintas and Budak (1995) neglects the axial stiffness of the system, which can be acceptable in some cases like tool chatter processes but not when chatter is the result of structure chatter, typical from face milling of steel, for instance.

For these reason, Jensen and Shin (1999a), following the methodology of Altintas and Budak (1995), showed a three-dimensional model, which includes the axial axis of the tool and takes into account the lead angle. This angle allows locating the chip regeneration direction in three dimensions. Altintas (2001) updated his algorithm to a three-dimensional model and obtained an analogue result as Jensen and Shin (1999a). Munoa et al. (2005) applied the model of Altintas and Budak (1995) for chatter stability prediction in steel roughing operations. The effect of the feed direction was taken into account and the machine dynamics were obtained for specific positions of the machine. This independence of the system stability limiting dynamics on the tool allows selecting the most convenient tool for a given roughing operation.

The single frequency approach has shown to be precise enough for most milling processes, but when radial immersion of the mill is small, the existence of additional stability lobes was proved. Davies et al. (2000) noticed the presence of a new family of lobes in the stability diagram as they used a discrete map model for highly interrupted milling processes, where the time in the cut is infinitesimal and the cutting process is modeled as an impact. Bayly et al. (2003) developed the method of time finite elements, obtaining similar results.

Insperger and Stépán (2000) used an approximation method called Fargue method and also detected these lobes and showed that the mathematical phenomenon which describes them is the *flip bifurcation* (classical stability lobes correspond to *Hopf bifurcations*). Later, they developed the semi-discretization (SD) method in order to solve the milling model described in a form of delayed differential equation (DDE) (Insperger and Stépán, 2001).

From this point on, two different types of chatter were distinguished: *flip* (or double period instability) and *Hopf*, depending on the mathematical phenomenon describing each case. The existence of chatter flip has been experimentally confirmed by several authors (Davies et al., 2000; Davies et al., 2002; Mann et al., 2004 and Gradišek et al., 2005).

The different stability calculation methods and their main advantages and disadvantages are described in Table 2.1.

Method	Advantages	Disadvantages
SINGLE FREQUENCY / ZEROTH ORDER APPROXIMATION (ZOA)	• Fast method. • Measured FRF direct input.	• Nonlinearities not supported. • Inaccuracies in interrupted cutting.
MULTI-FREQUENCY	• The simulation speed and precision depends on the number of harmonics selected. • Measured FRF direct input.	• Nonlinearities not supported. • Every type of cutting supported.
TIME DOMAIN BASED	• Very complex mill models can be handled. • Robustness.	• Modal parameter extraction from the FRF is needed. • Slower than ZOA method.
INITIAL VALUE TIME DOMAIN	• Nonlinearities can be taken into account. • Very accurate simulations.	• Time consuming. • Uncertainty in chatter determination. • Filtering problems. • Modal parameter extraction from the FRF is needed.

Table 2.1: Stability prediction method comparison (Munoa, 2007).

Flip lobes can also be described in the frequency domain if modulated components of the chatter frequency and more terms in the Fourier series of the directional factor matrix are considered. Although these models were developed in the 90s (Budak, 1994; Budak and Altintas, 1998), it was not until one decade later when flip lobes were obtained using these methods (Merdol and Altintas, 2004; Zatarain et al., 2004).
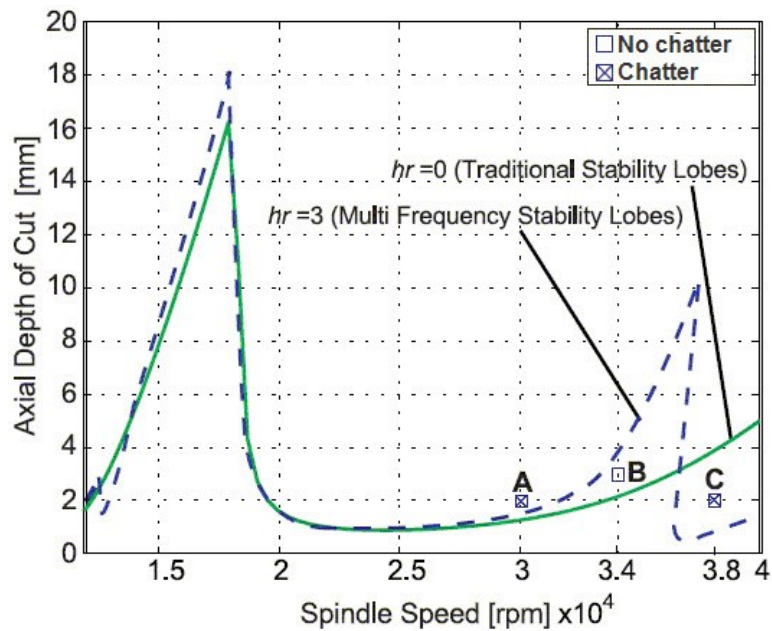
Figure 2.8: Differences of traditional zeroth order lobes versus multi-frequency stability lobes (Altintas and Weck, 2004).

By using the multi-frequency approach, Zatarain et al. (2006) showed that the helix of the tool produces the transformation of the added lobes (period doubling) into instability islands. This means that, contrary to what it had been thought until then, the helix of the tool increases the stability under certain specific relations between helix pitch and depth of cut. Insperger et al. (2006) reached the same conclusion by using the semi-discretization method. Later, Patel et al. (2008) obtained the same results by using the method of Time Finite Elements.

Budak (1994) had previously showed that the helix angle had no repercussion in the single frequency solution. This is due to the fact that this type of solution is just capable of simulating Hopf type lobes. Apart from flip type lobes, other error sources have been identified in ZOA solution when mode interaction phenomenon is present in low engagement milling processes (Munoa et al., 2009).

2.2.2 Last trends in stability models

Nowadays there are still several challenges in cutting modeling that are being intensively investigated.

In the aerospace sector, there is a growing need to reduce weight of components that has evolved in very **thin walled structures**. This type of structures poses a significant challenge in terms of machining, due to its intrinsic low dynamic stiffness.

Modeling of this type of machining is a complex task, given that the dynamic properties of the system are continuously changing as the tool moves to stiffer or more flexible positions in the workpiece and due to the material removal during the cutting process. The main trend in thin wall machining is to use FEM models to predict the modal parameters and shapes of the different vibrations modes, considering the variations due to the material removal. However, the damping estimation is more difficult due to the effect of the workpiece clamping on the different modes of the thin wall. Budak et al. (2009) applied experimentally fed frequency domain models for optimizing 5-axis machining processes performed with ball end-mills. Biermann et al. (2010) presented a general approach to simulate workpiece vibrations during five-axis milling of turbine blades. They combined time domain based simulations (Stepan et al., 2014) with dynamic parameters of the thin wall obtained by a FEM model and the surface topology of the final blade was predicted using advanced visualization techniques.

As the cutting technology advances, **new mill geometry types** are developed. These new geometries are usually rather complex, hence the frequency methods are not adequate for the modeling of these mills. Therefore initial value time domain and time domain based methods in combination with the orthogonal to oblique transformation are used instead. Yusoff and Sims (2010) use the semi-discretization method in order to optimize variable helix angle mills. Similarly, Sellmeier and Denkena (2010) use the Ackerman method for variable pitch mill optimization. They found stable closed areas within the instability zone. These zones were also identified in the case of uniformed pitched mills acting on systems with more than one mode (Munoa et al., 2009). Finally, Dombovari et al. (2010) and Munoa et al. (2010) obtained stability charts for serrated mills by means of the semi-discretization method. In this work, the stability increase of a serrated tool with respect to an equivalent conventional mill is shown, as well as the strong feed dependency of the stability chart for this type of tools (Figure 2.9).
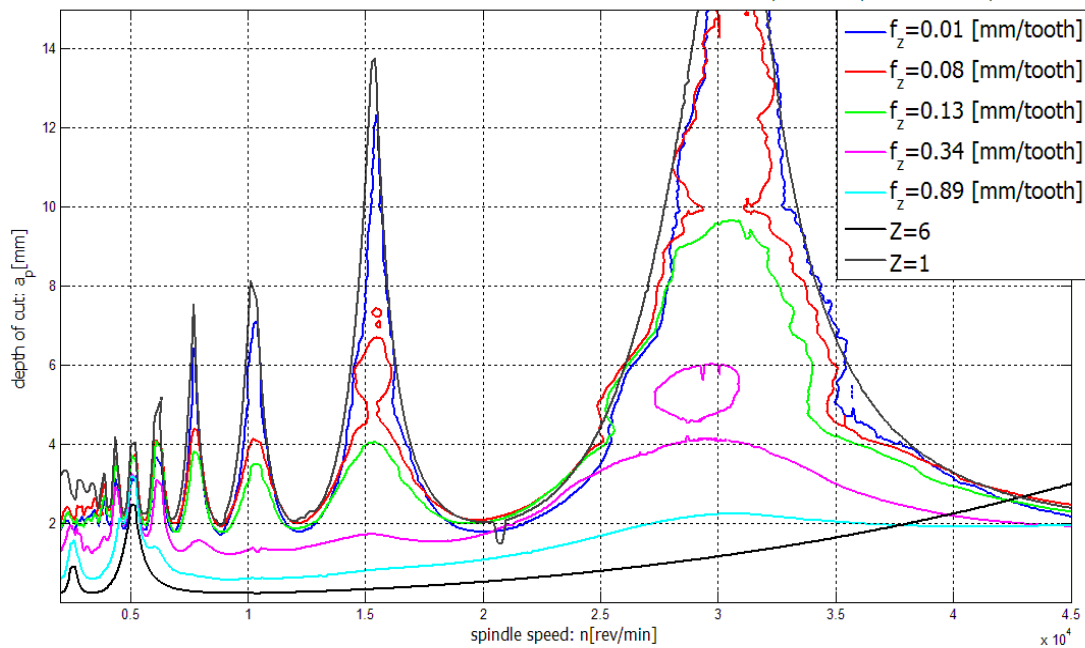
Figure 2.9: Stability lobes for a serrated mill. Feed dependency is observed. All the lobes are located between the one-tooth tool and the six-tooth tool.

The University of Florida (Karandikar and Schmitz 2010) has studied **the effect of tool wear** on cutting force coefficients. They have observed a notable change in the tangential cutting force coefficients as the tool wears out, which would entail a dramatic decrease in stability.

The investigation of **stability of turning processes** is another subject of current investigations, with two main difficulties: the process damping is present in most of the cases and some geometrical effects make the stability analysis more difficult. This is the case of boring processes where the feed influences the stability (Kurata et al., 2010).

A common growing practice in several industrial applications is **the use of two or more spindle heads milling simultaneously** in order to maximize productivity, what is called simultaneous or parallel milling. This set-up adds a higher difficulty in stability analysis. Lazoglu et al. (1998) were the first to model parallel turning operations using initial value time domain simulations where each tool was cutting a different surface and dynamic coupling between the tools occurs through the flexible workpiece. They showed that the dynamic coupling decreased the stability limits. Later, Ozdoganlar and Endres (1999) developed a parallel turning process on a modified vertical milling machine where they cut different surfaces in the same part. They developed an analytical solution for dynamically symmetric systems where the cutting tools have the same transfer functions, and validated the analytical solution

experimentally using a special flexible plate. Ozturk and Budak (2010) developed a time-domain model for parallel milling stability analysis, concluding that the material removal rate (MRR) could be increased with respect to a single milling tool process. Mori et al. (2011) increased the accuracy in the finishing operation of flexible plates by applying a double-sided single tooth milling process, in which thrust force is cancelled by synchronizing both tools. Brecher et al. (2011) presented a model for parallel milling and remarked the difficulty of this kind of simulation, since time relationship between both cutting processes must be taken into account.

Finally, there are researchers trying to pose **new numerical methods for calculation time reduction** purposes (Rock, 2010), multiple frequency strength identification (Dombovari et al., 2011b) or new solving approaches (Sellmeier and Denkena, 2010).

There are other topics such as **process damping** and the **unsafe zone** that will be discussed in 2.4.2.

2.2.3 Model integration in commercial off-the-shelf software

Up to now, the force and stability models developed have had little impact in production plants. This is due to the fact that these models have not been integrated in the most commonly used platforms by process engineers, such as CAM tools and verification and optimization tools (VERICUT® from CGTech, NCSIMUL® from SPRING TECHNOLOGIES...), in a 3D environment.
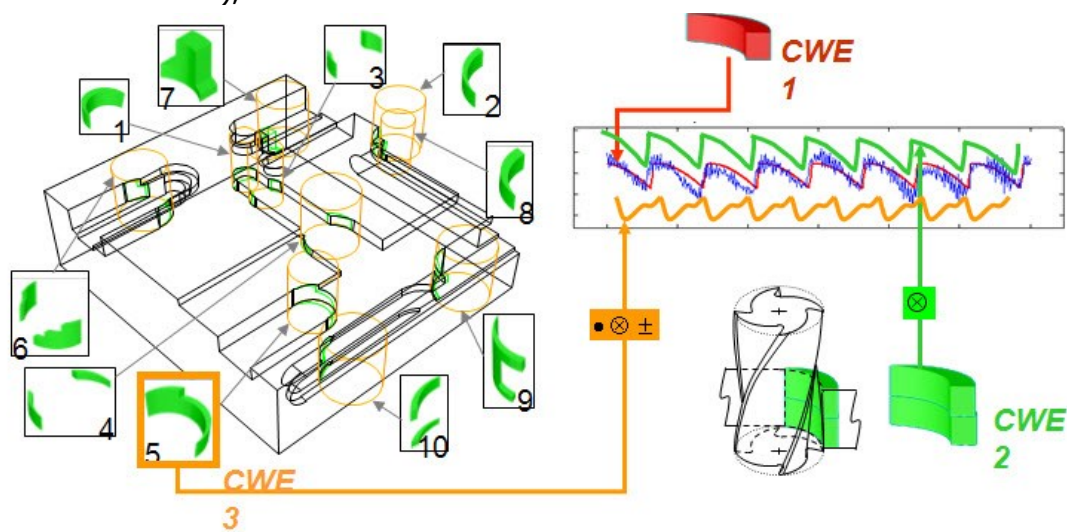
Figure 2.10: Tool engagement calculation from CAM model (Altintas, 2011).

Currently, there are different international research groups trying to sort out this issue. The instantaneous chip thickness computation along the tool rotating angle is the key point in this investigation (Figure 2.10). Current CAM and verification software are capable of computing the chip load according to tool's and workpiece's geometry and cutting teeth position, however, this information is not usually available for external use. The software ESPRIT® from DP Technology Corp. has an open network environment philosophy, which allows the addition of extra functionalities to the software core.

Regarding the international groups working in this area, Professor Altintas and his research group at University of British Columbia (UBC) have recently developed the *MACHpro Virtual Machining System* project (Merdol and Altintas, 2008). Before starting this general application, they have conducted specific works for titanium impeller machining (Ferry and Altintas, 2008a and Ferry and Altintas, 2008b), which deal with machining time optimization without overcoming several restrictions such as chip load and stress level in tool. The objective of *MACHpro Virtual Machining System* project is to develop reliable software for the computation of force, vibration and stability limits, usable for any kind of tool and workpiece geometry.

In Germany, the Institute for Machine Tools of the University of Stuttgart (IFW-Stuttgart) works on the joint simulation of the structure and the cutting process are being carried out (Heisel et al., 2010). In the University of Dortmund, Surmann and Enk (2007) developed a simulation system to calculate the regenerative tool vibrations along changing engagement conditions. The Technical University of Darmstadt has also presented a work in the joint dynamic simulation of structure and cutting process, aimed specifically for a robot application (Abele, 2010). An information exchange with the CAM application is done.

2.3   DYNAMIC MILLING MODEL

From all the models described in section 2.2, ZOA, multi-frequency solution and initial value time domain solutions for a 3-dimensional case are addressed, since these will be the main models used in this Thesis.

2.3.1   Dynamic chip thickness

Considering ϕ_{ji} the instantaneous angular immersion of tooth *j,* as shown in Figure 2.11, and a spindle angular speed of *N* (rpm), the immersion angle varies with time as:

$$\phi_j(t) = \frac{2\pi N t}{60}.$$ (2.3-1)
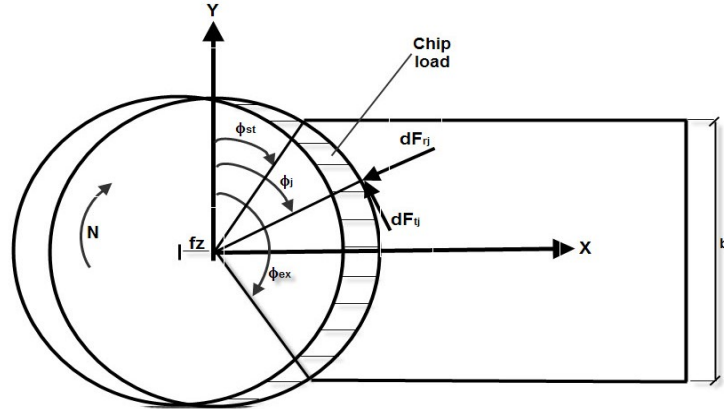
Figure 2.11: Angular immersion in milling processes.

Figure 2.12 shows a schematic representation of the milling process considering 3 degrees of freedom. Cutting forces affect the structure in the three Cartesian directions x, y and z, causing dynamic displacements. The resulting chip thickness h consists of a static part $h_s(\phi_j)$ and a dynamic part $h_d(\phi_j)$. The static part is attributed to the rigid body motion of the cutter

$$h_s(\phi_j) = f_z \sin\phi_j \sin\kappa,$$ (2.3-2)

where f_z is the feed rate per tooth and κ is the lead angle.

The dynamic component is caused by the vibrations of the tool at the present tooth period,

$$h_{d1}(\phi_j) = -x(t)\sin\phi_j \sin\kappa - y(t)\cos\phi_j \sin\kappa + z(t)\cos\kappa$$ (2.3-3)

and the previous tooth period

$$h_{d0}(\phi_j) = -x(t-\tau)\sin\phi_j \sin\kappa - y(t-\tau)\cos\phi_j \sin\kappa + z(t-\tau)\cos\kappa.$$ (2.3-4)

Therefore, the complete expression for the chip thickness is:

$$h(\phi_j) = h_s(\phi_j) - h_{d1}(\phi_j) - h_{d0}(\phi_j).$$ (2.3-5)
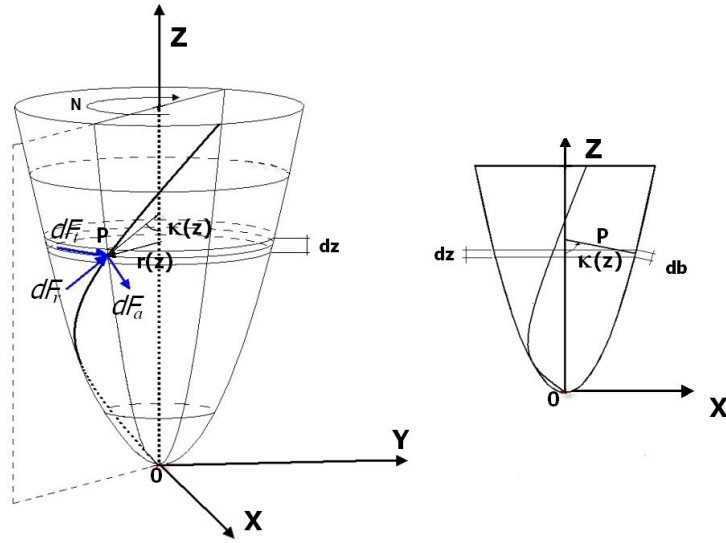
Figure 2.12: 3D view of and end mill with cutting forces acting over it (Munoa, 2007).

Considering $\Delta x = x(t) - x(t-\tau)$, $\Delta y = y(t) - y(t-\tau)$ and $\Delta z = z(t) - z(t-\tau)$:

$$h_d(\phi_j) = (\Delta x \sin\phi_j \sin\kappa + \Delta y \cos\phi_j \sin\kappa - \Delta z \cos\kappa) g(\phi_j). \tag{2.3-6}$$

Where τ is the regenerative delay, which is equal to the tooth passing frequency T for conventional uniform pitch cutters and function $g(\phi_j)$ is the screen function that determines whether the tooth is in or out of cut:

$$\begin{cases} g(\phi_j) = 1, & \text{if} & \phi_{st} < \phi_j < \phi_{ex}, \\ g(\phi_j) = 0, & \text{if} & \phi_j < \phi_{st} & \text{or} & \phi_j > \phi_{ex.} \end{cases} \tag{2.3-7}$$

Simplifying:

$$h_d(\phi_j) = \{n\}^{\mathrm{T}} \{\Delta r\} g(\phi_j). \tag{2.3-8}$$

2.3.2 Dynamic cutting force

A linear force model (Armarego and Epp, 1970) will be considered.

$$\{dF_{tra,j}(\phi_j)\} = (K_t \{K\} h(\phi_j) dz / \sin\kappa + \{K_e\} dS), \tag{2.3-9}$$

where $\{K\} = \{1, K_r, K_a\}^{\mathrm{T}}$, $\{K_e\} = \{K_{te}, K_{re}, K_{ae}\}^{\mathrm{T}}$, $dz / \sin\kappa$ is the differential chip length and dS is the length of the cutting edge.

The ploughing components of the cutting force $\{K_e\}$ do not contribute to the regeneration mechanism and they can be neglected, therefore, the resulting differential dynamic forces yield:

$$dF_{tj} = K_t \, h(\phi_j) \, dz / \sin \kappa,$$ (2.3-10)

$$dF_{rj} = K_r \, dF_{tj},$$ (2.3-11)

$$dF_{aj} = K_a \, dF_{tj}.$$ (2.3-12)

In a matrix form:

$$dF = \frac{K_t}{\sin \kappa} \{K\} h(\phi_j) \, dz.$$ (2.3-13)

In the Cartesian Coordinate System:

$$\begin{Bmatrix} dFx_j \\ dFy_j \\ dFz_j \end{Bmatrix} = \begin{bmatrix} -\cos\phi_j & -\sin\phi_j \sin\kappa & -\sin\phi_j \cos\kappa \\ \sin\phi_j & -\cos\phi_j \sin\kappa & -\cos\phi_j \cos\kappa \\ 0 & \cos\kappa & -\sin\kappa \end{bmatrix} \begin{Bmatrix} dFt_j \\ dFr_j \\ dFa_j \end{Bmatrix} = [Q_1] \begin{Bmatrix} dFt_j \\ dFr_j \\ dFa_j \end{Bmatrix}.$$ (2.3-14)

The total force is obtained integrating the differential force over the whole axial depth of cut. The force generated by each cutting edge is considered.

$$\{F\} = \int \{dF\} = K_t \int_0^a \frac{1}{\sin \kappa} \sum_{j=1}^Z [Q_1]\{K\} h(\phi_j) \, dz.$$ (.2.3-15)

$A(t)$ is defined as the directional cutting coefficient matrix for a differential disk:

$$[A(t)] = \sum_{j=1}^Z [Q_1]\{K\}\{n\}^T g(\phi_j).$$ (2.3-16)

The resulting vibration $r(t)$ is composed of a time-periodic stationary solution $r_p(t)$ and a perturbation $p(t)$ around it:

$$\{r(t)\} = \{r_p(t)\} + \{p(t)\}.$$ (2.3-17)

The stationary solution has no effect on the stability, therefore only the perturbation term is used for the calculation of the dynamic force:

$$\{F\} = K_t (a / \sin \kappa)[A(t)]\{\Delta p(t)\}.$$ (2.3-18)

The zeroth order solution (Altintas and Budak, 1995) considers just the mean value of the directional factor matrix, whereas in the multi-frequency solution (Minis and Yanushevski, 1993) more harmonics are considered. The more harmonics are considered the more accurate the approximation will be, but for non-interrupted cuttings it is not needed to consider many harmonics.

2.3.3 Dynamic parameters

The amplitude of the resulting vibration of a structure is defined by means of the frequency response function (FRF):

$$\{p(j\omega)\} = [\Phi(j\omega)]\{F(j\omega)\}, \tag{2.3-19}$$

where:

$$[\Phi(j\omega)] = \begin{bmatrix} \Phi_{xx}(j\omega) & \Phi_{xy}(j\omega) & \Phi_{xz}(j\omega) \\ \Phi_{yx}(j\omega) & \Phi_{yy}(j\omega) & \Phi_{yz}(j\omega) \\ \Phi_{zx}(j\omega) & \Phi_{zy}(j\omega) & \Phi_{zz}(j\omega) \end{bmatrix}. \tag{2.3-20}$$

In a milling process, the flexibility of the two points in contact, that is, tool and workpiece, must be taken into account, since both of them affect the regenerative effect. If $\{p_t(j\omega)\}$ is the dynamic displacement in the tool and $\{p_w(j\omega)\}$ is the dynamic displacement in the workpiece:

$$\{p_t(j\omega)\} = [\Phi_{tt}(j\omega)]\{F_t(j\omega)\} + [\Phi_{tw}(j\omega)]\{F_w(j\omega)\} \tag{2.3-21}$$

and

$$\{\Delta p_t(j\omega)\} = (1 - e^{j\omega_c T})([\Phi_{tt}(j\omega)]\{F_t(j\omega)\} + [\Phi_{tw}(j\omega)]\{F_w(j\omega)\}). \tag{2.3-22}$$

On the other hand:

$$\{p_w(j\omega)\} = [\Phi_{ww}(j\omega)]\{F_w(j\omega)\} + [\Phi_{wt}(j\omega)]\{F_t(j\omega)\} \tag{2.3-23}$$

and

$$\{\Delta p_w(j\omega)\} = (1 - e^{j\omega_c T})([\Phi_{ww}(j\omega)]\{F_w(j\omega)\} + [\Phi_{wt}(j\omega)]\{F_t(j\omega)\}). \tag{2.3-24}$$

The FRF of the tool is not independent from the response in the workpiece side and vice versa. The frequency response functions are defined as follows:

$$[\Phi_{tt}(j\omega)] = \begin{bmatrix} \Phi_{x_t x_t}(j\omega) & \Phi_{x_t y_t}(j\omega) & \Phi_{x_t z_t}(j\omega) \\ \Phi_{y_t x_t}(j\omega) & \Phi_{y_t y_t}(j\omega) & \Phi_{y_t z_t}(j\omega) \\ \Phi_{z_t x_t}(j\omega) & \Phi_{z_t y_t}(j\omega) & \Phi_{z_t z_t}(j\omega) \end{bmatrix}, \tag{2.3-25}$$

$$[\Phi_{tw}(j\omega)] = \begin{bmatrix} \Phi_{x_t x_w}(j\omega) & \Phi_{x_t y_w}(j\omega) & \Phi_{x_t z_w}(j\omega) \\ \Phi_{y_t x_w}(j\omega) & \Phi_{y_t y_w}(j\omega) & \Phi_{y_t z_w}(j\omega) \\ \Phi_{z_t x_w}(j\omega) & \Phi_{z_t y_w}(j\omega) & \Phi_{z_t z_w}(j\omega) \end{bmatrix}, \tag{2.3-26}$$

$$[\Phi_{ww}(j\omega)] = \begin{bmatrix} \Phi_{x_w x_w}(j\omega) & \Phi_{x_w y_w}(j\omega) & \Phi_{x_w z_w}(j\omega) \\ \Phi_{y_w x_w}(j\omega) & \Phi_{y_w y_w}(j\omega) & \Phi_{y_w z_w}(j\omega) \\ \Phi_{z_w x_w}(j\omega) & \Phi_{z_w y_w}(j\omega) & \Phi_{z_w z_w}(j\omega) \end{bmatrix}, \tag{2.3-27}$$

$$[\Phi_{wt}(j\omega)] = \begin{bmatrix} \Phi_{x_w x_t}(j\omega) & \Phi_{x_w y_t}(j\omega) & \Phi_{x_w z_t}(j\omega) \\ \Phi_{y_w x_t}(j\omega) & \Phi_{y_w y_t}(j\omega) & \Phi_{y_w z_t}(j\omega) \\ \Phi_{z_w x_t}(j\omega) & \Phi_{z_w y_t}(j\omega) & \Phi_{z_w z_t}(j\omega) \end{bmatrix}. \tag{2.3-28}$$

And the dynamic chip thickness yields:

$$h_d(\phi_j) = \{n\}^{\mathrm{T}}(\{\Delta p_t\} - \{\Delta p_w\}). \tag{2.3-29)}$$

From the reaction principle:

$$\{F_t(j\omega)\} = -\{F_w(j\omega)\}. \tag{2.3-30}$$

Therefore:

$$h(\phi_j) = \{n\}^T\left\{\left(1 - e^{j\omega_c T}\right)\left[\Phi_{tt}(j\omega) - \Phi_{wt}(j\omega)\right]\{F_t(j\omega)\} - \left(1 - e^{j\omega_c T}\right)\left[\Phi_{ww}(j\omega) - \Phi_{tw}(j\omega)\right]\{F_w(j\omega)\}\right\} =$$

$$= f_z \sin\phi_j \sin\kappa + \{u\}^T\left\{\left(1 - e^{j\omega_c T}\right)\left(\left[\Phi_{tt}(j\omega)\right] + \left[\Phi_{ww}(j\omega)\right] - 2\left[\Phi_{tw}(j\omega)\right]\right)\{F_t(j\omega)\}\right\} = \tag{2.3-31}$$

$$= f_z \sin\phi_j \sin\kappa + \{u\}^T\left\{\left(1 - e^{j\omega_c T}\right)\left[\Phi(j\omega)\right]\{F_t(j\omega)\}\right\}.$$

In order to consider flexibility of the whole system (tool and workpiece sides), the following matrix must be calculated:

$$[\Phi(j\omega)] = [\Phi_{tt}(j\omega)] + [\Phi_{ww}(j\omega)] - 2[\Phi_{tw}(j\omega)]. \tag{2.3-32}$$

Generally, the cross term $[\Phi_{tw}(j\omega)]$ does not have a significant influence in the overall $[\Phi(j\omega)]$ term, but there are some exceptions in which a mode can have a noticeable displacement both in the tool and the workpiece side. In these cases, this term can be of great weight in the overall compliance.

2.3.4   Feed direction

Until now, the cutting force has been defined in the process coordinate system (CS1), where x axis is oriented in feed direction, y axis in the perpendicular direction on the cutting plane and z axis in the axial direction (Figure 2.13).
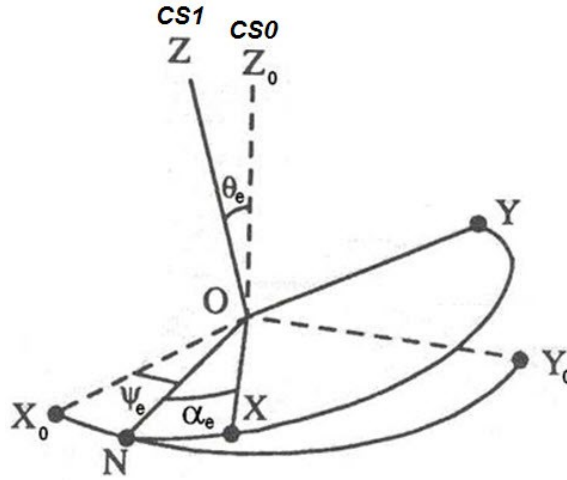
Figure 2.13: Relation of process coordinate system (CS1) with machine coordinate system (CS0) through the angles of Euler (Munoa, 2007).

The frequency response matrix $[\Phi(j\omega)]$ is obtained in the general coordinate system (CS0) which coincides with the axes of the machine. In order to relate the general coordinate system with the process coordinate system, the angles of Euler are used:

- precession (ψ_e): Rotation around z axis,
- nutation (θ_e): Rotation around x axis,
- intrinsic rotation (α_e): Rotation around z axis.

With these angles the frequency response matrix in the general coordinate system can be oriented according to the process coordinate system:

$$\left.\begin{array}{l}\{p_0\}=[\Phi_0]\{F_0\}\\\{p_0\}=[Q_2]\{p\}\\\{F_0\}=[Q_2]\{F\}\end{array}\right\} \quad \begin{array}{l}\{p\}=[Q_2]^{-1}\{p_0\}=[Q_2]^{-1}[\Phi_0]\{F_0\}=\\ =[Q_2]^{-1}[\Phi_0][Q_2]\{F\}=[\Phi]\{F\},\end{array} \quad , \tag{2.3-33}$$

where $[Q_2]$ is the rotation matrix from CS1 to CS0.

$$[Q_2]=\begin{bmatrix}\cos\psi_e\cdot\cos\alpha_e-\sin\psi_e\cdot\cos\theta_e\cdot\sin\alpha_e & -\cos\psi_e\cdot\sin\alpha_e-\sin\psi_e\cdot\cos\theta_e\cdot\cos\alpha_e & \sin\psi_e\cdot\sin\theta_e\\ \sin\psi_e\cdot\cos\alpha_e+\cos\psi_e\cdot\cos\theta_e\cdot\sin\alpha_e & -\sin\psi_e\cdot\sin\alpha_e+\cos\psi_e\cdot\cos\theta_e\cdot\cos\alpha_e & -\cos\psi_e\cdot\sin\theta_e\\ \sin\theta_e\cdot\sin\alpha_e & \sin\theta_e\cdot\cos\alpha_e & \cos\theta_e\end{bmatrix}. \tag{2.3-34}$$

2.3.5 ZOA solution

From equation (2.3-18), the directional cutting coefficient matrix is approximated by the mean term in the Fourier series,

$$\{F\}=K_t\,(a/\sin\kappa)[A_0]\{\Delta p\}.. \tag{2.3-35}$$

In the ZOA solution a dominant chatter frequency is considered:

$$\{p(t)\}=\{p\}e^{j\omega_c t}$$
$$\{p(t-\tau)\}=\{p\}e^{j\omega_c(t-\tau)}=\{p\}e^{j\omega_c t}e^{-j\omega_c\tau}\Bigg\}.$$

(2.3-36)

And the regenerative vector is represented as:

$$\{\Delta p(t)\}=\{p(t)\}-\{p(t-\tau)\}=(1-e^{-j\omega_c\tau})\{p\}e^{j\omega_c\tau}.$$

(2.3-37)

Substituting equation (2.3-33) in equation (2.3-37):

$$\{\Delta p\}=(1-e^{-j\omega_c\tau})[\Phi(j\omega_c)]\{F\}$$

(2.3-38)

and substituting this expression in equation (2.3-35):

$$\{F\}=K_t(a/\sin\kappa)(1-e^{-j\omega_c\tau})[A_o][\Phi(j\omega_c)]\{F\}.$$

(2.3-39)

$[A_0]$ can be calculated as follows:

$$[A_0]=\frac{1}{T}\int_0^T[A(t)]dt=\frac{1}{\phi_p}\int_{\phi_{st}}^{\phi_{ex}}[A(\phi)]d\phi=\frac{Z}{2\pi}\begin{bmatrix}\alpha_{xx}&\alpha_{xy}&\alpha_{xz}\\\alpha_{yx}&\alpha_{yy}&\alpha_{yz}\\\alpha_{zx}&\alpha_{zy}&\alpha_{zz}\end{bmatrix}=\frac{Z}{2\pi}[\alpha_0].$$

(2.3-40)

where ϕ_{st}: cutting start angle, ϕ_{ex}: cutting exit angle and α_{xx}, α_{xy}, α_{xz}, α_{xx}, α_{yx}, α_{yy}, α_{yz}, α_{zx}, α_{zy}, α_{zz} are the directional factors, which are those described in Altintas (2001), but divided by a factor of 2. This is because the factor ½ is previously taken out from $[A(\phi)]$ matrix.

Therefore equation (2.3-39) yields:

$$\{F\}=\frac{ZK_t a(1-e^{-j\omega_c\tau})}{2\pi\sin\kappa}[\alpha_o][\Phi(j\omega_c)]\{F\}.$$

(2.3-41)

The non-trivial solution of the system is encountered when the determinant of the previous equation is equal to zero:

$$\det\{[I]+\Lambda[\Psi]\}=0,$$

(2.3-42)

where

$$\Lambda=\Lambda_R+j\Lambda_I=-\frac{ZK_t a(1-e^{-j\omega_c\tau})}{2\pi\sin\kappa}.$$

(2.3-43)

Matrix $[\Psi]$ is the frequency response function oriented according to the directional cutting coefficients,

$$[\Psi]=[\alpha_0][\Phi(j\omega_c)].$$

(2.3-44)

From the real part of equation (2.3-43):

$$a = -\frac{\pi \sin \kappa \, \Lambda_R}{K_t Z}\left[1+\left(\frac{\Lambda_I}{\Lambda_R}\right)\left(\frac{\sin \omega_c \tau}{1-\cos \omega_c \tau}\right)\right].$$
(2.3-45)

From the imaginary part of equation (2.3-43):
$$\Lambda_I\,(1-\cos \omega_c \tau)-\Lambda_R \sin \omega_c \tau = 0.$$
(2.3-46)

Operating equation (2.3-46) and defining angle χ:
$$\tan \chi = \frac{\Lambda_I}{\Lambda_R} = \frac{\sin \omega_c \tau}{1-\cos \omega_c \tau}.$$
(2.3-47)

Combining equation (2.3-45) and equation (2.3-47):
$$a_{\lim} = -\frac{\pi \sin \kappa \, \Lambda_R}{Z\,K_t}(1+(\tan \chi)^2).$$
(2.3-48)

Only the eigenvalues with negative real part will result in limit points in the stability diagram.

Operating equation (2.3-47), the phase shift of the eigenvalue χ can be described as:
$$\tan \chi = \frac{\Lambda_I}{\Lambda_R} = \frac{\cos(\omega_c \tau/2)}{\sin(\omega_c \tau/2)} = \tan\left[\pi/2-\left(\frac{\omega_c \tau}{2}\right)\right].$$
(2.3-49)

The phase shift ε between the current and the previous surface is:
$$\varepsilon = \pi - 2\chi.$$
(2.3-50)

If l is the number of waves generated between each tooth:
$$\omega_c \tau = \varepsilon + 2\pi l.$$
(2.3-51)

And finally the rotating speed of the tool can be written as:
$$N = \frac{60}{Z\tau} = \frac{60\,\omega_c}{Z\,(\varepsilon + 2\pi l)}.$$
(2.3-52)

2.3.6 Multi-frequency model

Multi-frequency model was initially proposed by Minis and Yanushevski (1993) and Budak and Altintas (1998) and it was later generalized by Merdol and Altintas (2004) and Munoa (2007). This solution is a more accurate solution than ZOA. The main difference between these two solutions is that in ZOA a single chatter frequency ω_c is considered, whereas in the multi-frequency method several modulated chatter

frequencies are included in the dynamic model. Moreover, more than one Fourier terms in the directional factor matrix are taken into account.

From equation (2.3-18) and considering all the terms in the Fourier series, the force vector is represented according to:

$$\{F\} = \frac{K_t a}{\sin \kappa} \left(\sum_{m=-\infty}^{\infty} [A_m] e^{jm\Omega t} \right) \{\Delta p\},$$

(2.3-53)

where $[A_m]$ is the mth harmonic of the directional factor matrix.

As stated before, vibration energy is distributed over the main chatter frequency (ω_c) and several modulated frequencies of the main frequency (Dombovari et al., 2011b). The modulation is related to the tooth passing frequency ($\omega_c + l\Omega$):

$$p(t) = \sum_{l=-\infty}^{\infty} \left(p_l e^{j(\omega_c + l\Omega)t} \right)$$

(2.3-54)

Therefore the regenerative effect is produced according to all the involved harmonics:

$$\Delta p(t) = p(t) - p(t - \tau) = \sum_{l=-\infty}^{\infty} \left(p_l e^{j(\omega_c + l\Omega)t} - p_l e^{j(\omega_c + l\Omega)(t-\tau)} \right) =$$

$$= \sum_{l=-\infty}^{\infty} p_l e^{j(\omega_c + l\Omega)t} \left(1 - e^{-j(\omega_c + l\Omega)\tau} \right) = \left(1 - e^{-j\omega_c\tau} \right) \sum_{l=-\infty}^{\infty} p_l e^{j(\omega_c + l\Omega)t}.$$

(2.3-55)

Rewriting equation (2.3-53):

$$\{F\} = \frac{K_t a}{\sin \kappa} \left(\sum_{m=-\infty}^{\infty} [A_m] e^{jm\Omega t} \right) \left(\left(1 - e^{-j\omega_c\tau} \right) \sum_{l=-\infty}^{\infty} p_l e^{j(\omega_c + l\Omega)t} \right).$$

(2.3-56)

Equation (2.3-56) can be simplified as follows:

$$\sum_{l=-\infty}^{\infty} \{F_l\} e^{jl\Omega t} = \frac{K_t a}{\sin \kappa} \left(1 - e^{-j\omega_c\tau} \right) \sum_{m=-\infty}^{\infty} \sum_{l=-\infty}^{\infty} [A_m] p_l e^{j(m+l)\Omega t}.$$

(2.3-57)

If both sides on the equation are multiplied by $(1/\tau e^{-jh\Omega t})$ and integrated from 0 to T, using the orthogonality principle, equation (2.3-58) is obtained:

$$\{F_h\} = \frac{K_t a}{\sin \kappa} \left(1 - e^{-j\omega_c\tau} \right) \sum_{l=-\infty}^{\infty} [A_{h-l}] \{p_l\}.$$

(2.3-58)

Next, the displacement vector is related to the force vector through the frequency response function $[\Phi]$:

$$\{p_h\} = [\Phi(j(\omega_c + h\Omega))] \{F_h\},$$

(2.3-59)

where:

$$[\Phi(\mathrm{j}(\omega_c + h\Omega))] = \begin{bmatrix} \Phi_{xx}(\mathrm{j}(\omega_c + h\Omega)) & \Phi_{xy}(\mathrm{j}(\omega_c + h\Omega)) & \Phi_{xz}(\mathrm{j}(\omega_c + h\Omega)) \\ \Phi_{yx}(\mathrm{j}(\omega_c + h\Omega)) & \Phi_{yy}(\mathrm{j}(\omega_c + h\Omega)) & \Phi_{yz}(\mathrm{j}(\omega_c + h\Omega)) \\ \Phi_{zx}(\mathrm{j}(\omega_c + h\Omega)) & \Phi_{zy}(\mathrm{j}(\omega_c + h\Omega)) & \Phi_{zz}(\mathrm{j}(\omega_c + h\Omega)) \end{bmatrix}. \tag{2.3-60}$$

Substituting equation (2.3-58) into equation (2.3-59):

$$\{p_h\} = \frac{K_t\,a}{\sin\kappa}\left(1 - e^{-\mathrm{j}\omega_c\tau}\right)[\Phi(\mathrm{j}(\omega_c + h\Omega))]\sum_{l=-\infty}^{\infty}[A_{h-l}]\{p_l\}. \tag{2.3-61}$$

The stability equation results in an infinite dimensional matrix expression, which is truncated considering a finite number of harmonics sufficient to perform an accurate stability prediction. The number of harmonics of the coefficient matrix is twice the number of harmonics of the modulated chatter frequencies h considered:

$$\begin{Bmatrix} p_{-h} \\ \vdots \\ p_0 \\ \vdots \\ p_h \end{Bmatrix} = \frac{K_t\,a}{\sin\kappa}\left(1 - e^{-\mathrm{j}\omega_c\tau}\right) \begin{bmatrix} [\Phi_{-h}] & \cdots & 0 & \cdots & 0 \\ \vdots & \ddots & 0 & \ddots & \vdots \\ 0 & \cdots & [\Phi_0] & \cdots & 0 \\ \vdots & \ddots & & \ddots & \vdots \\ 0 & \cdots & 0 & \cdots & [\Phi_h] \end{bmatrix} \begin{bmatrix} [A_0] & \cdots & [A_{-h}] & \cdots & [A_{-2h}] \\ \vdots & \ddots & \vdots & \ddots & \vdots \\ [A_h] & \cdots & [A_0] & \cdots & [A_{-h}] \\ \vdots & \ddots & \vdots & \ddots & \vdots \\ [A_{2h}] & \cdots & [A_h] & \cdots & [A_0] \end{bmatrix} \begin{Bmatrix} p_{-h} \\ \vdots \\ p_0 \\ \vdots \\ p_h \end{Bmatrix}.$$

$$\tag{2.3-62}$$

The system will be solved as an eigenvalue problem:

$$\{p_h\} = \frac{K_t\,a}{\sin\kappa}\left(1 - e^{-\mathrm{j}\omega_c\tau}\right)[\Phi_h][A_h]\{p_h\} \tag{2.3-63}$$

and

$$\{0\} = \det\{[I] + \Lambda[\Phi_h][A_h]\}, \tag{2.3-64}$$

where:

$$\Lambda = -\frac{K_t a}{\sin\kappa}(1 - e^{-\mathrm{j}\omega_c\tau}). \tag{2.3-65}$$

2.3.7 Initial value time domain milling model

In this section the initial value time domain milling model (Bediaga et al., 2005; Mancisidor, 2014) used for time domain simulations with changing spindle speed is briefly described.

The general time domain equation is considered,

$$[M]\{\ddot{r}(t)\} + [C]\{\dot{r}(t)\} + [K]\{r(t)\} = \{F(t)\}. \tag{2.3-66}$$

The $[M]$, $[C]$ and $[K]$ matrices are the mass, damping and stiffness matrices respectively, which are obtained by curve fitting experimental data.

The tangential, radial, and axial cutting forces of the jth tooth of the milling cutter $\{F_{tra,j}\}$ are considered according to the linear model described in section 2.3.2.

For process simulation, equation (2.3-66) has to be solved by a numerical integration method. Any form of Runge-Kutta method is the most commonly used in dynamic system simulation.

The modal transformation of (2.3-66) can be performed using the modal vector matrix $[Q_i]$:

$$[Q_i]^{\mathrm{T}}[M][Q_i]\{\ddot{\eta}(t)\}+[Q_i]^{\mathrm{T}}[C][Q_i]\{\dot{\eta}(t)\}+[Q_i]^{\mathrm{T}}[K][Q_i]\{\eta(t)\}=[Q_i]^{\mathrm{T}}\{F(t)\}. \tag{2.3-67}$$

Assuming proportional damping, the matrix equation is diagonalized and decoupled, obtaining for each mode

$$\ddot{\eta}_i(t)+2\xi_i\omega_{\mathrm{n},i}\dot{\eta}_i(t)+\omega_{\mathrm{n},i}^2\eta_i(t)=\frac{P_i(t)}{m_i}, \tag{2.3-68}$$

where m_i, $\omega_{n,i}$ and ξ_i are the modal mass, the natural frequency and the damping of ith mode of structure, while $P_i(t)$ is the modal force.

Equation (2.3-69) can be written as a state space model:

$$\begin{Bmatrix}\dot{\eta}_i(t)\\\ddot{\eta}_i(t)\end{Bmatrix}=\begin{bmatrix}0&1\\-\omega_{\mathrm{n},i}^2&-2\xi_i\omega_{\mathrm{n},i}\end{bmatrix}\begin{Bmatrix}\eta_i(t)\\\dot{\eta}_i(t)\end{Bmatrix}+\begin{bmatrix}0\\1\end{bmatrix}\frac{P_i(t)}{m_i}, \tag{2.3-69}$$

which can be rewritten as the general linear-time invariant state equation:

$$\{\dot{y}_i(t)\}=[D_i]\{y_i(t)\}+[E]\frac{P_i(t)}{m_i}. \tag{2.3-70}$$

Operating equation (2.3-70),

$$\begin{Bmatrix}\eta_i(t_{k+1})\\\dot{\eta}_i(t_{k+1})\end{Bmatrix}=\begin{bmatrix}A_{11,i}&A_{12,i}\\A_{21,i}&A_{22,i}\end{bmatrix}\begin{Bmatrix}\eta_i(t_k)\\\dot{\eta}_i(t_k)\end{Bmatrix}+\begin{bmatrix}\dfrac{\Delta t^2}{2}\\\Delta t-\xi_i\omega_{\mathrm{n},i}\Delta t^2\end{bmatrix}\frac{P_i(t_k)}{m_i}, \tag{2.3-71}$$

where,

$$A_{11,i}=\left[\cos(\omega_{\mathrm{d},i}\Delta t)+\frac{\xi_i\omega_{\mathrm{n},i}}{\omega_{\mathrm{d},i}}\sin(\omega_{\mathrm{d},i}\Delta t)\right]e^{-\xi_i\omega_{\mathrm{n},i}\Delta t}$$

$$A_{12,i}=\frac{1}{\omega_{\mathrm{d},i}}\sin(\omega_{\mathrm{d},i}\Delta t)e^{-\xi_i\omega_{\mathrm{n},i}\Delta t}$$

$$A_{21,i}=\frac{\omega_{\mathrm{d},i}^2+\xi_i^2\omega_{\mathrm{n},i}^2}{\omega_{\mathrm{d},i}}\sin(\omega_{\mathrm{d},i}\Delta t)e^{-\xi_i\omega_{\mathrm{n},i}\Delta t}$$

$$A_{22,i}=\left[\cos(\omega_{\mathrm{d},i}\Delta t)-\xi_i\frac{\omega_{\mathrm{n},i}}{\omega_{\mathrm{d},i}}\sin(\omega_{\mathrm{d},i}\Delta t)\right]e^{-\xi_i\omega_{\mathrm{n},i}\Delta t},$$

and,

$$\omega_{d,i} = \omega_{n,i} \sqrt{1 - \xi_i^2} .$$

Finally, the Cartesian displacements, which will be used to calculate the cutting forces, are obtained from the modal displacements:

$$\{r(t_{k+1})\} = [Q]^T \{\eta(t_{k+1})\}. \tag{2.3-72}$$

In the simulations, just as in the real measurement, the spindle speed can be varied steadily, from a spindle speed of N_1 to N_2. The integration is performed along the time frame of the spindle speed sweep, keeping a constant $\Delta\phi$ angle step. As the speed is variable, the time integration step is also variable:

$$\Delta t = \frac{\Delta\phi}{\omega_i} . \tag{2.3-73}$$

$$\omega_i = \omega_1 + \frac{\omega_2 - \omega_1}{\phi_{total}} \Delta\phi \, i \ \ and \ \ \omega_i = \frac{2\pi N_i}{60} . \tag{2.3-74}$$

where ϕ_{total} is the total angle rotated during the sweep, $i=1\ldots n_i$ is the integration step, ω_i is the angular speed and N_i the spindle speed at each integration step.

2.3.8 Comparison of stability models

In Chapters 2.3.5, 2.3.6 and 2.3.7, the ZOA, the multi-frequency and the initial value time domain solutions to the stability problem have been described. These solutions, together with the initial value time domain methods and the time domain based methods (semi-discretization) are the main methods for stability prediction (see Table 2.1).

In Figure 2.14, an example of the stability limit calculated by some of these methods is shown (Munoa et al., 2009).

The precision of ZOA method is reduced when the cutting force becomes interrupted. These inaccuracies have two main sources: double period chatter (point C in Figure 2.14) and variations due to mode interaction (point B in Figure 2.14). It is also noticeable that mode interaction causes a depth of cut minimum variation at higher order lobes (see Figure 2.14). This effect is also not predictable through the ZOA method. When the number of flutes is low, these effects appear even with considerable engagements.

The multi-frequency and semi-discretization methods can describe the double period lobes and the effects of mode interaction in the stability diagram, thus driving to the same exact solution.
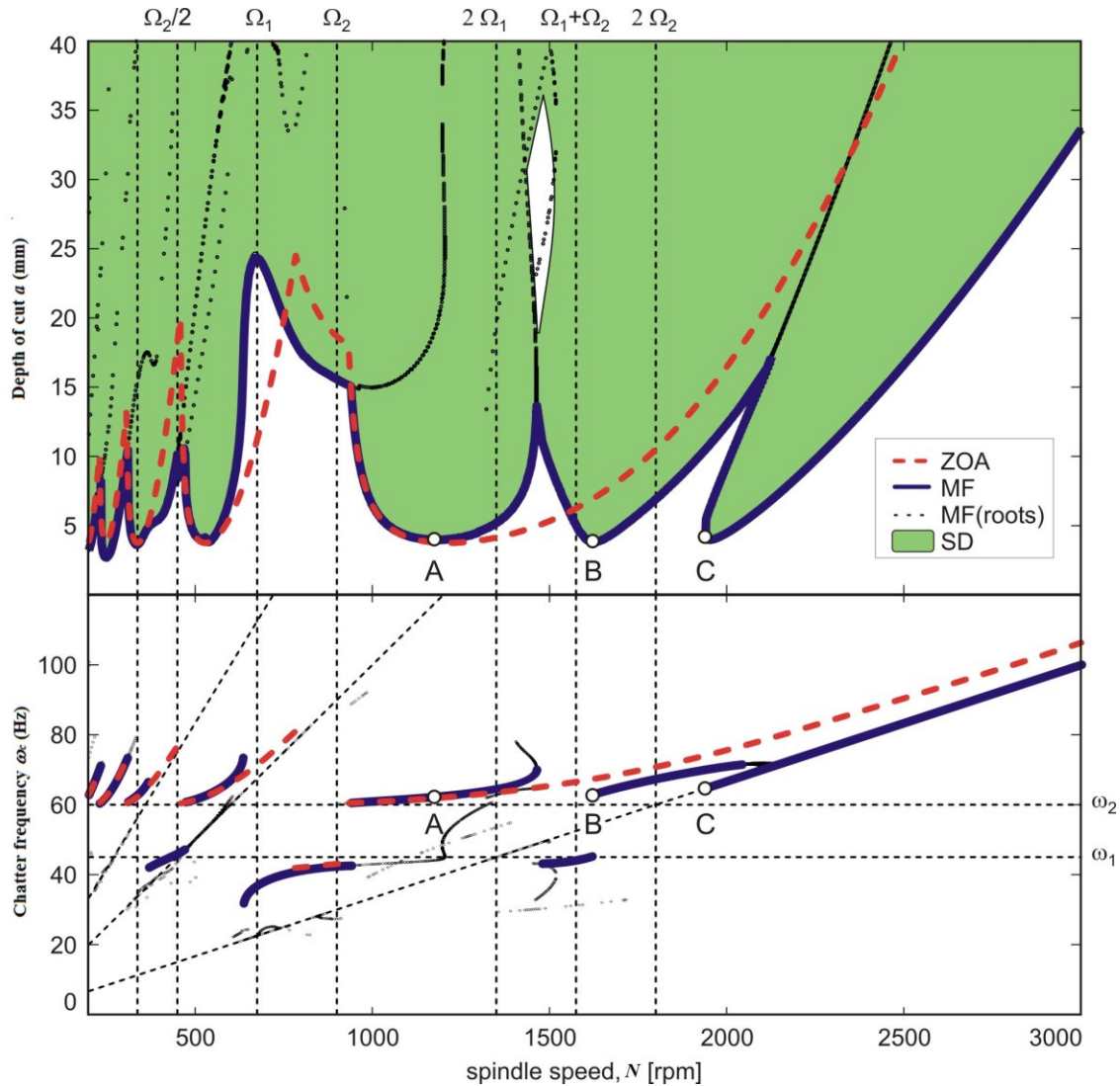
Figure 2.14: Stability limit calculated by ZOA, multi-frequency and semi-discretization method in a cutting process with presence of flip type lobes and mode interaction effect (Munoa et al., 2009).

2.4   INACCURACIES OF THE PREDICTION MODELS

An accurate prediction of the stability of the system is crucial in order to improve productivity, increasing material removal rate according to the stability charts. This requires an accurate measurement of the input parameters of the model. The input data subject to higher uncertainty are cutting coefficients and compliance of the machine (Brecher and Esser 2007).

Table 2.2 summarizes the main factors affecting the accuracy of current stability models according to the different researches carried out:

	Factor	Effect on stability	Reference
MACHINE RELATED FACTORS	Gyroscopic effect	Reduction of chatter frequency Decrease of stability	Tian and Hutton (2001) Xiong et al. (2003) Movahhedy and Mosaddegh (2006) Cao et al. (2012)
	Centrifugal forces	Reduction of chatter frequency Decrease of stiffness	Lin et al. (2003) Chen and Hwang (2006) Cao et al. (2010)
	Bearing temperature increase	Increase of chatter frequency Increase of stiffness	Abele and Fielder (2004) Hongqi and Yung (2004)
	Structure joints	Increase of damping Change of stiffness	Koenigsberger and Tlusty (1970) Mancisidor (2009)
	Torsional stiffness	Decrease of stability	Rivin and Kang (1992)
PROCESS RELATED FACTORS	Tool and workpiece contact	Increase of dynamic stiffness	Jensen and Shin (1999b) Zaghbani and Songmene (2009)
	Moving of the tool outside the workpiece	Increase of stability Lobe shape remains unchanged	Tlusty and Ismail (1981) Zatarain et al. (2004) Bediaga et al. (2005).
	Process damping effect	Increase of stability	Altintas et al. (2008) Bachrathy et al. (2010) Dombovari and Stepan (2010) Eynian (2010) Turner (2010) Ahmadi and Ismail (2011) Turkes et al. (2011) Tunç and Budak (2012)
	Variable cutting coefficients	Change of stability.	Jensen and Shin (1999b)
	Exact kinematics of milling process	Negligible change of stability.	Montgomery and Altintas (1991)

Table 2.2: Factors affecting stability prediction accuracy.

2.4.1 Machine related factors

Many researchers have observed the inaccuracies that often arise in the stability prediction due to the static frequency response function extraction. Several reasons have been pointed out to explain these errors:

Gyroscopic effects

The gyroscopic effect causes a splitting of the natural frequency into two backward and forward frequencies (Figure 2.15). The amplitude of the backward frequency is the

determining factor in defining the stability border (Tian and Hutton, 2001). This is because the tangential milling forces that act against the spindle rotation are mostly in phase with the velocity of a backward-wave mode. It has to be noticed that gyroscopic effects are only significant at very high rotating speeds, being negligible at conventional speeds.

Although there is consensus about the bigger effect of damping on the backward frequency (Pedersen, 1972), there are several researchers who reported a decrease in stability and chatter frequency due to the gyroscopic effect. Tian and Hutton (2001) developed a milling stability model including gyroscopic effects and concluded that gyroscopic effects reduce both stability and chatter frequency. Xiong et al. (2003) investigated the influence of the gyroscopic effect of a rotating spindle through a finite element modeling based on Timoshenko beam theory, concluding that it reduces both chatter frequency and axial depth of cut. Movahhedy and Mosaddegh (2006) described gyroscopic effect as a negative damping effect, which lower the borders of stability.
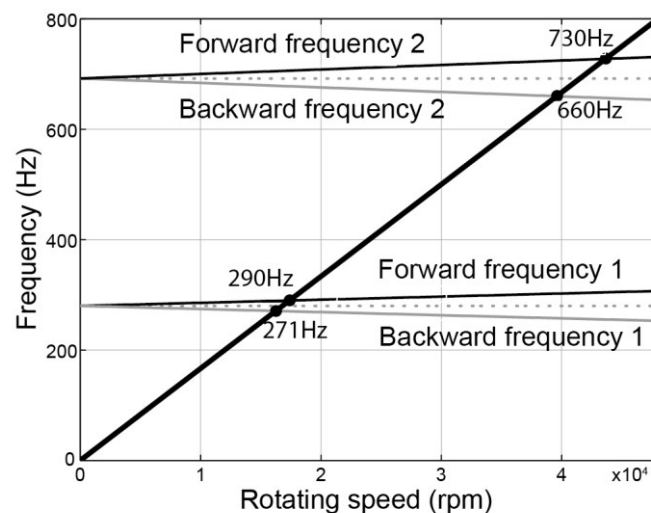
Figure 2.15: Gyroscopic effect in spindle's natural frequency: forward and backward frequencies show up.

Cao et al. (2012) modeled the gyroscopic effect on milling stability adding the gyroscopic term to the equation of motion of the spindles. They found that the gyroscopic moment of the spindle shaft can increase the cross FRFs, but can hardly affect the direct FRFs. Moreover, they claimed that the gyroscopic effects have much less effect than centrifugal forces on bearing stiffness.

Spindle bearing preload change with centrifugal forces, cutting forces and thermal deformations.

When spindle bearing preload is increased, the dynamic stiffness of the system is increased (Ozturk el al, 2012).

During the milling process, centrifugal forces and cutting forces push the balls of the bearings against the race, changing bearing's stiffness and damping values. According to Lin et al. (2003), system stiffness increases with bearing preload and therefore, given that centrifugal forces press bearing balls against the outer race reducing its preload, high rotational speeds result in a bearing stiffness decrease. This was also confirmed by Chen and Hwang (2006) or Cao et al. (2010). The latest modeled rigid and constant preload spindles. They verified that the spindle speed decreases the bearing stiffness, shifting chatter stability pockets from higher to lower speeds. Later, Cao et al. (2012) modeled both gyroscopic and centrifugal forces effects and confirmed stability model results with experiments.

Abele and Fiedler (2004) also derived the same conclusion and, moreover, pointed at the temperature increase at the bearings as another cause for dynamic stiffness change. Centrifugal forces produce an enlargement of normal force and a decrease of the contact angle at the outer race. In order to ensure equilibrium, the normal force at the inner ring will become smaller and the contact angle will increase (Figure 2.16). The enlargement of the difference between contact angles at the inner and outer race will reduce the bearing stiffness. On the other hand, the temperature difference between the inner and the outer race also affects the bearing stiffness. In most bearing assemblies, rotating speed gives rise to a differential temperature between the inner and the outer race of the bearing, being the latter cooler. This effect reduces bearing clearance, reduces the contact angle and, in turn, leads to an increase of bearing stiffness.
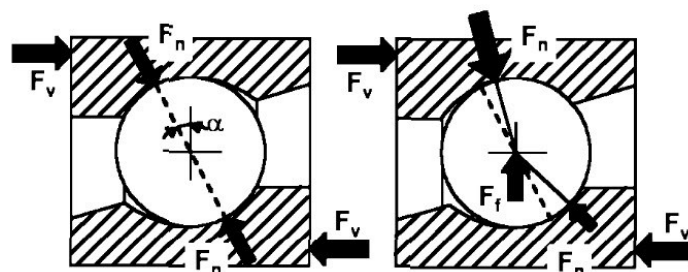
Figure 2.16: Bearing contact forces distribution change due to centrifugal forces (Abele and Fiedler, 2004).

Hongqi and Yung (2004) developed and validated a dynamic thermo-mechanical model for high speed spindles considering the bearing preload change under thermal expansions.

Although most of the researchers agree claiming that stability decreases at high rotating speeds, there are other works pointing just at the opposite direction (Gagnol et al., 2007).

Effect of the machine control parameters

Altintas et al. (2005) pointed out the necessity of coupling the control loops to the structural dynamics in order to simulate properly machine tool structures.

The tuning parameters in the velocity control loop play an important role in machine tool mode damping or amplification. Parameters such as the proportional gain or the integral time have been demonstrated to be influencing parameters on the machine dynamic response at IK4-Ideko internal research (Figure 2.17).
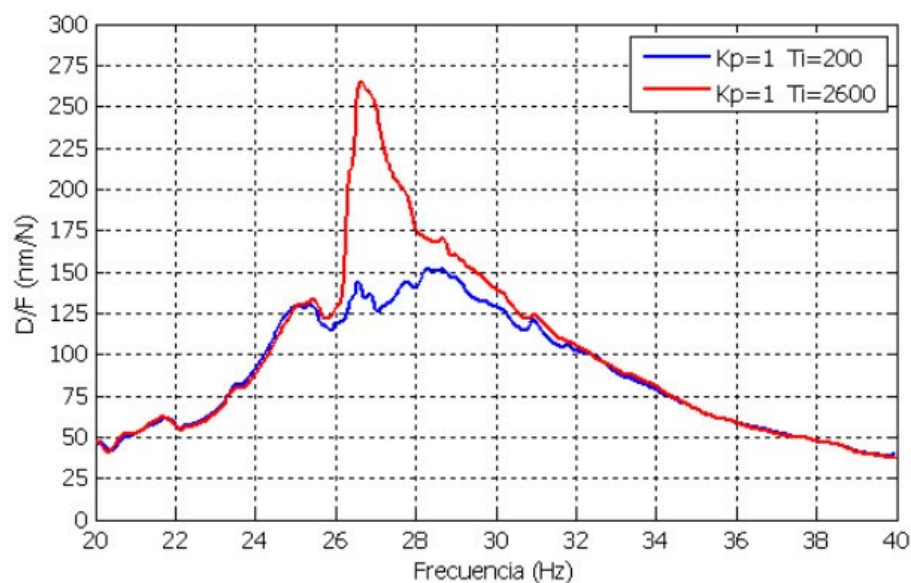
Figure 2.17: Effect of integral time of the velocity loop on the dynamic stiffness of a milling machine.

Nonlinearities of structure joints

The stiffness of the joints defines in a great extent the overall stiffness and the dynamic behavior of the whole machine tool system. Much effort has been done in bolted joints and other type of fasteners modeling, but many difficulties have been found due to non-smooth, nonlinear and time variant behavior of these joints. Ibrahim

and Pettit (2005) offered a review of current problems and uncertainties regarding joint dynamic modeling.

The damping of the system is virtually defined by structure joints (Koenigsberger and Tlusty, 1970). Mancisidor (2009) measured damping successive times during the assembly process of a key-cutting machine, verifying that global damping of the system is composed by the damping provided by the system joints. The overall damping value increases as the number of joints is increased (see Figure 2.18).
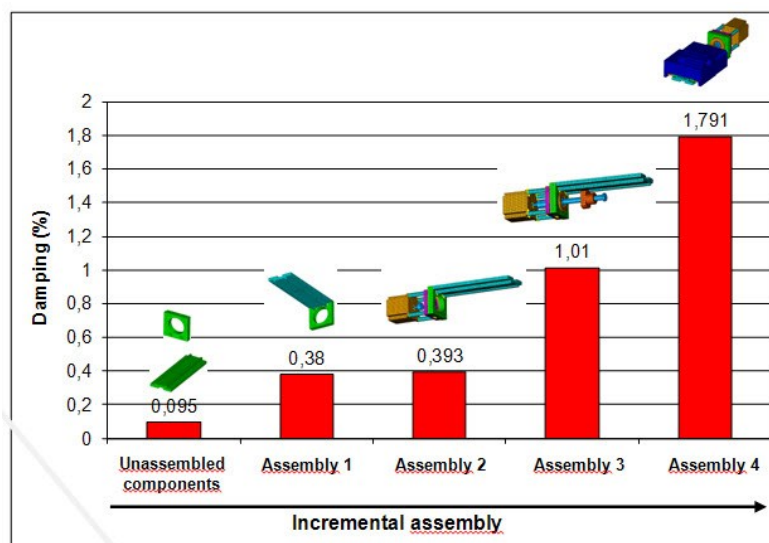
Figure 2.18: Damping increase with assembled components (Mancisidor, 2009).

Torsional stiffness effect

Although the torsional stiffness of the cutting tool is considered in drilling (Roukema and Altintas, 2006) or plunge milling (Ko and Altintas, 2005), it is neglected in current milling stability models; however, Rivin and Kang (1992) obtained a direct relationship between process stability and torsional stiffness. According to their experiments, when the torsional stiffness decreases, process stability increases. From this finding, they proposed the construction of torsional compliant heads to increase system's stability.

This effect was also observed at IK4-Ideko when investigating a machinist's problem when milling the disk brakes of a car. The machine was a multi-head milling station in which there were two identical heads (Figure 2.19) with two identical milling cutters milling alternatively over the same workpiece position. One of the heads was able to cut the disk brake smoothly whereas the other one gave rise to strong chatter vibrations and poor surface finish (Figure 2.20) under the same cutting conditions.
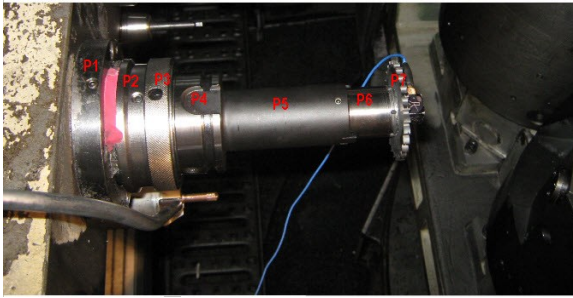
Figure 2.19: Side and face cutter used for disk brake machining.

Figure 2.20: Chatter marks on disk brake.

The only possible reason for this different behavior was the drive system, which was different for both heads. Although the drive motor was the same for both heads, the transmission path was much longer in the one with a good cutting performance (Figure 2.21).
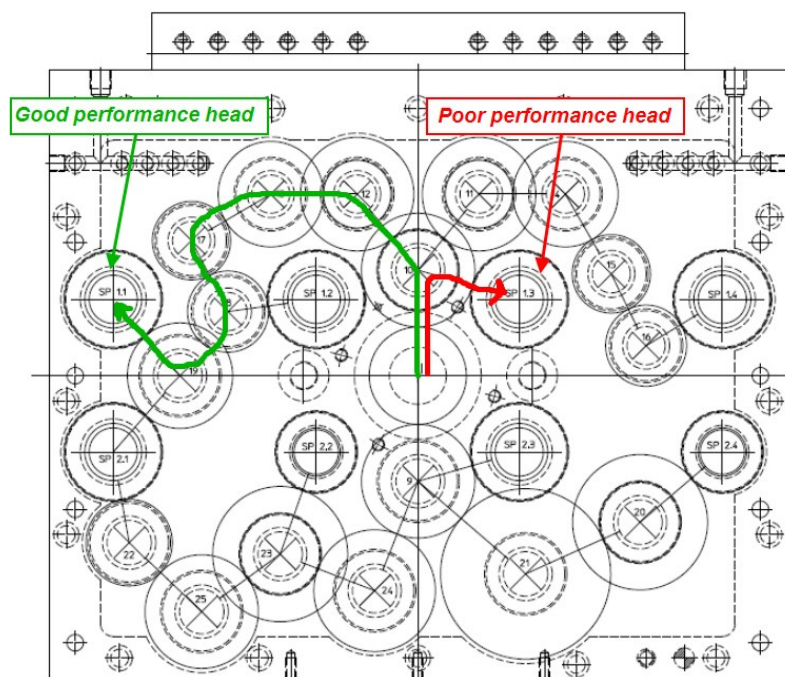
Figure 2.21: Transmission path scheme of the multi-head station. Poor performance head path (red) versus good performance head path (green).

This finding supports Rivin's theory about higher stability at a lower torsional stiffness.

2.4.2   Process related factors

During the cutting process, there exist several factors that introduce nonlinear effects and cannot therefore be analytically modeled. These effects give raise to simulation

errors and consequently failure in model prediction. Initial value time domain stability models are often used to handle process nonlinearities.

In the following lines, several factors related to the cutting process that affect stability are described:

Exact kinematics of milling process

Most of milling models consider that the static chip thickness changes according to the sine of the radial immersion angle (2.3-2).
However, each flute of the tool describes a cycloidal trajectory, since the tool moves forward as it is rotating. In theory this introduces nonlinearity through the so-called state-dependent delay mechanism (Bachrathy et al., 2011).

In order to describe the exact kinematics of the flute time domain simulations are carried out. The trajectory of each flute must be discretized and the real chip thickness is calculated according to this trajectory.

Some authors who pose the exact kinematics (Montgomery and Altintas, 1991) state that the usual static chip thickness consideration does not bring up noticeable changes in the models of milling operations.

Tool and workpiece contact

Jensen and Shin (1999b) state that the natural frequency of the structure varies significantly when the machine is in contact with the workpiece with respect to when it is not. Zaghbani and Songmene (2009) also reported considerable deviations in the FRF obtained through tap testing of a tool in contact and without contact with a workpiece.

One of the reasons that may explain this effect is the own stiffness of the cutting process, which can alter the intrinsic stiffness of the idle system to some extent. Moreover, the rubbing of the tool against the workpiece during cutting could provide additional damping to the system.

Weck (1984) proposed the use of electrohydraulic or electromagnetic relative exciters to analyze this effect. These shakers are capable of providing a static preload to the system, which can simulate the tool and workpiece contact, before applying the dynamic load.

Moving of the tool outside of the cut

When the process destabilizes and the vibration amplitude becomes too big, some insert of the tool can jump out of the cut and stop cutting (Tlusty and Ismail, 1981). For that particular insert, the chip thickness becomes null and so does the cutting force. This kind of nonlinearity has a stabilizing effect on the vibration, since the regenerative effect is interrupted and the amplitude of the vibration stops growing continuously and gets stabilized in a limit cycle.

This nonlinearity influences the magnitude of the vibration and the surface roughness, but it does not influence the linear stability diagram definition to a large extent (Zatarain et al., 2004; Bediaga et al., 2005).

When the calculation of this effect is done, the trajectories of every insert/flute has to be followed in order to determine if they are out of cut or not, thus computing the real surface left for the forthcoming inserts/flutes.

In the next figure, the results of the simulation of the vibration under consideration of the moving of the tool outside of the cut are presented. Figure 2.22a considers this effect whereas Figure 2.22b does not take it into account. A great error is made in vibration assessment if the explained effect is not considered.
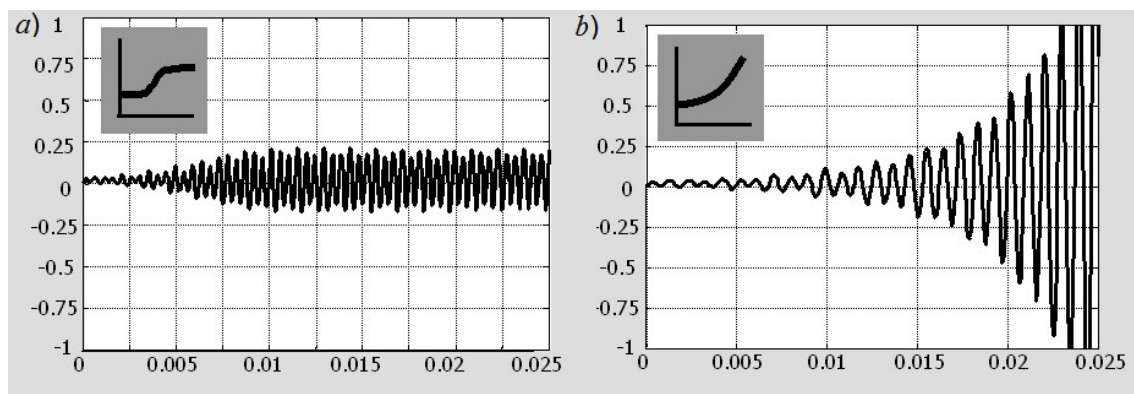
Figure 2.22: Moving of the tool outside the cut simulation. Munoa (2007).

Process damping effect

When the tooth passing frequency is much lower than the chatter frequency $\Omega << \omega_c$, the stability lobes rise, increasing the limit depth of cut. This is due to the process damping effect.

There is no consensus about the physical description of the process damping effect and there are different theories to explain the involved mechanisms. The most extended one explains process damping as the result of the rubbing of the flank of the tool against the machined surface (Eynian, 2010). When there are many oscillations in a single tool revolution, the effective rake angle becomes negative in the slope-down motion of the tool. This means that the rake face of the tool rubs against the workpiece surface when the material is being cut and this friction adds extra damping to the cutting process. When this happens, self-excited vibrations are less likely to occur. According to some authors (Altintas et al., 2008), as the tool wears out, process damping usually becomes more prominent and the stability grows.

Although the modeling of this effect is a complex task, it has become one of the major subjects of investigation in the last years. The proper modeling of this zone is of capital interest for difficult-to-cut materials such as titanium, which are usually machined in the process damping zone due to the high relation between the chatter frequency and the tooth passing frequency.

The International Academy for Production Engineering (CIRP) created a group to deal with this issue. This work group proposed a method to obtain dynamic cutting coefficients that would take into account the process damping effect, according to the results of the ring-shaped cutting tests designed by Vanherck and Peters. The obtained results were collected by Tlusty (Tlusty, 1978).

Montgomery and Altintas (1991) used the contact laws in order to model the penetration mechanism of a harder material into a softer wavy one. This model, as well as other related models, has problems for a proper stability prediction at low speeds. According to Altintas and Weck (2004) the modeling of the process damping is crucial in order to determine the stability at low speeds ($5\Omega < \omega_c$).

Altintas et al. (2008) defined a new dynamic force model for orthogonal cutting with three different cutting coefficients: the static coefficient (K_f), proportional to the chip thickness and the dynamic coefficients (C_i, α_i), proportional to velocity and acceleration terms respectively. These coefficients were obtained by means of controlled oscillating tests with the aid of a fast tool servo.

Nowadays, SD is regarded as the first method for the modeling of the process damping zone. Stepan proposed the short delay theory (Stepan, 1989). He ascertained that, using distributed DDE with different shape functions, a stability increase at low speeds would be produced, similar to the experimentally proven process damping. The assumption of the short delay model is that there is a pressure instead of a point force

between tool and workpiece. This pressure has a special distribution along the contact length between the rake face and the chip itself.

Bachrathy et al. (2010) built stability charts including the first order approximation of the short delay model. Dombovari and Stepan (2010) presented a work in which it was experimentally demonstrated that there is a phase shift between the chip thickness and the cutting force and an extended short delay model was proposed.

The Advanced Manufacturing Research Center (AMRC) of the University of Sheffield is exploring another method based on the early models from the 60s for the modeling of this effect (Turner, 2010).

More recently, Ahmadi and Ismail (2011) obtained stability lobes based on a linearized iterative analytical model of the process damping, dependent on the vibration amplitude. The followed approach was to substitute the nonlinear damping pulse by an equivalent viscous damper. They defined two limits: an upper limit which corresponds to the limit at which the tool disengages from the workpiece periodically and a lower limit where the vibration stabilizes at a value between zero and the disengagement amplitude. This method agreed with the time domain simulations, reducing considerably the computation time and giving a good approximation to experimental tests.

Turkes et al. (2011), on the other hand, determined a new analytical model in which the process damping ratio is calculated. The advantage of this model is that it can be used for different cutting parameters, workpiece materials and tool types.

Tunç and Budak (2012) have also extensively explored process damping phenomena. They suggested cylindrical flank face geometries rather than planar flank faces to achieve higher process damping.

Process damping is, therefore, a very important phenomenon which is being widely studied but it has not been accurately modeled yet. The achievement of an accurate model would give rise to new process techniques to increase stability through the use of process damping effect (Siddhpura and Paurobally, 2012).

Variable cutting coefficients

Cutting coefficients are the coefficients used in the semi-empirical methods for quantification of cutting forces. These coefficients are usually supposed constant and dependent on the tool-workpiece combination. However, different works have

demonstrated that parameters like feed, cutting speed and depth of cut also affect cutting coefficients.

At low feeds the specific force needed to cut the material is higher (Jensen and Shin 1999b). This is usually noticeable in cutting processes where the increase of feed stabilizes the arisen instability. Budak (1994) defined the cutting coefficient as a function of the average chip thickness raised to a specific exponent. Munoa et al. (2006) applied this model for chatter prediction in frequency domain. Endres and Loo (2002) also calculated variable cutting force coefficients raising chip thickness, cutting speed and rake angle to an empirical exponent.

On the other hand, Lamikiz (2003) used axial depth of cut dependent cutting forces in order to model ball end mill forces.

A clear example of cutting coefficient variability is encountered in complex geometry end mills. For these cases, the orthogonal to oblique transformation is a suitable approximation procedure for cutting coefficient determination. The force is then calculated by the integration of the previously discretized geometry of the tool cutting edge. Dombovari et al. (2010) followed this procedure for serrated tool cutting coefficient identification.

Unsafe zone

The unsafe or bistable zone is the region in the stability chart where the process can be stable or unstable depending on the magnitude of the existing perturbations (Figure 2.23). This phenomenon was described by Shi and Tobias (1984) and demonstrated mathematically by Dombovari et al. (2011a).
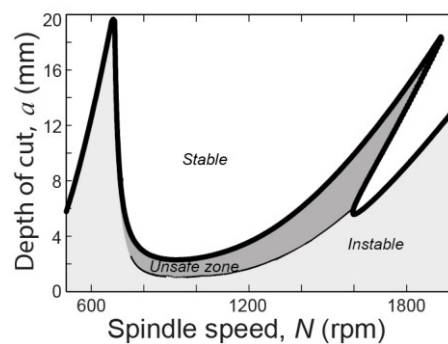
Figure 2.23: Unsafe zone. Dombovari and Stepan (2015).

Stepan et al. (2011) claimed that the size of unsafe zone of regenerative chatter has a maximum for increasing feed.

Tool engagement variations due to vibrations

When strong vibrations arise from highly interrupted processes, the width of cut could undergo noticeable variations that could affect stability prediction. This is a factor that is not usually taken into account in stability prediction models, but has been pointed out by Jensen and Shin (1999a).

2.5   EXPERIMENTAL CHARACTERIZATION TECHNIQUES

In this section, several experimental techniques are described for force and machine dynamics characterization. The aim of these techniques is to minimize the uncertainty of the model input data and take into account process and machine nonlinearities, in order to increase stability simulations accuracy.

2.5.1   New force characterization methods

The improvement in cutting force characterization is becoming a matter of interest in the recent years. Some authors have proposed methods to compensate distortions produced by the dynamometric plate used to measure force (Magnevall et al., 2010). An inverse filtering is used in order to counteract unwanted dynamic effects.

Gonzalo et al. (2010) proposed a method in which cutting coefficients are directly identified over the time signal. This method permits to obtain the cutting coefficients from a single experimental set, in contrast with the several tests needed in the traditional cutting force identification methods. Outside the machine tool field, Lourens et al. (2010) used an extended Kalman filter for cutting force estimation.

Another issue related to the cutting force characterization is the most appropriate mathematical model to use. Apart from the models which introduce process damping by means of dynamic cutting coefficients proportional to vibration velocity (Bachrathy et al., 2010), other authors (Dombovari et al., 2011a) bring up the option of using a cubic law for the cutting force modeling. Stepan et al. (2010) used this cubic law for chip thickness dependent cutting force identification. This new approach is more accurate since the feed dependent behavior of an unsafe zone in the chatter stability charts is explained mathematically.

With the increasing complexity of tools' cutting edge profile, general methods to calculate cutting force for any kind of tool geometry have become subject of study in the last years. Tukora and Szalay (2011) used an instantaneous cutting force prediction method, which can be applied for multi-axis machining. In this case, the geometric information of the workpiece to cut is not a limiting factor for cutting force coefficient determination and is gained directly from the CAM model. Hosseini et al. (2011) presented a new algorithm for chip load and cutting force calculation out of the cutting edge definition as a NURBS curve. This method can be applied to any kind of tool geometry. Kilic (2015) also described a general model for arbitrary tool geometry.

2.5.2 Dynamic parameter extraction methods

Rasper et al. (2010) state that machine dynamics is the main source of errors in stability models. Current dynamic characterization procedures have been called into question and the need of new theoretical and experimental characterization procedures has been highlighted (Ehmann et al., 1997). These new procedures are mostly based on experimental methods.

Traditional methods

Nowadays, impact hammer testing is the usual method for dynamic parameter identification. When a nonlinear system is analyzed, sometimes a shaker is used for excitation, although the time consuming set-up makes it usually not worthwhile. The FRF traditional concept is doubtful since the shape of the response curves vary significantly with the level of force or displacement (Figure 2.24). From the theoretical point of view the nonlinear systems lead to bifurcations which make the perturbation magnitude determinant in the system's final response. Extensive research is being carried out in nonlinear systems, from both experimental and theoretical point of view. From the experimental point of view, the analysis of the system nonlinearity requires the use of specific shaker excitation methods for the dynamic characterization. One of the most commonly used methods is the frequency sweep with different controlled force and displacement levels ("swept sine"). This sort of investigations is usually very costly and time consuming.

Rasper et al. (2010) encountered big differences in the dynamics of a machine measured with an impact hammer compared to the results obtained by means of a shaker excitation. Certain variability in the mobility when changing the angular position of the spindle was also observed. They effect was explained as a result of measuring the mobility on an idle machine tool state, where dynamic stiffening effects cannot be

detected. Therefore, rotating spindle measurement methods development is regarded as indispensable.
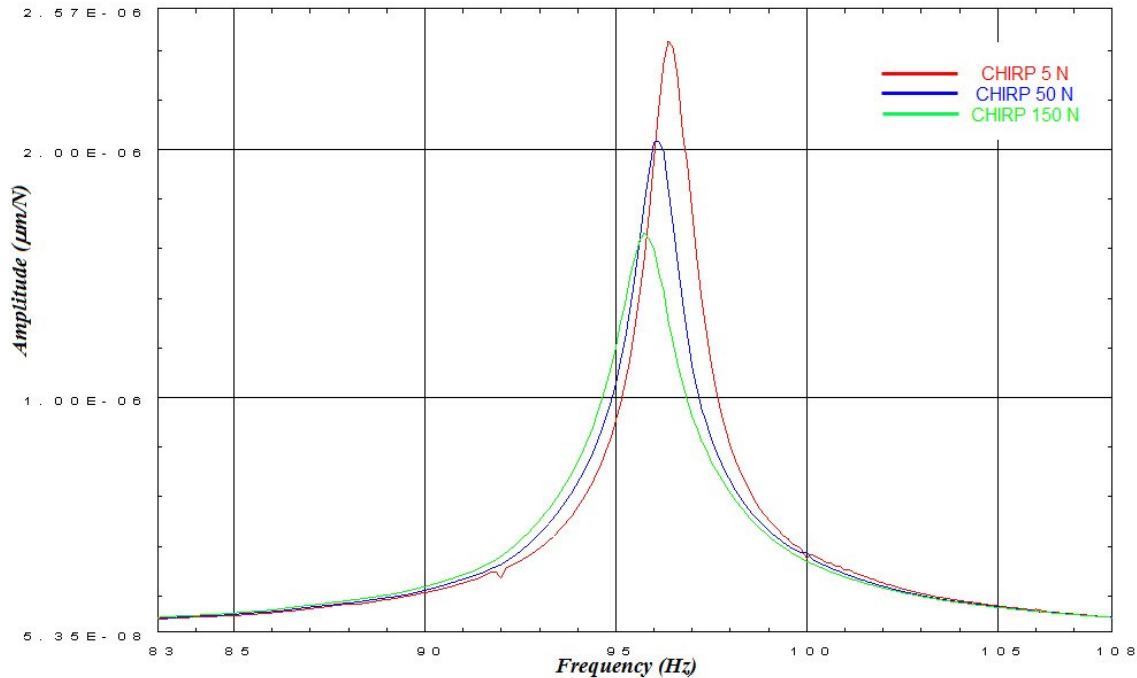
Figure 2.24: FRFs of a non-linear clamping unit under different force levels (Astarloa, 2011).

The gyroscopic effects and the spindle bearing preload change with centrifugal forces could be analyzed by means of tip testing with rotating spindle. Some authors have tried this option (Faassen et al., 2003; Cheng et al., 2007; Brecher and Esser, 2008), but it requires a complex set-up which often makes the procedure unfeasible.

Sims et al. (2005) described the use of piezoelectric sensors and actuators for tool excitation and response measurement. They recommended this method for small milling tools, which may be difficult to test with a modal hammer.

Active magnetic bearings (AMB) have also been used in order to identify the spindle tool system's frequency response function (FRF). Abele et al. (2006) used an AMB to identify the spindle tool system's FRF. This method allows making non-contact measurements when the spindle is running. By means of the substructure receptance coupling techniques the theoretical dynamics of the tool can be added to the spindle's and the response at the tool tip can be estimated for different tools. Rantatalo et al. (2007) also used AMB in order to excite the structure and non-contact displacement sensors to measure the response. All these authors reported differences between 0rpm and rotating spindle FRFs.

Recently, Matsubara et al. (2015) used a non-contact excitation device for FRF analysis in rotating spindles. They analyzed the changes in FRFs and stability lobes due to speed and force changes, concluding that the last induces larger variations.

Inverse methodology for dynamic parameter extraction from cutting tests

Other authors have gone further, aiming to avoid all the error sources listed in 2.4 and have proposed inverse methodology to identify system parameters directly by conducting experiments during cutting. Quintana et al. (2008) carried out a work in which they performed cutting tests on a roof shape workpiece at different speeds, printing the real stability lobes in the workpiece itself. Ismail and Soliman (1997) proposed a similar approach, but using a speed-ramp instead. They used the R-value chatter indicator in order to define stability borders and compared them with cutting tests successfully, although they observed mismatches when very high speeds were used. Grossi et al. (2015) also used a speed-ramp test, but unlike Ismail and Soliman, they kept the feed per tooth constant.

Kruth et al. (2002) considered the structure having a dominant mode in a single direction. They developed an inverse analytical formulation based in zeroth order solution. They assumed a single mode direction and predicted modal parameters using experimental data. However, this method cannot take account of mode coupling in case of having two perpendicular mode directions. Suzuki et al. (2008) studied a spindle which has symmetric modes in two orthogonal directions. They used an iterative numerical method in order to adjust dynamic parameters to fit experimental data based on zeroth order solution. Özsahin et al. (2015) developed a similar inverse approach based on stability tests. They simulated and validated experimentally that tool point FRF is affected by spindle speed and cutting forces simultaneously. They discovered that when the stability of the cutting operation is determined by the tool modes, the tool point FRF is not affected by rotating speeds. However, when spindle and holder modes are involved, deviations due to operational conditions become crucial for a proper stability prediction.

Operational Modal Analysis

The operational modal analysis (OMA) technique is a different approach for the dynamic characterization of the machining system. The OMA is an output-only analysis method; the natural frequencies, mode shapes and damping ratios can be obtained from an output signal without knowing the input signal. It is not possible to extract

modal mass and modal stiffness values, since they depend on the unknown input force.

There are two main different mathematical approaches to deal with the input data from the OMA analysis. On the one hand, the frequency domain decomposition (FDD) methods consist in calculating the spectral density matrix $G_{yy}(\mathrm{j}\omega)$ for each measurement and performing a Singular Value Decomposition approximating the spectral density matrix as:

$$G_{yy}(\omega) = [\varphi]^H [\Pi][\varphi],$$

(2.5-1)

where $[\Pi]$ is the singular value matrix, which contains the natural frequency values and $[\varphi]$ is the singular vectors unitary matrix, which contains the mode shapes.

There are two derivations of the FDD method. In the enhanced frequency domain decomposition (EFDD) method, a SDOF power spectral density function is identified around a natural frequency and then it is transformed back to the time domain through the Inverse Discrete Fourier Transform (IDFT). On the other hand, in the curve-fitting in the frequency domain decomposition (CFDD) method, the curve-fitting of the SDOF function around a peak is performed directly in the frequency domain, resulting generally in a more accurate estimation of the dynamic parameters. Both EFDD and CFDD can estimate damping ratios and can also handle possible harmonics in the input signal. Effective harmonic detection and removal of harmonics is one of the major challenges for an accurate operational modal analysis and different novel methods have been proposed for that purpose (Agneni et al., 2012 and Dion et al., 2012).

Whereas FDD methods are frequency domain methods, suited for stationary excitation, stochastic subspace identification (SSI) is a time domain algorithm suited for both stationary and non-stationary excitations. It is a more powerful method than FDD. It is non-iterative, since it identifies the "states" of the system before identifying the system itself.

Burney et al. (1976) determined the dynamic parameters of a machine tool under working condition using a time-series-technique (ARMA). The method was based on the analysis of the displacement signal between the tool and the workpiece. The same authors used this technique to study further the dynamics of the machine tool under different cutting conditions. Recently, Zaghbani and Songmene (2009) developed and applied a complete methodology for applying OMA under real working conditions in a milling process. Two different methods were applied: autoregressive moving average method (ARMA) and least square complex exponential (LSCE) method. They demonstrated experimentally that the dynamic parameters obtained from OMA were more accurate than those obtained through impact testing at 0rpm. According to the

experimental results, the stability limit calculated using the data obtained through the OMA analysis is lower and more accurate than the stability limit obtained using the static FRF. Schedlinski applied a classical operational modal analysis on a laser cutting machine (Schedlinski and Lüscher, 2002) and a milling and a turning machine (Schedlinski et al., 2010). Some authors have even performed an OMA on a machine tool with microphones as sensors (Archenti and Nicolescu, 2010). Cai et al. (2014) also used OMA for structural dynamics identification in machine tools. They observed that the dynamics of machine tools presented in operation varied significantly from those results obtained by the traditional experimental modal analysis.

Li et al. (2013b) and Mao et al. (2014) performed an evolution of the OMA analysis and used the active excitation modal analysis (AEMA) instead. This method consists of exciting the machine tool with the drive system. Li et al. performed a pure OMA post-processing of the obtained signals and came up with noticeable damping decrease with respect to a standard hammer test. Mao et al. scaled the mode shapes using the dynamic modification technique and synthetized an alternative FRF. They found differences in frequency with respect to the traditionally obtained FRF.

Real cutting force excitation modal analysis

Finally, the estimation of the modal parameters using the real cutting force as input excitation has been also tested.

Opitz and Weck (1969) and Minis et al. (1990) used randomly distributed channels for random excitation approach. They measured system compliance through random cutting force excitation by recording both force and response signals, they built theoretical stability lobes out of these measurements and finally they correlated them with actual cutting tests. Deviation with respect to the compliance measurements through impact hammer excitation was observed and parameters like preload, direction of preload, feed rate or damping were addressed as the main causes of this deviation.

Liu et al. (2002) used the ARMAX module of Simulink (Matlab) to perform the experimental modal analysis. They measured the force by means of a 3-component dynamometric plate and the response by means of an accelerometer in real-time.

Later, Özsahin et al., (2011) used two different approaches. First, they obtained the FRF for discrete frequency points at specific cutting speeds, measuring the force and response at the corresponding speed. Secondly, in order to avoid the harmonic content problem of the cutting forces, a specially designed workpiece with randomly distributed channels was cut (Figure 2.25). This way a random excitation of the system was

achieved. Both approaches showed significant changes in system dynamic parameters in comparison with the standard hammer test.
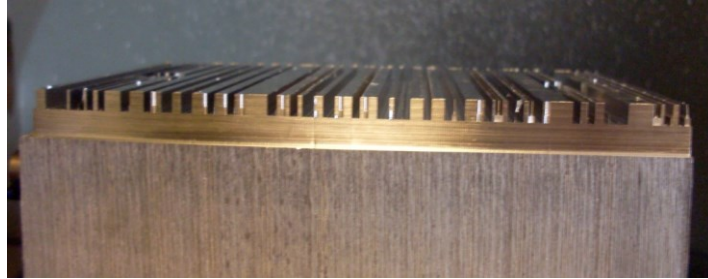
Figure 2.25: Workpiece with random surface profile (Özsahin et al., 2010).

More recently, Li et al. (2013a) and Cai et al. (2015) developed similar techniques to obtain dynamic parameters from a random cutting force excitation. They pre-machined a thin wall on a workpiece and performed cutting tests in order to apply a random excitation. Li et al. reported a damping decrease with respect to hammer test results.

2.6   CHATTER DETECTION

Chatter is usually an easily identifiable vibration process. Typical chatter marks and the generated noise are usually a good indicative of the generation of chatter.

There are special cases, however, where chatter noise is masked or not clearly identifiable and chatter marks are not evident or are erased by forthcoming operations. An example of this case is for example high speed milling in aluminum, where it is possible to mix up the typical stable milling sharp noise with the high-pitched chatter vibration. This fact brings along that, in some workshops, parts are machined under chatter conditions and the machine operators are not aware of it. The awareness arises when the mechanical parts of the machine begin to fail in a recurrent basis.

In cases where feed marks are severe, misjudgment could be made (Figure 2.26).
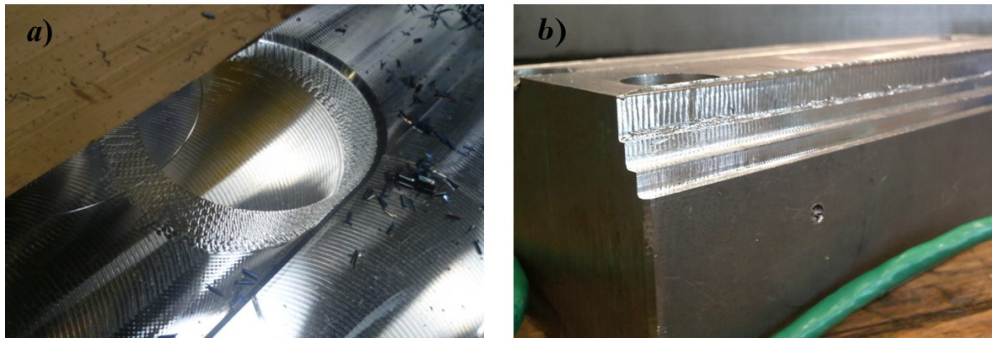
Figure 2.26: *a*) shows visible chatter marks in face milling whereas *b*) shows deep feed marks, which could be mistaken for chatter marks.

As human perspective is sometimes deceptive, it is always more appropriate to implement reliable chatter detection procedures. In some delicate operations, it is very important that the detection takes place immediately after the onset of chatter, in order to remove it as soon as possible. Also when online chatter suppression techniques are applied, an early detection is crucial, since actuation after chatter has reached high amplitudes of vibration could be useless (Bediaga et al., 2009).

2.6.1 Detection sensors

Different sensor types can be used for chatter monitoring. Accelerometers and microphones are the most commonly used ones, but there are other types of sensors for special applications. Accelerometers are easy-to-use, accurate and they are very appropriate for non-rotating part monitoring. Force sensors are always a more illuminating solution, since it gives a direct measure of the cutting force during the process, regardless the dynamic stiffness of the measured point. The drawback is that the mounting procedure is more demanding in order to have a good measure of the force.

When a non-contact sensor is needed the microphone is a good alternative, although it has several drawbacks, i.e. environmental noise influence, high sensitivity to shocks, inaccuracy of measures in the low frequency range. Another alternative for non-contact measurement are laser displacement sensors, vibrometers or inductive or capacitive displacements sensors. These are mainly for laboratory use and their performance is poorer in industrial environments.

2.6.2 Detection procedures

Once some kind of physical variable of the process is monitored, a detection procedure or algorithm must be applied in order to determine whether the process is unstable or

not. The detection procedure consists of a signal processing method of the acquired signal followed by a chatter classification criterion of this processed signal.

Significant research effort has been done in this field, which is an indicator of the difficulty of developing general-use chatter detection algorithms. Table 2.3 shows a summary of some of the state of the art references in chatter detection procedures:

	Detection procedure	Sensing device	Reference
FREQUENCY METHODS	Fast Fourier transform (FFT)	Microphone	Delio (1992)
	Fast Harley transform (FHT)	Microphone	Stern (1999)
	Wavelet transform	Accelerometer and dynamometer	Khraisheh et al. (1995)
		Accelerometer	Yao et al. (2010) Choi and Shin (2003) Stepan et al. (2011) Sun et al. (2014)
	Fuzzy interference system	Accelerometer	Bediaga (2009)
TIME METHODS	False nearest neighbours Mutual information	Accelerometer	Berger et al. (2005)
	False nearest neighbours Information theory functionals	Dynamometer	Gradišek et al. (1998b)
	Signal entropy measurements	Dynamometer	Gradišek et al. (1998a) Gradišek et al. (2003)
		Accelerometer	Pérez-Canales et al. (2012)
	Variance analysis	Microphone	Schmitz et al. (2002) Schmitz (2003)
		Dynamometer	Tangjitsitcharoen and Pongsathornwiwat (2012)
	Rescaled range analysis of the Hurst exponent	Accelerometer	Vela-Martinez et al. (2009)
	Hidden Markoz model (HMM)	Acoustic emission	Varma and Baras (2002)
	Index based reasoning (IBR)	Dynamometer	Tansel et al. (2010)
	Variance ratio	Accelerometer	Bailey et al. (1995)
		Spindle drive current	Soliman and Ismail (1997)
	Energy and Kurtosis index	Motor current	Liu et al. (2011)
	Recursive least square method (RLS)	Accelerometer and eddy current	Abele et al. (2012)
	Cyclostationarity	Spindle encoder	Lamraoui et al. (2014)

Table 2.3: Chatter detection methods.

Frequency methods are more widely spread than time domain methods, however the last ones are usually faster in chatter onset detection.

Frequency methods

The most common detection procedure is the analysis of the frequency content of the acquired signal by means of a Fourier analysis. The fast Fourier transform (FFT) proposed by Cooley and Tukey (1965) was a revolution for the frequency domain analysis and became extensively used in the 90s, due to advances in digital signal processing.

A stable milling operation will show a main frequency peak at the tooth passing frequency Ω. Its harmonics will also be present, the greater the more interrupted the process is. As there is always a certain degree of unbalance, misalignment and run-out of the cutter, the rotating frequency ω_g and its harmonics will also be typically visible in the spectrum.

On the other hand, in an unstable milling operation, apart from the typical stable milling operation frequency content, new frequency components show up. The chatter frequency peak ω_c is visible and also the chatter modulated frequencies $\omega_c + h\Omega$ (the greater the more interrupted the process is). More than one chatter frequency may appear.

The FFT is usually a good approach to detect the chatter onset instant but is not always accurate enough, since FFT method requires a relatively large data processing time. If a higher precision in the chatter onset exact moment is needed, more advanced detection techniques must be applied. Moreover, when chatter frequency is very close to one of the cutting force harmonics, chatter spectral content could be hidden when doing a simple Fourier analysis.

In 1992 the first commercial chatter monitoring and control system was installed in a Makino machine, which was later purchased by McDonell-Douglas company. The system, based on subsequent FFT calculations, was called chatter recognition and control system (CRAC) and was developed by Thomas Delio from Manufacturing Laboratories Inc. (Delio, 1992).

Later, in 1999, Design & Manufacture Solutions (DMS) patented a portable chatter detection and suppression system (Stern, 1999). The detection method is based on the fast Harley transform (FHT), which is similar to the FFT but in this case, the coefficients are real numbers instead of complex coefficients. After the FHT is

computed, the RMS (root mean square) value of the spectrum is calculated and the maximum component frequency (MCF) is identified. At this point, a discrete Hartley transform (DHT) centered over the MCF is performed, which turns into a high resolution spectrum. If an established amplitude limit is exceeded, the system will diagnose chatter.

Khraisheh et al. (1995) presented the wavelet technique as the most proper technique for primary (non-regenerative) chatter detection. They also used phase plane, power spectra, Poincaré map and fractal dimensions methods, which supported the results obtained through the wavelet transform. Later, Choi and Shin (2003) used a wavelet based maximum likelihood algorithm for chatter detection in turning and milling processes. Yao et al. (2010) also proposed an online chatter detection method based on wavelet and support vector machine (SVM). Stepan et al. (2011) also used wavelet transforms to illustrate the transitions between the stable and the unstable zones of a cutting process. Finally, Sun et al. (2014) used the weighted wavelet packet entropy method for early chatter detection during the transient stage.

Bediaga (2009) developed a fuzzy inference system in order to determine the existence of chatter. It was based on the FFT analysis of the signal, filtering and subsequent indicator diagnosis.

Time signal processing methods

The Poincaré map is especially useful when the chatter frequency is very close to one of the cutting force harmonics and it is difficult to judge if an unstable cut is being produced or if amplification by a nearby resonance has taken place at that particular frequency (Dombovari et al., 2011a). It consists of synchronizing the acquired signal with the rotating speed. A signal value is acquired periodically and the current time value is compared with the previous period value. It the values diverge, the process is unstable.

Berger et al. (2005) worked on chatter detection by analyzing time series. They analyzed *false nearest Neighbours* and *mutual information* techniques, achieving satisfactory results. However, these techniques require a big computation effort. Gradišek et al. (1998b) also presented a work focused on the detection of chatter from cutting force signals using different techniques such as *false nearest neighbours*, dimensional correlation and *information theory functionals*.

Several works deal with statistical descriptors for chatter detection. The national institute of standards and technology (NIST) researchers Tony Schmitz and Matthew

Davies patented in 2002 a novel method in chatter detection, based on the synchronous sampling of the signal and a subsequent analysis of the signal variance (Schmitz and Davies, 2002). During stable cutting the variance reading is constant, whereas under unstable cutting, the variance value increases notably. Later they published the developed system (Schmitz et al., 2002; Schmitz, 2003). Tangjitsitcharoen and Pongsathornwiwat (2012) also developed a method to detect chatter based on the variance of the dynamic cutting force signals, analyzing the scaled variance difference between the negative and the positive part of the force signal. Vela-Martinez et al. (2009) developed a method to monitor and predict the emergence of chatter using the rescaled range analysis (R/S) of the Hurst exponent, which allows a statistical measure of the variability of time series.

The stable and unstable conditions can also be distinguished by nonlinear characteristics analysis, such as the entropy and the Lyapunov exponentials. This analysis is time consuming and requires a large amount of acquired data with low noise level. This made Gradišek et al. (1998a) pose the coarse grained entropy rate (CER) method for real-time chatter detection in turning processes. Later, it was also applied in grinding process (Gradišek et al., 2003). The entropy rate gives a measure of the loss of information with respect to the previous state along time. When a stable process is turned into unstable, the entropy rate decreases dramatically. Pérez-Canales et al. (2012) also used an entropy related method, the approximate entropy (AE), method in order to identify chatter in cutting. In this case a high value of the entropy randomness indicates the presence of instability.

It is also possible to perform chatter detection through hidden Markov models (HMM), which were exposed by Varma and Baras (2002) as an alternative method. In their work they recorded an acoustic emission signal and obtained the characteristic vectors. Then, the signal is classified according to hidden Markov model and the chatter onset is determined comparing it with the normal operation condition of the machine. Zhang et al. (2010) proposed a hybrid approach between hidden Markov model (HMM) and artificial neural networks (ANN). The HMM allows the temporal modeling of features extracted from recorded signals and the artificial neural network integrates the inputs.

Tansel et al. (2010) used an index-based reasoning (IBR) for chatter detection in milling through the torque signal of a rotary dynamometer. The IBR system is a simple reasoner that classifies the signals with the help of a lookup table.

Detection algorithms based on limit values require a subjective determination of empirical limits in order to assess chatter onset. If the process is stationary setting the limit is simple, but if the conditions of the process are not known, it becomes more

complex. For those processes in which a limit value is not selectable, Bailey et al. (1995) pose a detection method by means of an accelerometer close to the cutting point. The calculated parameter is the variance ratio:

$$R = (\sigma_s / \sigma_n)^2, \qquad\qquad (2.6\text{-}1)$$

where σ_s and σ_n are the variances in the low and high frequency range of the accelerometer, respectively. Chatter will be detected when $R \ll 1$. Based on the same technique, Soliman and Ismail (1997) investigated a new method for chatter detection using spindle drive current signal.

Besides Soliman and Ismail, there are other authors who have dealt with internal machine signals for chatter detection (Lamraoui et al., 2014; Lamraoui et al., 2015), this way simplifying and reducing the required hardware. Liu et al. (2011) used feed motor current signal in order to detect onset of chatter in a turning process. They claimed an accuracy rate above 95% for chatter recognition, by means of the analysis of energy and kurtosis indexes change in time. Although Abele et al. (2012) used accelerometer and eddy current sensor signals for chatter monitoring, they also simplified the detection set-up by processing the signals on the PLC of the main spindle drive.

2.7   CHATTER SUPPRESSION

Self-excited vibrations depend on many factors, such as dynamic stiffness of the structure or the tool, cutting parameters, and workpiece and tool characteristics. This makes chatter a complex problem to solve but, at the same time, it offers many different options to tackle the problem.

In general, it can be stated that there are three main approaches to address chatter vibrations (Figure 2.27): mechanical design approach, machining process approach and control approach.
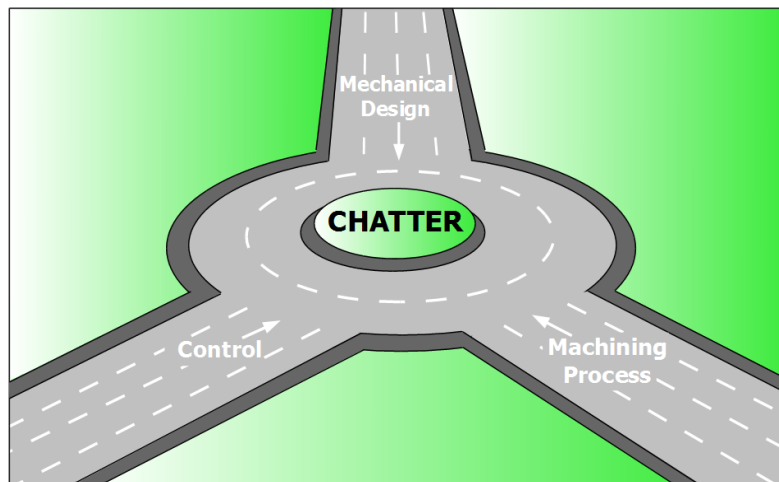
Figure 2.27: Chatter suppression approaches. Mancisidor (2014).

2.7.1   Machining Process Approach

In order to have a chatter free process, it is fundamental to design a proper machining strategy and select the most appropriate cutting conditions. The most intuitive and used technique is to reduce the cutting stiffness (product of the principal cutting coefficient by the axial depth of cut). Since the cutting coefficients depend mainly on the material of the workpiece, the usual way to reduce cutting stiffness and avoid chatter is reducing the axial depth of cut. Having a cutting stiffness lower than the dynamic stiffness guarantees chatter free machining over the whole spindle speed range.

Another method is to take advantage of process damping effect. When worn cutting tools are used, self-excited vibrations are less likely to occur. This effect becomes more noticeable as the ratio between chatter frequency and tooth passing frequency becomes higher. Hence, this method usually requires reducing the spindle speed.

The two methods explained above lead to a productivity decrease. Nevertheless, the reduction of the spindle speed is not always necessary to suppress chatter vibrations. If the stability lobes diagram is obtained, the spindle speed can be tuned in order to match the high stability zones (sweet spots). There are some commercial software packages to calculate the stability lobes, like CUTPRO^{TM} or MetalMAX^{TM}.

Another method, also based in stability lobe theory, is to select automatically the optimum spindle speed. First, the chatter frequency has to be measured and then, spindle speed is changed in such way that the tooth passing frequency matches the measured chatter frequency, which implies machining in resonance conditions. In

these conditions, there is no phase shift between the current cut and the previous waveform, so the regeneration of vibration is reduced considerably (Delio et al., 1992; Bediaga et al., 2009). There are some commercial software applications (Harmonizer®), or machine tool builder optional functions for CNC (Machining Navi), which perform this task automatically.

A proper selection of the tool overhang can also suppress chatter vibrations. This method has been principally studied for aluminum rough milling, due to the importance of tool modes in chatter generation. By means of the variation of the geometric characteristics of the tool, an increase on the stability of the process can be also obtained.

Tlusty et al. (1996) proposed a technique in order to determine the proper overhang of the tool. The University of British Columbia (UBC) has developed an application called SpindlePro® inside the software CUTPRO™ which provides the possibility of testing different tools or tool holders theoretically.

Continuing with the tool design, some special tool geometries have been developed for the distortion of the regenerative effect (Figure 2.28). The idea of using variable pitch cutter for chatter suppression was proposed by Slavicek (1965), who applied Tlusty's orthogonal cutting chatter theory on milling cutters with two different pitch angles. He claimed that the maximum depth of cut can be doubled if compared to uniform pitch angles. Vanherck (1967) further developed Slavicek's technique by considering more than two pitch angles on the cutter. Other cutter design techniques for chatter suppression include a serrated design of the cutting edges (Dombovari et al., 2010) or alternating helix angle design (Vanherck, 1967).
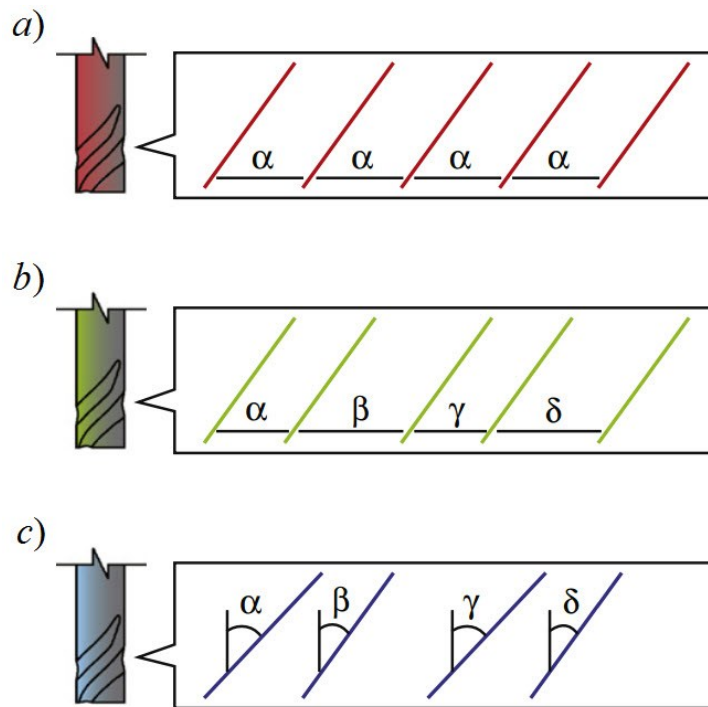
Figure 2.28: *a*) Conventional cutting tool; *b*) Variable pitch cutting tool; *c*) Variable helix cutting tool; (Quintana and Ciurana, 2011).

In 1983, Tlusty, Ismail and Zaton used chatter theory for orthogonal cutting and numerical simulations, analyzing the influence of variable pitch angles, serrated edges and alternating helix angles on stability. In the 90's the first semi-analytical solutions of milling stability of variable pitch cutters were developed (Minis and Yanushevsky, 1993; Budak 1994; Altintas and Budak, 1995). Later, Altintas et al. (1999) presented a semi-analytical method in frequency domain.

2.7.2 Mechanical Design Approach

The dynamic stiffness of the structure and the spindle head must be maximized in order to have the best possible dynamic behavior. However, machine tool designers and manufacturers do not usually focus on increasing damping on machine tool structures, but only structure stiffness maximization is sought.

If one-dimensional chatter is considered, a static stiffness increase will improve process stability (Koenigsberger and Tlusty, 1970). However, real conditions are more complex when more than one mode, multiple flutes and changing cutting directions are present. In some cases, such as bolted or welded joints, an increase of the static stiffness can entail reduction of damping (Munoa, 2007).

Nowadays, one of the most popular solutions to increase dynamic stiffness of structures is the addition of passive dampers to the vibrating structure. The most used passive dampers are the dynamic vibration absorbers (DVA), also known as tuned mass dampers (TMD), which are inertial force devices.
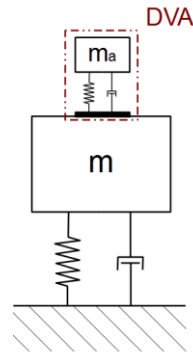
Figure 2.29: Scheme of a DVA. Mancisidor (2014).

By means of these devices, the target mode is split into two new modes which can be effectively damped and, thus, the dynamic stiffness can be increased. These devices have to be accurately tuned for the target frequency and their obtainable damping is limited, while their great advantages are the simplicity and reliability. The idea was introduced by Hahn (1951) when he proposed to use a Lanchester passive damper with the objective of stabilizing the cutting process and suppressing chatter.

In recent years, a number of various passive damping systems, such as dampers with multiple degrees of freedom (Zuo and Nayfeh, 2006) and multiple TMDs (Yang et al., 2010), have been developed to damp a single mode. It has been demonstrated that multiple TMDs are more effective than a single TMD solution, whenever they have the same mass ratio.

For general vibration problems, a suitable tuning strategy was developed by Den Hartog (1956). The special nature of chatter stability problem, however, makes classical tuning methodology not optimal for chatter minimization purposes. Hence, optimal tuning strategies to suppress chatter by considering stability of metal cutting systems were studied by Sims (2007). He tuned a single DVA to flatten the negative real part of the main structure analytically.

Although the proposed strategies are not too complex, the achievement of an accurate tuning is a knotty work. Considering that the design of a specific damping value is a complex task, it is almost impossible to get the optimum tuning parameters. Recently, a self-tuned eddy current damper has been presented by Aguirre et al. (2012), where the stiffness and damping are independent parameters and hence, the controllability of

these parameters is more feasible. Stein et al. (2012) have reported a similar damping technique, where the stiffness depends on the resistance of a magnetic circuit. Du Bois et al. (2012) presented another novel damping technique by means of tensioned cables, whose tuning is claimed to be simple.

Apart from dynamic absorbers, there are other working principles for passive dampers. Friction dampers use the frictional force that results from the relative movement between the vibrating element and the added auxiliary mass (Figure 2.30a). Impact dampers are based on the dissipated energy when an impact between two bodies occurs (Figure 2.30b). Some dampers, such as the granular dampers, combine the friction and impact force damping principles.
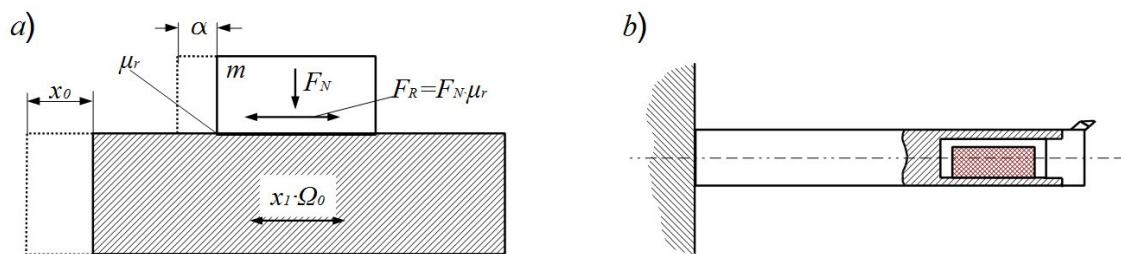
Figure 2.30: a) Friction damper (Gimenez and Iriondo, 1997); b): Impact damper (Tobias, 1965).

Viscous dampers are usually based on a sprung mass inside a cavity which is filled with a viscous fluid. When the vibration of the mass occurs, the fluid is forced to flow through a small gap between the casing and the body. The damping value depends on the gap left and the viscosity of the fluid.

Finally, the surface treatments and coatings are useful means to increase damping, principally on panels and sheet metal structures. Viscoelastic materials can be sprayed or bonded over the surface of the vibratory structure to increase damping.

2.7.3   Control Approach

The behavior of a machine is defined by the control driven by actuators and sensors located in the machine. For instance, as explained in section 2.7.1, a proper selection of the spindle speed can enhance cutting performance and the control of the machine could perform this action automatically.

In the 70's, some authors proposed the distortion of the regenerative effect by a continuous spindle speed variation (CSSV) (Hoshi et al., 1977; Sexton and Stone,

1978). Several studies where the effectiveness of this technique is demonstrated have been presented in the literature (Altintas and Chan, 1992; Jayaram et al., 2000).
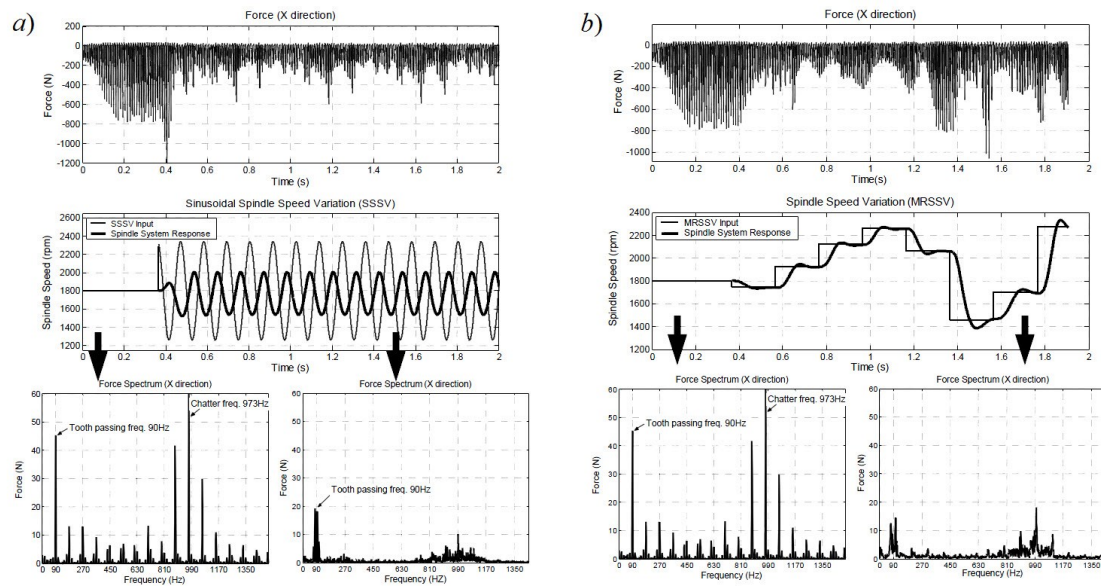
Figure 2.31: Application of *a*) SSSV; *b*) MRSSV; (Bediaga et al., 2004).

According to Bediaga et al. (2004), there are different methods to vary the spindle speed (Figure 2.31). The most studied in the literature is the sinusoidal spindle speed variation (SSSV) method, consisting on a sinusoidal variation of the spindle speed around the mean speed value. There have been many research efforts on this strategy for turning process (Al-Regib et al., 2003; Yang et al., 2003). In milling, Sastry (Sastry et al., 2002) developed an analytical method that allowed the analysis of stability with SSSV.

There are also other types of spindle speed variation. Seguy et al. (2010) studied a triangular spindle speed variation for high-speed milling process. Another alternative is to vary the spindle speed randomly through a Multi-level random spindle speed variation (MRSSV). Yilmaz et al. (2002) presented the effectiveness of this method in turning. Zatarain et al. (2008) developed the general theory for analysis of milling processes in time and frequency domains, for any speed variation strategy.

Nevertheless, the active control technique is regarded as one of the most promising chatter suppression methods from control point of view. Generally, such control is based on the measurement of a parameter related to the vibration, the processing of this signal and the introduction of a controlled force signal as a response to the input signal through internal drives or added actuators. Thus, a dynamically correlated external energy is applied onto the machine structure (Figure 2.32). The actuation force could be also introduced by means of the own drives of the machine.

An active system consists of mechanical and electrical components; therefore, it is understood as a mechatronic system. If sensors integrated into the structure are used as autonomous actuators, those systems are called smart materials, e.g. piezoceramics or shape memory alloys.
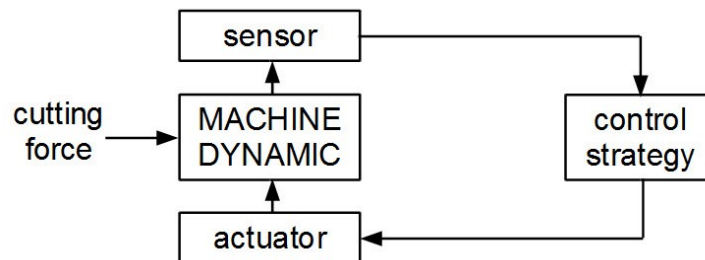
Figure 2.32: A common active vibration control scheme. Mancisidor (2014).

The active vibration control guarantees adaptability to changing conditions. Hence, the cutting parameters remain as defined by the machine user and the productivity is not reduced.

The actuators to perform active damping can present serial or parallel location. The actuators working in parallel with the structure are easier to integrate in the machine and their integration does not affect the original stiffness of the machine. This is the case of inertial actuators. On the other hand, actuators located in serial must be carefully integrated not to affect the global machine geometry and stiffness.

According to Alter and Tsao (1994), in the late 1960s, some works on active control of the direct-drive turning process were carried out (Comstock et al., 1969; Nachtigal and Cook, 1970; Nachtigal, 1972). The results showed the significant stability improvement obtained through active cutting control. In 1970, Cowley and Boyle proposed to use an electromagnetic inertial drive commanded by an accelerometer signal in order to introduce active damping in the structure of the machine tool. Their proposal is still used nowadays with excellent results.

Mancisidor (2014) successfully designed and validated two active damping devices optimally controlled through a direct velocity feedback strategy in order to suppress chatter in milling processes.

Chapter 3

Critical Analysis and Objectives

In this chapter, the analysis of the state of the art (Chapter 2) is summarized. In order to improve both chatter prediction and suppression, overcoming the current weaknesses identified, the main objectives to pursue in the work developed by this Thesis are described.

3.1 CRITICAL ANALYSIS

Stability models are a powerful simulation tool that provides valuable information for an efficient and chatter-free process planning. Considerable effort has been dedicated to this subject in the last years and a good insight has been gained into the describing equations of the different cutting processes.

Until now, these models have been used for academic or research purposes, as well as for cutting process definition and optimization, but they are generally regarded as a side consultancy tool, since they lack of the necessary reliability so as to integrate them in production planning processes (Esser et al., 2006). However, nowadays the international research community, together with the most advanced manufacturing industries, have already started the task of an effective integration of these models in

the process definition procedure as an automated tool. The main goal is to add an extra module to current CAM software in order to calculate process stability at every process simulation step and provide automatic cutting condition suggestions according to the calculated stability charts.

In spite of the accurate process mathematical description achieved, there are some handicaps that jeopardize stability models' usefulness. In section 2.4, the numerous stability model sources of error have been described. Theoretical simplifications, nonlinearities and experimentally obtained inaccurate input data have been pointed out as the main sources of error.

In this Thesis the main sources of error will be investigated and specific new models and techniques will be proposed so as to overcome these limitations in milling processes. The final purpose is to obtain a fast and precise mathematical description of the milling process and high quality experimental input data, which will result in a trustful determination of the stability limits.

As cited in Chapter 2, several errors in stability lobe prediction have been reported by the scientific community. Currently existing stability models are more suitable for light alloy milling operations, where the modes limiting stability are related to the cutting tool or the machined workpiece. However, heavy-duty rough milling operations have specific features that are not considered by current stability models, such as feed direction and machining position dependency. Moreover, the important characteristic in this type of process is the diameter to inserts or flutes (D/Z) relation of the tool, which is not reflected in current SLDs.

Current stability models are not optimized for every kind of milling stability analysis. On the one hand, semi-discretization, multi-frequency and time domain models are more universal but too time consuming, whereas typical frequency domain ZOA is fast but does not consider double period lobes.

Another current problem in stability prediction is the dynamic parameter inputs for the model. The dynamic parameters are usually obtained by artificial excitation methods with an idle an isolate machining system, which does not include the real boundary conditions produced in a real machining environment.

Nevertheless, due to the high number of sources of inaccuracies in stability prediction, the obtained stability lobes will be always subject to a certain degree of uncertainty. It is therefore necessary to foresee chatter suppression techniques to handle unstable

processes in those cases in which the prediction is not accurate or when the required cutting conditions are unavoidably located in unstable regions.

There are many possible ways to tackle chatter and the appropriateness of each method depends on the milling process characteristics. Current well-known chatter suppression methods are not in a mature stage yet and many improvements can still be done in order to reduce the cost of the solutions and facilitate its integration in current machining systems.

The systems currently used for automatic on-line chatter detection usually require wired solutions or use monitoring sensors which are not close enough to the machining point. This makes current solutions not applicable in some specific operations.

Passive dampers are an effective and commonly used solution for critical mode damping in industrial applications. However, they are passive systems that lack of capability of adaptation to variable machining conditions. Moreover, the use of elastomers to generate the required stiffness makes the tuning of these systems a difficult task, due to their lack of linearity and the uncoupled contribution of stiffness and damping they provide.

Finally, current active damping devices for machine tools have proven their effectiveness for machining performance enhancement under changing machining conditions. However, these systems are usually very expensive and difficult to integrate due to the large volume occupied.

3.2 OBJECTIVES

The work developed under this Thesis is focused on:

- Analyzing stability model inaccuracies through experimental demonstration.

- Improving current stability models.

- Developing experimental methods for model input data refinement and stability lobe determination.

- Proposing novel chatter suppression techniques.

According to the analysis drawn from the State of the art, the specific objectives to fulfill have been defined:

1. **Analysis of stability model inaccuracies in heavy-duty roughing milling operations and adaptation of SLD diagrams according to the specific features of this type of operations.**

   The first objective in this Thesis will be to apply current stability lobe models for chatter prediction in different machines, with the purpose of assessing the obtained accuracy.

   Current stability calculation will be enriched with feed direction and machine position dependency and the SLD diagram will be modified to visualize the D /Z relation of the different tool ranges available.

2. **Development of new analytical expressions to enrich current stability models and gain a deeper insight in double period type instability.**

   New analytical expressions to speed up time consuming stability methods and gain knowledge in double period instability analysis will be developed.

3. **Improvement of current ZOA method including flip lobe calculation maintaining the same modus operandi and the calculation speed.**

   A new improved combined analytical model that boosts today's ZOA model will be developed in order to improve stability prediction, making it feasible for industrial environment application.

4. **Development of experimental methods to improve accuracy in dynamic parameters used as inputs for the stability model.**

   Experimental methods present a big potential for accurate milling prediction, due to the absence of theoretical assumptions typical from theoretical methods and the "close-to-reality" contour conditions. The experimental methodology will be applied at two different levels.

   On the one hand, a direct fitting of the stability lobe curves from experimental cutting tests to assess stability limits will be studied. From these results, new dynamic parameters will be determined from cutting data post-processing.

On the other hand, the frequency response function of the structure will be directly obtained out of experimental cutting tests. Then, the obtained FRFs will be used to feed the model for stability prediction.

5. **Development of an automatic cutting parameter selection algorithm based on a microphone monitored wireless signal.**

An automatic parameter selection algorithm will be developed, in order to correct process parameters on-line, processing the monitoring signal of a microphone located inside the machine enclosure.

6. **Manufacturing and validation of a tunable mass damper with variable stiffness.**

A tuned mass damper in which a circular spring sets the stiffness will be built. The stiffness tuning will be uncoupled from the damping, which will be provided through the eddy current effect.

7. **Development of an active damping system through the own drives of the machine tool.**

An active damping solution using the own drives of the machine as actuators will be developed. The machining process will be monitored by means of an accelerometer, whose feedback signal will be used to perform the control by an additional acceleration feedback loop on the machine CNC.

Part II
Milling Stability Prediction Improvement

In this part, current stability modeling is enhanced through different developments. First, current stability prediction models pitfalls in accurate chatter assessment for heavy-duty process planning are highlighted (Chapter 4). In order to overcome this problem several actions to improve the stability models and the quality of the data used by these models are taken. Thus, specific improvements on the stability lobes for heavy-duty milling operations (Chapter 4), an easy formulation for double period type lobes calculation (Chapter 5), a combined analytical model based on ZOA method (Chapter 6), an inverse methodology for dynamic parameter extraction out of experimental cutting tests (Chapter 7) and a methodology for an accurate FRF estimation based on the real cutting force (Chapter 8) are developed.

Chapter 4

Heavy-duty Milling Process Planning Method Based on Stability Model

The present chapter proposes a standard stability model with specific new improvements focused on heavy-duty operations: the dependency of stability on machine position in the whole workspace and the dependency of stability on feed direction. These factors are not taken into account by current stability models, which make them unsuitable for the stability prediction of this kind of operations. This new model is used as the basis for the development of a universal process planning and tool selection methodology.

Although the developed model is considering important factors which affect stability in milling operations, additional stability prediction pitfalls are found.

4.1   STABILITY   IN   HEAVY-DUTY   FACE   MILLING   OPERATIONS

Two main assumptions are made when performing heavy-duty milling operations:

- Although a different cutting tool is used, the FRF remains unchanged.
- As non-interrupted cutting processes are involved, ZOA method is providing an accurate result.

Vibration modes involved in heavy-duty roughing operations have big modal masses, and therefore the FRFs are independent of the tool. Hence, the same FRF can be used to obtain the stability lobes of different tools. This is experimentally demonstrated in Figure 4.1, where frequency response functions of two tools in different frequency regions are shown. Mode frequencies involving machine elements are up to roughly 200Hz and the frequency response is independent of the clamped tool in this case, whereas mode frequencies involving tool and tool holders are at higher frequencies and in that case the clamped tool has a significant effect on the frequency response.
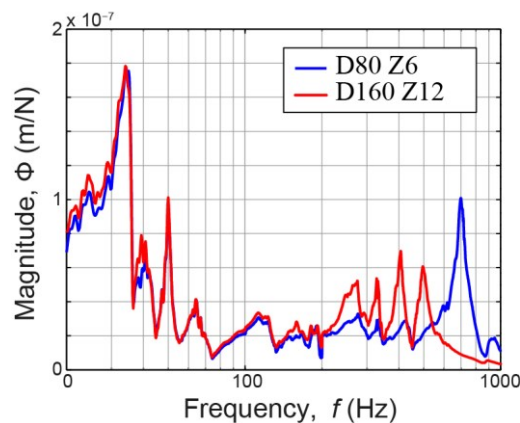
Figure 4.1: Comparison of tool tip FRF on the ram-type travelling column milling machine; an 80mm diameter and 6-insert tool with a 160mm and 12-insert tool from 20 to 1000Hz.

When machine chatter occurs, the dynamics of the structure depends on the position of the machine. The architecture of the machine tool defines the magnitude of dynamical variation inside the workspace. These variations can be handled discretizing the workspace in different points and measuring experimentally the different FRFs in each point (see Figure 4.2).
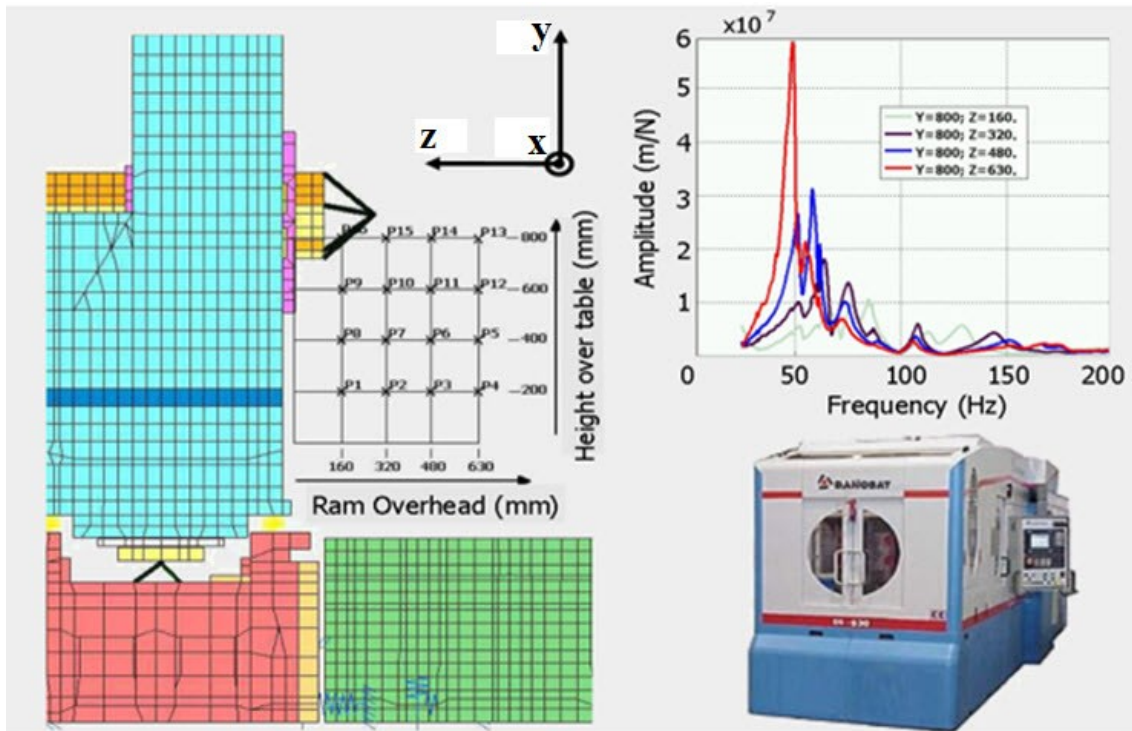
Figure 4.2: Discretization of the workspace of the vertical ram-type machining center and the variation of the drive point FRF in *x* direction depending on the ram overhang. Munoa, 2007.

The single frequency model (ZOA) allows a fast and accurate stability lobe calculation for non-interrupted milling processes. Due to the fact that heavy-duty milling operations are usually performed with large (75-80%) tool engagements and high number of flutes, the created harmonics are usually weak and the single frequency method can provide an accurate solution. Figure 4.3 serves as an example of the achievable precision by means of the single frequency method. The stability of a typical face milling operation has been obtained through the single frequency model (ZOA) and multi-frequency model. The operation consists of a 100mm width milling operation using a 125mm diameter and 8-fluted tool. The cutting coefficients and dynamic parameters used in the simulation are specified in Table 4.1 and Table 4.2 respectively. The figure shows that the predicted stability is almost identical.
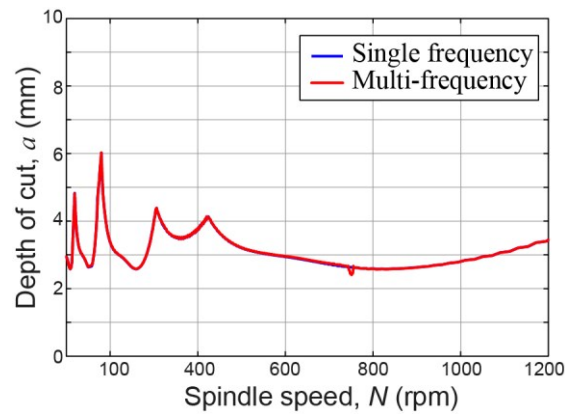
Figure 4.3: Single frequency simulation vs. multi-frequency simulation in a standard roughing milling process.

K_t	K_r	K_a	K_{te}	K_{re}	K_{ae}
1883N/mm²	0.38	0.25	98N/mm	186 N/mm	147 N/mm

Table 4.1: Cutting coefficient for F1140/SANDVIK R245-12T3M-PH 4030.

	Natural Frequency (f_n)	Damping ratio (ξ)	Modal Stiffness (k)	Modal vector [Q_i]	
				Tool {p}	Ram Tip {q}
1	33.3Hz	5.5%	20.5 N/μm	(-0.61,0.69,-0.39)	(-0.4, 0.43,-0.28)
2	43.8Hz	6.8%	55.8 N/μm	(0.51, 0.78, -0.35)	(0.27, 0.48,-0.22)
3	51Hz	2%	273 N/μm	(0.99, -0.12,0)	(0.55, -0.06,-0.03)
4	193Hz	1.5%	639 N/μm	(0.7,-0.56, 0.43)	(0.2, 0.04, 0.06)

Table 4.2: Dynamic parameters of a ram-type travelling column milling machine.

4.2   PROCESS PLANNING METHODOLOGY

4.2.1   Methodology development

The heavy-duty face milling of steel and cast iron is mainly limited by the machinability characteristics of the material and chatter vibrations. Comparing with high speed machining of light alloys, the window of suitable spindle speeds for each tool is narrow due to machinability reasons. The objective of the process planning is to select a tool where the optimal cutting speeds (from machinability point of view) coincide with the most stable zone. The stability models should be used in this process.

First of all, the machine dynamics must be characterized in order to introduce them in the stability model. As stated before, in heavy-duty operations, the stability of the cut depends only on the dynamics of the machine structure and workpiece, which are machine position dependent. If the effect of the machine spindle or tool is involved in cutting capability limitation, the receptance coupling methodology can be used in order to add the spindle or tool effect to the machine dynamics (Schmitz et al., 2007).

When the machine tool user requires a face milling process planning, a large number of tools with different diameters and number of flutes are available for the same tool insert geometry (see Table 4.3). All those tools share the same dynamic parameters, cutting coefficients and cutting speed V_c range. The diameter and the number of flutes are the only different properties for their stability simulation. Therefore, a common stability diagram can be defined considering the same relative radial immersion and immersion angles, modifying the solutions obtained from ZOA method, described in equations (2.3-48) and (2.3-52), that is:

$$a_{\lim} = -\frac{\pi \sin \kappa \, \Lambda_R}{Z \, K_t}(1+(\tan \chi)^2) \tag{4.2-1}$$

and

$$N = \frac{60}{Z \, \tau} = \frac{60 \, \omega_c}{Z \, (\varepsilon + 2\pi l)}. \tag{4.2-2}$$

Therefore, taking into account that $V_c=\pi ND/1000$, equations (4.2-1) and (4.2-2) can be transformed to:

$$Z \, a_{\lim} = \left(-\pi \Lambda_R / K_t\right)\left(1+\left(\Lambda_I / \Lambda_R\right)\right)\sin \kappa, \tag{4.2-3}$$

$$D/Z = \left(\frac{1000}{60} V_c / \omega_c\right)\{1-(2/\pi)\arctan(\Lambda_I / \Lambda_R)+2l\} \quad l=0,1,2,... \tag{4.2-4}$$

Tool manufacturers offer several cutter bodies to perform the particular milling operation, dividing the cutter bodies in groups with different insert pitches sharing the same diameter range (see Table 4.3). Currently, in most cases, the cutter body is selected without following a clear criterion.

As the spindle speed N range is defined according to the cutting speed V_c which is recommended for the mounted inserts and the material to cut, the D/Z ratio is the important parameter to consider in heavy-duty milling operations. Thus, SLD can be plotted as a function of D/Z ratio instead of spindle speed N. Therefore, this new SLD adapted to heavy-duty roughing milling operations offers a useful stability criterion to select the most proper cutter body.

Work material	Tool group	Tool picture	Diameter (mm)	Insert number	*D/Z*
	Coarse Pitch		80	4	20
			100	5	20
			125	6	20.83
			160	7	22.86
	Close pitch		80	6	13.33
			100	7	14.29
			125	8	15.63
			160	10	16
	Extra close pitch		80	8	10
			100	10	10
			125	12	10.42
			160	16	10

Table 4.3: SANDVIK-Coromill R245 tool family.

Apart from the theoretical achievable stability, other a_{lim} constraints such as maximum cutting length of the insert or tool, maximum machine torque and maximum machine power are limiting factors for the process planning. The equations describing these limits are presented below:

- **Insert cutting length.**
  One of the limitations of the depth of cut is the maximum depth of cut a_{max} attainable by the used inserts:

$$Z\, a_{\lim} = Z\, a_{\max},$$ (4.2-5)

  where a_{max} is the maximum physical depth of cut of the used inserts.

- **Machine spindle maximum torque.**
  The maximum achievable depth of cut is also limited by the torque of the main spindle:

$$\overline{F}_{tj} = \frac{\int_{\phi_{st}}^{\phi_{ex}} \left(K_t f_z \sin\phi\, a + K_{te} a / \sin k \right) d\phi}{\Delta\phi_j},$$

$$\overline{T}_c = (D/2)\sum_{j=1}^{Z} \overline{F}_{tj},$$

$$Z\, a_{\lim} = \frac{\overline{T}_{c,\max}\, 4\pi}{D\left(K_t f_z \left(\cos\phi_{st} - \cos\phi_{ex}\right) + \left(K_{te}/\sin k\right)\left(\phi_{ex} - \phi_{st}\right) \right)}.$$ (4.2-6)

- **Machine spindle maximum power.**

  The power of the spindle unit is another factor that could limit the depth of cut:

  $$\overline{P} = \overline{T}\, V_c\, /(30D),$$

  $$Z\, a_{\lim} = \frac{\overline{P}_{\max} 120\pi}{1000 V_c \left(K_t f_z \left(\cos\phi_{st} - \cos\phi_{ex} \right) + \left(K_{te} / \sin k \right) \left(\phi_{ex} - \phi_{st} \right) \right)}. \tag{4.2-7}$$

Combining all these limiting factors, the combined tool selection chart relating $Za_{\lim}$ vs. D/Z (see Figure 4.4) is built. This chart shows the optimum diameter per flute ratio and therefore, the tool providing the highest material removal rate (MRR) for the process can be selected. The maximum attainable MRR is described in equation (4.2-8):

$$\mathrm{MRR} = Z\, a_{\lim} d\, V_c\, f_z\, /\, \pi, \tag{4.2-8}$$

where $d = a_e/D$ is the immersion ratio and a_e is the radial immersion.

Figure 4.4 sets the stability limit at different ram overhangs (z=160-320-480-630mm) through colored lines (blue, red, green and black respectively). On the other hand, the power and torque limits, which are dependent on the number of teeth of the tool, are drawn in grey. The maximum aZ (MRR) value for each of the tool range specified on top of the graph is marked with different shaped points ($\bullet$,$\star$,$\blacksquare$ and $\blacktriangle$), with the same color code as the stability limiting lines.
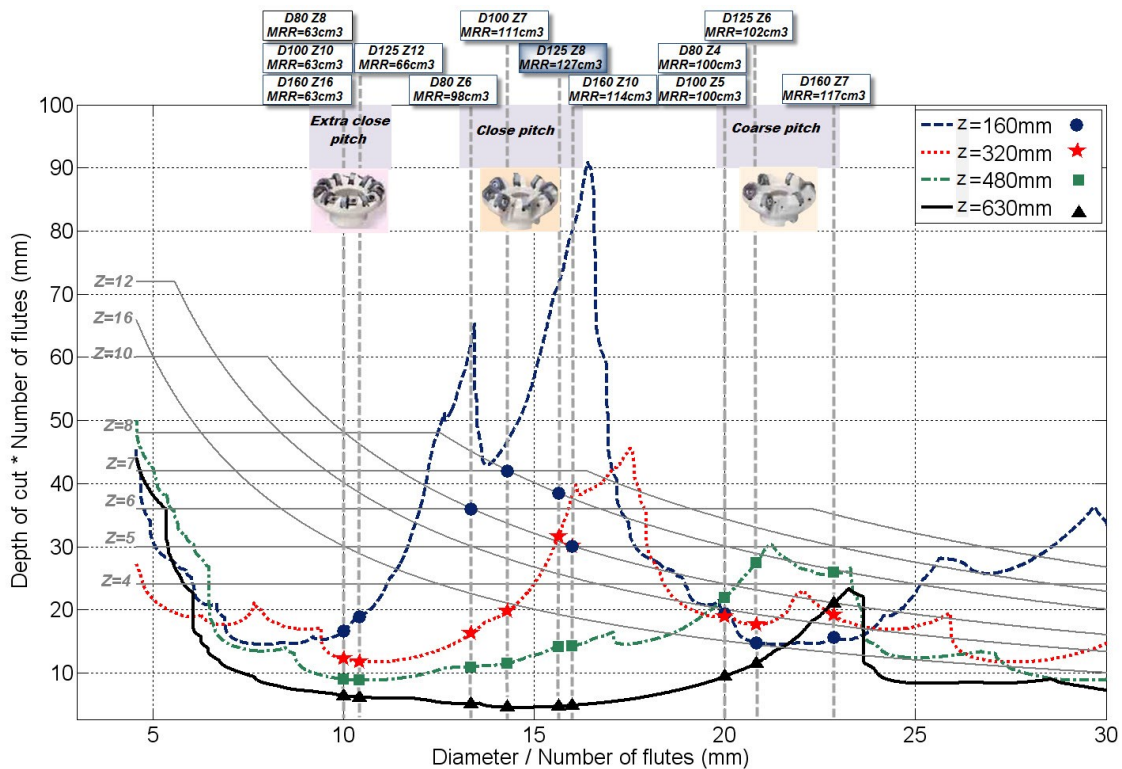
Figure 4.4: Tool selection chart for SANDVIK R245 tool family for V_c=225m/min. Case study 1.

Once the tool is selected, the process planning can be refined through conventional stability diagrams. The conventional stability calculation is performed in the whole workspace, obtaining the maximum stability depending on different feed directions and different cutting speeds.

The process planning starts from the target workpiece characteristics (material and shape). The process planner selects the proper insert geometry and cutting conditions according to that target operation. These cutting conditions, together with spindle power and torque limits and the experimentally characterized cutting force and machine dynamic characteristics, feed the tool selection SLD (see Figure 4.4) in order to select the cutter body. After this step the whole process is already defined and at this point, the standard SLD is applied for process optimization in terms of spindle speed N, depth of cut a and feed direction. Figure 4.5 summarizes schematically process planning procedure.
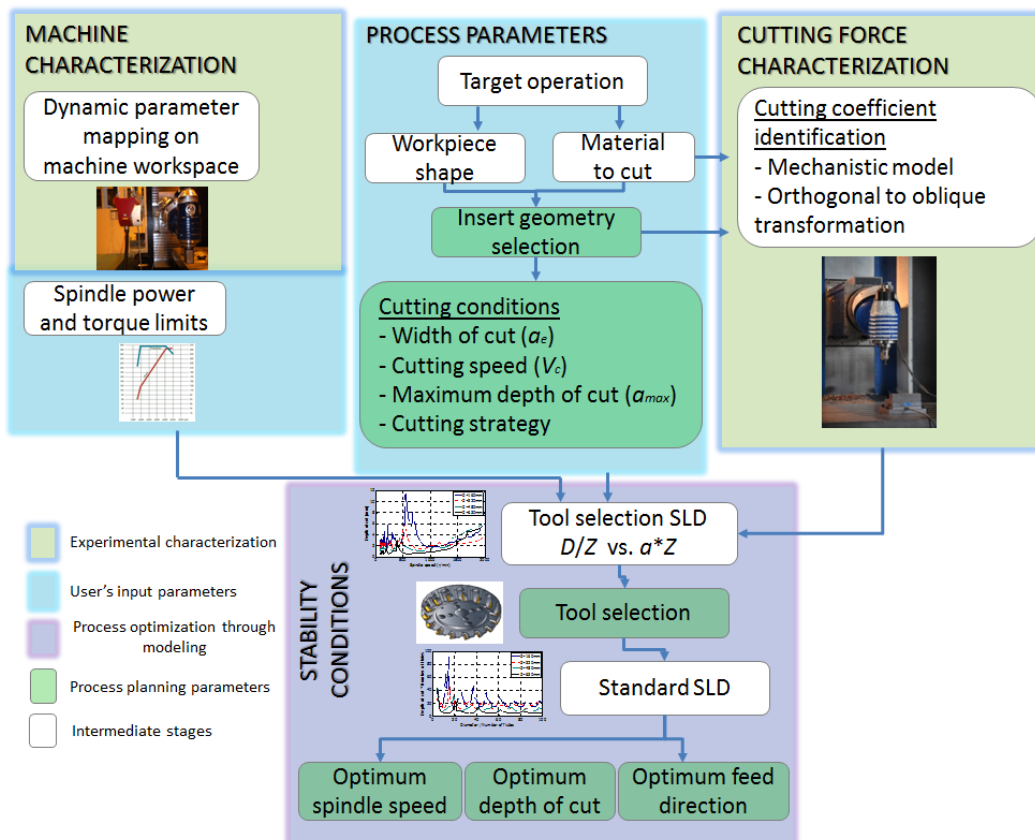
Figure 4.5: Process planning procedure.

4.2.2   Case study 1: vertical ram-type machining center

A face milling of a (F1140 / C45k) steel block in the *xy* plane was optimized using a vertical ram-type machining center (see Figure 4.2). This machine shows a rated torque of 240Nm, a rated power of 35kW and a maximum speed of 12000rpm. In this case the workpiece is supposed to be totally rigid in roughing processes. The workspace was discretized in 16 different points. For process planning, each machine position requires its own stability calculation; therefore, in each position nine FRFs were needed. The FRFs were obtained by means of an impact hammer excitation and a triaxial accelerometer response measurement.

A SANDVIK-Coromill R245 tool family (see Table 4.3) was considered with R245-12 T3 M-PM 4030 insert geometry. This insert type allows a maximum cutting depth of 6mm. The associated cutting coefficients are shown in Table 4.1.

The selected cutting strategy was down-milling machining with 80% tool engagement, that is, a width of cut of 100mm. The feed was 0.1mm/Z. Figure 4.4 shows the tool selection chart relating Za_{lim} vs. D/Z at V_c=225m/min. This graph shows that the close pitch cutter body family D/Z ratio (D/Z around 15) is located in a wide sweet spot area, with a very high MRR, clearly limited by spindle torque and power limits at low ram overhangs. However, as the ram extends, the stability drops considerably. Regarding coarse pitch cutter body family (D/Z around 20), a small sweet spot allows increasing stability at long ram overhangs, which makes this tool family the most appropriate for machining with long ram overhangs. On the other hand, the extra close pitch cutter body family (around D/Z=10) shows a low stability in any ram position.

According to Figure 4.4, considering the SANDVIK-Coromill R245 tool family, the 125mm diameter and 8-insert tool (D/Z=15.6) is the most appropriate tool for this operation in this specific machine, since the highest average material removal rate (MRR) along the ram traverse (z) is achieved.

Next conventional stability calculation was performed for this tool. The workspace stability chart shows at first glance that stability depends strongly on the ram overhang creating almost vertical iso-stability lines (see Figure 4.6). The chatter frequency is also reducing with ram overhang. In this example, the tool speed should be reduced from 550 to 400r/min as the tool overhang is increased (see Figure 4.7) in order to refine machining center cutting performance.
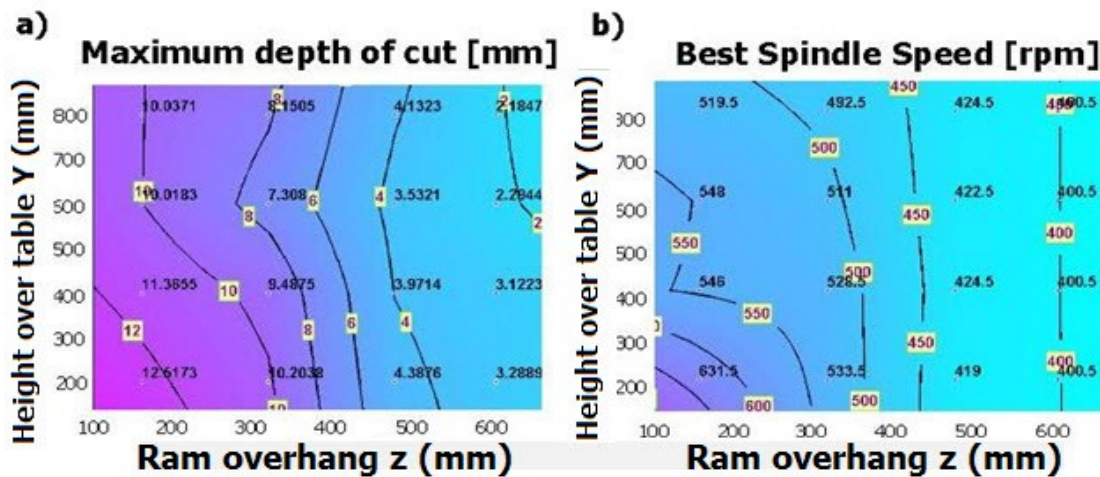
Figure 4.6: Variation of the stability diagram in the workspace. Munoa, 2007.
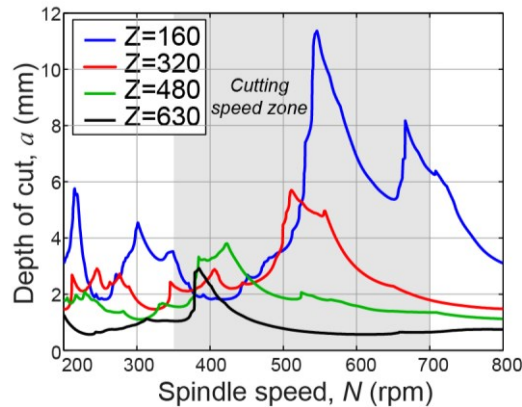
Figure 4.7: Stability diagrams for SANDVIK-Coromill R245-125Q40-12M with 8 inserts. Case study 1.

Figure 4.8 shows the variability of maximum and minimum stability around the cutting plane. Green dashed circles indicate minimum and maximum cutting depth values among angular directions of the plane. This kind of plot indicates the optimum direction to perform cutting. In the example provided, the right selection of the direction can improve cutting performance by 35%.
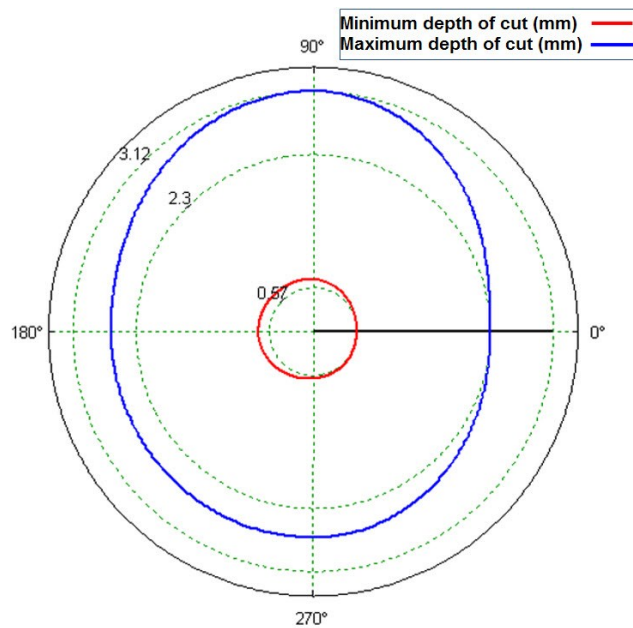
Figure 4.8: Polar depth of cut plot in Case study 1 (y=400mm, z=630mm). Munoa, 2007.

On the other hand, according to Figure 4.4, a 125mm diameter and 12-insert tool (D/Z=10.4) is one of the tools offering a lowest average MRR along the ram traverse. Stability lobes for this tool (Figure 4.9) indicate that low speeds are preferable for low ram overhangs.
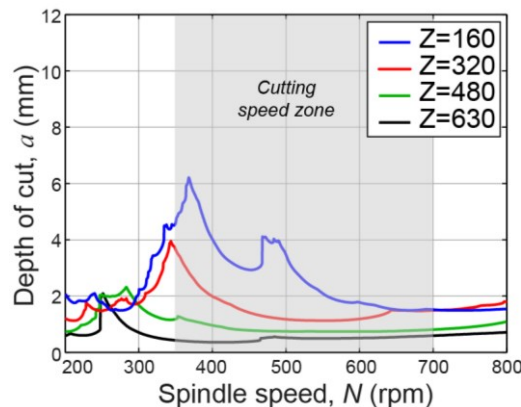
Figure 4.9: Stability diagrams for SANDVIK-Coromill R245-125Q40-12H with 12 inserts. Case study 1.

4.2.3 Case study 2: ram-type travelling column milling machine

The process planning methodology was also applied to a ram-type travelling column milling machine. This machine shows a rated torque of 900Nm, a rated power of 32kW and a maximum speed of 4000rpm (Figure 4.10). The machined material was F-1140

(C45k) steel and it was clamped on a working table. In this case the flexibility of the working table is similar to the machine in some positions; therefore, both frequency response functions were added as shown in section 2.3.3.

Figure 4.10: Ram-type travelling column milling machine overview.

As in case study 1, a SANDVIK-Coromill R245 tool family was considered with R245-12 T3 M-PM 4230 type inserts and 80% width. Down-milling direction was considered, as it is the weakest direction for this particular machine. The feed was 0.2mm/Z.

Figure 4.11 shows the tool selection chart for this case. According to it, a 125mm diameter and 12-insert (D/Z=10.4) is one of the most appropriate tools, whereas a 125mm diameter and 8-insert (D/Z=15.6) is among those offering the lowest MRR.
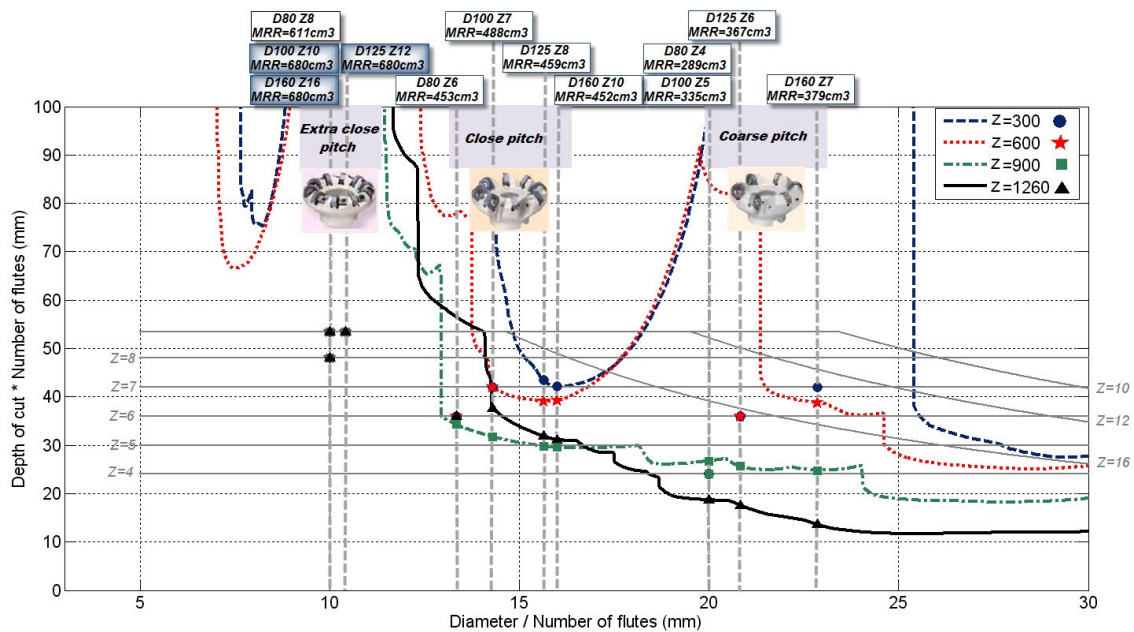
Figure 4.11: Tool selection chart for SANDVIK R245 tool family for V_c=250m/min. Case study 2 (20-200Hz).

Next, conventional stability calculation was performed for the 125mm diameter and 8-insert tool (Figure 4.12). As a general trend, it can be stated that the higher the cutting speed in the recommended cutting speed range, the higher the stability, especially at high ram overhangs.
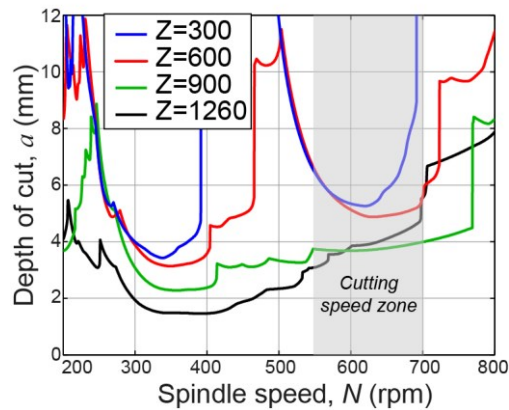
Figure 4.12: Stability diagrams for SANDVIK-Coromill R245-125Q40-12M with 8 inserts. Case study 2.

4.3 EXPERIMENTAL VALIDATION

An experimental validation was run in order to confirm the predictions of the stability models. Two practical cases were analyzed where, the highest stability D/Z region in the tool selection chart is opposite to each other. Whereas in the vertical ram-type machining center the 125mm and 8-insert tool (SANDVIK-CoromillR245-125Q40-12M, D/Z=15.6) offers the highest removal rate, in the ram-type travelling column milling machine this tool is one of the worst choices. Besides, the 125mm and 12-insert tool (SANDVIK-Coromill R245-125Q40-12H, D/Z=15.6) is predicted as one of the least appropriate tools for the vertical ram-type machining center, but it is the best choice for the ram-type travelling column milling machine. Both tools will be used in order to validate the process planning methodology.

4.3.1 Case study 1: vertical ram-type machining center

Four different ram overhangs tests were carried out (see Table 4.4). The best and worse cutting speed regions according to the stability model for face milling were correlated for the two selected tools. A test part with different depth steps was used. With this configuration the depth of cut was increased step by step in a single cutting test (see Figure 4.13).

D125 Z8 (SANDVIK-Coromill R245-125Q40-12M)								D125 Z12 (SANDVIK-Coromill R245-125Q40-12H)							
Position [mm]		Milling Conditions		Simulation		Experimental		Position [mm]		Milling Conditions		Simulation		Experimental	
z	y	N [r/min]	Direction	a_{lim} [mm]	ω_c [Hz]	a_{lim} [mm]	ω_c [Hz]	MaxMRR [cm³/min]	z	y	N [r/min]	Direction	a_{lim} [mm]	ω_c [Hz]	a_{lim} [mm]	ω_c [Hz]	MaxMRR [cm³/min]
160	300	410	Up	1.3	88.8	1.5	84.4	**220**	160	600	730	Down	1.5	88	1.7	83.1	**149**
		550	Down	10.92	119.9	>5	TL				350	Down	4.6	127	>3	TL	
320	300	730	Up	1.17	72.1	1.5	70	**204**	320	600	730	Down	1.5	79.5	1.2	75	**105**
		510	Down	5.75	60.4	>5	TL				350	Down	3.7	61.3	2.2	70.3	
480	600	730	Up	1	61.4	1	58.4	**170**	480	600	730	Down	0.9	61.8	0.8	66.9	**70**
		425	Down	3.7	50.3	5	56.82				350	Down	1.2	54.8	1.2	57.5	
630	600	550	Up	0.47	51	1.5	55.2	**66**	630	600	350	Down	0.4	50	0.6	53.8	**70**
		400	Up	2.12	49.5	2	47.5				730	Down	0.6	56.5	0.8	59.4	

TL=Torque limit

Table 4.4: Experimental correlation of Case study 1.
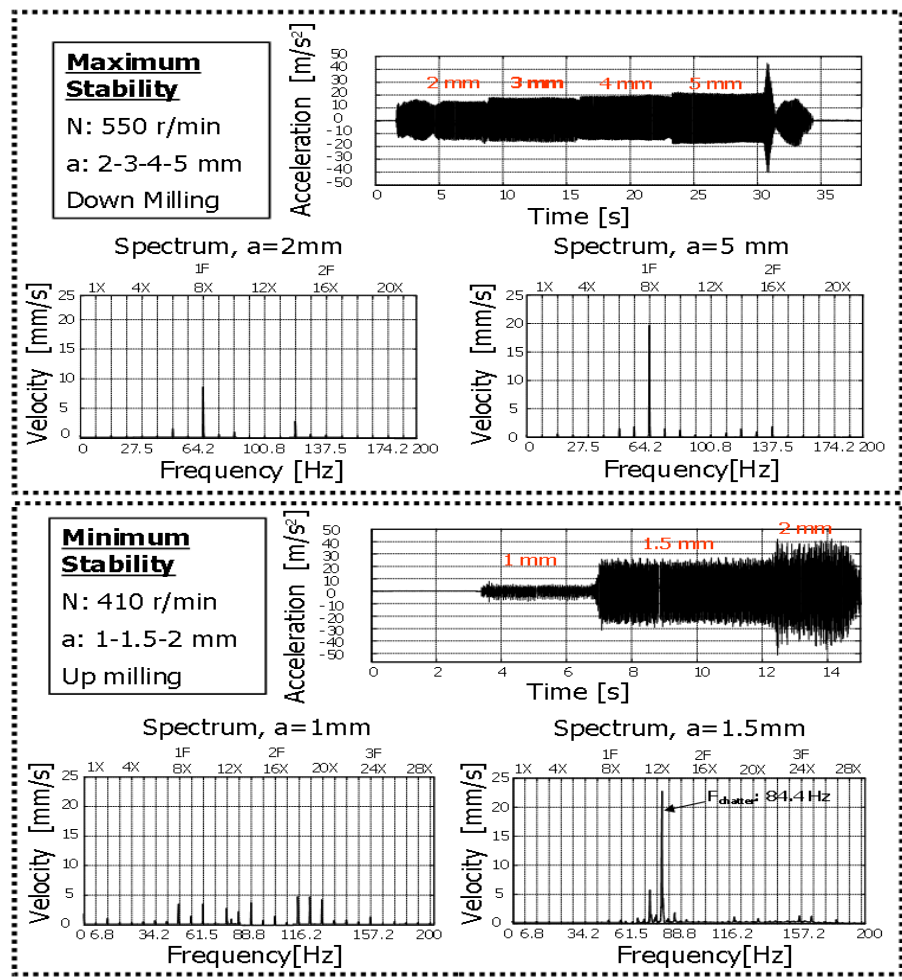
Figure 4.13: Cutting test at the same position (y=300mm, z=160mm) with optimal and worst stability conditions. Case study 1. Munoa, 2007.

The experiments confirm the existence of a sweet spot in the stability chart, and the movement of the best spindle speed from 550 to 400r/min as the ram overhang is increased. In general, the limit depth of cut is well predicted with the stability model, although slight discrepancies can be detected, especially in the minimum value. This minimum depth of cut is underrated in the simulations, probably due to damping value underrating. Frequency values are also in good agreement with simulations.

The MaxMRR value (Table 4.4) shows that the diameter 125mm and 8-insert tool pointed out as the best tool for this machining center outperforms the 125mm and 12-insert tool to a large extent.

4.3.2 Case study 2: ram-type travelling column milling machine

Unlike the Case study 1, in this case the 125mm diameter and 12-insert tool has the highest MRR according to the obtained tool selection chart (Figure 4.11), whereas the 125mm and 8-insert tool is one of the worst choices for this particular machine. For both tools, four different overhangs simulated were selected for the experimental tests. The optimum and worst cutting speed regions were selected for model validation. Figure 4.12 shows the stability diagram for the 8-insert tool.

Experimental results are shown in Table 4.5. In this case the theoretical estimation is far from the experimental results. Stability lobes overrate the cutting capability of the machine. Concerning the frequency prediction, correlation is reasonably accurate for the 8-insert tool, but not for the 12-insert tool. The mismatch of the latter is due to the onset of high frequency chatter, which is related to machine tool spindle.

D125 Z8 (SANDVIK-Coromill R245-125Q40-12M)									D125 Z12 (SANDVIK-Coromill R245-125Q40-12H)								
Position [mm]		Milling Conditions		Simulation		Experimental			Position [mm]		Milling Conditions		Simulation		Experimental		
z	y	N [r/min]	Direction	a_{lim} [mm]	ω_c [Hz]	a_{lim} [mm]	ω_c [Hz]	MaxMRR [cm³/min]	z	y	N [r/min]	Direction	a_{lim} [mm]	ω_c [Hz]	a_{lim} [mm]	ω_c [Hz]	MaxMRR [cm³/min]
300	1300	550	Down	6.4	61.8	4.5	60	**672**	300	1300	700	Down	>10	118	3.5	498	**595**
		700	Down	>10	73	>6	DL				620	Down	>10	124	>4	PL	
600	1300	700	Down	5.6	63.2	3.5	35	**392**	600	1300	700	Down	9.1	119	3.5	504	**595**
		550	Down	6.5	61.5	3.5	60.5				620	Down	>10	115	>4	PL	
900	1300	550	Down	3.7	39.8	2.5	34.3	**280**	900	1300	575	Down	6.6	115	2.5	36	**420**
		700	Down	4	40.2	2.5	35				700	Down	>10	123	2.5	507	
1260	1300	550	Down	3.1	36.8	2.5	31.8	**280**	1260	1300	575	Down	3.6	71	2.5	34	**420**
		700	Down	5.6	39.5	2.5	33.8				700	Down	5.6	135	2.5	505	

Table 4.5: Experimental correlation of Case study 2.

However, the 12-insert tool (Table 4.5) shows a higher MRR capability, even when an unexpected machine spindle mode was limiting the stability. Therefore, although stability limit is not accurately predicted, tool selection chart helped selecting the most appropriate tool to be used in this particular machine.

4.4   CONCLUSIONS

The machinability and the dynamic stiffness of the milling machine structure limit the productivity in heavy-duty roughing due to chatter vibrations. A new procedure based on a frequency model has been proposed for process planning. The model has been adapted introducing the dynamic cross effects between machine and workpiece response, the effect of feed direction and the variation of the dynamics with the machining position. A different way to obtain the stability charts as a function of the D/Z ratio has been proposed to select the most suitable tool considering machinability reasons. FRF only depends on machining position and it allows simulating stability lobes for different tools with the same FRF. The procedure has been validated experimentally.

The experimental results match with the predictions for the machine in case study 1, confirming that the optimal speeds have been selected for the different ram overhangs. However, in case study 2, experimental results are not accurately predicted. There are two main reasons for this: the involvement of higher frequency spindle modes in stability limitation and the deviation of the experimentally extracted dynamic parameters with respect to reality. The main mismatches have been found when predicting the maximum cutting depth, whereas the frequency prediction has been reasonably accurate in most cases. This indicates that current milling stability prediction models are not accurate for every type of machine. Impact hammer excitation is widely used for dynamic parameter extraction but in view of the results of this work, the development of alternative dynamical measurement methods closer to the cutting conditions might be needed in order to improve the quality of the predictions.

The tool selection chart has been successfully used to select the proper tool for both practical cases. Paradoxically, the best tool for one of the machines has turned out to be the worst for the other machine and vice versa. This demonstrates that there is not a specific D/Z ratio that could be regarded as a universal MRR maximization solution, but a proper combination of the D/Z ratio with each machine, considering its dynamics properties, must be sought. In this context, the process planning methodology proposed in this work meets this need.

Contribution 1:

A new procedure based on a frequency model has been proposed for heavy-duty milling process planning, where machine structural chatter limits productivity. The model has been adapted introducing the dynamic cross effects between machine and workpiece response, the effect of feed direction and the variation of the dynamics with the machining position. The model accounts for the machinability and machine capacity constraints in order to offer the most suitable D/Z tool ratio.

Contribution 2:

It has been demonstrated that there is not a universal tool that holds the higher cutting capability in every machine tool as it is usually perceived by machinists, but the cutting capability is set by the combination between the tool characteristics and the machine dynamics. Thus, a specific tool that can be a good choice for a particular machine could be the worst choice for another machine with a different dynamic behavior.

Contribution 3:

The assessment of the stability of milling operations can be considerably inaccurate depending on the specific case studied. Whereas the frequency prediction is usually accurate, the maximum achievable depth of cut presents important deviations in specific cases. Therefore, apart from the adaptation of the stability model to heavy-duty milling operations carried out, current stability prediction models need to add additional effects which affect stability that have not been taken into account so far.

Related Publications:

Iglesias, A., Munoa, J., & Ciurana, J. (2014). Optimisation of face milling operations with structural chatter using a stability model based process planning methodology. *The International Journal of Advanced Manufacturing Technology*, 70(1-4), 559-571.

Chapter 5

Analytical Expressions for Chatter Analysis in Milling Operations

New analytical formulae are proposed related to both Hopf and period doubling type stability boundaries emerging in the regenerative mechanical model of time periodical milling processes with one dominant mode.

The lack of accuracy in stability predictions described in Chapter 4 can be partially improved considering the double period related instability that is not considered by several of the proposed stability models in the literature.

Furthermore, the time domain based methods that do consider this type of instability can benefit from a previous rough calculation of the stability limits by means of the developed analytical expressions. This previous estimation can be used to limit the scanning point range, thus speeding up the calculation to a large extent.

The destabilization mechanism of double period chatter is explained, creating an analogy with the chatter related to the Hopf bifurcation, considering one dominant mode and using concepts established by the Pioneers of chatter research. Thus the physics behind this cutting instability are properly explained and important new relations between Hopf and flip instability are found, stressing the importance of the ratio between the main harmonics of the directional factors.

5.1   GENERAL MULTI-FREQUENCY FORMULATION IN MODAL COORDINATES

A simple form of the multi-frequency solution is derived in this section for the milling operation in modal coordinates. By using these simplified equations and the special characteristics of the double period chatter, analytic expressions for one dominant mode are derived for Hopf related chatter and double period chatter limits.

5.1.1   Dynamic cutting force definition in modal coordinates

The dynamic force expression in equation (2.3-18) can be transformed into the modal space. In this case, the modal displacement $\{\eta\}$ and the modal force $\{P\}$ are described as:

$$\{\Delta p\} = [Q_3]\{\Delta\eta\}, \tag{5.1-1}$$

$$\{P(t)\} = [Q_3]^{\mathrm{T}}\{F(t)\}, \tag{5.1-2}$$

where $\{\Delta\eta(t)\} = \{\eta(t) - \eta(t\text{-}\tau)\}$ and $[Q_3]$ is the geometrically normalized modal transformation matrix (see Figure 5.1).
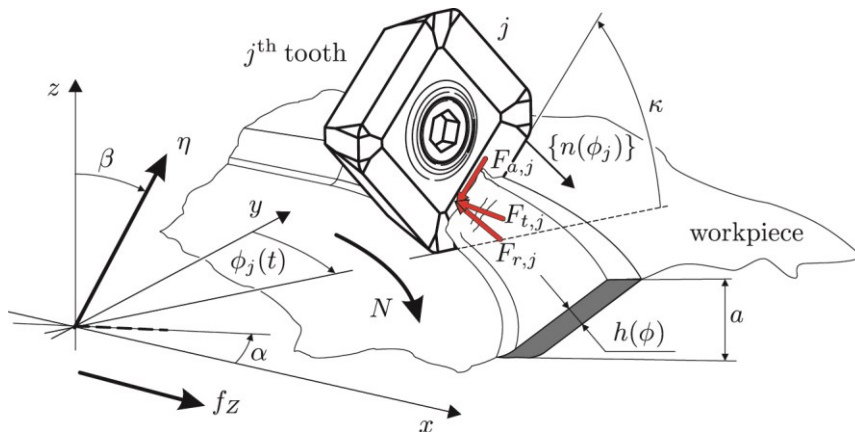
Figure 5.1: Geometry of the face milling cutter. The cutting forces can be written in Cartesian coordinate system (*x*, *y*, *z*) or spherical coordinate system (α, β, η).

Hence, the dynamic milling force can be written in modal coordinates defining the modal directional factor matrix $[B(t)]$:

$$\{P(t)\} = -\frac{K_t \, a}{\sin \kappa}[B(t)]\{\Delta \eta(t)\},$$

(5.1-3)

where

$$[B(t)] = -[Q_3]^T[A(t)][Q_3].$$

(5.1-4)

In most cases, $[B(t)]$ results in a negative value and, therefore, to be consistent with the convention fixed by earlier works (Tlusty and Polacek, 1957; Tobias and Fishwick, 1958), the negative sign has been adopted in equation (5.1-4) from the original $[B(t)]$.

5.1.2   Stability analysis in frequency domain

Following the developments by Minis and Yanushevsky (1993), Munoa et al. (2013a) and Budak and Altintas (1998), it is possible to obtain a closed loop formulation. The process stability analysis drives to an infinite dimension matrix expression similarly to Hill's infinite determinant method (Farkas, 1994), that is,

$$
\begin{Bmatrix} \{\eta_{-h}\} \\ \vdots \\ \{\eta_0\} \\ \vdots \\ \{\eta_h\} \end{Bmatrix} = -\left(\frac{K_t \, a}{\sin \kappa}\right)(1-e^{-j\omega_c\tau})
\begin{bmatrix} [\Phi_{-h}] & \cdots & [0] & \cdots & [0] \\ \vdots & \ddots & \vdots & \ddots & \vdots \\ [0] & \cdots & [\Phi_0] & \cdots & [0] \\ \vdots & \ddots & \vdots & \ddots & \vdots \\ [0] & \cdots & [0] & \cdots & [\Phi_h] \end{bmatrix}
\begin{bmatrix} [B_0] & \cdots & [B_{-h}] & \cdots & [B_{-2h}] \\ \vdots & \ddots & \vdots & \ddots & \vdots \\ [B_h] & \cdots & [B_0] & \cdots & [B_{-h}] \\ \vdots & \ddots & \vdots & \ddots & \vdots \\ [B_{2h}] & \cdots & [B_h] & \cdots & [B_0] \end{bmatrix}
\begin{Bmatrix} \{\eta_{-h}\} \\ \vdots \\ \{\eta_0\} \\ \vdots \\ \{\eta_h\} \end{Bmatrix},
$$

(5.1-5)

where $\{\eta_h\}$ are the eigenvectors of the corresponding eigensolution containing the relative strengths of all the considered modes for h^{th} modulated frequency, while $[\Phi_h] = [\Phi(\omega_c + h\Omega)]$ and $[B_h]$ are the frequency response function (FRF) and the modal directional factor matrix evaluated at the hth modulated chatter frequency. In a theoretical basis, the size of the matrices is infinite, but in practice the FRF takes very small values for frequencies far from the natural frequencies. Therefore, the system can be truncated without noticeable loss of accuracy.

The frequency domain consideration restricts the eigensolution of equation (5.1-5) to be formulated coefficient-wise defining

$$\Lambda(\omega_c) = \left(\frac{K_t \, a}{\sin \kappa}\right)(1-e^{-j\omega_c\tau}),$$

(5.1-6)

which drives to indirect 'eigenvalues' related to the spindle speeds Ω/Z and depths of cut a. Note that, different numerical methods have been proposed to obtain the multi-

frequency solution (Minis and Yanushevsky, 1993; Budak and Altintas, 1998; Merdol and Altintas, 2004).

In general, the accuracy of the modeling of the milling force increases with the number of harmonics calculated. The magnitude of the harmonics depends on the engagement, the direction of the milling force and the mode and the number of flutes. As the cutting process becomes more interrupted, the influence of the harmonics is more significant.

5.1.3   Zero Order Approximation (ZOA)

If only the zeroth order term is considered a fast parametric analytical solution is possible. This simplification provides a spindle speed independent equation and therefore it can be solved considering chatter frequency as a varying parameter and obtaining the corresponding depth of cut and spindle speeds (Altintas and Budak, 1995) using

$$\{\eta_0\} = -\left(\frac{K_t\, a}{\sin\kappa}\right)(1 - e^{-j\omega_c\tau})[\Phi_0][B_0]\{\eta_0\}.$$ (5.1-7)

The Cartesian consideration of equation (5.1-7) is the mostly used reference to perform milling process stability analysis using measured FRFs (Altintas and Budak, 1995). Practically, when the number of considered modes is bigger than three, the approach based on modal coordinates drives to bigger matrix dimensions and longer calculation times.

5.1.4   Double period chatter

The double period stability loss of the stationary (forced) vibration $\{r_p(t)\}$ has some particularities that can be helpful to define the stability boundaries. The main characteristic of this double period chatter is that there is a proportional relationship between the chatter frequency and the excitation/tooth passing frequency (Davies et al., 2000):

$$2\omega_c = m\Omega.$$ (5.1-8)

In terms of frequency domain, the double period chatter happens when the chatter frequency and one of the modulated chatter frequencies are shaking the same mode. Only the odd modulated chatter harmonics can create the double period chatter. The regenerative term explains this effect and can be rewritten as a function of the involved harmonics resulting zero for all the even harmonics.

$$f_r = 1 - \mathrm{e}^{-\mathrm{j}\omega_c \tau} = 1 - \mathrm{e}^{-\mathrm{j}\omega_c \frac{2\pi}{\Omega}} = 1 - \mathrm{e}^{-\mathrm{j}m\pi} = \begin{cases} 0, & \text{if } m = 0, 2, 4, ..., \\ 2, & \text{otherwise}. \end{cases} \tag{5.1-9}$$

Applying these effects in the main equation (5.1-5):

$$\begin{Bmatrix} \{\eta_{-h}\} \\ \vdots \\ \{\eta_0\} \\ \vdots \\ \{\eta_h\} \end{Bmatrix} = -\left(\frac{2K_t a}{\sin\kappa}\right) \begin{bmatrix} [\Phi_{-h}] & \cdots & [0] & \cdots & [0] \\ \vdots & \ddots & \vdots & \ddots & \vdots \\ [0] & \cdots & [\Phi_0] & \cdots & [0] \\ \vdots & \ddots & \vdots & \ddots & \vdots \\ [0] & \cdots & [0] & \cdots & [\Phi_h] \end{bmatrix} \begin{bmatrix} [B_0] & \cdots & [B_{-h}] & \cdots & [B_{-2h}] \\ \vdots & \ddots & \vdots & \ddots & \vdots \\ [B_h] & \cdots & [B_0] & \cdots & [B_{-h}] \\ \vdots & \ddots & \vdots & \ddots & \vdots \\ [B_{2h}] & \cdots & [B_h] & \cdots & [B_0] \end{bmatrix} \begin{Bmatrix} \{\eta_{-h}\} \\ \vdots \\ \{\eta_0\} \\ \vdots \\ \{\eta_h\} \end{Bmatrix},$$

$$\tag{5.1-10}$$

where:

$$[\Phi_h] = [\Phi\,(\mathrm{j}\,(\omega_c + h\Omega))] = \left[\Phi\left(\mathrm{j}\omega_c\left(1 + \frac{2h}{m}\right)\right)\right]. \tag{5.1-11}$$

The eigenvalue problem is now independent from the tooth passing frequency and the spindle speed. Therefore it is possible to obtain the limit of the double period chatter similarly to Altintas and Budak (1995). The eigenvalue $\Lambda(\omega_c)$ is solved for each frequency or spindle speed. These eigenvalues should fulfill the following conditions to ensure physical solutions:

$$\Lambda(\omega_c) = \Lambda_\mathrm{R}(\omega_c) + \Lambda_\mathrm{I}(\omega_c)\,\mathrm{j} = \frac{K_t a Z}{\pi \sin\kappa}, \tag{5.1-12}$$

(C1) $\Lambda_\mathrm{R}(\omega_c) > 0$,

(C2) $\Lambda_\mathrm{I}(\omega_c) = 0$,

(C3)   the average term should have the biggest value in the eigenvector (Merdol, 2008).

The stability limits for double period are only considered for the real valued eigenvectors. In fact, the different double period are obtained scanning different lines $\omega_c(\Omega) = m\Omega/2$ ($m = 1, 3, 5, ...$) in the chatter frequency diagram.

$$a(\omega_c) = \frac{\pi \Lambda_\mathrm{R}(\omega_c)\sin\kappa}{Z K_t}, \tag{5.1-13}$$

$$N(\omega_c) = \frac{60\,\omega_c}{\pi Z m}. \tag{5.1-14}$$

5.2 DOUBLE PERIOD LOBES WITH ONE DOMINANT MODE: ANALYTICAL SOLUTIONS AND A COMPARISON WITH TRADITIONAL CHATTER

The analytical solution for Hopf and flip lobes is obtained from the dynamic milling equation (5.1-3).

5.2.1 Directional factor

First of all, it is important to define the directional factor (Koenigsberger and Tlusty, 1970) or the direction coefficient (Opitz and Bernardi, 1970) of one mode $B(t)$ in a certain milling process, because it defines decisively the shape of the stability diagram and the presence of the double period chatter.

The directional factor is a geometrical term which captures the projection of the cutting force onto the direction of the mode and the vibration onto the direction of the chip thickness. Operating, the time-periodic directional factor, defined in equation (5.1-4):

$$B(t) = \sum_{j=1}^{Z} g(\phi_j)(\sin\beta\sin\kappa\sin(\alpha+\phi_j) - \cos\beta\cos\kappa) \cdot$$

$$(\cos\beta(K_r\cos\kappa - K_a\sin\kappa) - \sin\beta(\cos(\alpha+\phi_j) + (K_a\cos\kappa + K_r\sin\kappa)\sin(\alpha+\phi_j))) =$$

$$= \sum_{j=1}^{Z} g(\phi_j)s(\phi_j),$$

(5.2-1)

where $\phi_j = \phi_j(t)$. In milling there are several flutes acting at the same time and the cutting direction is changing with the rotation of the tool. In one word, the directional factors are time dependent and periodic with the tooth passing frequency. Therefore, a discrete Fourier development is possible as

$$B(t) = \sum_{r=-\infty}^{\infty} B_r\, e^{jr\Omega t} = \frac{Z}{2\pi}\sum_{r=-\infty}^{\infty}\beta_r\, e^{jr\Omega t},$$

(5.2-2)

where different definitions of harmonics are obtained as

$$B_r = \frac{Z}{2\pi}\int_{\phi_{st}}^{\phi_{ex}} s(\phi)\, e^{-jrZ\phi}\, \mathrm{d}\phi = \frac{Z}{2\pi}\beta_r.$$

(5.2-3)

The β_0 is the average value of this factor and coincides with the direction coefficient proposed by Opitz and Bernardi, 1970.

If only one dominant mode is considered, all the matrices involved in the stability problem become one dimensional. Therefore, the general characteristic equation is simplified:

$$
\begin{Bmatrix} \eta_{-h} \\ \vdots \\ \eta_0 \\ \vdots \\ \eta_h \end{Bmatrix} = -\left(\frac{K_t\, a}{\sin \kappa}\right)(1-e^{-j\omega_c \tau})
\begin{bmatrix} \Phi_{-h} & \cdots & 0 & \cdots & 0 \\ \vdots & \ddots & \vdots & \ddots & \vdots \\ 0 & \cdots & \Phi_0 & \cdots & 0 \\ \vdots & \ddots & \vdots & \ddots & \vdots \\ 0 & \cdots & 0 & \cdots & \Phi_h \end{bmatrix}
\begin{bmatrix} B_0 & \cdots & B_{-h} & \cdots & B_{-2h} \\ \vdots & \ddots & \vdots & \ddots & \vdots \\ B_h & \cdots & B_0 & \cdots & B_{-h} \\ \vdots & \ddots & \vdots & \ddots & \vdots \\ B_{2h} & \cdots & B_h & \cdots & B_0 \end{bmatrix}
\begin{Bmatrix} \eta_{-h} \\ \vdots \\ \eta_0 \\ \vdots \\ \eta_h \end{Bmatrix}.
$$

$$(5.2\text{-}4)$$

In the case of a mechanical system with only one mode, there are no mode couplings; consequently, the ZOA can theoretically provide a good approach for the traditional chatter related to the Hopf bifurcation (Altintas and Budak, 1995; Munoa et al., 2013a). However, some harmonics have to be considered to capture the period-doubling chatter.

5.2.2   Traditional Chatter: Hopf-bifurcation

If only one dominant mode is considered a simple approximation is obtained for the characteristic equation:

$$
\eta_0 = -\left(\frac{K_t\, a_H\, Z}{2\pi \sin \kappa}\right)(1-e^{-j\omega_c \tau})\, \beta_0\, \Phi_0\, \eta_0 .
$$

$$(5.2\text{-}5)$$

The equation is almost the same as the one proposed by Tlusty and Polacek (1957) and Tobias and Fishwick (1958), with the only difference of the presence of the directional factor orienting the FRF.

Operating equation (5.2-5), an analytical expression of the depth of cut a, the phase between the inner and the outer modulation ε and the spindle speed N as a function of the chatter frequency ω_c can be obtained as

$$
a_H(\omega_c) = -\frac{\pi \sin \kappa}{K_t\, Z\, \beta_0 G(\omega_c)} ,
$$

$$(5.2\text{-}6)$$

$$
N_H(\omega_c) = \frac{60\,\omega_{c,H}}{Z\,(2\psi(\omega_c)+(2l+3)\,\pi)} ,
$$

$$(5.2\text{-}7)$$

and

$$
\varepsilon_H(\omega_c) = 2\psi(\omega_c) + 3\pi.
$$

$$(5.2\text{-}8)$$

$G(\omega_c)$ is the real part and $\psi(\omega_c)$ is the phase of the FRF $\Phi(\omega_c)$, which depends on the chatter frequency.

There are three main graphs that are usually employed for stability analysis: the limit depth of cut graph (a_H versus N), the chatter frequency graph (ω_c versus N) and the phase shift graph (ε versus N). In this work the dimensionless form of these plots has been used: the cutting stiffness to dynamic stiffness ratio σ as a function of the tooth passing frequency to natural frequency ratio ν (Figure 5.2c and Figure 5.3c) and the dimensionless chatter frequency λ as a function of ν (Figure 5.2b and Figure 5.3b).

The dimensionless forms of the depth of cut a, the spindle speed N and the chatter frequency ω_c are defined as:

$$\sigma = \frac{K_t \, Z \, \beta_0}{4 \, \pi \, k \, \xi \sin \kappa} a, \tag{5.2-9}$$

$$\lambda = \frac{\omega_c}{\omega_n}, \tag{5.2-10}$$

and

$$\nu = \frac{2 \, \pi \, Z}{60 \, \omega_n} N. \tag{5.2-11}$$

Two different shapes are possible depending on the sign of the directional factor. When the directional factor is positive, the negative side of the real part of the FRF leads to the feasible stability boundary and, therefore, chatter frequency is always bigger than the natural frequency (Figure 5.3b). An opposite case is possible when the directional factor is negative (Figure 5.2b). Figure 5.2c and Figure 5.3c

Figure 5.2 and Figure 5.3 graphs present several characteristic points (minutiae) that can be analytically described through simple expressions.

Tool			
Diameter (D)	Number of flutes (Z)	Lead angle (κ)	Helix angle
20mm	3	90	0
Cutting conditions & Coefficients			
Engagement	Feed direction	K_t [N/mm²] K_r	K_a
1mm (Down-milling)	(1,0,0)	804 0.314	0.15
Dynamic Parameters			
Mode f_n [Hz]	ζ [%]	k [N/µm] m [kg]	Case Orientation
1 178	0.54	19.78 15.81	Case 1 ($\beta_0 < 1$) (1,0,0) Case 2 ($\beta_0 > 1$) (0,1,0)

Table 5.1: Cutting conditions and dynamic parameters for case 1, $\beta_0 < 1$, with the dominant mode oriented in x direction and case 2, $\beta_0 > 1$, with the dominant mode oriented in y direction.
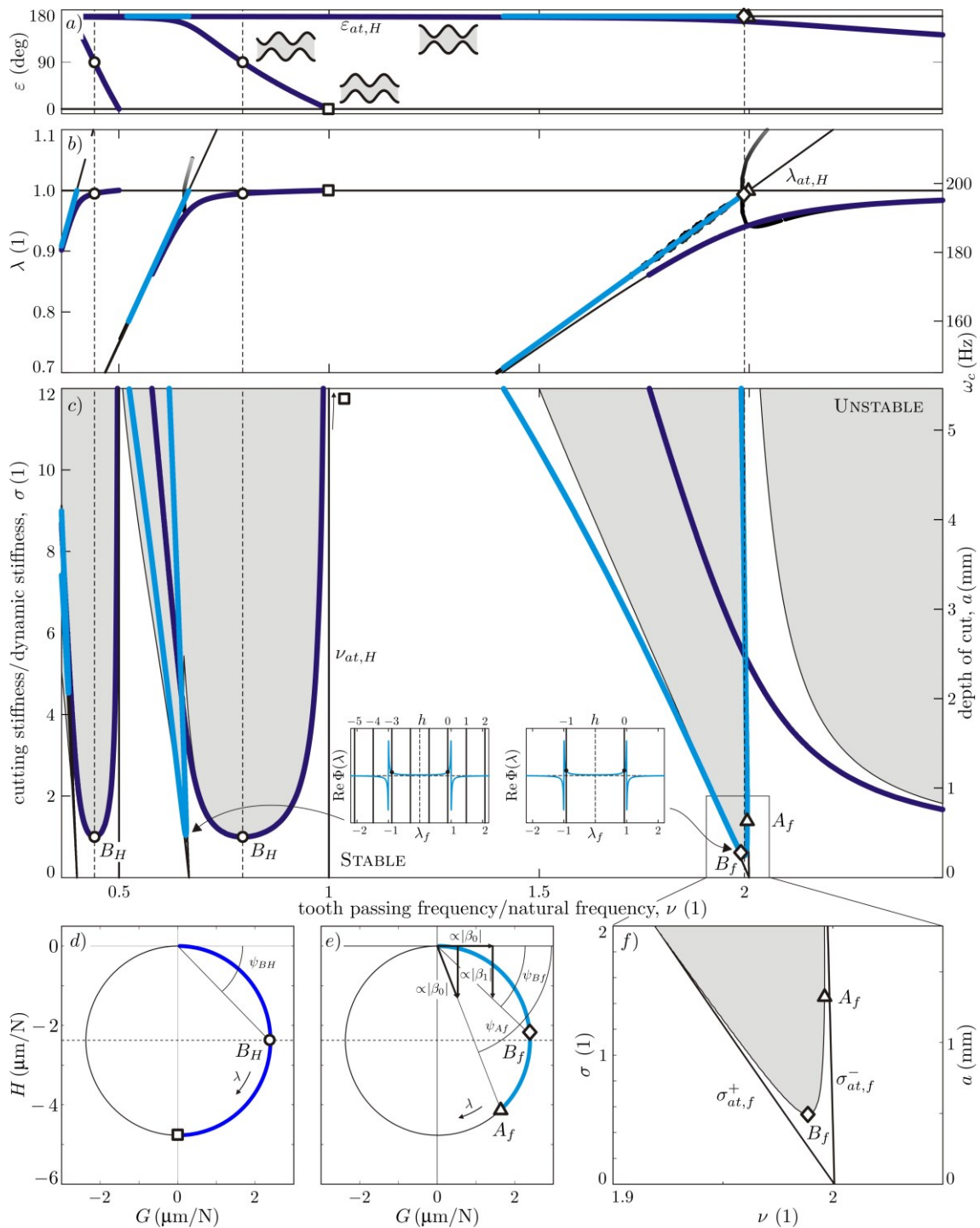
Figure 5.2: Comparison of the analytical solution, Hopf solution (dark blue) and flip solution (light blue), versus semi-discretization solution (shaded area) in milling stability analysis with negative directional factor (parameters in Table 5.1). Minutiae of the curves can be observed: Hopf minimum stability (B_H), Hopf depth of cut asymptote ($N_{at,H}$), Hopf chatter frequency asymptote ($\lambda_{at,H}$), Hopf phase shift asymptote ($\varepsilon_{at,H}$), flip intersection point (A_f), flip minimum stability (B_f) and flip lobe asymptotes ($\sigma^{-}_{at,f}$ and $\sigma^{+}_{at,f}$). *a)* modulation phase ε; *b)* dimensionless chatter frequency λ; *c)* cutting stiffness / dynamic stiffness σ; *d)* Nyquist plot with Hopf minutiae; *e)* Nyquist plot with flip minutiae; *f)* flip minimum detail.

Figure 5.3: Comparison of the analytical solution, Hopf solution (dark blue) and flip solution (light blue), versus semi-discretization solution (shaded area) in milling stability analysis with positive directional factor (parameters in Table 5.1). Minutiae of the curves can be observed: Hopf minimum stability (B_H), Hopf depth of cut asymptote ($N_{at,H}$), Hopf chatter frequency asymptote ($\lambda_{at,H}$), Hopf phase shift asymptote ($\varepsilon_{at,H}$), flip intersection point (A_f), flip minimum stability (B_f) and flip lobe asymptotes ($\sigma^-_{at,f}$ and $\sigma^+_{at,f}$). Experimental data are shown as green points (stable cut) and red crosses (unstable cut) at flip lobe and Hopf minimum area. a) modulation phase ε; b) dimensionless chatter frequency λ; c) cutting stiffness / dynamic stiffness; d) Nyquist plot with Hopf minutiae; e) Nyquist plot with flip minutiae; f) flip minimum detail.

Minimum depth of cut (B$_H$)

The stability lobe defines a minimum of the Hopf related stability limit (a_{BH}), when the real part of the FRF has a minimum or a maximum, in case of positive or negative directional factor respectively.

Deriving the expression of the real part, the chatter frequencies related to this minimum are obtained:

$$\omega_{BH} = \begin{cases} \omega_n \sqrt{1+2\xi}, & \beta_0 > 0, \\ \omega_n \sqrt{1-2\xi}, & \beta_0 < 0. \end{cases} \tag{5.2-12}$$

Introducing this value in the real part of the FRF of equation (5.2-6), the next value is obtained for the minimum value of the depth of cut:

$$a_{BH} = \begin{cases} \dfrac{4\pi k\,\xi(1+\xi)\sin\kappa}{K_t\,Z\,\beta_0} \cong \dfrac{4\pi k\,\xi\sin\kappa}{K_t\,Z\,\beta_0}, & \beta_0 > 0, \\[3mm] -\dfrac{4\pi k\,\xi(1-\xi)\sin\kappa}{K_t\,Z\,\beta_0} \cong -\dfrac{4\pi k\,\xi\sin\kappa}{K_t\,Z\,\beta_0}, & \beta_0 < 0, \end{cases} \tag{5.2-13}$$

where k is the modal stiffness.

This minimum can be observed in Figure 5.2c and Figure 5.3c.

Rearranging, a meaningful expression is obtained:

$$\frac{Z\,K_t\,a_{BH}}{\pi\sin\kappa} \cong \frac{4\,k\,\xi}{\beta_0}. \tag{5.2-14}$$

In the left side, the cutting stiffness of a milling operation is defined with cutting process dependent parameters. In the right side the oriented dynamic stiffness is obtained after multiplying the peak value of the FRF with the directional factor. This expression explains that if the oriented dynamic stiffness is higher than the cutting stiffness, a stable cut is assured (Merrit, 1965).

The minimum depth of cut a_{BH} coincides with a phase shift between modulations of $\varepsilon_{BH} = 3\pi/2$ if $\beta_0 > 0$ or $\varepsilon_{BH} = \pi/2$ if $\beta_0 < 0$. This fact contradicts the usual thinking of considering the worst chatter scenario a phase shift of $\varepsilon_{BH} = \pi$, that is, the largest chip thickness fluctuation case.

Depth of cut asymptote $N_{at,H}$

An asymptote $N_{at,H}$ defines the maximum depth of cut when the tooth passing frequency is exactly the natural frequency, that is, the resonant condition (see $v_{at,H}$ in Figure 5.2*c* and Figure 5.3 *c*). At this asymptote, $\omega_c = \omega_n$ and $\varepsilon = 2\pi$.

Chatter frequency asymptote $\omega_{c,at,H}$

The chatter frequency is always bigger or smaller than the natural frequency depending on the sense of the directional factor but never intersects the natural frequency if a single mode is considered. An interaction between modes is required to cross this asymptote (Munoa et al., 2013a). Moreover, a complete family of oblique asymptotes (see $\lambda_{at,H}$ in Figure 5.2*b* and Figure 5.3*b*) is defined considering the order *l* of the different lobes:

$$\omega_{c,at,H} = \left(\frac{2l+1}{60}\right)\pi\, N\, Z. \tag{5.2-15}$$

Phase shift asymptote $\varepsilon_{at,H}$

The phase shift between modulations presents an asymptote at high chatter frequencies at $\varepsilon_{at,H} = \pi$, in the complete out of phase case (see Figure 5.2*a* and Figure 5.3*a*).

Nyquist plot

If a Nyquist plot (see Figure 5.2*d* and Figure 5.3*d*) is used to represent the possible values for the chatter frequency in the FRF of the main mode, the sense of the directional factor defines the operative "side" of the FRF. The maximum of the stability diagram has always the closest chatter frequency to the natural frequency and, therefore, it is close to the resonance at $\psi = -\pi/2$. The minimum coincides with the maximum real part. The phase shift between modulations can be calculated using the Nyquist diagram.

5.2.3   Double-period chatter at first lobe: Flip bifurcation

Flip chatter is originated basically when the chatter frequency and one of the modulated chatter frequencies are exciting the same mode. In Figure 5.2*c* and Figure 5.3*c* the chatter frequency is exciting the mode in the positive part of the FRF and the modulation with the harmonic -1, -3 or -5 (depending on the lobe) of the main frequency Ω is exciting the mode in the negative part.

In this approach the matrices in equation (5.2-4) will be truncated to consider only harmonic 0 and harmonic -1, which is considered enough to describe double period type chatter (Munoa et al., 2013; Zatarain et al., 2010):

$$\det\left(\begin{bmatrix} 1 & 0 \\ 0 & 1 \end{bmatrix} + \frac{K_t\, a\, Z}{\pi \sin \kappa} \begin{bmatrix} \Phi_{-1} & 0 \\ 0 & \Phi_0 \end{bmatrix} \begin{bmatrix} \beta_0 & \beta_{-1} \\ \beta_1 & \beta_0 \end{bmatrix}\right) = 0.$$

(5.2-16)

In this case the dynamics related to the -1 harmonic are the conjugate of the zero term.

$$\Phi_{-1} = \Phi_0\, e^{-j2\psi}.$$

(5.2-17)

Therefore the determinant can be rewritten:

$$\det\left(\begin{bmatrix} 1 & 0 \\ 0 & 1 \end{bmatrix} + \frac{K_t\, a\, Z}{\pi \sin \kappa} \Phi_0 \begin{bmatrix} e^{-j2\psi} & 0 \\ 0 & 1 \end{bmatrix} \begin{bmatrix} \beta_0 & \beta_{-1} \\ \beta_1 & \beta_0 \end{bmatrix}\right) = 0.$$

(5.2-18)

The eigenvalue problem can be solved easily:

$$\det\left(\begin{bmatrix} 1 & 0 \\ 0 & 1 \end{bmatrix} + \Delta \begin{bmatrix} e^{-j2\psi} & 0 \\ 0 & 1 \end{bmatrix} \begin{bmatrix} \beta_0 & \beta_{-1} \\ \beta_1 & \beta_0 \end{bmatrix}\right) = 0.$$

(5.2-19)

$$\Delta = \frac{K_t\, a\, Z}{\pi \sin \kappa} \Phi_0.$$

(5.2-20)

Operating:

$$\Delta = \frac{1}{\beta_{eq}} = \left(\frac{-\cos\psi \pm \sqrt{r_\beta^2 - \sin^2\psi}}{\beta_0\,(1-r_\beta^2)}\right) e^{j\psi},$$

(5.2-21)

where $r_\beta = |\beta_1| / |\beta_0| = |\beta_{-1}| / |\beta_0|$.

Following the methodology posed by the pioneers of the chatter research, an equivalent directional factor for the double period chatter can be defined. This factor is slightly different from the original definition of a geometrical directional factor, since it is weakly dependent on the phase ψ of the FRF.

$$\beta_{eq} = \frac{\beta_0\,(1-r_\beta^2)}{R(\psi)} e^{-j\psi},$$

(5.2-22)

where $R(\psi) := -\cos\psi \pm \sqrt{r_\beta^2 - \sin^2\psi}$.

This value β_{eq} is an imaginary number with a phase opposite to the phase of the FRF. The modulus depends on the zero order directional factor (β_0), the ratio between the harmonics of the directional factor (r_β) and a phase dependent function $R(\psi)$. The phase ψ changes abruptly between 0 to $-\pi$ close to the resonance but has a constant

value as it shifts away. Therefore, these equivalent directional factors also have a constant value when the frequency is far from the natural frequency and also when damping $\xi=0$.

Introducing the value of the equivalent directional factor, it is possible to define the depth of cut as a function of the real part of the oriented FRF ($\beta_{eq}\Phi_0$).

$$1-\frac{K_t Z}{\pi \sin \kappa} a\,\beta_{eq}\Phi_0 = 0 \quad \Rightarrow \quad a_f(\omega_c)=\frac{\pi \sin \kappa}{K_t\,Z\,\mathrm{Re}(\beta_{eq}(\omega_c)\,\Phi_0(\omega_c))}, \tag{5.2-23}$$

where $\mathrm{Im}(\beta_{eq}\Phi_0)=0$. In order to fulfill this condition, the phase dependent value $R(\psi)$ must be real valued.

Operating in the imaginary part of the oriented FRF, a relationship between the phase and the directional factor can be obtained:

$$\tan\psi = \frac{H}{G} = -\frac{\beta_{eq,\,I}}{\beta_{eq,\,R}}, \tag{5.2-24}$$

where $\Phi_0 = G + \mathrm{j}\,H$, $\beta_{eq} = \beta_{eq,R} + \mathrm{j}\,\beta_{eq,I}$.

Substituting this equation in the real part:

$$\mathrm{Re}(\beta_{eq}\Phi_0) = \left(\beta_{eq,R} + \frac{\beta_{eq,I}^2}{\beta_{eq,R}}\right)G = \frac{\left|\beta_{eq}\right|}{\cos\psi}\,G = \left|\beta_{eq}\right|\left|\Phi_0\right|. \tag{5.2-25}$$

An analytical expression can be obtained for double period chatter lobes with one dominant mode:

$$a_f = \frac{\pi \sin \kappa}{K_t\,Z\,|\beta_{eq}|\,|\Phi_0|} = -\frac{\pi \sin \kappa \left(\cos\psi \pm \sqrt{r_\beta^2 - \sin^2\psi}\right)}{K_t\,Z\,\beta_0\,(1-r_\beta^2)\,|\Phi_0|}. \tag{5.2-26}$$

Equation (5.2-26) brings along different possible lobe shapes depending on the sign of the different terms of the equation (see Table 5.2).

		$\beta_0 < 0$	$\psi \in [\psi(A_f),0]$	$\psi(A_f) > -\pi/2$	$\omega \in [0,\,\omega(A_f)]$
$r_\beta < 1$					
		$\beta_0 > 0$	$\psi \in [-\pi,\psi(A_f)]$	$\psi(A_f) < -\pi/2$	$\omega \in [\omega(A_f),\infty]$
$r_\beta > 1$	-		$\psi \in [-\pi,0]$	-	$\omega \in [0,\infty]$

Table 5.2: Flip lobe casuistry and characteristics.

If $r_\beta < 1$, an intersection point A_f exists in the flip lobe. In this case, the flip lobe is only defined for higher ($\beta_0 > 0$) or lower ($\beta_0 < 0$) values of this A_f point. In this case, the flip

lobe is composed of two branches: an upper branch related to $\left(\cos\psi + \sqrt{r_\beta^2 - \sin^2\psi}\right)$ and a lower branch related to $\left(\cos\psi - \sqrt{r_\beta^2 - \sin^2\psi}\right)$.

If $r_\beta > 1$, there is no intersection point and the lobe is not limited to a single quadrant of ψ (see Table 5.2). In this case, only one of the branches produces real results, depending on the sign of β_0.

In most practical cases $r_\beta < 1$, although $r_\beta > 1$ is not only possible but quite frequent. Figure 5.4 shows an example (see Table 5.3 for conditions) of the different values that β_0 and β_1 can take under different mode directions. In this example there are two ranges of values between 20º and 60º and between 140º and 180º where $r_\beta > 1$.
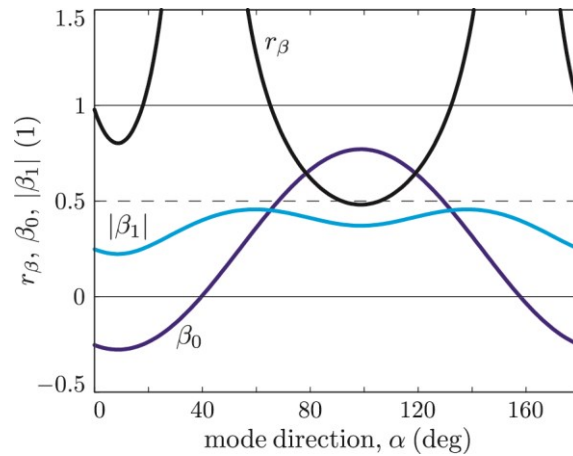
Figure 5.4: r_β, β_0, $|\beta_1|$ values as a function of mode direction α, according to cutting conditions defined in Table 5.3. The value of r_β is bigger than 0.5 for almost any mode direction (flip dominance) and bigger than 1 at two wide mode direction ranges (single branch flip shape).

Tool			
Diameter (D)	*Number of flutes (Z)*	*Lead angle (κ)*	*Helix angle*
20mm	3	90	0
Cutting conditions & Coefficients			
Engagement	*Feed Direction*	*K_t [N/mm²] $\quad K_r$*	*K_a*
10mm (Down-milling)	(1,0,0)	804 $\qquad$ 0.314	0.15
Dynamic Parameters			
Mode $\quad$ *f_n [Hz]*	*ζ [%]*	*k [N/µm] $\quad$ m [kg]*	*Orientation*
1 $\qquad$ 178	1	19.78 $\qquad$ 15.81	From (1,0,0) to (-1,0,0)

Table 5.3: Cutting conditions and dynamic parameters for β_0, β_1 and r_β calculation as a function of the mode direction.

Equation (5.2-26) can also be defined as a function of the dimensionless chatter frequency $\lambda_f = m\Omega/2/\omega_n$. This way a closed analytical expression is obtained for the flip lobe.

$$a_f(\lambda_f) = -\frac{\pi k \left[(1 - \lambda_f^2) \pm \sqrt{r_\beta^2 (1 - \lambda_f^2)^2 - 4(1 - r_\beta^2)\xi^2 \lambda_f^2} \right] \sin\kappa}{K_t Z \beta_0 (1 - r_\beta^2)}.$$

(5.2-27)

where $\beta_0 > 0$ ($\beta_0 < 0$) induces $\lambda_f > 1$ ($\lambda_f < 1$). Examples of flip lobes are shown in Figure 5.2*c* ($r_\beta < 1$, $\beta_0 < 0$, $\lambda_f < 1$) and Figure 5.3*c* ($r_\beta < 1$, $\beta_0 > 0$, $\lambda_f > 1$). On the other hand, when $r_\beta > 1$ the flip shape is different, as shown in Figure 5.5 (see Table 5.4 for simulation conditions).

Tool			
Diameter (D)	*Number of flutes (Z)*	*Lead angle (κ)*	*Helix angle*
20mm	3	90	0
Cutting conditions & Coefficients			
Engagement	*Feed Direction*	K_t *[N/mm²]* K_r	K_a
10mm (Up-milling)	(1,0,0)	804 0.314	0.15
Dynamic Parameters			
Mode f_n *[Hz]*	ζ *[%]*	k *[N/μm]* m *[kg]*	*Orientation*
1 178	1	19.78 15.81	$(\cos(60), \sin(60), 0)$

Table 5.4: Cutting conditions and dynamic parameters for $r_\beta > 1$ case.

The spindle speed as a function of the dimensionless chatter frequency λ_f yields:

$$N(\lambda_f) = \left(\frac{60\,\lambda_f}{\pi Z\,m}\,\omega_n \right).$$

(5.2-28)

When $r_\beta < 1$, the chatter frequency ω_c is always below the natural frequency ω_n for $\beta_0 < 0$ and over it for $\beta_0 > 0$ (see Figure 5.2*a* and Figure 5.3*b*). When the spindle speed approaches the intersection point A_f, the chatter frequency is very similar to the natural frequency of the mode. On the other hand, when $r_\beta > 1$, the chatter frequency can take any value from 0 to ∞ (see Table 5.2), crossing the natural frequency line close to the spindle speed corresponding to the minimum B_f (see Figure 5.5*a*). It is also worth remarking that, in the N vs. ω_c plot, the chatter frequency coincides with the asymptote of the Hopf chatter frequency $\omega_{c,at,H}$ defined in (5.2-15).

The phase shift between modulations is given by

$$\varepsilon_f = m\pi,$$

(5.2-29)

where $m = 1, 3, 5, \dots$

The phase shift ε_f is independent from the spindle speed or the chatter frequency, being always in complete out of phase. Two important points can be analyzed in detail: the intersection point (A_f) and the point with the minimum stability (B_f).
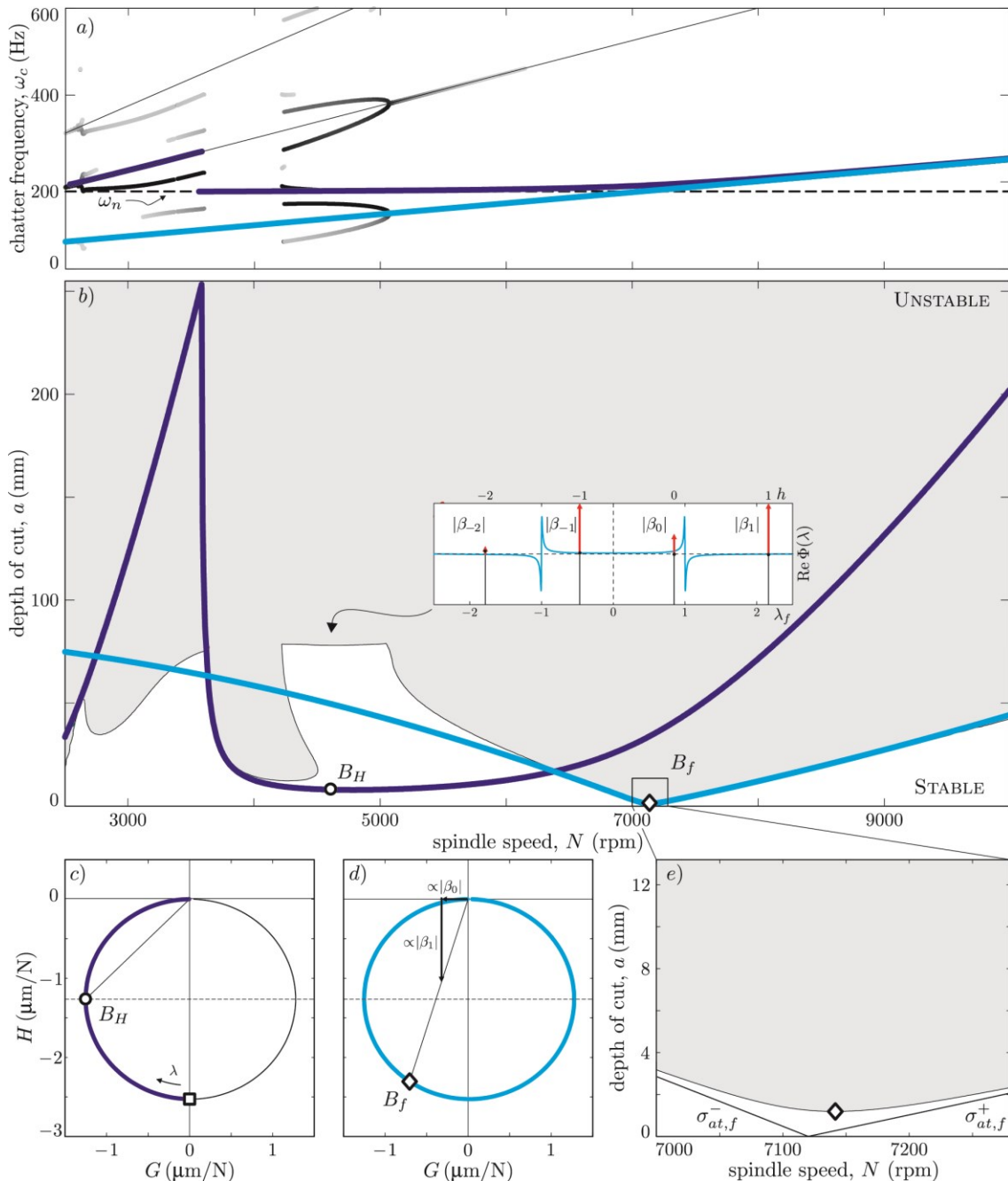
Figure 5.5: Cutting stability limit when $r_\beta > 1$ calculated by different models: analytical expressions for Hopf (dark blue), analytical expressions for flip (light blue) and semi-discretization (black and shaded). $r_\beta > 1$ cases result in significant deviations of the analytical formulae due to harmonic truncation. a) chatter frequency ω_c; b) depth of cut a; c) Nyquist plot with Hopf minutiae; d) Nyquist plot with flip minutiae.

Intersection point (A_f) for $r_\beta < 1$

The intersection point (A_f) defines the starting point of the flip lobe (only when $r_\beta < 1$) and it is associated with the point which has only one root in equation (5.2-21), that is, the point at which the phase ψ corresponds to the arcsine of the ratio between harmonics r_β.

$$r_\beta^2 = \sin^2 \psi_{Af} . \tag{5.2-30}$$

which leads to

$$\psi_{Af} = \begin{cases} -\pi + \arcsin r_\beta, & \beta_0 > 0, \quad \cos \psi_{Af} < 0, \\ -\arcsin r_\beta, & \beta_0 < 0, \quad \cos \psi_{Af} > 0. \end{cases} \tag{5.2-31}$$

Note that, if the FRF is represented in a Nyquist plot, this intersection point can be found graphically (see Figure 5.2*e* and Figure 5.3*e*). This is achieved through the sine of the phase ψ_{Af}, that is, representing the harmonic -1 of the Fourier development of the directional factor in the vertical axis and representing the harmonic 0 at an angle such that its horizontal projection equals the length of harmonic -1. The phase ψ_{Af} is the angle between these two vectors (Zatarain et al., 2010).

It is possible to obtain the dimensionless chatter frequency λ_{Af} of the intersection point A_f taking into account the next expression.

$$\tan \psi_{Af} = -\frac{2\,\xi\,\lambda_{Af}}{1 - \lambda_{Af}^2} = \begin{cases} \dfrac{r_\beta}{\sqrt{1 - r_\beta^2}}, & \beta_0 > 0, \quad \cos \psi_{Af} < 0, \quad \lambda_{Af} > 1, \\ \dfrac{-r_\beta}{\sqrt{1 - r_\beta^2}}, & \beta_0 < 0, \quad \cos \psi_{Af} > 0, \quad \lambda_{Af} < 1. \end{cases} \tag{5.2-32}$$

Operating with these formulae, the frequency of the intersection point A_f (see Figure 5.2*c*, Figure 5.2*f*, Figure 5.3*c* and Figure 5.3*f*) can be defined as a function of the damping ratio and the ratio between harmonics.

$$\lambda_{Af} = \begin{cases} \sqrt{\sqrt{1 + \left(1 - r_\beta^2\right)\left(\dfrac{\xi}{r_\beta}\right)^2} + \sqrt{1 - r_\beta^2}\left(\dfrac{\xi}{r_\beta}\right)}, & \beta_0 > 0, \\ \sqrt{\sqrt{1 + \left(1 - r_\beta^2\right)\left(\dfrac{\xi}{r_\beta}\right)^2} - \sqrt{1 - r_\beta^2}\left(\dfrac{\xi}{r_\beta}\right)}, & \beta_0 < 0. \end{cases} \tag{5.2-33}$$

And finally the depth of cut associated with this point can be obtained from equation (5.2-27).

$$a_{Af} = \frac{4\,\pi\,k\,\xi\,\lambda_{Af} \sin \kappa}{K_t\,Z\,\beta_0 \sin 2\psi_{Af}} . \tag{5.2-34}$$

Minimum depth f cut (B_f)

The other important point is the point related to the minimum depth of cut (B_f). When $r_\beta < 1$ and the milling process is not highly interrupted, the minimum depth of cut can be approximated by using the intersection point (A_f). However, when the cutting process is highly interrupted this approximation drives to big inaccuracies.

To obtain the real stability limit, it is necessary to derive the depth of cut defined in equation (5.2-27) with respect to the dimensionless chatter frequency. The dimensionless frequency related to the minimum stability can be obtained equating the derivative to 0. Only the branch that is defining the minimum stability is taken into account in this process.

$$\frac{\partial}{\partial \lambda_f}\left(1 - \lambda_f^2 + \sqrt{r_\beta^2\left(1 - \lambda_f^2\right)^2 - 4\left(1 - r_\beta^2\right)\xi^2\, \lambda_f^2}\,\right) = 0\,.$$

(5.2-35)

Solving the equation, an approximation of the minimum is obtained:

$$\lambda_{Bf} \cong \begin{cases} \sqrt{1 + \left(\dfrac{\xi}{r_\beta}\right)^2} + \dfrac{\xi}{r_\beta}, & \beta_0 > 0, \\[4mm] \sqrt{1 + \left(\dfrac{\xi}{r_\beta}\right)^2} - \dfrac{\xi}{r_\beta}, & \beta_0 < 0. \end{cases}$$

(5.2-36)

If the phase of this point is analyzed, an impressive result is achieved, namely, the minimum of the stability is obtained when the tangent of the phase is equal to the harmonic ratio. Hence, in this point the relation between the imaginary and real part of the FRF is exactly the ratio between different harmonics of the directional factors.

$$\tan \psi_{Bf} = \frac{-2\,\xi\,\lambda_{Bf}}{1 - \lambda_{Bf}^2} \cong \begin{cases} r_\beta, & \beta_0 > 0, \\ -r_\beta, & \beta_0 < 0. \end{cases}$$

(5.2-37)

Whereas for the intersection point (A_f) the ratio between harmonics was equal to the sine of the phase ψ_{Af}, in the flip minimum (B_f) it is equal to the tangent of the phase ψ_{Bf} and it can be calculated graphically in the Nyquist plot (see Figure 5.2e, Figure 5.3e and Figure 5.5d), in a similar way as the intersection point case. The harmonic 0 is plotted in the vertical axis and the harmonic -1 in the horizontal axis. The angle these two vectors form is equal to ψ_{Bf}. It has to be noted that for $r_\beta < 1$ case, the minimum point has always a phase ψ_{Bf} smaller than $-3\pi/4$ ($\beta_0 > 0$) or bigger than $-\pi/4$ ($\beta_0 < 0$), whereas for $r_\beta > 1$ ψ_{Bf} is between $-\pi/4$ and $-3\pi/4$ (normally close to $-\pi/2$).

Finally, the minimum depth of cut a_{Bf} (see Figure 5.2c, Figure 5.2f, Figure 5.3c, Figure 5.3f, Figure 5.5b and Figure 5.5e) can be defined introducing the dimensionless chatter frequency in the analytic equation.

$$a_{Bf} \cong \begin{cases} \dfrac{2\pi k \xi \lambda_{Bf} \sin\kappa}{K_t Z \beta_0 r_\beta}, & \beta_0 > 0, \\[4mm] -\dfrac{2\pi k \xi \lambda_{Bf} \sin\kappa}{K_t Z \beta_0 r_\beta}, & \beta_0 < 0. \end{cases}$$

(5.2-38)

Flip lobe asymptotes $a_{at,f}$

Corpus and Endres (2000) found that these double period lobes have two asymptotes corresponding with the no damped case. Eliminating the relative damping inside equation (5.2-27), an analytical formulation can be obtained for these two asymptotes.

$$a_{at,f}(\lambda_f, \xi = 0) = \pm \frac{\pi k \sin\kappa}{K_t Z \beta_0 (1 \pm r_\beta)} (1 - \lambda_f^2).$$

(5.2-39)

These two asymptotes define the boundaries of the zone where the double period chatter can grow. Equation (5.2-39) is valid for both $r_\beta < 1$ and $r_\beta > 1$ cases. Their dimensionless form can be visualized in Figure 5.2f, Figure 5.3f and Figure 5.5e as $\sigma^-_{at,f}$ and $\sigma^+_{at,f}$:

$$\sigma^-_{at,f} = -\frac{(1 - \lambda_f^2)}{4\xi(1 - r_\beta)},$$
$$\beta_0 > 0,$$
$$\sigma^+_{at,f} = -\frac{(1 - \lambda_f^2)}{4\xi(1 + r_\beta)},$$

(5.2-40)

$$\sigma^-_{at,f} = \frac{(1 - \lambda_f^2)}{4\xi(1 - r_\beta)},$$
$$\beta_0 < 0.$$
$$\sigma^+_{at,f} = \frac{(1 - \lambda_f^2)}{4\xi(1 + r_\beta)},$$

(5.2-41)

They are joining always in the same point corresponding with a zero depth of cut and a spindle speed related to a tooth passing frequency coincident with $(2/m)$ times the natural frequency.

When $r_\beta < 1$, the two asymptotes cover the same spindle speed range, whereas when $r_\beta > 1$, each asymptote covers a different speed range over and below the intersection point at $\Omega = (2/m)\omega_n$.

5.2.4   Absolute depth of cut limit

It is interesting to know which lobe type (Hopf or flip) defines the absolute minimum stability. Equating Hopf a_{BH} (5.2-13) and flip a_{Bf} (5.2-38) limit depths of cut, it yields:

$$2(1+\xi) = \frac{\lambda_{Bf}}{r_\beta}, \quad \beta_0 > 0,$$

$$2(1-\xi) = \frac{\lambda_{Bf}}{r_\beta}, \quad \beta_0 < 0.$$

$$(5.2\text{-}42)$$

The dominance of flip or Hopf lobes in the stability diagram depends only on two parameters: the damping ratio ξ and the ratio between harmonics r_β. Depending on the relation between these two parameters it is possible to know if the minimum in the stability diagram is delimited by the Hopf or the flip type lobes. Operating:

$$\beta_0 > 0, \quad r_\beta = \frac{1+2\xi}{2+2\xi},$$

$$(5.2\text{-}43)$$

$$\beta_0 < 0, \quad r_\beta = \frac{1-2\xi}{2-2\xi}.$$

When the conditions in equation (5.2-43) are met, the Hopf and flip lobes present the same minimum. These conditions depend on two variables only: r_β and, to a lesser extent, ξ. As the ratio between harmonics ($r_\beta = |\beta_1| / |\beta_0|$) becomes higher (more interrupted cutting process) the flip type lobes have lower minimum a than Hopf lobes. The limit at which flip lobes become more limiting than Hopf lobes occurs approximately when the harmonic β_1 turns bigger than half of the main harmonic β_0 ($r_\beta > 0.5$). This is exactly true when the relative damping $\xi = 0$ and it varies according to Figure 5.6 as the damping is increased.
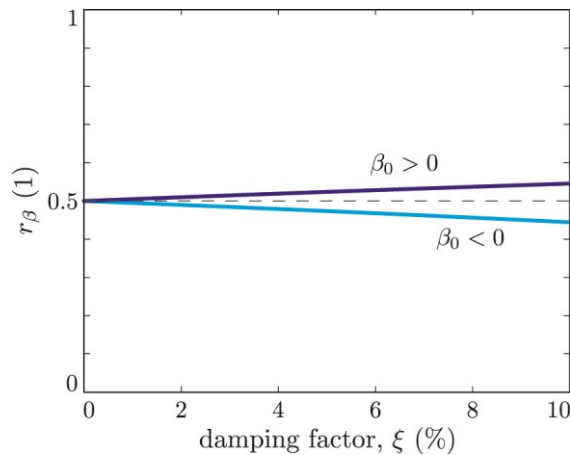
Figure 5.6: r_β threshold at which flip lobes set a lower minimum than Hopf lobes. This occurs when r_β becomes roughly bigger than 0.5 (this is exactly true for $\xi=0$).

The harmonics of the directional factor β_0 and β_1 depend on the tooth geometry, the immersion angle and the mode direction with respect to the feed direction. The value of the harmonics as a function of the mode direction is depicted in Figure 5.4. Considering the ratio between harmonics r_β, the conditions at which flip lobes become more limiting than Hopf lobes can be obtained. In the example in Figure 5.4, flip lobes are more limiting for every mode direction except for a narrow region around 100º.

5.3   VALIDATION

The developed formulae have been correlated with the semi-discretization method, which has confirmed its accuracy and rapidness. A vast set of simulations was carried out under different cutting conditions and dynamic parameters, with the basic simulation defined according to Table 5.1 (case 2). Parameters like mode orientation, immersion, cutting direction and modal damping were combined in order to analyze stability prediction under different directional factors and damping ratios. The error incurred in Hopf and flip estimation is also presented as:

$$Error_H = \frac{\left| a_{BH,S} - a_{BH,A} \right|}{a_{BH,S}},$$

$$Error_f = \frac{\left| a_{Bf,S} - a_{Bf,A} \right|}{a_{Bf,S}}.$$

(5.3-1)

The results are shown in Table 5.5:

Mode orientation	Immersion	Direction	β_0	$|\beta_1|$	r_β	Damping (%)	$a_{BH,S}$ (mm)	$a_{BH,A}$ (mm)	$Error_H$ (%)	$a_{Bf,S}$ (mm)	$a_{Bf,A}$ (mm)	$Error_f$ (%)
0	5	Up	0.004	0.004	0.998	1	267.9	269.1	**0.4**	133.6	134.8	**0.9**
						5	1372	1399	**2**	675.7	701.6	**3.8**
						10	2858	2931	**2.6**	1360	1475	**8.5**
	45	Up	0.295	0.252	0.854	1	3.6	3.53	**1.9**	2.14	2.07	**3.3**
						5	20.24	18.35	**9.3**	10.74	10.85	**1**
						10	47.12	38.45	**18.4**	22.37	23.01	**2.9**
	90	Up	0.747	0.381	0.51	1	1.41	1.39	**1.41**	1.45	1.38	**2.8**
						5	7.58	7.25	**4.4**	7.61	7.46	**2**
						10	16.44	15.18	**7.7**	16.6	16.44	**1**
	135	Up	0.698	0.429	0.614	1	1.51	1.49	**1.3**	1.25	1.22	**2.4**
						5	8.23	7.75	**5.8**	6.56	6.52	**0.6**
						10	18.12	16.23	**10.4**	14.28	14.13	**1.1**
	180	Slotting	0.493	0.409	0.829	1	2.16	2.11	**2.3**	1.3	1.28	**1.5**
						5	12.43	10.97	**11.7**	6.7	6.7	**0**
						10	29.55	22.98	**22.2**	14.22	14.22	**0**

						n	$a_{BH,S}$	$a_{BH,A}$	$Error_H$	$a_{Bf,S}$	$a_{Bf,A}$	$Error_f$
60	5	Up	0.057	0.057	0.997	1	18.14	18.18	**0.2**	9.11	9.11	**0**
						5	93.14	94.5	**1.5**	45.56	47.5	**4.3**
						10	194.8	198	**1.6**	92.1	99.8	**8.4**
	45	Up	0.057	0.057	0.997	1	3.3	3.23	**2.1**	1.94	1.93	**0.5**
						5	18.56	16.8	**9.5**	10.1	10.1	**0**
						10	43.22	35.2	**18.6**	20.81	21.43	**3**
	90	Up	0.133	0.434	3.27	1	12.17	7.85	**35.5**	1.2	1.19	**0.8**
						5	50.17	40.81	**18.7**	6.06	6.03	**0.5**
						10	60.7	85.5	**40.9**	12.15	12.24	**0.7**
	135	Up	0.057	0.501	8.77	1	14.93	18.21	**22**	1.04	1.03	**1**
						5	25.83	94.66	**266.5**	5.14	5.17	**0.6**
						10	33.5	198.3	**491.9**	10.27	10.4	**1.3**
	180	Slotting	0.493	0.724	1.47	1	2.29	2.11	**7.9**	0.75	0.72	**4**
						5	33.15	10.97	**66.9**	3.68	3.68	**0**
						10	37.85	22.98	**39.3**	7.61	7.62	**0.1**
120	5	Up	-0.02	0.020	0.997	1	51.46	50.98	**0.9**	26.01	25.56	**1.7**
						5	256.6	244.6	**4.7**	128.6	122.8	**4.5**
						10	511.4	463.5	**9.4**	257.9	233.6	**9.4**
	45	Up	-0.25	0.200	0.81	1	4.15	4.13	**0.5**	2.57	2.54	**1.2**
						5	20.32	19.82	**2.5**	12.24	12.08	**1.3**
						10	39.64	37.56	**5.2**	23.3	22.73	**2.4**
	90	Up	-0.14	0.330	2.39	1	7.6	7.32	**3.7**	1.55	1.54	**0.6**
						5	41.1	35.13	**14.5**	7.54	7.56	**0.3**
						10	87.67	66.55	**24.1**	14.32	14.8	**3.4**
	135	Up	0.354	0.527	1.49	1	3.18	2.94	**3.4**	1	0.98	**2**
						5	24.76	15.27	**6.5**	5.06	5.05	**0.2**
						10	56.66	32.15	**43.3**	10.47	10.45	**0.2**
	180	Slotting	0.493	0.445	0.903	1	2.17	2.11	**2.8**	1.2	1.17	**2.5**
						5	12.75	10.97	**13.9**	6.13	6.12	**0.2**
						10	56.66	22.98	**59.4**	12.92	12.93	**0.1**

Table 5.5: Validation of the analytical expressions versus semi-discretization model. $a_{BH,S}$: Hopf minimum prediction in semi-discretization simulation, $a_{BH,A}$: Hopf minimum prediction with analytical formulae, $Error_H$: Error incurred in Hopf minimum estimation, $a_{Bf,S}$: flip minimum prediction in semi-discretization simulation, $a_{Bf,A}$: flip minimum prediction with analytical formulae, $Error_f$: Error incurred in flip minimum estimation.

The minutiae of the lobes are satisfactorily predicted by the analytical formulae. It is noticeable that all r_β values are over 0.5 (flip dominance) even if the immersion has been swept from very small values to 100% immersion. This indicates that flip importance is not conditioned by the milling immersion as it has been stated in previous researches, but by the oscillating nature of the cutting forces for a specific milling operation.

Flip minimum prediction error with respect to semi-discretization simulation is always within 10% for every studied case. The error becomes more important when damping is increased or when immersion becomes smaller. For damping values $\xi < 5\%$, which are the vast majority of the practical cases, the error range is reduced to less than 5%.

Regarding Hopf minimum error, every $r_\beta < 1$ simulation is within 25% error. In this case the error also increases as damping is increased. For damping values $\xi < 5\%$, Hopf minimum error drops to less than 15%. When $r_\beta > 1$, the developed analytical formulae for Hopf minimum determination are not valid any more due to harmonic truncation. This is mainly due to harmonic -1, which is exciting the mode in the negative part of the FRF at higher speeds in lobe $l=0$, in an analogue way as it happens with flip chatter. As harmonic -1 becomes larger, the effect on the stability limit is more noticeable.

Therefore, the following unexpected conclusion is drawn: flip minimum analytical expression is fairly more accurate than Hopf minimum. The reason for this is that two harmonics 0 and -1 are considered for flip calculation, whereas in Hopf the truncation is done considering only harmonic 0.

Concerning the complete analytical curves correlation (see Figure 5.2 and Figure 5.3), typical slight deviations due to harmonic truncation of the analytical formulae of the flip lobes can be observed. As the ratio between the tooth passing frequency and the natural frequency ν becomes smaller, the deviation of the analytical formulae is bigger due to the influence of truncated higher harmonics of the directional factor. This is the reason for observing greater deviation in the negative directional factor $\beta_0 < 0$ case (see Figure 5.2c). In general, Hopf lobes also show slight deviations due to the interrupted nature of the cut.

However, both flip and Hopf lobe approximation is not accurate when $r_\beta > 1$, where the error incurred can be really significant (Figure 5.7). This $r_\beta > 1$ case aside, even if the approximation is not completely precise, it is good enough to have a clear picture of the stability of the system and select proper scanning limits for the classical simulation methods (time domain, semi-discretization,…).
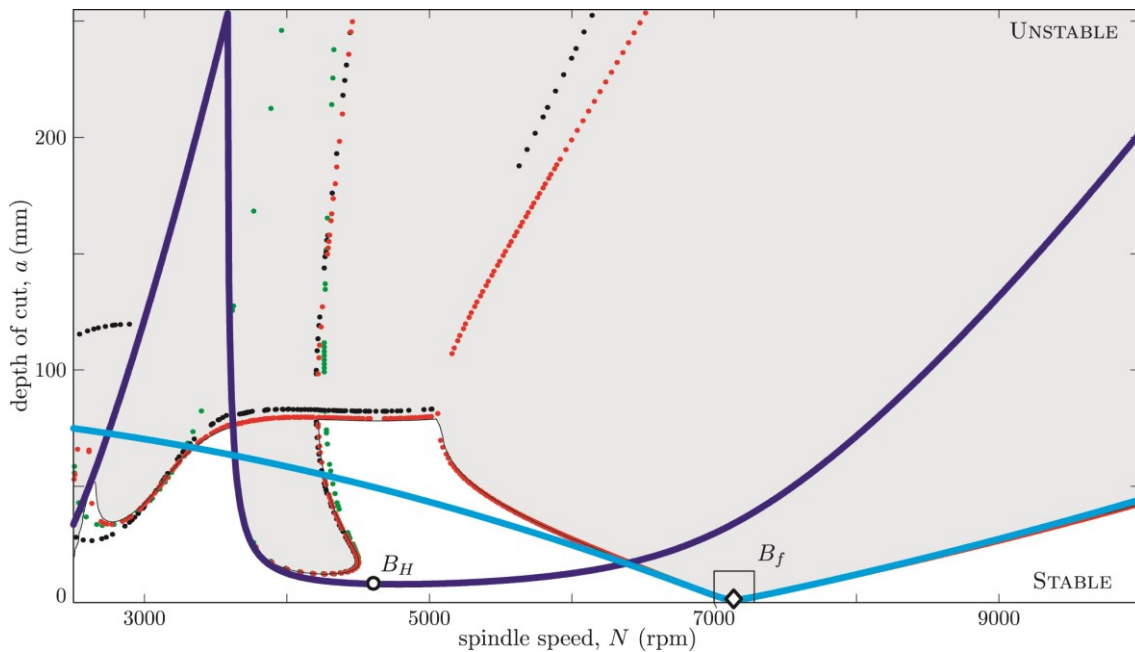
Figure 5.7: Cutting stability limit when $r_\beta > 1$ calculated by different models for conditions specified in Table 5.4: analytical expressions for Hopf (dark blue), analytical expressions for flip (light blue), multi-frequency -1 harmonic (green), multi-frequency -2 harmonics (black), multi-frequency -3 harmonics (red), semi-discretization (black and shaded). $r_\beta > 1$ cases result in significant deviations of the analytical formulae due to harmonic truncation.

5.4   CONCLUSIONS

Analytical expressions have been developed in order to describe Hopf and flip limits in a simple manner for a dominant mode system. Flip instability has been solved in a similar way to the Hopf limit, introducing an equivalent directional factor β_{eq}, which is weakly dependent on the machine dynamic response. The novel analytical expressions developed in this work are those related to the flip minimum a_{Bf} and the absolute depth of cut limit calculation.

The performed development leads to handy discoveries to assess chatter limits according to the values of r_β, that is, the relation between the harmonic 1 and harmonic 0 of the directional factor. Thus, flip dominates over Hopf for r_β values bigger than 0.5 roughly and, when r_β turns bigger than 1, flip lobes become different from the currently known in terms of shape and features.

The minutiae of both limit lobes (flip and Hopf) have been identified and shown in comparable graphs.

These formulae are useful to understand Hopf and flip instabilities in a deeper way, with a clear insight of the main parameters affecting stability. Moreover, this approximate limit identification can be useful to speed up classic time and semi-discretization stability models, whose calculation time depends to a great extent on the boundary conditions defined when launching the simulation.

The analytical expressions obtained in this work have been compared with the semi-discretization method, obtaining a good approximation for every case except for $r_\beta > 1$, where harmonic truncation introduces a significant error and only flip lobe minimum determination formula remains accurate. Both flip and Hopf lobes are affected by harmonic truncation, being low speeds of flip lobes and especially high speeds of Hopf lobes the most sensitive to truncation.

Until now, researchers have claimed the accuracy of ZOA solution for large immersion milling processes, however, in this work it was observed that a large immersion process simulation by ZOA can result in very inaccurate solutions, not only by flip lobe presence but also due to significant changes at the Hopf lobe. Therefore, the key point for ZOA validity assessment is the value of r_β, which gives a measure of how oscillating the milling force is.

Contribution 4:

Several analytical expressions have been developed in order to describe Hopf and flip limits in a simple manner for a dominant mode system. Among them, the expressions related to the flip minimum analytical expression a_{Bf} and the absolute minimum in the stability diagram (considering Hopf and flip limits) had never been previously described.

The formulae described in this chapter are useful to understand Hopf and flip instabilities in a deeper way, with a clear insight of the main parameters affecting the stability. Moreover, this approximate limit identification can be useful to speed up classic time and semi-discretization stability models, whose calculation time depends to a great extent on the boundary conditions defined when launching the simulation.

The results have been correlated with the semi-discretization prediction method, resulting in a good approximation with slight deviations that become larger as the process becomes more interrupted (r_β grows) and as damping increases.

Contribution 5:

The importance of the directional factor harmonic ratio r_β has been highlighted. Thus, flip dominates over Hopf for r_β values bigger than 0.5 roughly and, when r_β turns bigger than 1, flip lobes become different from the currently known in terms of shape and features.

Contribution 6:

Although researchers had claimed the accuracy of ZOA solution for large immersion milling processes, it was observed that a large immersion process simulation by ZOA can result in very inaccurate solutions, not only by flip lobe presence but also due to significant changes at the Hopf lobe. Therefore, the key point for ZOA validity assessment is the value r_β, which gives a measure of how oscillating the milling force is.

Related Publications:

Iglesias, A., Munoa, J., Ciurana, J., & Dombovari, Z. (2015). Analytical expressions for chatter analysis in milling operations with one dominant mode. *Journal of Sound and Vibration*, submitted.

Chapter 6

Analytical Stability Model for Interrupted Milling Processes

The ZOA method developed by Altintas and Budak (1995) is a basic reference in stability calculation, being the most cited paper related to chatter research. It features an unbeatable efficiency, since it offers an acceptable prediction for most milling processes in a very short calculation time. Moreover, it can handle experimental FRFs, without the need of curve fitting to obtain dynamic parameters.

Although it shows a good accuracy for continuous or fairly continuous milling processes, it suffers from important pitfalls when dealing with interrupted milling processes, since it cannot predict the appearance of flip type lobes. This was clearly observed in Chapter 5, where the analytical formulae developed could predict new instable areas not foreseen by ZOA.

In this chapter, this well-known single frequency method has been improved including an analytical calculation of the flip type lobes in an analogue way as the Hopf chatter. Thus, the high simulation speed of the original method is maintained, while increasing its accuracy when dealing with interrupted milling processes.

The solution of the method ends up with simple expressions describing depth of cut a and spindle speed N:

6.1   APPROXIMATED ANALYTICAL SOLUTIONS

6.1.1   Hopf Bifurcation: Zero Order Approximation (ZOA).

If only the zero order term is considered in the milling stability equation (2.3-62), a fast analytical solution is possible to trace the linear stability border related to Hopf-bifurcation. This simplification provides a spindle speed independent equation and therefore it can be solved considering different chatter frequencies and obtaining for each one the corresponding depth of cut and spindle speed (Altintas and Budak, 1995) as described in

$$\{p_0\} = \left(\frac{K_t\, a}{\sin \kappa}\right)(1 - e^{-j\omega_c \tau})\left[\Phi_0\right]\left[A_0\right]\{p_0\},$$

(6.1-1)

$[A_0]$ matrix is calculated as described in equation (2.3-40):

Following the development by Altintas and Budak (1995), the stability analysis drives to an eigenvalue problem where the eigenvalues ($\Lambda = \Lambda_R + j\Lambda_I$) can be related with the maximum stable depth of cut and different cutting speeds:

$$a_{\lim} = -\frac{\pi \sin \kappa\, \Lambda_R}{Z\, K_t}\left(1 + \left(\frac{\Lambda_I}{\Lambda_R}\right)^2\right),$$

(6.1-2)

$$N = \frac{60}{Z\,\tau} = \frac{60\,\omega_c}{Z\,(\varepsilon + 2\,\pi\, l)}.$$

(6.1-3)

6.1.2   Flip Bifurcation: New analytical approach

The period doubling chatter related to flip bifurcation produces an independent family of lobes with some particularities that can be useful to define the stability boundaries. The main characteristic of this double period chatter is that there is a linear relationship between the chatter frequency and the tooth passing frequency. When a double period or flip bifurcation appears, the chatter frequency keeps a linear relationship with respect to the main frequency Ω (Davies et al., 2000):

$$2\,\omega_c = m\,\Omega.$$

(6.1-4)

In terms of frequency domain, the double period chatter or the flip bifurcation happens when the chatter frequency and one of its modulated chatter frequencies are exciting

the same mode. Only the odd modulated chatter harmonics can create the double period chatter. The regenerative term explains this effect. This term can be rewritten as a function of the involved harmonic and is null for all the even harmonics,

$$f = 1 - e^{-j\omega_c\tau} = 1 - e^{-j\omega_c\frac{2\pi}{\Omega}} = 1 - e^{-jm\pi} = \begin{cases} 2, & \text{if } m = 1, 3, 5, \dots \\ 0, & \text{otherwise.} \end{cases} \tag{6.1-5}$$

Considering equation (6.1-5), equation (2.3-63) becomes:

$$\begin{Bmatrix} \{p_{-h}\} \\ \vdots \\ \{p_0\} \\ \vdots \\ \{p_h\} \end{Bmatrix} = \left(\frac{K_t\, a\, Z}{\pi \sin\kappa} \right) \begin{bmatrix} [\Phi_{-h}] & \cdots & [0] & \cdots & [0] \\ \vdots & \ddots & \vdots & \ddots & \vdots \\ [0] & \cdots & [\Phi_0] & \cdots & [0] \\ \vdots & \ddots & \vdots & \ddots & \vdots \\ [0] & \cdots & [0] & \cdots & [\Phi_h] \end{bmatrix} \begin{bmatrix} [\alpha_0] & \cdots & [\alpha_{-h}] & \cdots & [\alpha_{-2h}] \\ \vdots & \ddots & \vdots & \ddots & \vdots \\ [\alpha_h] & \cdots & [\alpha_0] & \cdots & [\alpha_{-h}] \\ \vdots & \ddots & \vdots & \ddots & \vdots \\ [\alpha_{2h}] & \cdots & [\alpha_h] & \cdots & [\alpha_0] \end{bmatrix} \begin{Bmatrix} \{p_{-h}\} \\ \vdots \\ \{p_0\} \\ \vdots \\ \{p_h\} \end{Bmatrix},$$

$$\tag{6.1-6}$$

where

$$[\Phi_h] = [\Phi(j\,(\omega_c + h\Omega))] = \left[\Phi\left(j\omega_c\left(1 + \frac{2h}{m} \right) \right) \right]. \tag{6.1-7}$$

The eigenvalue problem is now independent from tooth passing frequency and spindle speed. Therefore, it is possible to obtain the limit of the double period chatter scanning the frequency range like in the method proposed by Altintas and Budak (1995) or, more straightforward, scanning the spindle speed range. For each frequency or spindle speed the eigenvalue problem is solved.

The eigenvalues of equation (6.1-6) can be calculated through its determinant:

$$\det([I] + \Lambda[\Phi][\alpha]) = 0. \tag{6.1-8}$$

These eigenvalues should fulfill these conditions to define a border of the stability lobe:

$$\Lambda = \Lambda_R + j\Lambda_I = -\frac{K_t\, a\, Z}{\pi \sin\kappa}, \tag{6.1-9}$$

$\Lambda_R < 0$, $\Lambda_I = 0$.

The stability limits for double period chatter are defined using the eigenvectors with only real values. In fact, the different double period lobes are obtained scanning different lines (*m*) in the chatter frequency diagram (*m*=1,3,5,...).

$$a_{\lim} = -\frac{\pi \sin\kappa}{Z\, K_t} \Lambda_R, \tag{6.1-10}$$

$$N = \frac{60\, \omega_c}{\pi\, Z\, m}, \tag{6.1-11}$$

where *m* = 1, 3, 5, ...

6.1.3   Combined analytical frequency method

Hopf and flip analytical methods can be combined to create a new analytical frequency domain algorithm. This new method improves the accuracy of the ZOA but the main advantages are maintained: experimental FRF can be introduced directly and the calculation time is not severely increased. The combined method adds double period chatter lobes (flip bifurcation) to the approximated solution (Hopf bifurcation) proposed by the ZOA. The algorithm is described in Figure 6.1 and it can be divided in four steps:
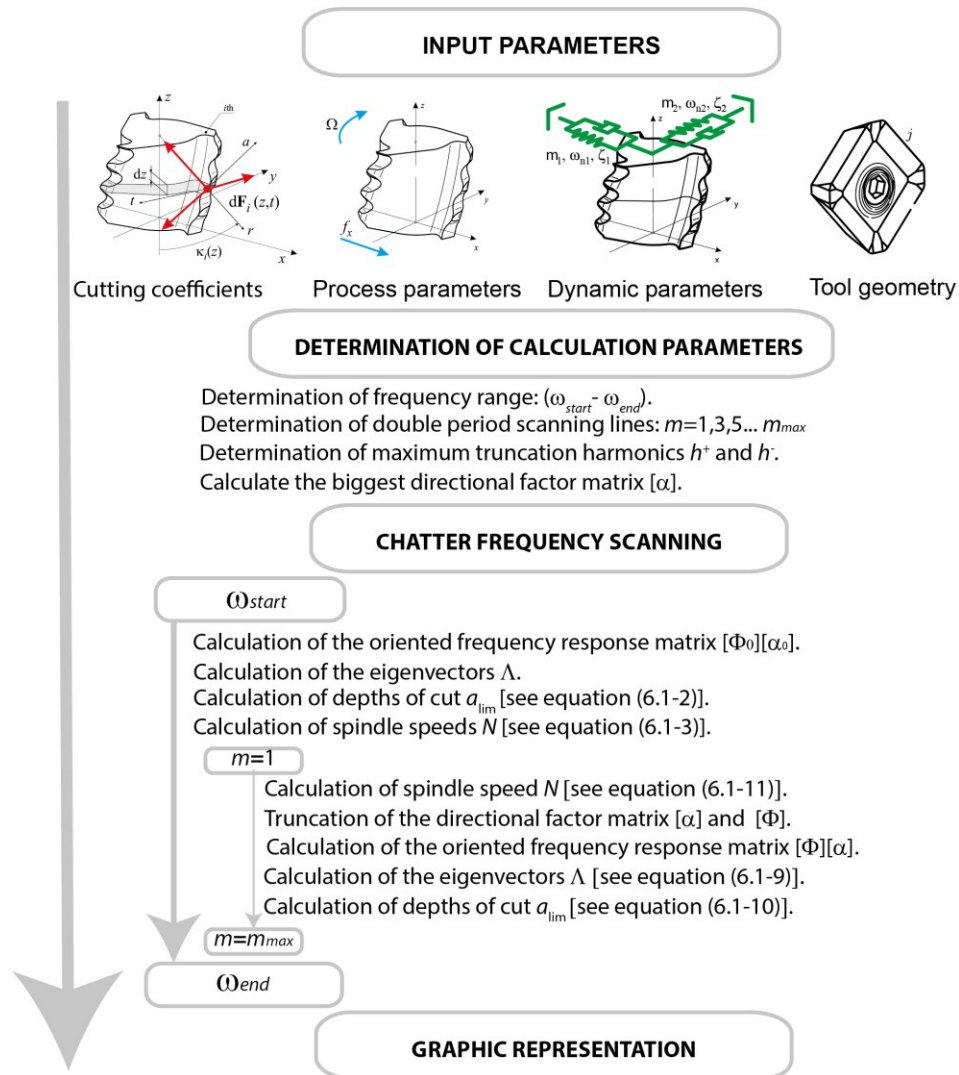

Figure 6.1: Combined analytical frequency method algorithm.

Step 1: Input parameter determination

The input parameters are obtained and introduced in the model. The cutting coefficients and the dynamic parameters can be theoretically or experimentally obtained, whereas the process parameters and tool geometry are given by the machining operation to perform.

Step 2: Determination of the calculation parameters

Before starting the frequency scanning in Step 3, the algorithm sets several limits which will help to perform the scanning in the range of interest.

- **Determination of the frequency range [ω_{start}, ω_{end}]**: It is selected considering the main flexibility of the dynamic system and eliminating frequencies where the system is really stiff compared with the most flexible frequency. The limit can be customized according to the user needs, but a good approximation could be achieved accounting for the range of those frequencies whose flexibility is over 10% of the most flexible frequency peak.

- **Determination of the number of double period scanning lines m**: Once the frequency range has been calculated, the number of double period scanning lines m that fall in the scanning region in the N vs. ω_c plot (Figure 6.2) is obtained from equation (6.1-11):

$$\frac{60\,\omega_{start}}{\pi\,Z\,N_{end}} < m < \frac{60\,\omega_{end}}{\pi\,Z\,N_{start}}, \tag{6.1-12}$$

where N_{start} and N_{end} are the spindle speed limits defined in Step 1 and m must be an odd number.
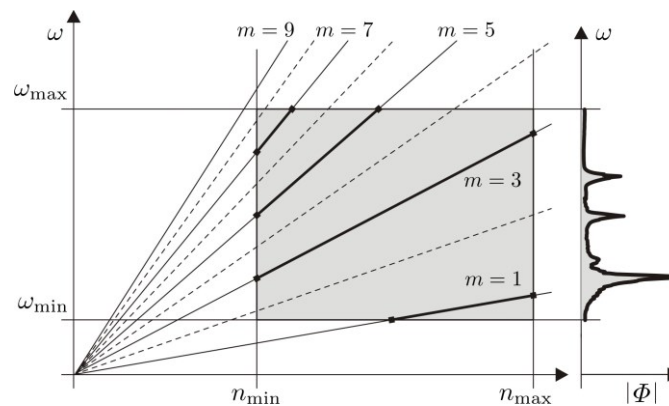

Figure 6.2: Scanning region delimited by ω_{start} - ω_{end} and N_{start} - N_{end}. In the example shown, only the $m=1$, $m=3$, $m=5$ and $m=7$ must be scanned for a proper lobe determination.

- **Determination of the maximum truncation harmonics h^+ and h^-:** The number of positive h^+ and negative h^- significant harmonics is determined considering always a positive scanning according to the frequency range of interest $\omega_c \in [\omega_{start}, \omega_{end}]$.

$$h^- = \left\lfloor \frac{\omega_{end} + \omega_c}{\Omega} \right\rfloor \ and \ h^+ = \left\lfloor \frac{\omega_{end} - \omega_c}{\Omega} \right\rfloor. \tag{6.1-13}$$

- **Calculation of the biggest directional factor matrix $[\alpha]$:** For each chatter frequency and/or spindle speed, the oriented frequency response matrix $([\Phi][\alpha])$ is truncated according to the number of positive h^+ or negative harmonics h^- determined previously.

Step 3: Chatter frequency scanning

After all the calculation parameters have been set, the model starts scanning the defined frequency range and calculates the zeroth order solution as in the well-known ZOA method, in order to determine the Hopf lobes. The solution for every flip lobe m is obtained scanning the different flip lines in the N vs. ω_c plot defined in Step 2 (Figure 6.2) along the defined frequency range. The procedure is to truncate the directional matrix according to the previously defined truncation harmonics h^+ and h^-, calculate the product of $[\Phi][\alpha]$, the eigenvectors of the resultant matrix and finally the resultant depth of cut limit a_{lim} and its correspondent spindle speed N for every lobe.

Step 4: Graphic representation

Finally, the resultant values of a_{lim} and N are plotted to build the SLD with Hopf and flip type lobes included.

6.2   COMPARISON OF STABILITY MODELS

The accuracy of the proposed method has been compared with traditional ZOA approximation, multi-frequency solution and semi-discretization models. The comparison has been carried out selecting three representative examples from the literature. The ZOA simulations have been carried out using the algorithm described by Altintas and Budak (1995), the multi-frequency solution has been obtained following Budak and Altintas (1998), and finally the semi-discretization model has been implemented considering the method proposed by Insperger and Stepan (2000). Several works have compared semi-discretization and multi-frequency methods concluding that the two methods are providing the same result (Munoa et al., 2013a).

This has also been proved in this work and, for that reason, only the semi-discretization method comparison with the developed method will be shown.

6.2.1 Case 1: Heavy-duty milling with face milling cutter.

The case of a heavy-duty operation with a face milling cutter has been considered first (Munoa, 2007). The cutting conditions and dynamic parameters are summarized in Table 6.1. The dynamic properties have been obtained making a curve fitting on DS630 machining center for different positions. The dynamic behavior is changing inside the workspace and, hence, the workspace has been discretized in 16 different positions. In each position, 8 high engagement (80%) cutting process simulations have been performed for different cutting directions. C45 steel has been considered in these simulations.

Tool			
Diameter (D)	*Number of flutes (Z)*	*Lead angle (κ)*	*Helix angle*
125mm	8	45°	0°
Cutting conditions & Coefficients			
Engagement	*Feed Direction*	*K_t [N/mm²]* *K_r*	*K_a*
100mm (Down Milling)	(1,0,0)	1889 0.4105	0.1928
Dynamic Parameters			
Mode *f_n [Hz]*	*ζ [%]*	*k [N/μm]* *m [kg]*	*Orientation*
1 36.1	5.1	56.6 1105	(0.128,-0.674,0.728)
2 50.6	3	42 415	(0,1,0)
3 84.6	2.5	52.6 186	(0.969,-0.246,-0.013)
4 89.8	4.3	48.9 154	(0.267,0.961,-0.075)
5 135.1	2.6	30.6 42.5	(1,0,0)

Table 6.1: Parameters for simulation of case 1 (Munoa, 2007).

In this case, the ZOA approximation is able to predict accurately the stability compared with semi-discretization. A representative example is presented in Figure 6.3.
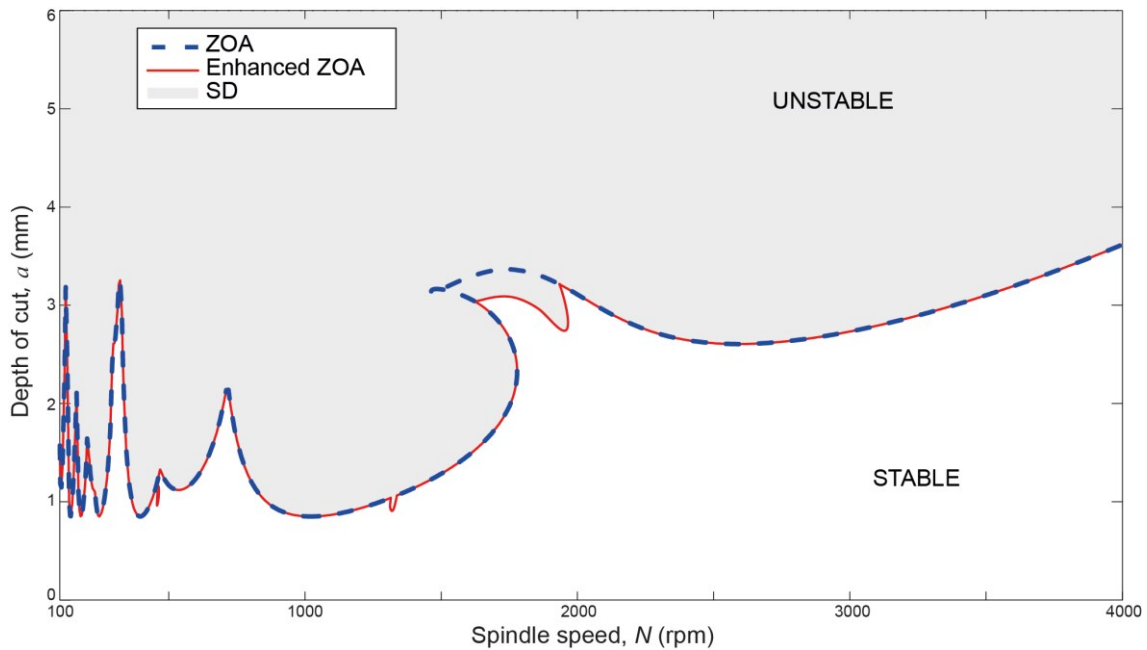
Figure 6.3: Stability diagram for case 1 comparing ZOA, semi-discretization and combined frequency method. (Munoa, 2007).

Considering the machinability issues for the selected tool, spindle speeds between 300 and 800 rpm are suitable for steel machining. Hence, the ZOA method provides a fast and precise solution at the same time. There is an anecdotal discrepancy around 1800 rpm due to the presence of a closed flip instability region. The combined frequency method offers the exact solution.

The ZOA is a powerful tool when low oscillation cutting forces are present, as it is the case in heavy-duty cutting where the engagement and the number of flutes are high. For these cases ZOA method is suitable to perform multiple simulations taking into account different positions, cutting planes and cutting directions.

6.2.2   Case 2: Highly interrupted cutting.

Insperger and Stepan (2000) reported an example of highly interrupted cutting using 1 fluted tool (Table 6.2). This example is far from a real cutting case but it has been experimentally verified and used for comparison with the multi-frequency model in the literature (Merdol and Altintas, 2004).

Tool			
Diameter (D)	*Number of flutes (Z)*	*Lead angle (κ)*	*Helix angle*
19.05mm	1	90°	0°
Cutting conditions & Coefficients			
Engagement	*Feed Direction*	*K_t [N/mm²]*	*K_r*	*K_a*
6.35mm (Centered)	(1,0,0)	550	0.364	0
Dynamic Parameters			
Mode	*f_n [Hz]*	*ζ [%]*	*k [N/μm]*	*m [kg]*	*Orientation*
1	146.8	0.38	2.2	2.586	(1,0,0)

Table 6.2: Parameters for simulation of case 2 (Merdol and Altintas, 2004).

In this example, the double period chatter (flip lobe) defines the minimum stability (Figure 6.4). In general, the flip lobes are as important as the Hopf lobes especially considering a finishing operation of a highly flexible part.
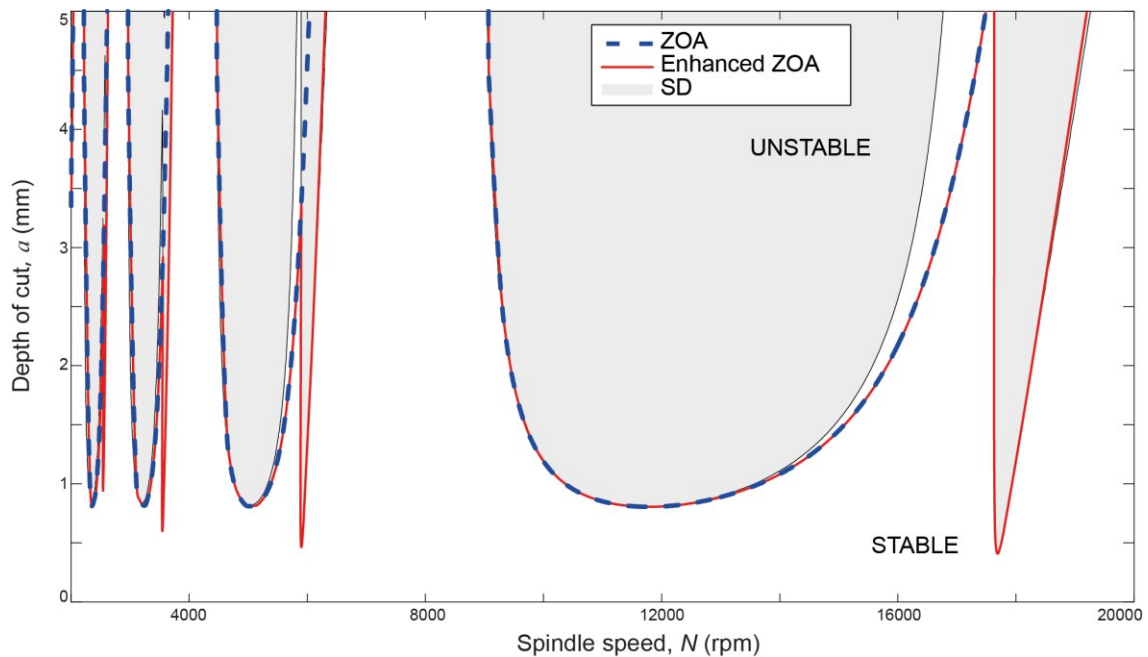
Figure 6.4: Stability diagram for case 2 comparing ZOA, semi-discretization and combined frequency method. (Merdol and Altintas, 2004).

In this case, the ZOA method is not able to describe the double period chatter and therefore important disagreements between methods are found. The combined method is able to predict exactly the double period chatter and therefore this fast prediction is good enough and can have practical applications when interrupted cutting is performed.

6.2.3   Case 3: Interrupted cutting with mode coupling.

Finally a third example has been chosen considering mode couplings due to the existence of more than one significant vibration mode when an interrupted milling process is performed (Munoa et al., 2013). The characteristics of this example are summarized in Table 6.3.

Tool			
Diameter (D)	*Number of flutes (Z)*	*Lead angle (κ)*	*Helix angle*
50mm	4	90°	0°
Cutting conditions & Coefficients			
Engagement	*Feed Direction*	*$K_t [N/mm^2]$*	*K_r* *K_a*
12.5mm (Down Milling)	(1,0,0)	2000	0.3 0
Dynamic Parameters			

Mode	*f_n [Hz]*	*ζ [%]*	*k [N/μm]*	*m [kg]*	*Orientation*
1	45	4	30	375	(1,0,0)
2	60	4	30	211	(0,1,0)

Table 6.3: Parameters for simulation of case 3. (Munoa et al., 2013).

The combined method is able to improve the accuracy of the ZOA method introducing exact double period lobes, but it is not able to capture the variations due to mode coupling effect (see Figure 6.5). Therefore, important divergences are found in some regions.
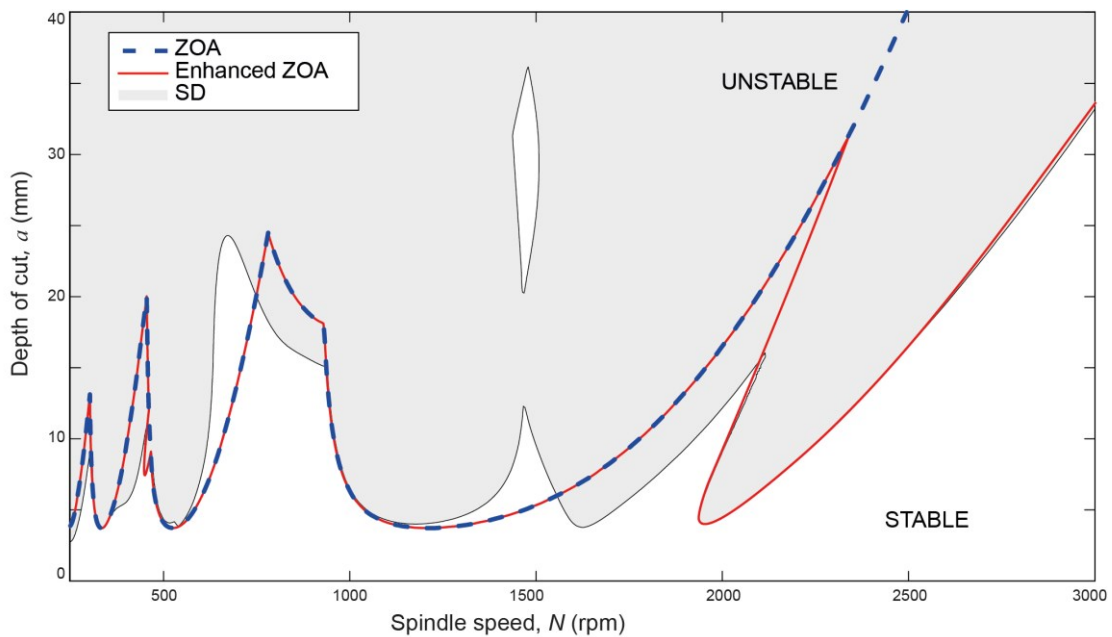

Figure 6.5: Stability diagram for case 3 comparing ZOA (dashed blue line), semi-discretization (shaded area) and combined frequency method (solid orange line). (Munoa et al., 2013a).

In general, the combined analytical model improves the accuracy of the traditional ZOA method, while maintaining the speed and the possibility to use experimental FRFs directly. The flip lobes are accurately predicted and the only pitfalls occur when mode interaction is present.

6.3   EXPERIMENTAL VALIDATION

Finally, an experimental validation of the analytical model was carried out. A special workpiece fixture system with a clear dominant mode in the direction perpendicular to the cutting direction has been tested. An aluminum workpiece was placed on top of it (see Figure 6.6). This fixture simulates a flexible set-up in which both Hopf and flip chatter at $m=1$ can emerge with low radial immersion cuts. A 20mm diameter straight fluted end mill was used to perform interrupted cutting tests. The straight flutes allow achieving a "pure" flip lobe, without the island effect typical from the helix angle effect (Patel et al., 2008). A 3 fluted tool was selected in order to facilitate the flip chatter onset detection, since it appears at odd multiples of the tooth passing frequency, which avoids mixing the chatter peaks with rotating frequency harmonics.

Figure 6.6: Experimental setup.

In Figure 6.7 the comparison between a stable and a flip chatter test in terms of surface marks is shown. According to equation (6.1-4), the flip chatter presents a frequency which is exactly the half of the main cutting frequency Ω for $m=1$. This

makes the flip chatter marks have a similar aspect to a stable cut, but with a longer spacing between marks and a deeper relief.
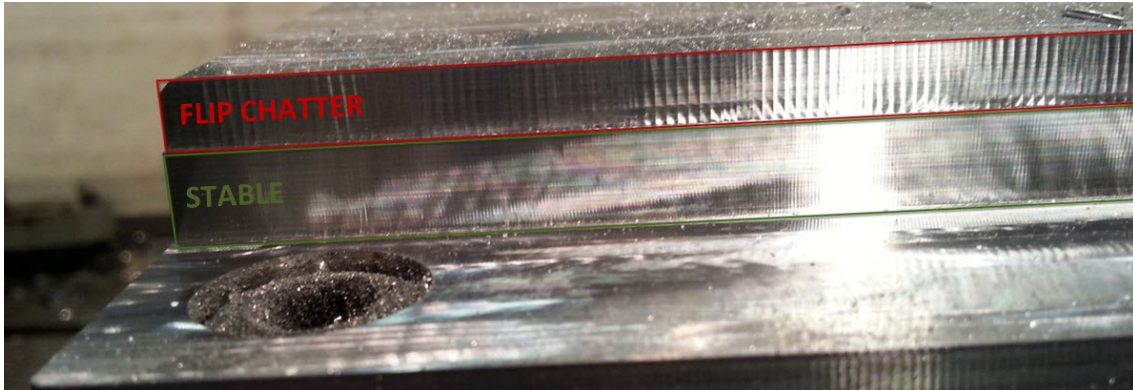

Figure 6.7: Surface roughness of flip chatter test versus stable test.

In order to validate the developed method, several cutting tests have been carried out in the region of the first Hopf lobe (l=0) and the flip lobe at m=1. The cutting conditions and the dynamics of the flexible fixture are indicated in Table 6.4.

Tool			
Diameter (D)	*Number of flutes (Z)*	*Lead angle (κ)*	*Helix angle*
20mm	3	90°	0°
Cutting conditions & Coefficients			
Engagement	*Feed Direction*	*K_t [N/mm²]*	*K_r* *K_a*
1mm (Down Milling)	(1,0,0)	804	0.39 0.15
Dynamic Parameters			
Mode *f_n [Hz]*	*ζ [%]*	*k [N/μm]* *m [kg]*	*Orientation*
1 178	0.54	19.78 15.81	(0,1,0)

Table 6.4: Parameters for experimental validation.

Both Hopf and flip lobes were studied. The obtained results are shown in Figure 6.8. The chatter frequency ω_c versus the spindle speed N (Figure 6.8a) and the cutting depth of cut a versus the spindle speed N (Figure 6.8b) have been plotted. If the typical ZOA model was used to predict stability, important errors would have been incurred in the speed region around N=7000rpm ($\Omega\approx2\omega_n$) since, as opposed to the combined analytical frequency model developed, the classical ZOA model does not account for the flip lobes. Figure 6.8d shows the time signal and the spectrum of a stable cut and an unstable cut in the flip and Hopf minimum areas.
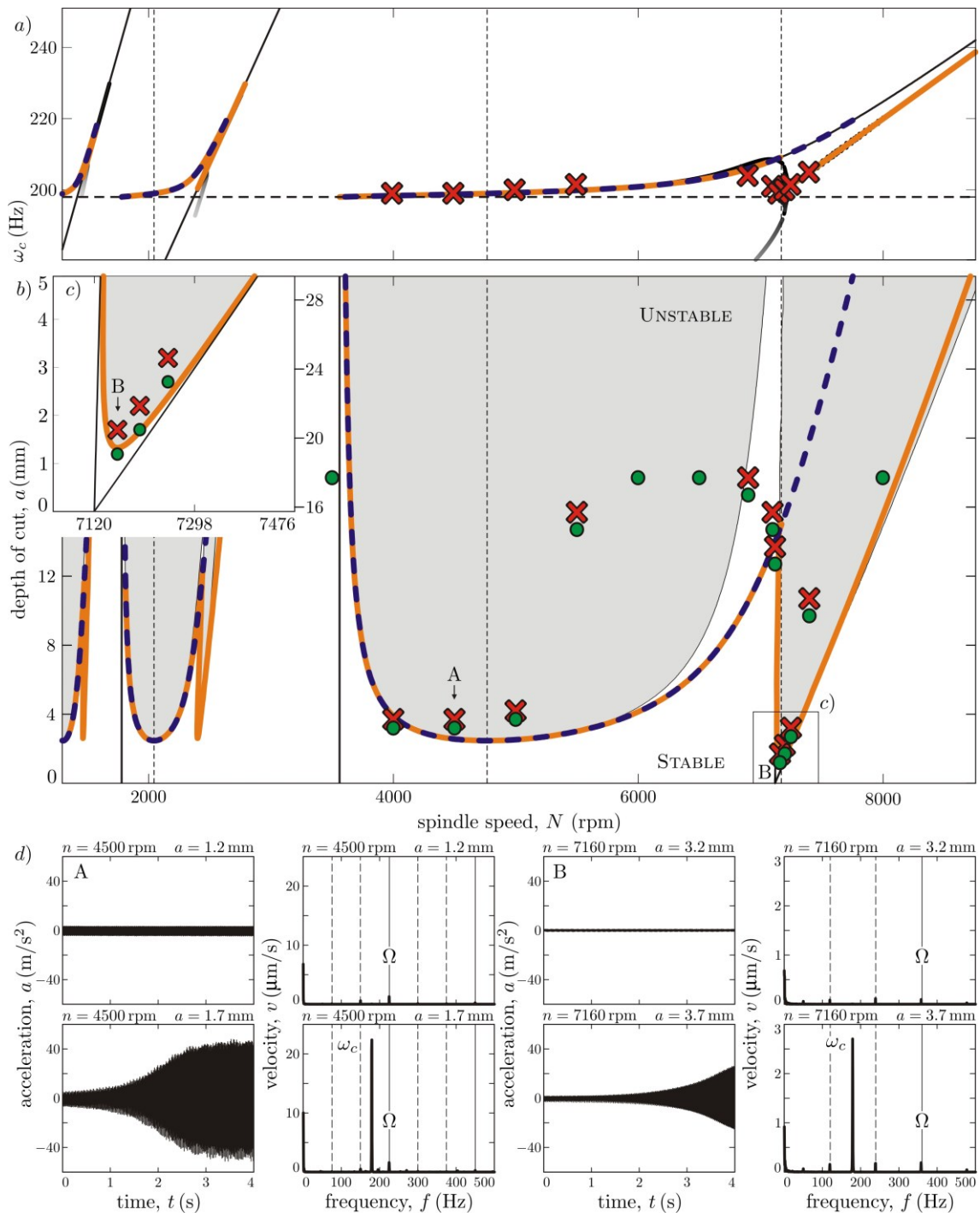
Figure 6.8: Experimental validation of the analytical stability model for interrupted milling. ZOA (dashed blue line), semi-discretization (shaded area) and combined frequency method (solid orange line) simulation results for *a*) chatter frequency ω_c and *b*) depth of cut *a* are shown. The experimental tests are plotted over the theoretical stability curve as green circles (stable cut) or red crosses (unstable cut). The time signal and the spectrum of a stable and an unstable test in the Hopf (A) and flip (B) minimum are shown in *d*).

According to the experimental tests, there is still a significant deviation in the prediction of the stability in the region around N=5500-7000rpm ($\Omega \approx$1.5-2ω_n), probably

due to the effect of mode interactions by the not considered modes (only the main mode has been introduced in the model). However, the remaining spindle speed range, including Hopf and flip minimum, has been satisfactorily predicted and a good correlation is obtained with the experimental data.

6.4   CONCLUSIONS

The single frequency or zero order approximation (ZOA) method is the basic reference in milling stability because it provides fast and accurate determination of the stability for continuous cutting making possible the introduction of experimental FRF functions without any fitting. This method is accurate enough to predict stability in industrial problems like a heavy-duty face milling operation.

A combined frequency domain method has been proposed based on a simple frequency scanning, following the same calculation procedure as the traditional ZOA method. This combined method has improved the accuracy of the ZOA approximation in milling conditions with interrupted cutting, maintaining the main advantages of the ZOA. These advantages are the great accuracy to calculation time ratio and the possibility of dealing with experimental FRFs, without need of curve fitting. Moreover, the solution it provides for flip type lobes shows a great accuracy in comparison with the recognized method of semi-discretization.

The new simulation model shows a good agreement with experiments, whereas the classical ZOA method fails in the flip lobe influence area, since it is not capable of describing the double period chatter. Nevertheless, further improvements are needed in the model in order to achieve an accurate prediction of the stability border.

Contribution 7:

A new combined frequency domain analytical method has been developed. This method calculates the standard ZOA solution combined with the double period chatter limit in a single frequency scanning loop. This new combined model maintains the main advantages of ZOA, fast calculation and possibility to introduce the experimental FRF of the system directly in the model, with the addition of the accurate prediction of flip type lobes.

The experimental results indicate that despite the prediction improvement achieved, further improvements are required for a trustful stability prediction.

Related Publications:

Iglesias, A., Munoa, J., Ciurana, J., & Dombovari, Z. (2015). Analytical model for interrupted milling: ZOA method enhancement including double period instability. *International Journal of Machine Tools and Manufacture*, submitted.

Iglesias, A., Munoa, J., Ciurana, J., & Dombovari, Z. (2015). Analytical stability model for interrupted milling processes. *International Journal of Advanced Manufacturing Technology*, submitted.

Chapter 7

Inverse Methodology for Dynamic Parameter Extraction

Apart from the new stability calculation model (Chapter 6) and formulae (Chapter 5) developed in order to improve stability prediction, new experimental characterization techniques pose another approach to increase model input data quality and, therefore, milling stability prediction.

In this Chapter, there are two main objectives. First, the modal parameters of a machine tool are experimentally obtained based on a new inverse analytical formulation of zero order stability solution. The new formulation is applied to a dominant mode case and a two equal orthogonal mode case. The purpose is to improve the accuracy of the extracted dynamic parameters of the system and avoid severe errors in stability prediction, as those verified in Chapter 4. The second objective is investigating the effect of tool wear on the stability of the cutting process.

7.1 IDENTIFICATION OF STRUCTURE'S MODAL PARAMETERS THROUGH INVERSE STABILITY

7.1.1 Slope cutting test

A sloped workpiece, which allows increasing axial depth of cut, is milled to identify critical chatter stability conditions needed for the proposed inverse identification method (Figure 7.1a). The cutting conditions are listed in Table 7.1. The cutting tests are conducted at different spindle speeds to cover the range of speed and axial depth of cut for the construction of stability curves. In Figure 7.1a, cutting speed and y-coordinate of cutter is set constant when cutting along x-direction. Vibration of tool is measured throughout the cutting process. At a certain spindle speed when depth of cut reaches limit depth of cut, chatter occurs, and the chatter frequency dominates measured force and vibration signals. Critical spindle speed, limit depth of cut and chatter frequency are collected at each test.

a) Schematics of slope cutting experiment

b) Principal u and v directions of FRF for fixed (nonrotating) modes.
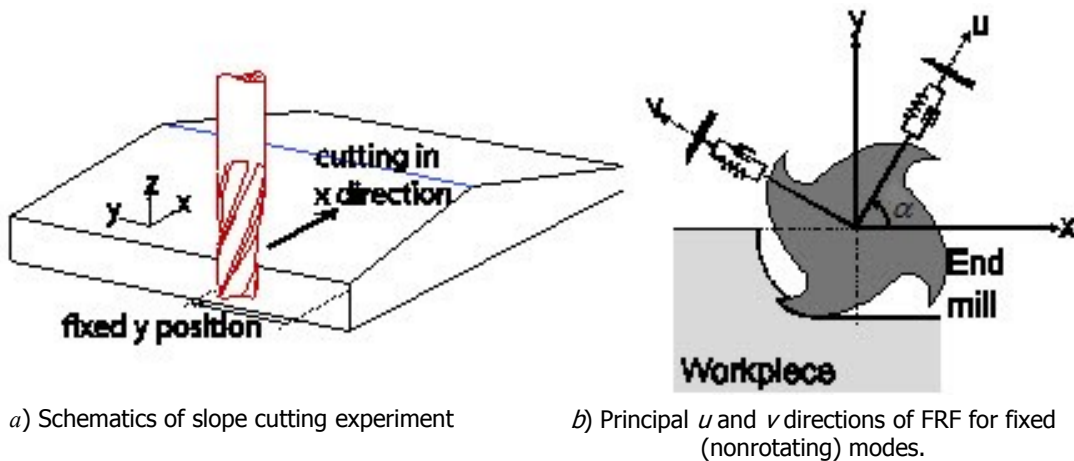
Figure 7.1: Slope cutting test with simple dynamics.

Workpiece material	Steel F1140 (C45)
Type of cutter	Inserted cutter SANDVIK 490-032A25-08M
Cutter diameter (D)	32 [mm]
Number of teeth on cutter (Z)	4
Type of milling	Slotting
Maximum axial depth of cut on slope	4 [mm]
Angle of slope on workpiece	2.78 [deg]
Type of toolholder	ISO50, great power collet chuck.
Name of machine tool	Solaruce SV6000
Cutting fluid	No coolant or cutting fluid used
Spindle speeds (N)	1420, 1480, 1600, 1750, 2000, 2400, 2600, 3000 [rpm]
Feed per tooth (f_z)	0.20 [mm]

Table 7.1: Technical information of slope cutting experiment.

The reason of decreasing depth of cut towards the other end of sloped workpiece is to observe difference between limits while cutting with increasing and decreasing depth of cut (Shi and Tobias, 1984). In Figure 7.2, when the depth of cut increases, steady state amplitude of vibration jumps from A to B. However, while decreasing depth of cut, amplitude of vibration jumps from B' to A'. Because of nonlinearities related to the cutting force, A-B and B'-A' do not correspond to the same depths of cut. The region between A and A' is called unsafe zone.
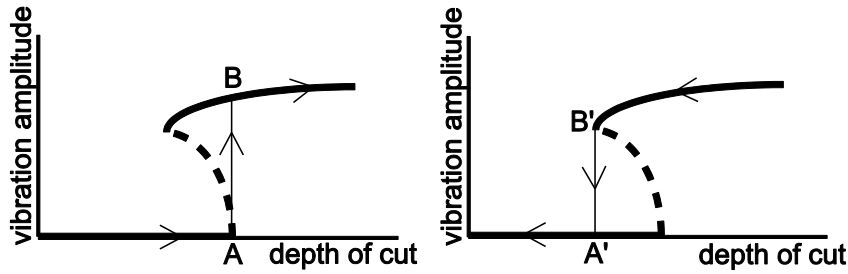

Figure 7.2: Changes in steady state vibration amplitude when depth of cut is increasing (left) and depth of cut is decreasing (right).

For a system whose FRF can be approximated by means of simple dynamics, an inverse method to predict modal parameters using experimental data is introduced. Inverse formulation is applied to each set of experimental data collected from each lobe, separately. This method can be considered as updating stability diagram which is predicted by tap testing to include the effects of process.

The two cases considered are FRF with one dominant mode (case 1) and FRF with two symmetric, orthogonal equal modes (case 2). Tool tip FRF (transfer function) matrix identified at the cutter-workpiece contact zone can be expressed as shown in Figure 7.1*b*:

$$[\Phi(j\omega)] = \begin{bmatrix} \Phi_{uu}(j\omega) & \Phi_{uv}(j\omega) \\ \Phi_{vu}(j\omega) & \Phi_{vv}(j\omega) \end{bmatrix}, \tag{7.1-1}$$

where, $\Phi_{uu}(j\omega)$, $\Phi_{vv}(j\omega)$: direct tool tip FRF in principal u and v directions, $\Phi_{uv}(j\omega)$, $\Phi_{vu}(j\omega)$: cross tool tip FRFs. If the modes are assumed to be orthogonal, $\Phi_{uv}(j\omega)$, $\Phi_{vu}(j\omega)$=0. As shown in Figure 7.1*b*, the principal mode directions may not coincide with the machining directions. Transforming FRF matrix from (u,v) to (x,y) coordinate system yields

$$[\Phi(j\omega)] = \begin{bmatrix} \Phi_{uu}\cos^2\alpha + \Phi_{vv}\sin^2\alpha & (\Phi_{uu}-\Phi_{vv})\sin\alpha\cos\alpha \\ (\Phi_{uu}-\Phi_{vv})\sin\alpha\cos\alpha & \Phi_{uu}\sin^2\alpha + \Phi_{vv}\cos^2\alpha \end{bmatrix}, \tag{7.1-2}$$

The characteristic equation for two degree-of-freedom milling is

$$\det\left(\left[I\right]-\frac{1}{2\pi}ZK_t a(1-e^{-j\omega_c T})\left[\alpha_0\right]\left[\Phi(j\omega_c)\right]\right)=0. \tag{7.1-3}$$

The directional factor matrix is written as

$$[\alpha_0]=\begin{bmatrix}\alpha_{xx} & \alpha_{xy}\\ \alpha_{yx} & \alpha_{yy}\end{bmatrix}, \tag{7.1-4}$$

where α_{xx}, α_{xy}, α_{yx}, α_{yy} are the average directional milling coefficients.

The eigenvalue problem can be solved from the characteristic equation

$$\det([I]+\Lambda[\psi])=0, \tag{7.1-5}$$

as:

$$\det([\Psi])\Lambda^2+\mathrm{trace}([\Psi])\Lambda+1=0, \tag{7.1-6}$$

7.1.2   Case 1: Inverse analytical formulation for one dominant mode

This case describes a one dominant mode direction system. If the mode direction is u, it can be set that $\Phi_{uu}(j\omega)=\Phi(j\omega)$ and $\Phi_{vv}(j\omega)=0$, and equation (7.1-2) becomes $[\Phi(j\omega)]=\Phi(j\omega)[R]$. The FRF of a single degree-of-freedom system is,

$$\Phi(j\omega)=\frac{\omega_n^2}{k\,(\omega_n^2-\omega^2+j2\xi\omega_n\omega)}. \tag{7.1-7}$$

Also,

$$[\Phi(j\omega)]=\Phi(j\omega)[R]=\Phi(j\omega)\begin{bmatrix}\cos^2\alpha & \sin\alpha\,\cos\alpha\\ \sin\alpha\,\cos\alpha & \sin^2\alpha\end{bmatrix}. \tag{7.1-8}$$

Rewriting the characteristic equation from equation (7.1-3), it yields:

$$\det\left(\left[I\right]-ZK_t a(1-e^{-j\omega_c T})\Phi(j\omega_c)\left(\frac{1}{2\pi}[\alpha_0][R]\right)\right)=0, \tag{7.1-9}$$

where $\Lambda=-ZK_t a\,(1-e^{-j\omega_c T})\Phi(j\omega_c)$ and

$$[\Psi]=\frac{1}{2\pi}[\alpha_0][R]=\begin{bmatrix}\alpha_{xx}\cos^2\alpha+\alpha_{xy}\sin\alpha\cos\alpha & \alpha_{xx}\sin\alpha\cos\alpha+\alpha_{xy}\sin^2\alpha\\ \alpha_{yx}\cos^2\alpha+\alpha_{yy}\sin\alpha\cos\alpha & \alpha_{yx}\sin\alpha\cos\alpha+\alpha_{yy}\sin^2\alpha\end{bmatrix}. \tag{7.1-10}$$

Terms in equation (7.1-6) yield:

$$\det([\Psi])=\det([A_0])\det([R])=0 \tag{7.1-11}$$

and

$$\Lambda=-1/\mathrm{trace}([\Psi]). \tag{7.1-12}$$

The equivalent directional coefficient can be defined as:

$$\alpha_{eq} = -\text{trace}([\Psi]) = -\frac{1}{2\pi}[\alpha_{xx}\cos^2\alpha + \alpha_{yy}\sin^2\alpha + (\alpha_{xy}+\alpha_{yx})\sin\alpha\cos\alpha].$$
(7.1-13)

Since α_{eq} is a real number, eigenvalue ($\Lambda=1/\alpha_{eq}$) of this system is real. Rewriting equation (7.1-12):

$$-1 = ZK_t a(1 - e^{-j\omega_c T})\alpha_{eq}\Phi(j\omega),$$
(7.1-14)

where chatter frequency (ω_c), limit depth of cut (a) and tooth passing period (T) are recorded from experiments.

Damping can be obtained from the phase shift equation of the FRF function

$$\tan(\psi) = \frac{H}{G} = \frac{-2\xi\lambda}{1-\lambda^2},$$
(7.1-15)

from any of the recorded experiments:

$$\xi = -\tan(\psi_1)\frac{1-\lambda^2}{2\lambda},$$
(7.1-16)

where, $\lambda=\omega_c/\omega_n$.

Knowing the relation of the phase shift of the frequency response function

$$2\psi = \omega_c\tau - 3\pi + 2\pi l,$$
(7.1-17)

the natural frequency is obtained from two experiments at different spindle speeds, since ω_{c1} and ω_{c2} and thus, $\tan\psi_1$ and $\tan\psi_2$ are known. From Equation (7.1-15):

$$\omega_n = \sqrt{\frac{\omega_{c2}^2 - \dfrac{\tan\psi_1\omega_{c2}}{\tan\psi_2\omega_{c1}}\omega_{c1}^2}{1 - \dfrac{\tan\psi_1\omega_{c2}}{\tan\psi_2\omega_{c1}}}}.$$
(7.1-18)

Equating real part of Equation (7.1-14) the limit depth of cut is obtained:

$$a_{\lim} = \frac{-1}{2ZK_t\alpha_{eq}G},$$
(7.1-19)

which leads to estimation of modal stiffness from any of the two experiments,

$$k = -2ZK_t a_1\alpha_{eq}\frac{1-\lambda_1^2}{(1-\lambda_1^2)^2 + (2\xi\lambda_1)^2},$$
(7.1-20)

where $\lambda_1=\omega_{c1}/\omega_n$ and a_1 is the limit depth of cut from the first experiment.

7.1.3　Case 2: Inverse analytical formulation for two equal orthogonal modes

This case consists of two symmetric modes in two orthogonal directions, i.e. $\Phi_{uu}(j\omega)=\Phi_{vv}(j\omega)=\Phi(j\omega)$. Equation (7.1-2) becomes $[\Phi(j\omega)]=\Phi(j\omega)[I]$, where FRF of single degree-of-freedom system is the same as equation (7.1-7).

Rewriting the characteristic equation (7.1-3):

$$\det\left([I]-ZK_t a(1-e^{-j\omega_c T})\Phi(j\omega_c)\left(\frac{1}{2\pi}[\alpha_0]\right)\right)=0, \tag{7.1-21}$$

and

$$\det([I]+\Lambda([\alpha_0]))=0, \tag{7.1-22}$$

where

$$\Lambda=-ZK_t a(1-e^{-j\omega_c T})\Phi(j\omega_c)/2\pi. \tag{7.1-23}$$

Similarly to equation (7.1-6), equation (7.1-22) can be written as

$$\det([\alpha_0])\Lambda^2+\text{trace}([\alpha_0])\Lambda+1=0, \tag{7.1-24}$$

where $\det([\alpha_0])=(\alpha_{xx}\alpha_{yy}-\alpha_{xy}\alpha_{yx})$ and $\text{trace}([\alpha_0])=\alpha_{xx}+\alpha_{yy}$. Therefore, eigenvalues are

$$\Lambda_\pm=\frac{\alpha_{xx}+\alpha_{yy}\pm\sqrt{(\alpha_{xx}-\alpha_{yy})^2+4\alpha_{xy}\alpha_{yx}}}{\alpha_{xy}\alpha_{yx}-\alpha_{xx}\alpha_{yy}}. \tag{7.1-25}$$

The equivalent directional coefficient is defined as

$$\alpha_{eq\pm}=\frac{\alpha_{xx}\alpha_{yy}-\alpha_{xy}\alpha_{yx}}{\alpha_{xx}+\alpha_{yy}\pm\sqrt{(\alpha_{xx}-\alpha_{yy})^2+4\alpha_{xy}\alpha_{yx}}}. \tag{7.1-26}$$

Unlike in case 1, the equivalent directional coefficient may be complex (depending on immersion) in Case 2.

$$\alpha_{eq\pm}=\alpha_R+j\alpha_I, \tag{7.1-27}$$

where α_R and α_I are the real and imaginary parts of α_{eq}. Since α_{eq} may be a complex number, imaginary part of $\Phi(j\omega_c)$, $H(\omega_c)$, may also affect the limit depth of cut. Due to this effect, the maximum stability asymptote can move from the theoretical resonance.

The equation (7.1-23) can be re-written as:

$$-1=ZK_t a(1-e^{-j\omega_c T})\alpha_{eq}\Phi(j\omega_c), \tag{7.1-28}$$

Similar to derivation of case 1, equating imaginary part of equation (7.1-28):

$$\tan(\chi) = \frac{H\alpha_{\mathrm{R}} \pm G\alpha_{\mathrm{I}}}{G\alpha_{\mathrm{R}} - H\alpha_{\mathrm{I}}} = \frac{\sin(\omega_c T)}{1 - \cos(\omega_c T)} = \tan\left(\frac{\pi}{2} - \frac{\omega_c T}{2}\right).$$
(7.1-29)

The angular displacement of the chatter vibration in one tooth period is,

$$\omega_c T = \pi - 2\chi + 2\pi l = 2\pi l + \varepsilon.$$
(7.1-30)

Angle χ can be related to the phase shift of the frequency response function as:

$$\chi = \psi + a\tan\frac{\alpha_{\mathrm{I}}}{\alpha_{\mathrm{R}}},$$
(7.1-31)

and therefore:

$$2\psi = \pi - \omega_c T + 2\pi l - 2a\tan\frac{\alpha_{\mathrm{I}}}{\alpha_{\mathrm{R}}}.$$
(7.1-32)

α_{eq}, K_t and N can be determined (for known immersion) beforehand. By performing experiments, two sets of data (a_1, N_1, ω_{c1} and a_2, N_2, ω_{c2}) can be collected from experimental data. χ_1 and χ_2 can be also derived from $\varepsilon = \omega_c T - 2\pi l$ and $\chi = (\pi - \varepsilon)/2$.

Equation (7.1-29) can be written in the same form as equation (7.1-15):

$$\tan(\chi) = \frac{-2\xi\lambda}{1 - \lambda^2}$$
(7.1-33)

where,

$$\tan(\chi) = \frac{\tan\psi\,\alpha_{\mathrm{R}} \pm \alpha_{\mathrm{I}}}{\alpha_{\mathrm{R}} - \tan\psi\,\alpha_{\mathrm{I}}}.$$
(7.1-34)

The rest of the derivation is similar to case 1. Thus,

$$\omega_n = \sqrt{\frac{\omega_{c2}^2 - \dfrac{\tan\chi_1\omega_{c2}}{\tan\chi_2\omega_{c1}}\omega_{c1}^2}{1 - \dfrac{\tan\chi_1\omega_{c2}}{\tan\chi_2\omega_{c1}}}}.$$
(7.1-35)

and

$$\xi = -\tan(\psi_1)\frac{1 - \lambda^2}{2\lambda}.$$
(7.1-36)

As the limit depth of cut can be calculated as follows:

$$a_{\mathrm{lim}} = \frac{-1}{2ZK_t\,\mathrm{Re}(\alpha_{eq}\Phi)},$$
(7.1-37)

modal stiffness is obtained from any experiment:

$$k = -2ZK_t a_1\frac{(1 - \lambda_1^2)\alpha_R \pm 2\xi\lambda_1\alpha_{\mathrm{I}}}{(1 - \lambda_1^2)^2 + (2\xi\lambda_1)^2}.$$
(7.1-38)

7.1.4   Verification of Inverse Analytical Formulation with Simulation

First, the inverse solution is verified on the ideal, simulated data based on the real system described in section 7.2. The FRF of the system is measured with impact modal test when the machine is at rest. If the structure is represented as shown in Figure 7.1b, α=90º, i.e. u-direction is equivalent to y-direction and v-direction is x-direction. Furthermore, FRFs of u and v directions are approximated by single modes. Natural frequency, modal damping ratio and modal stiffness of mode in u-direction are ω_n=94Hz, ξ=0.66% and k=58.4N/μm respectively. Modal parameters of dominant mode in v-direction are ω_n=230.6Hz, ξ=1.00% and k=161N/μm. The mode in u-direction is more flexible than v-direction.

The stability lobe l=0 is represented using the identified modal parameters for 1 mode and 2 modes case (Figure 7.3). Up to speeds around N=2000rpm, assuming only one mode in u-direction and ignoring mode in v-direction gives satisfactory results.
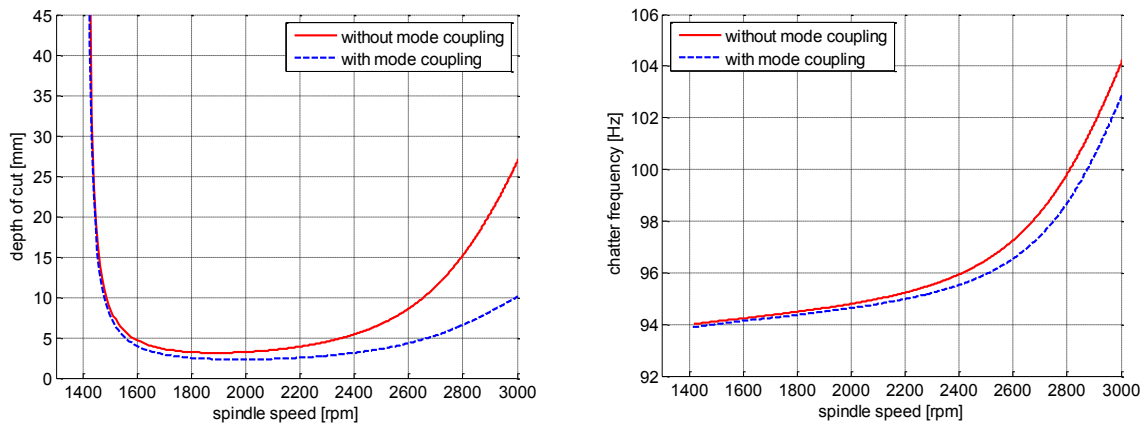
a) Limit depth of cut with and without considering mode coupling.

b) Chatter frequency with and without considering mode coupling.

Figure 7.3: Theoretical stability lobe (corresponding to lobe number l=0) obtained by hammer test. Cutting condition: Full immersion.

The proposed inverse solution is illustrated by taking five sample points from the stability lobe shown in Figure 7.3 (with and without mode coupling). Spindle speeds, chatter frequencies and limit depths of cut of these data points are used in the inverse prediction of modal parameters. When the mode coupling is neglected by considering the mode in u-direction only, the estimated modal parameters (ω_n=94Hz, ξ=0.70% and k=56.2N/μm) are in excellent agreement with the real values used in the stability lobe. Stability lobes based on the actual and estimated parameters exactly matched as shown in Figure 7.4. When sample points from stability lobe with mode coupling are

taken, identified modal parameters based on assuming only one mode in u-direction are ω_n=94Hz, ξ=0.52% and k=50.3N/μm. The predicted stability lobe based on the estimated and exact parameters also agrees acceptably well with each other as shown in Figure 7.5. While the chatter frequency estimation is excellent, there is a slight deviation in the estimated depth of cut due to estimation errors in the stiffness and damping of the structure.
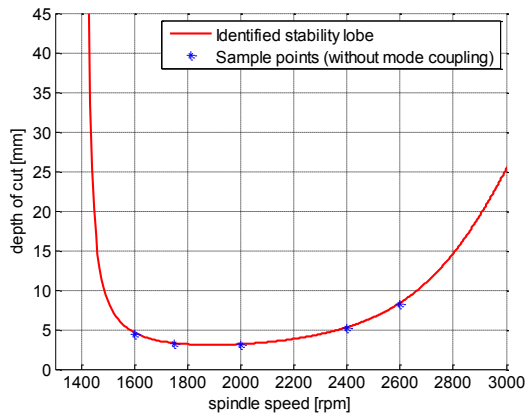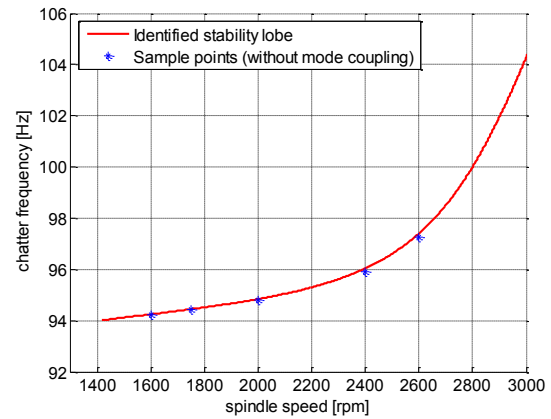
a) Limit depth of cut comparison   *b*) Chatter frequency comparison

Figure 7.4: Comparison of sample points with lobe obtained by inverse method for one dominant mode case. Sample points are taken from stability lobe which is obtained without mode coupling.
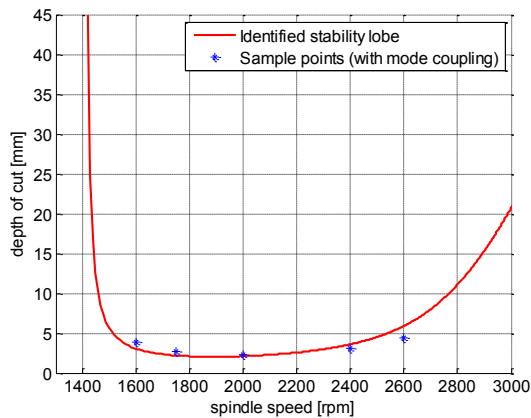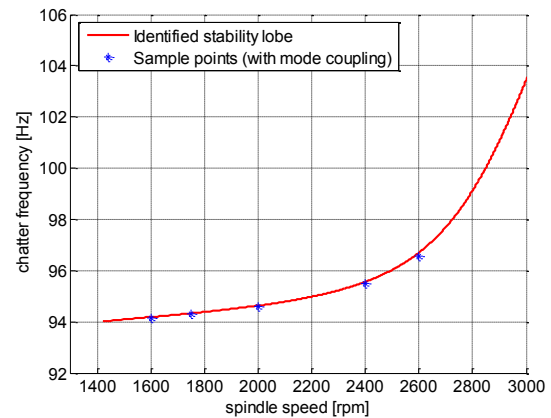
a) Limit depth of cut comparison   *b*) Chatter frequency comparison

Figure 7.5: Comparison of sample points with lobe obtained by inverse method for one dominant mode case. Sample points are taken from stability lobe which is obtained with mode coupling.

7.2   EXPERIMENTAL VALIDATION

7.2.1   Experimental setup

The cutting conditions used in the slot milling experiments are given in Table 7.1. The experiment setup is shown in Figure 7.6. The workpiece is mounted on a fixture which has single dominant mode direction.
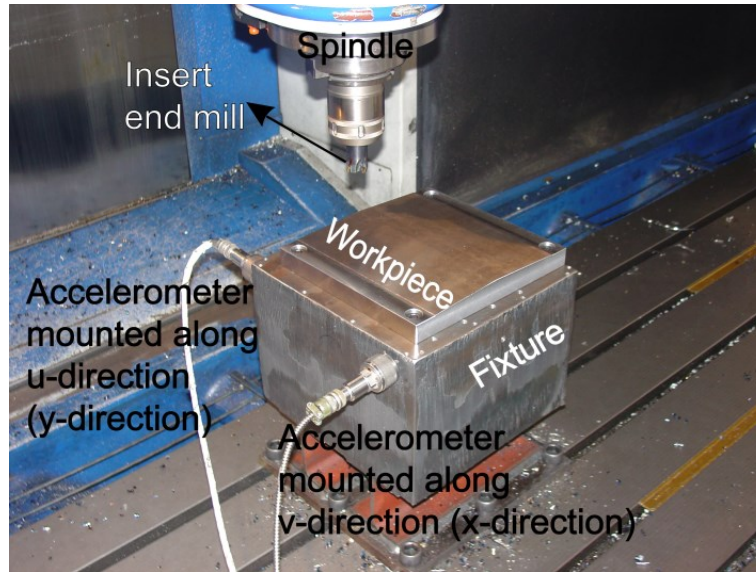
Figure 7.6: Experimental setup.

In each experiment, the procedure is composed of three parts. First, a series of slope cutting experiments are conducted at eight different spindle speeds. Secondly, the cutting coefficients of the tool are measured using a mechanistic method (Altintas, 2000). In the third part, wear is created in the tool via cutting a steel block. The procedure is repeated with same inserts until the end of the life of the tool, in order to analyze the progressive effect of tool wear.

Vibrations have been recorded by accelerometers attached on the workpiece (Figure 7.6).

7.2.2   Inverse method results

The sloped workpiece after the cutting test is shown in Figure 7.7. The lobular shape is printed on the machined surface at different cutting speeds.
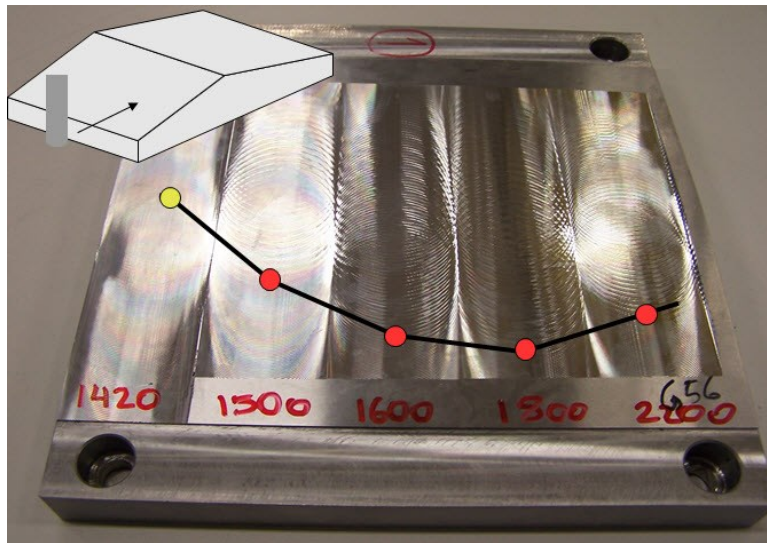
Figure 7.7: Workpiece surface roughness after slope chatter tests with the lobular shape printed on it.

The data collected in time domain is converted to a waterfall plot in frequency domain (by FFT) at each time step. Start of chatter can be recognized when waterfall plot is followed, as exemplified in a sample measurement shown in Figure 7.8. In order to determine start of chatter more efficiently, the vibration signal is first converted to mobility (velocity). The criterion for determining start of chatter is taking the time at which mobility of tooth passing frequency and chatter frequency become equal.

a) Sample waterfall plot. Time frame: 4 [s], time step of FFT: 0.5 [s]

b) Sample time history. Sampling frequency: 65,54 Hz

Figure 7.8: Sample plots used in chatter identification. Chatter frequency: 95.25Hz, spindle speed: 2000rpm (133.3Hz), start of cutting: 7.1s.

To determine end of chatter, time domain acceleration data and waterfall plot are used together. The time at which chatter frequency diminishes completely is regarded as the end of chatter.

Considering the test carried out with a new tool, chatter or unstable vibrations have been observed at five spindle speeds during experiment, and the results are summarized in Table 7.2. The modal parameters of the dominant mode in u-direction are estimated by inverse analytical formulation. As only two tests are enough to obtain the required dynamic parameters, the solutions provided by the 5 chatter tests have been combined in groups of two and the result for the dynamic parameters has been calculated by least squares method. Natural frequency, modal damping ratio and modal stiffness yield ω_n=93.3Hz, ξ=1.82% and k=12.2N/μm, respectively. Compared to the results obtained using the impact hammer, the natural frequency remained almost the same (f_n=93.3Hz) as in traditional hammer tests, the damping rat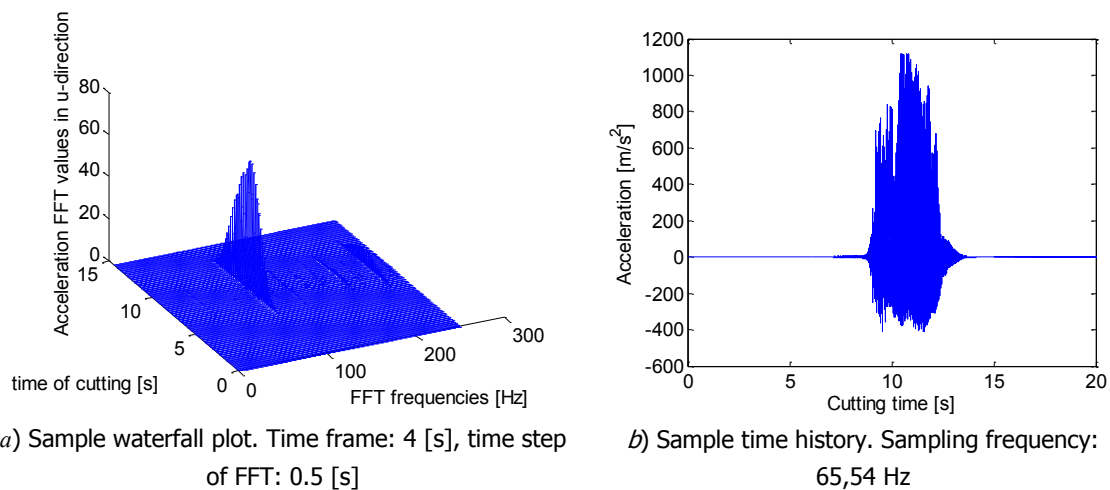io is increased from ξ=0.70% to ξ=1.82% and the estimated modal stiffness dropped from k=50.3N/μm to k=12.2N/μm.

Cutting speeds [rpm]	1420	1480	1600	1750	2000	2400	2600	3000
Feed speed [mm/s]	18.9	19.7	21.3	23.3	26.7	32.0	34.7	40.0
Limit depth of cut when depth of cut is increasing [mm]	S	S	3.18	2.51	1.95	2.39	3.40	S
Limit depth of cut when depth of cut is decreasing [mm]	S	S	2.53	1.71	1.53	1.92	2.68	S
Identified chatter frequency [Hz]	S	S	94.00	94.50	95.25	98.00	100.3	S

Table 7.2: Summary of chatter tests with new tool ('S' refers to stable cut)

The stability lobe is reconstructed by using the estimated modal parameters, and shown in Figure 7.9, together with the critical chatter conditions observed from the experiments.

a) Limit depth of cut fit.   *b*) Chatter frequency fit.
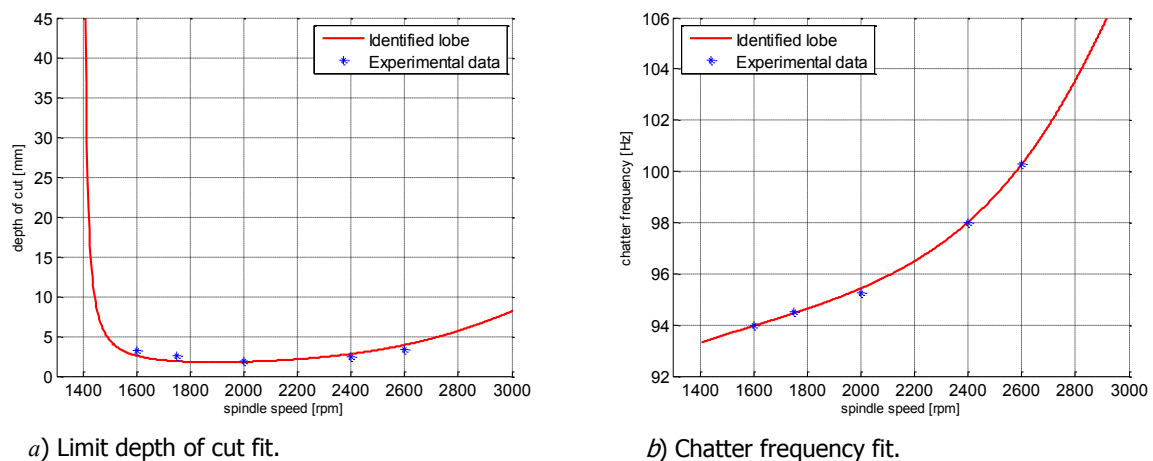
Figure 7.9: Comparison of experimental data points with identified stability lobe for first experiment.

The change in modal stiffness can be due to the fact that in the real process more than one mode is affecting the stability and the chatter frequencies in this spindle speed

range. The high experimental chatter frequencies define a high damping ratio if only one dominant mode is considered, and consequently this high damping brings along a low modal stiffness. The model is probably too simple to reflect the real behavior of the system and, for that reason, inconsistent values can be obtained for modal parameters. An improvement is required in the inverse method to introduce at least the effect of the flexibility in other directions.

Finally, as observed in Table 7.2, the limit depths of cut when slope is increasing and decreasing are different from each other. Using the results obtained with increasing and decreasing depth of cut, two different set of parameters can be obtained and consequently two different lobes can be created as shown in Figure 7.10. The area between the two lobes is defining an unsafe zone (Figure 7.10a) where the cutting can be stable depending on the perturbation or the vibration characteristics (Shi and Tobias, 1984).
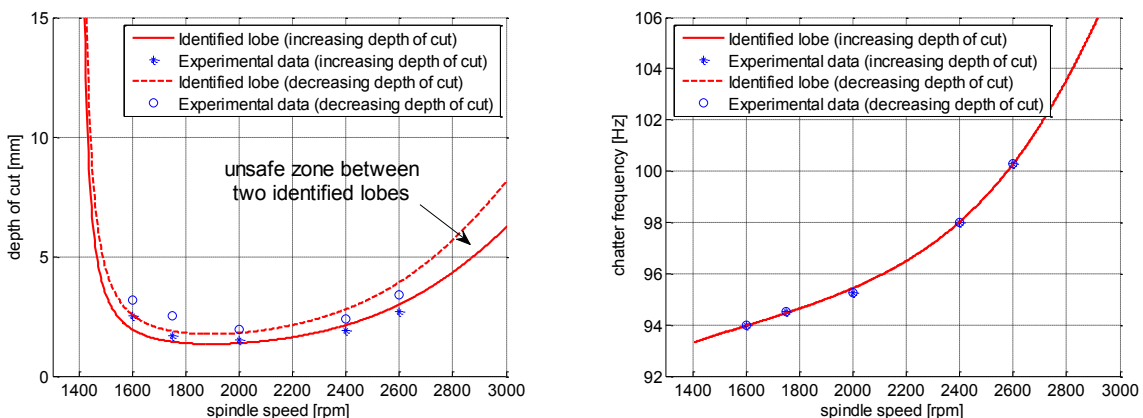
a) Limit depth of cut comparison. Unsafe zone appears between two identified stability lobes.

b) Chatter frequency comparison.

Figure 7.10: Comparison of identified stability lobes fitted to data measured when depth of cut is increasing and decreasing (for first experiment).

7.2.3   Effect of Tool Wear

At the beginning of each experiment, the flank wear on both primary and secondary clearance faces of the tool is measured as listed in Table 7.3.

	Tool life	Flank Wear Width (V_B) on primary clearance face	Flank Wear Width (V_B) on secondary clearance face	Tangential cutting coefficient (K_t)	Radial cutting coefficient (K_r)
Experiment 1	0	New tool	New tool	1459 [MPa]	257 [MPa]
Experiment 2	25 [m]	179 [μm]	82 [μm]	-	-
Experiment 3	51 [m]	245 [μm]	100 [μm]	1457 [MPa]	257 [MPa]
Experiment 4	75 [m]	260 [μm]	138 [μm]	-	-
Experiment 5	100 [m]	275 [μm]	164 [μm]	1455 [MPa]	259 [MPa]
Experiment 6	156 [m]	971 [μm]	184 [μm]	1767 [MPa]	384 [MPa]

Table 7.3: Technical information of slope cutting experiment.

The slope milling experiments with worn tools are analyzed as shown in (Table 7.3) with the corresponding estimated modal parameters listed in Table 7.4. There is almost no change in chatter frequency for all experiments (Figure 7.11*b*). Similarly, limit depths of cut do not change significantly (Figure 7.11*a*). Modal damping ratio increases slightly, but, in general the estimated modal stiffness and damping for all worn tools are almost similar for all flank wear values. Only the last test carried out using a completely worn out secondary flutes (clearance face) yields different results.

	Natural frequency [Hz]	Modal damping ratio [%]	Modal stiffness [N/μm]	$2k\xi$ [N/μm]
Hammer test	94.0	0.66	58.4	0.78
Experiment 1	93.3	1.82	12.2	0.44
Experiment 2	93.5	1.81	14.0	0.51
Experiment 3	93.0	1.90	12.6	0.49
Experiment 4	93.1	1.90	12.1	0.46
Experiment 5	93.0	1.92	12.0	0.46
Experiment 6	92.4	2.05	14.0	0.58

Table 7.4: Modal parameters of mode in *u*-direction estimated for all experiments (defined in Table 7.3).

a) Measured limit depth of cut

b) Measured chatter frequency
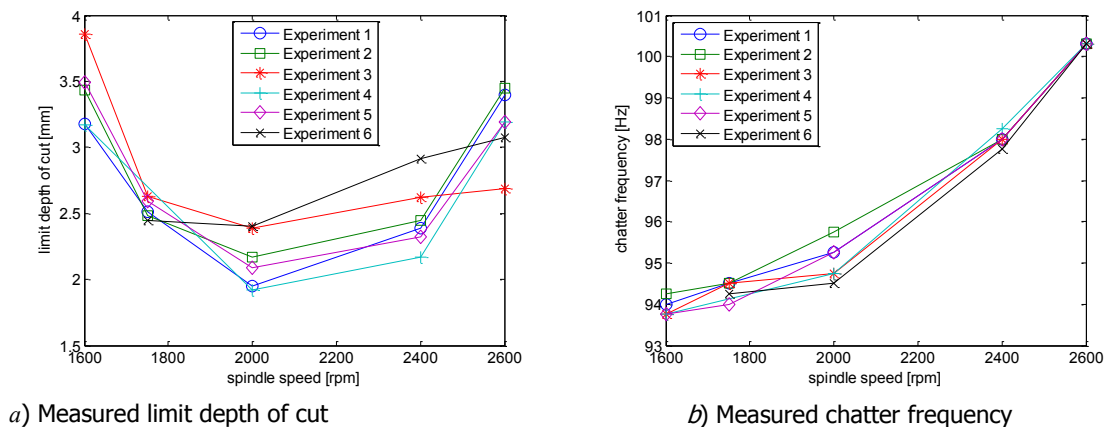
Figure 7.11: Comparison of experimental data measured when wear is increasing.

As a conclusion, experiments showed that critical depth of cut does not change cutting steel with increased flank wear when the chatter frequency is lower than the tooth passing frequency (in the highest stability lobe, l=0).

However, as the speed is reduced significantly, the flank wear surface will rub against the waves and increase the process damping, which will in turn increase the depth of cut as reported in (Altintas et al., 2008a). The same procedure can be repeated in higher order lobes to confirm this effect and obtain wear dependent parameters using inverse methods.

7.3   CONCLUSIONS

Structural dynamic parameters of a spindle-tool system are traditionally identified from impact modal test when the machine is not rotating. However, some spindles and mechanical systems may exhibit varying stiffness and damping at different speeds during milling operations.

This chapter presented an inverse modal parameter estimation method from chatter tests. An analytical procedure has been presented for the cases with one dominant mode and two equal and orthogonal modes based on the determination of an equivalent directional factor. In the case of two modes, the directional factor is complex and therefore the imaginary part of FRF of the mode also affects the depth of cut value.

When the system dynamics are dominated by a single mode in one direction, the proposed estimation method leads to highly accurate modal parameter estimation, which in turn leads to accurate prediction of stability charts. However, when there are different modes in two directions, the mode coupling affect the accuracy of the modal parameters.

The model is too simple to cover the behavior of the system in a realistic way and, for this reason, inconsistent solutions for the extracted dynamic parameters may be obtained. In the experimental study, workpiece is considered flexible in one direction and machine tool is assumed rigid. In reality, workpiece mode in other direction and machine tool modes may also affect stability. In that case, inverse method should be improved by introducing new parameters to consider such additional flexibility sources. New parameters would be static or residual stiffness of mode directions if the new additional modes are far from the dominant mode. Moreover, if the machine tool had a mode close to dominant workpiece mode a new formulation would have to be derived.

Thus, the observed drop in modal stiffness of the workpiece mode would become more reasonable.

The influence of tool wear on stability has been investigated using the inverse method in the highest stability lobe (l=0). The experiments carried out and the modal parameters obtained with the inverse method show that the influence of wear is negligible in this cutting speed range.

Contribution 8:

An inverse modal parameter estimation method from chatter tests has been described. A new analytical formulation for the case of two equal and orthogonal modes has been developed, based on the determination of an equivalent directional factor.

Contribution 9:

The inverse methodology can improve chatter prediction by more accurate dynamic parameter identification in systems with one dominant mode. An increase of damping and a decrease of stiffness with respect to traditional dynamic parameter extraction methods have been observed.

Nevertheless, the model employed is too simple to describe the system and, for this reason, unrealistic dynamic parameter oscillations may be found. The developed methodology loses accuracy when more than one mode is involved in stability limitation, as it is the usual case in machine tool dynamics.

Contribution 10:

The effect of tool wear on cutting coefficients or dynamic parameters is negligible for the conventional spindle speed range tested. These parameters are only affected when tool wear is in a very advanced state (faults visible to the human eye). Therefore, it can be concluded that in normal cutting conditions, tool wear can be neglected for stability analysis.

Related Publications:

Kilic, Z. M., Iglesias, A., Munoa, J., & Altintas, Y. (2010). Investigation of tool wear on the stability of milling process using an inverse method. *CIRP 2nd International Conference on Process Machine Interactions*, Vancouver, Canada.

Chapter 8

FRF Estimation through Sweep Milling Force Excitation (SMFE)

The method proposed here intends to go one step further than the inverse methodology proposed in Chapter 7, simplifying the necessary cutting tests and extending the validity of the methodology to any kind of dynamic system through a different approach.

A new method to obtain FRFs using the milling force itself as the input excitation is presented. The structure is excited through a machining operation with increasing or decreasing speed and the resulting forces and accelerations on the structure are measured. Thus, the structure dynamics are characterized under real machining conditions and the nonlinear effects related to the rotating spindle or the cutting process are also considered.

This new method, which has been named sweep milling force excitation (SMFE) approach, will produce more accurate FRFs than traditional methods, such as impact tests or shaker excitation, which are currently regarded as one of the main sources of inaccuracies for model stability input data. These inaccuracies can cause severe stability misjudgments, as it was demonstrated in Chapter 4.

The approach is simple and fast to execute, although a certain degree of knowledge is required in order to design a proper cutting test. Force and acceleration measuring sensors are also needed to apply this novel technique.

Next, the procedure to apply the method is described, the simulations carried out to verify the feasibility of the method and prepare the most appropriate test plan are presented and the experimental validation of the method is shown.

8.1   FRF ESTIMATION PROCEDURE: SMFE METHOD.

This work presents a new method called swept milling force excitation (SMFE) to obtain the dynamic response of the structure in a fast and easy way, using the cutting force itself as the input excitation for the FRF calculation.

Previous researches in this field (Opitz and Weck, 1969; Minis et al., 1990) used especial workpieces in order to produce random forces, which would consequently apply a random excitation in the structure. They tried to avoid the typical harmonic content of the milling force. However, in this work this harmonic content will be the input excitation used to obtain the FRF, analyzing the frequency response function in an analogue way as a chirp excitation case.

The experimental procedure is divided in next steps.

8.1.1   Selection of the excitation parameters

First of all, the frequency range of interest is defined. The main modes involved in the process stability must be within this range, in order to perform a complete dynamic characterization. The milling rotating speed is varied continuously in time over a defined range, in such way that the tooth passing frequency and/or its first harmonics are swept over the desired frequency range. It is important that these harmonics have high energy content in order to apply a strong excitation. An interrupted cutting process, with a small width of cut, is therefore used for this purpose. Figure 8.1 shows the spectrogram of three different tools when performing the SMFE method. Figure 8.1a, Figure 8.1b and Figure 8.1c correspond to a 2-insert tool, 6-insert tool and 1-insert tool respectively. It is noticeable that the main tooth passing harmonic Ω is swept from the beginning to the end of the frequency range of interest (12-42Hz in this case). This explains the different spindle speed range selected for each of the different tools. Depending on the number of inserts of each tool, there are other strong harmonics exciting partially the frequency range of interest.
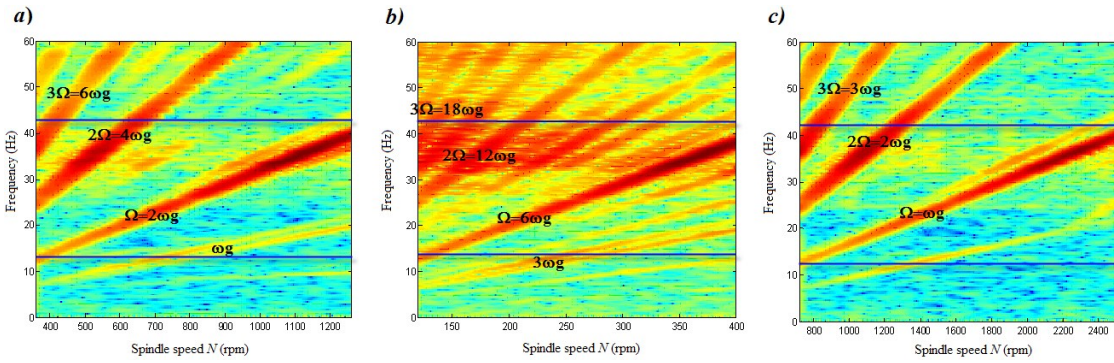
Figure 8.1: Spectrogram of the SMFE method for 3 different tools: *a*) *D*=125, *Z*=2; *b*) *D*=125mm, *Z*=6; *c*) *D*=32, *Z*=1.

8.1.2   Test plan definition

The frequency response function $\Phi(\phi)$, which relates the input excitation and the output response, can be calculated by different methods. In this case the Φ_1 estimate will be used:

$$\Phi_1 = \frac{G_{rF}}{G_{FF}}, \tag{8.1-1}$$

where G_{rF} is the cross spectrum between the output *r* and the input *F* and G_{FF} is the power spectrum of the input *F*.

According to previous works (Orlando et al., 2008), single-block DFT computation along the entire sweep data collection leads to a good FRF estimation. The cross and power spectra are computed as:

$$G_{rF}(f) = \frac{1}{N_a} \sum_{i=1}^{N_a} r_i(f)\, F_i(f), \tag{8.1-2}$$

$$G_{rr}(f) = \frac{1}{N_a} \sum_{i=1}^{N_a} r_i(f)\, r_i(f),$$

$$G_{FF}(f) = \frac{1}{N_a} \sum_{i=1}^{N_a} F_i(f)\, F_i(f),$$

where N_a is the number of averages.

The cutting force is divided into three spatial components, according to the model derived in Chapter 2. The system is regarded as a MIMO system, where multiple inputs and multiple outputs are produced with each cutting speed sweep.

$$G_{xFx} = \Phi_{xx}\, G_{FxFx} + \Phi_{xy}\, G_{FyFx} + \Phi_{xz}\, G_{FzFx},$$

$$G_{yFx} = \Phi_{yx}\, G_{FxFx} + \Phi_{yy}\, G_{FyFx} + \Phi_{yz}\, G_{FzFx}, \cdot \tag{8.1-3}$$

$$G_{zFx} = \Phi_{zx}\, G_{FzFx} + \Phi_{zy}\, G_{FzFx} + \Phi_{zz}\, G_{FzFx}.$$

As there are nine unknowns to solve, at least three different cutting tests must be performed in order to solve the system. If a 90º lead angle tool is used, the axial force F_z can be neglected and a 2-input 2-output system is obtained. In this case, at least two cutting tests are needed to obtain as many equations as unknown terms.

It has to be considered that the measurements must be independent from the previous tests, modifying the ratio of amplitudes or phases between the different force terms F_x, F_y and F_z. This can be accomplished by a substantial change in the tool immersion for each test. When two dimensions are considered, an easy way to accomplish this condition is changing the cutting strategy from down-milling to up-milling direction, whereas for three directions, at least three cutting tests are needed. A good option for this case is performing cutting tests in down-milling, up-milling and central-milling, as defined in Figure 8.2:
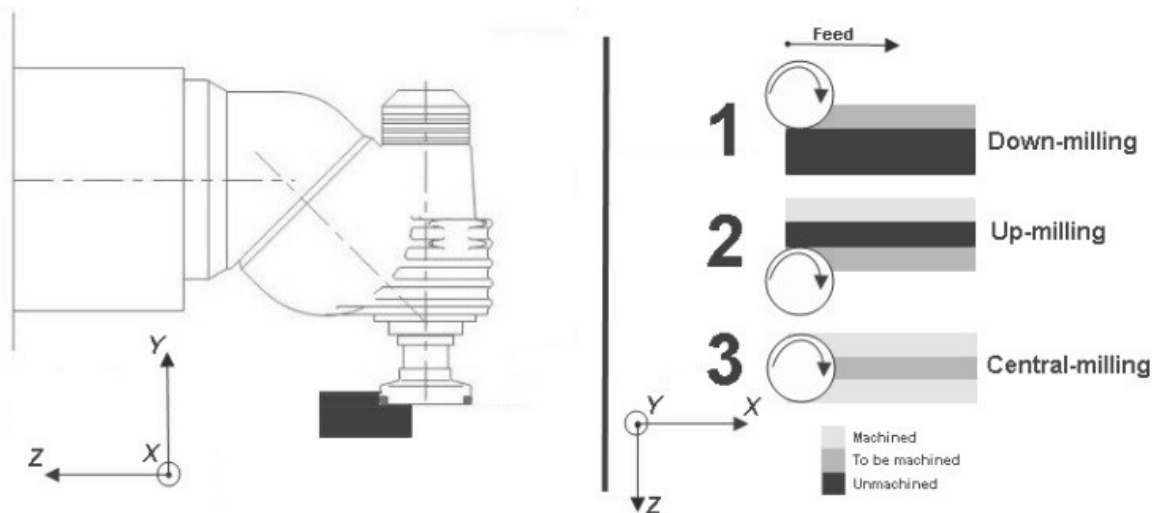
Figure 8.2: Cutting tests outline. Three different cutting tests are performed order to obtain the 9 terms [Φ] matrix of the system: down-milling cut, up-milling cut and central-milling cut.

The frequency response functions will be calculated from the cutting tests. Therefore, the force must be measured by means of a dynamometric plate or a dynamometric toolholder, whereas the response could be measured by means of accelerometers. Initial value time domain simulations are useful in order to define the parameters of the cutting tests to perform.

8.1.3   Test performance and post-processing

The cutting test plan defined in section 8.1.2 is performed and the measured data post-processed, solving the following system of 9 equations:

$$
\begin{bmatrix} G_{xF_x1} \\ G_{yF_x1} \\ G_{zF_x1} \\ G_{xF_x2} \\ G_{yF_x2} \\ G_{zF_x2} \\ G_{xF_x3} \\ G_{yF_x3} \\ G_{zF_x3} \end{bmatrix} = \begin{bmatrix} [\Phi] & . & . & 0 & . & . & 0 \\ . & & & & . & . \\ . & & & . & & . \\ . & & & . & & . \\ 0 & & [\Phi] & & & 0 \\ . & . & & & & . \\ . & . & & & & . \\ 0 & . & . & 0 & . & . & [\Phi] \end{bmatrix} \begin{bmatrix} G_{F_xF_x1} \\ G_{F_yF_x1} \\ G_{F_zF_x1} \\ G_{F_xF_x2} \\ G_{F_yF_x2} \\ G_{F_zF_x2} \\ G_{F_xF_x3} \\ G_{F_yF_x3} \\ G_{F_zF_x3} \end{bmatrix}, \tag{8.1-4}
$$

where the 3×3 FRF is defined as:

$$
[\Phi] = \begin{bmatrix} \Phi_{xx} & \Phi_{xy} & \Phi_{xz} \\ \Phi_{yx} & \Phi_{yy} & \Phi_{yz} \\ \Phi_{zx} & \Phi_{zy} & \Phi_{zz} \end{bmatrix}. \tag{8.1-5}
$$

A higher number of tests could be carried out in order to have a redundant system and increase the accuracy of the solution.

8.1.4 Measurement quality check

It is important to check the following indicators, in order to make sure that the $[\Phi]$ matrix obtained is reliable.

- **Condition number.**
  When the set of equations to solve the system is built, it is important to check the conditioning of the coefficient matrix in order to make sure that the system is completely independent. A low condition number will be proof of a well-conditioned matrix.

- **Coherence function.**
  The coherence function, which gives an estimate of the quality of the measurement by analyzing the repeatability of the performed averages, is defined as:

$$
\gamma_{rF}^2 = \frac{G_{rF}\, G_{rF}^*}{G_{rr}\, G_{FF}}. \tag{8.1-6}
$$

8.2 FRF SIMULATIONS

The theoretical FRFs have been simulated according to the SMFE method described in section 8.1. The excitation forces and responses needed for the simulation are calculated according to the theoretical time domain model described in section 2.3.7. The objective of these simulations is to determine the feasibility of the SMFE method, analyze the influence of the sweep length and find the ideal cutting conditions for an optimum FRF estimation through the SMFE method.

The analyzed system is a flexible fixture with a dominant mode in each axis x and y (see Figure 8.3).
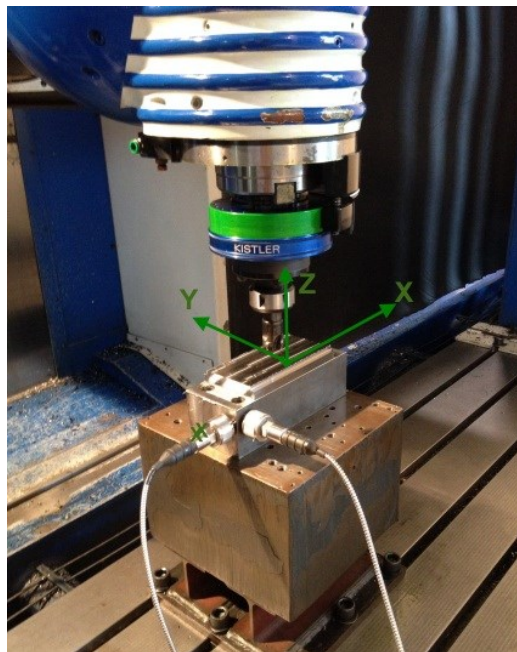
Figure 8.3: Flexible fixture with one dominant mode in each direction x and y.

A hammer test is conducted in order to extract the modal parameters in the traditional way. The SMFE is simulated and the FRF estimation procedure is tested and compared with the "static" FRF. The cutting conditions of the SMFE are described in Table 8.1:

The milling sweep borders, that is, the rotating speeds between which the simulation is done, are selected according to the frequency range of interest. From the hammer test it is known that the flexible fixture presents two modes at around 71Hz (y axis) and 159Hz (x axis). If the 71Hz mode must be excited, a frequency sweep from 50Hz to 100Hz should be considered. This implies the use of a rotation speed from 1500rpm to 3000rpm, since the excitation is achieved by means of the insert passing frequency

(2X). This means that the second harmonic of the insert passing frequency will excite the range between 100-200Hz and therefore, the *x* axis mode.

Direction	Down-milling / Up-milling
Workpiece material	C45k
Tool	490-032A25-08M
Inserts	490R-08T308M-PH
Diameter	32 [mm]
Number of inserts	2
Cutting speed range	150-300 [m/min]
Rotation speed range	1500-3000 [rpm]
Depth of cut	1 [mm]
Width of cut	6.4 [mm]

Table 8.1: Cutting conditions of the milling sweep tests.

In order to have enough equations to solve the system, two independent tests are simulated. The conditions are exactly the same for both tests but the cutting strategy is changed from down-milling to up-milling.

In order to guarantee the coherence of the system, each test is repeated four times and a frequency averaging of the results is done. Uncorrelated noise is added to the theoretical system with the purpose of simulating a real system in which noise is also recorded. The coherence of the direct FRFs is calculated from the four repetitions (Figure 8.4) and, in this way, the useful frequency range is detected. As the harmonic content is basically limited to the insert passing frequency 2X (50-100Hz) and its second harmonic 4X (100-200Hz), the useful frequency range is about 50-200Hz . Out of this range, the harmonic content is very weak and the signal to noise ratio is too small to consider the frequency response function as a reliable value.
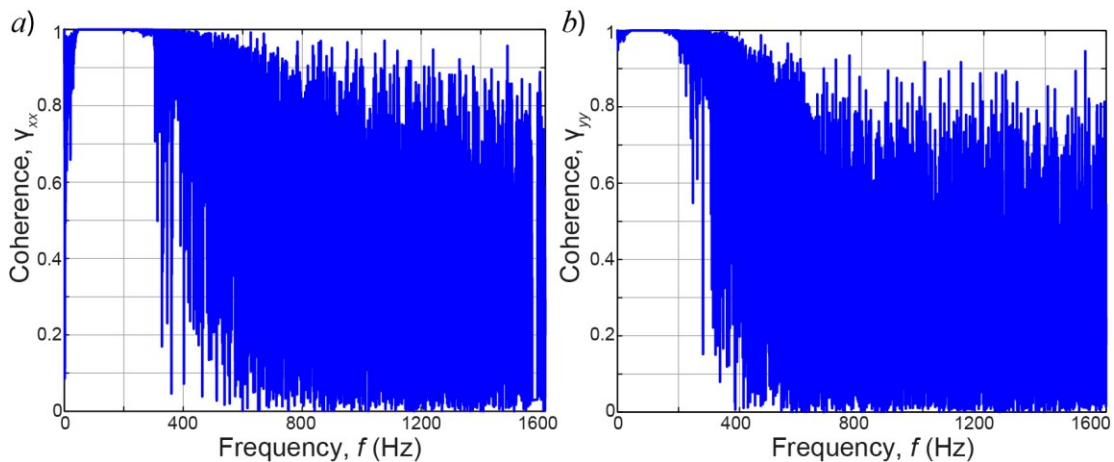
Figure 8.4: Simulated coherence functions in SMFE FRFs.

Three different milling sweeps (T=30s, T=10s and T=5s) are performed in order to analyze the influence of the milling force sweep rate and select the one with best accuracy versus consumed time rate. The machine spindle speed is increased linearly in order to cover the whole frequency range.

In Figure 8.5 different milling sweep simulations at different speed rates are compared with the standard experimental FRF (hammer test):
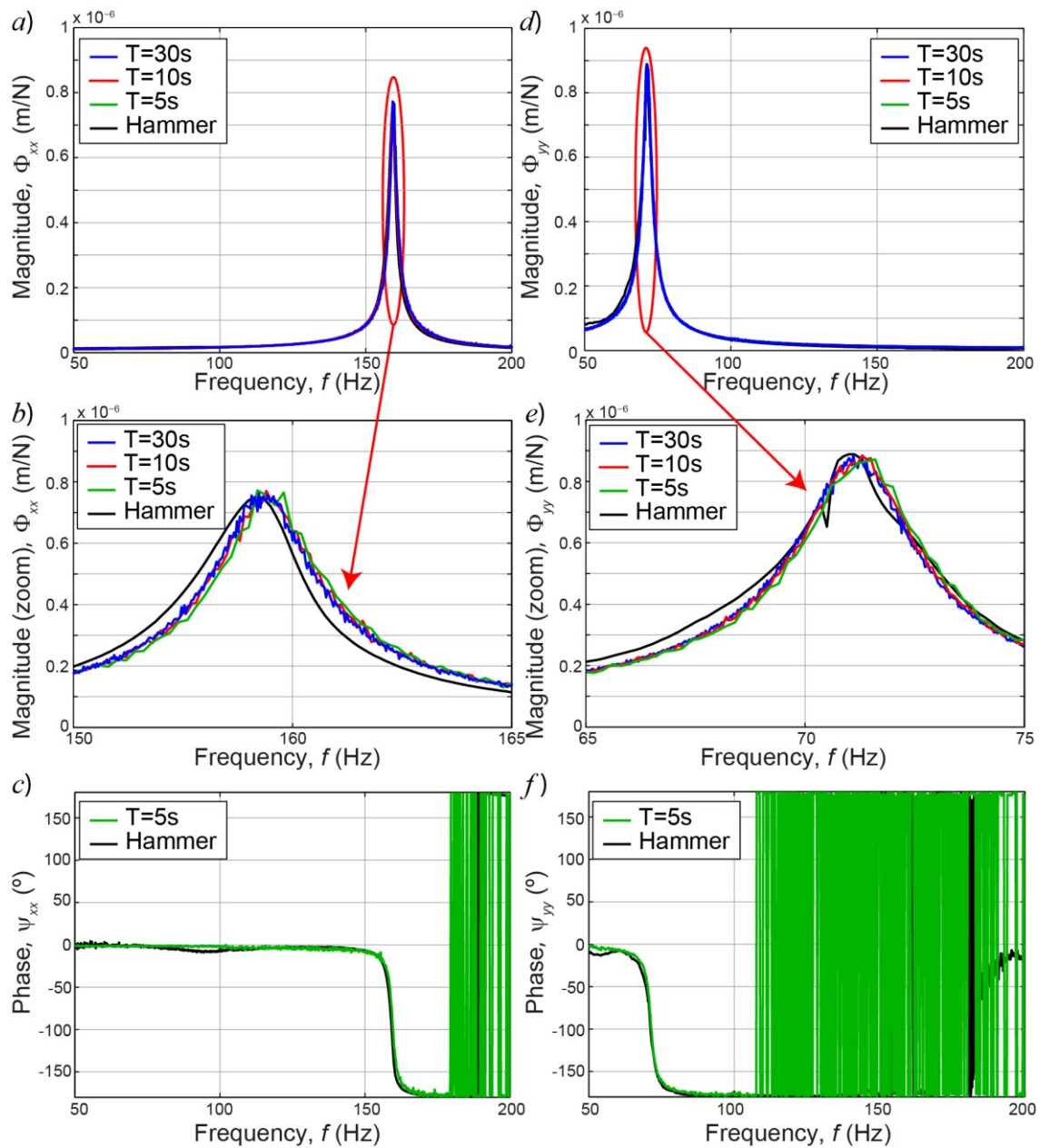
Figure 8.5: Hammer test and SMFE test comparison in *x* and *y* axes.

According to Figure 8.5, the milling sweep test introduces a certain delay in the frequency peaks related to the main modes. The faster the sweep the bigger this delay is, although the difference is not that significant. The amplitude is also well simulated, so it is concluded that the procedure to obtain the FRF is theoretically valid.

8.3   EXPERIMENTAL VERIFICATION

8.3.1   Experimental setup

Real SMFE experiments have been carried out on a 3+2 axes SV milling machine. The forces in the three axes x, y and z have been measured with a dynamometric tool holder (Kistler 9124B1111) and a dynamometric plate (Kistler 9257BA) attached to the machined workpiece, whereas the response in the spindle head has been measured by means of three accelerometers, as shown in Figure 8.6. Every cutting test has an approximate duration of 30s and three different cutting tests are performed in order to completely define the matrix in equation (8.1-5).
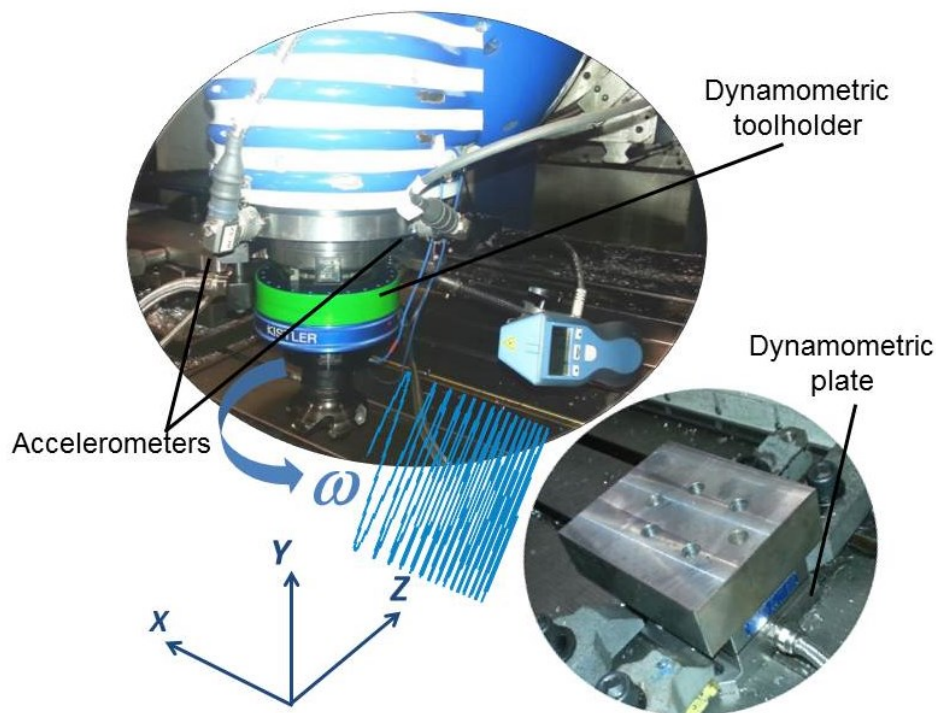
Figure 8.6: Experimental test configuration. The forces are recorded by means of a dynamometric tool holder and a dynamometric plate below the test workpiece. The response is measured through three accelerometers located on the spindle head.

Finally, every test is repeated four times and frequency averaging is carried out in order to minimize noise.

8.3.2   Influence of the tool

Different types of tools have been used for SMFE implementation. The purpose was to test different ratios between the applied cutting forces in the Cartesian axes, due to their different insert geometry (see Table 8.2).
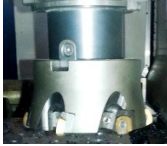
Tool number	Picture	Number of inserts	Lead angle	Tool reference
1		2	45°	Sandvik R245-080Q27-12M
2		6	~0°	Hitachi GFH476 ASF5125RM
3		1	90°	Sandvik 490-032A25-08 M

Table 8.2: Tools used for SMFE experimental tests.

The cutting conditions used for each type of tool vary, due to their different diameter to number of teeth D/Z ratio, in order to excite the same frequency region. The conditions used for each tool are summarized in Table 8.3.

Tool n.	N range (rpm)	a (mm)	f_z (mm/Z)	Immersion (%D)	Cutting direction
1	1260-360	1	0.2	12.5	x- Down-milling
					x- Up-milling
					x- Central-milling
2	400-120	0.2	0.2	12.5	x- Down-milling
					x- Up-milling
					x- Central-milling
3	2520-720	1	0.2	12.5	x- Down-milling
					x- Up-milling
					x- Central-milling

Table 8.3: Cutting conditions for SMFE.

In Figure 8.7, the FRF results achieved with the tests by each tool separately and the FRF obtained with the tools 1 & 2 (taking every test performed with these tools into account) have been compared.
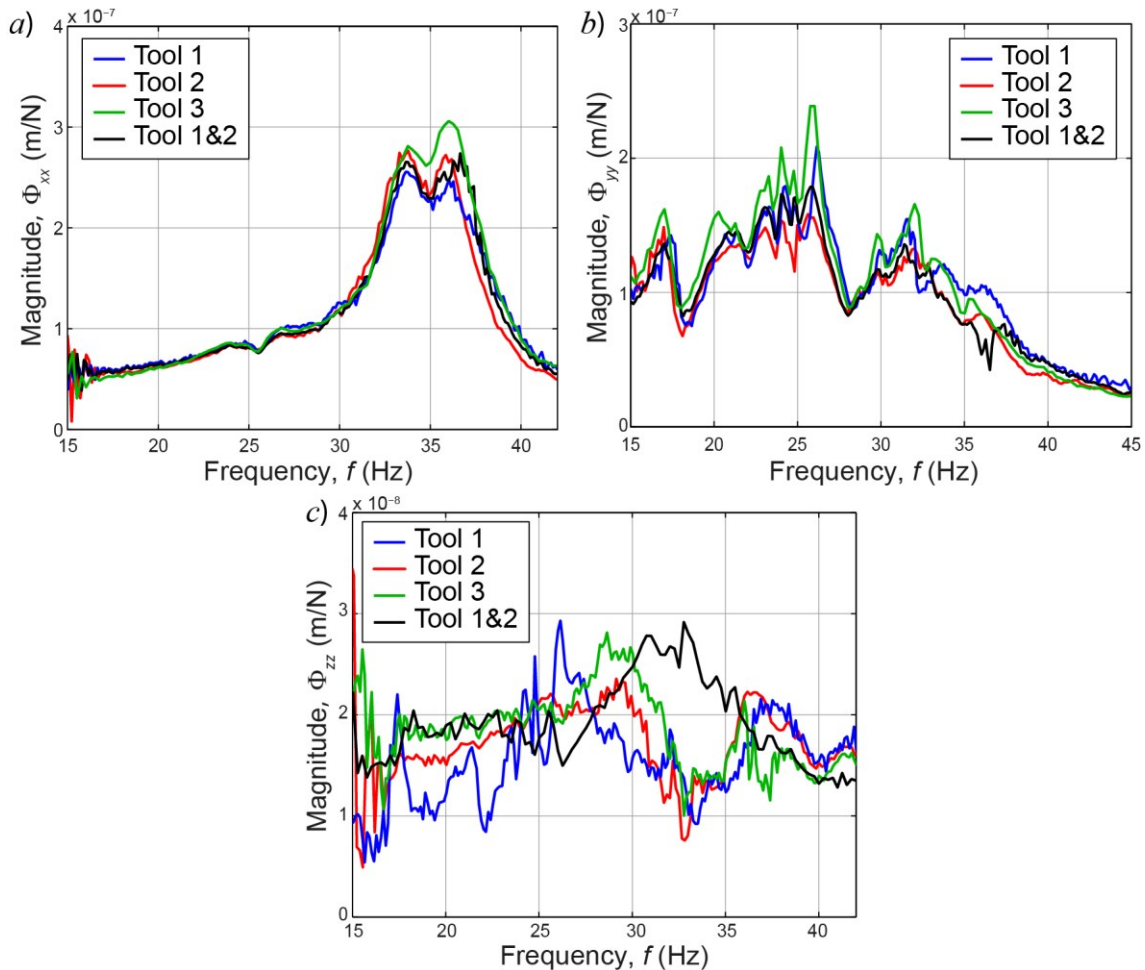
Figure 8.7: Comparison of the FRFs in x, y and z axes obtained with the SMFE method using different tools. *a)* Φ_{xx}; *b)* Φ_{yy}; *c)* Φ_{zz}.

The obtained FRFs do not vary significantly, although tool number 3 results in a noisier FRF and less coherent results (see Figure 8.8). This is due to the fact that its 90º lead angle does not allow a proper excitation in *y* axis. It is therefore crucial that a sufficiently strong excitation is applied in every direction of interest in order to achieve good quality FRFs.
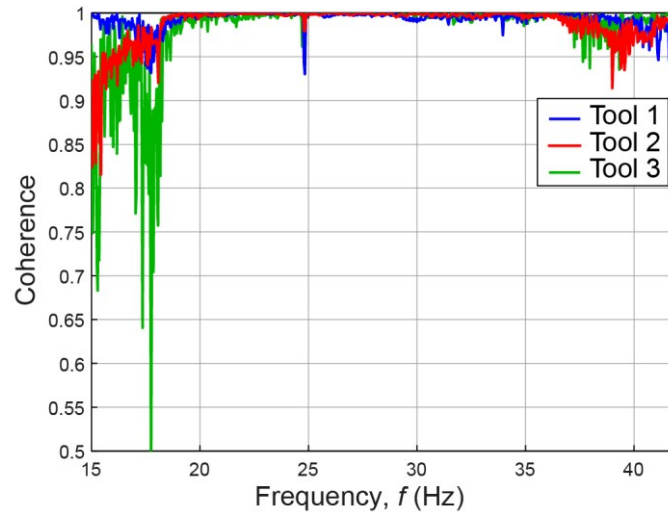
Figure 8.8: Comparison of the coherence functions of SMFE in *y* direction.

8.3.3   Influence of the force level

With the purpose of analyzing the influence of the cutting force level on the obtained FRF, different SMFE procedures have been repeated for tool number 1, varying only the depth of cut, thus, varying the excitation force level. This is an important test to observe the degree of nonlinearity of the machine.

The results are summarized in Figure 8.9. The resulting FRFs show a very slight decrease of static stiffness and increase of the amplitude of the peaks on the FRF as the excitation force increases.
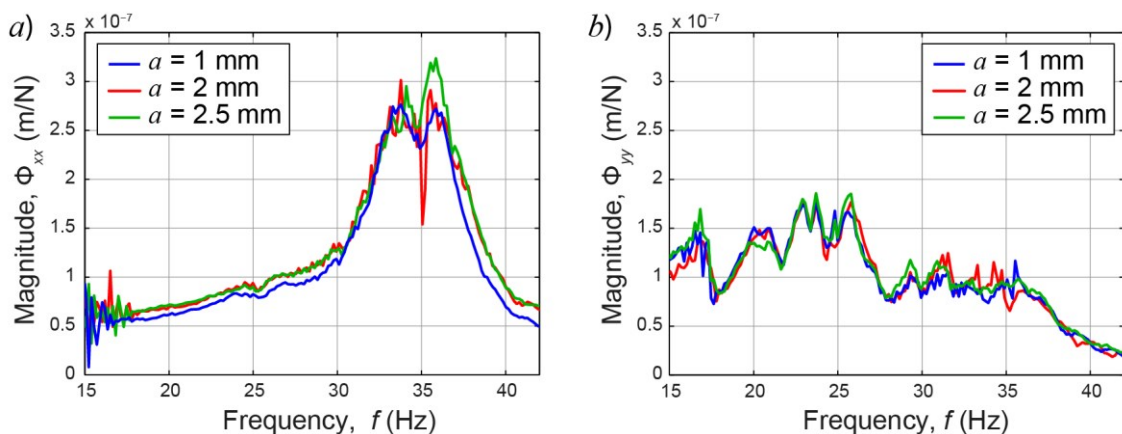
Figure 8.9: Comparison of the SMFE FRFs with different cutting depths. *a)* Φ_{xx}; *b)* Φ_{yy}. The FRFs remain almost unchanged with increasing depth of cut.

8.3.4 SMFE comparison with traditional FRF by means of hammer and shaker

Finally, the SMFE FRF was compared with the hammer and shaker FRF. The characteristics of these tests are described in Table 8.4 whereas the results can be observed in Figure 8.10.
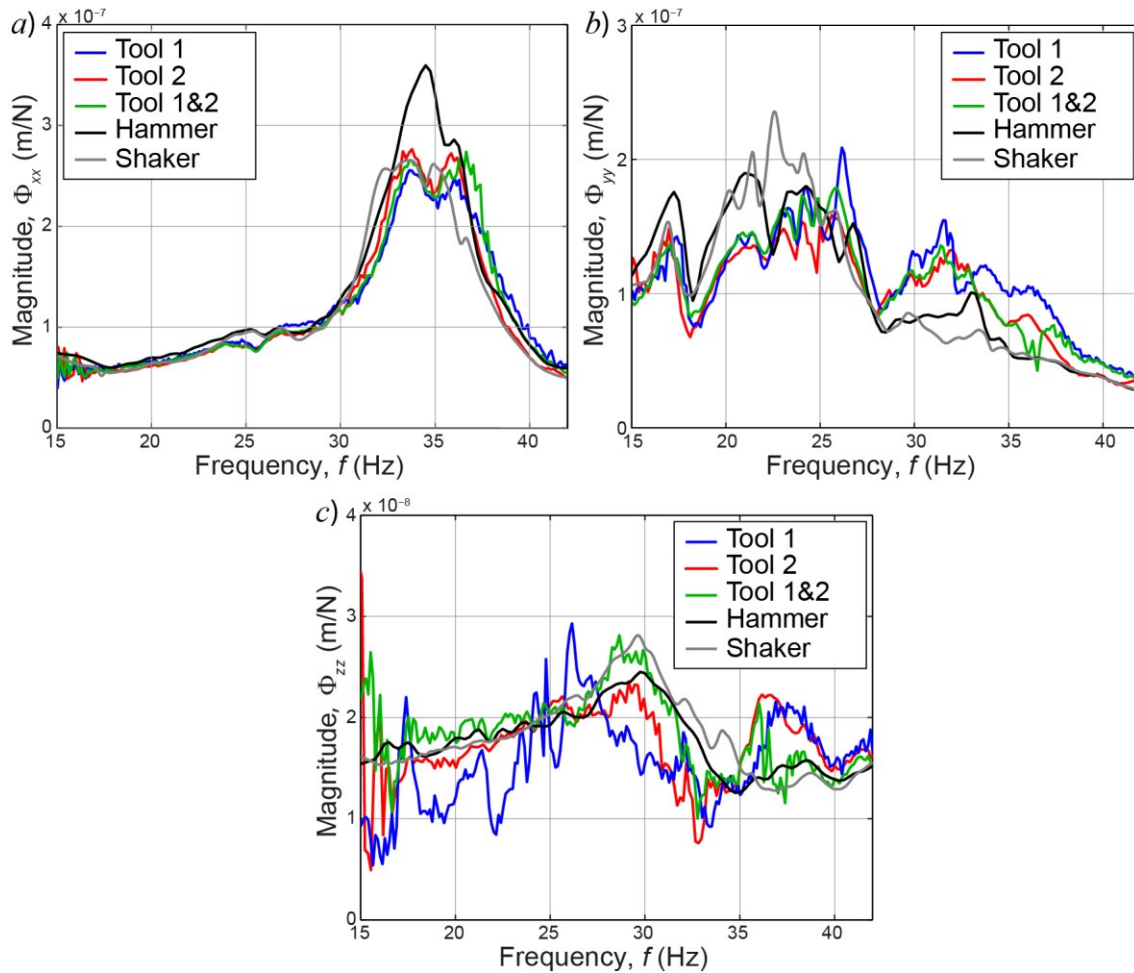
Figure 8.10: Comparison of the SMFE FRFs with traditionally obtained FRFs. a) Φ_{xx}; b) Φ_{yy}, c) Φ_{zz}.

FRF estimation methods	Type of excitation	Frequency resolution (Hz)	Number of averages	Test time (s)
Hammer test	Impulse	0.25	4	4
Shaker test	Stepped sine	0.25	1	240
SMFE	Sweep milling	0.25	4	26

Table 8.4: Cutting parameters for stability lobe calculation and experimental validation through cutting tests.

In x direction, two very close peaks can be observed. The first peak is higher for the hammer test, whereas the second one remains almost unchanged. In such close frequency peaks, one of the peaks could have a disruptive effect on the other one, attending to the real part plot. This could make that even if the amplitude is higher for the hammer FRF, the real part could be changed in such way that the stability would be higher. In y direction the traditional FRFs show a differentiated shape from the SMFE FRFs, with a noticeable drop at frequencies over 27Hz.

8.4   STABILITY LOBE VALIDATION

The FRFs obtained in the previous section (see Figure 8.10) will be used for the stability prediction through the theoretical lobes. The theoretical stability lobes can be calculated according to the model shown in section 2.3. The conditions of the cutting process that has been simulated are shown in Table 8.5. With these conditions the first lobe, $l = 0$ in (2.1-1), which is related to the low frequency modes, limits the stability. Therefore, it is suitable to compare the new FRF estimation method developed versus the traditional methods to obtain the FRF.

Tool				
Diameter (*D*)	Number of flutes (*Z*)	Picture	Lead angle (*κ*)	Helix angle (º)
125mm	12		45	0
Cutting conditions & coefficients						
Engagement	f_z (mm/Z)	Feed direction	*N* (rpm)	K_t (N/mm²)	K_r (1)	K_a (1)
118mm (Down-milling) 118mm (Up-milling)	0.2	*x*-	180 200 250 300 360	1889.1	0.411	0.193

Table 8.5: Cutting parameters for stability lobe calculation and experimental validation through cutting tests.

In order to assess the accuracy of stability prediction, real cutting tests were carried out under the same cutting conditions. The comparison of the theoretical and experimental results is shown in Figure 8.11.
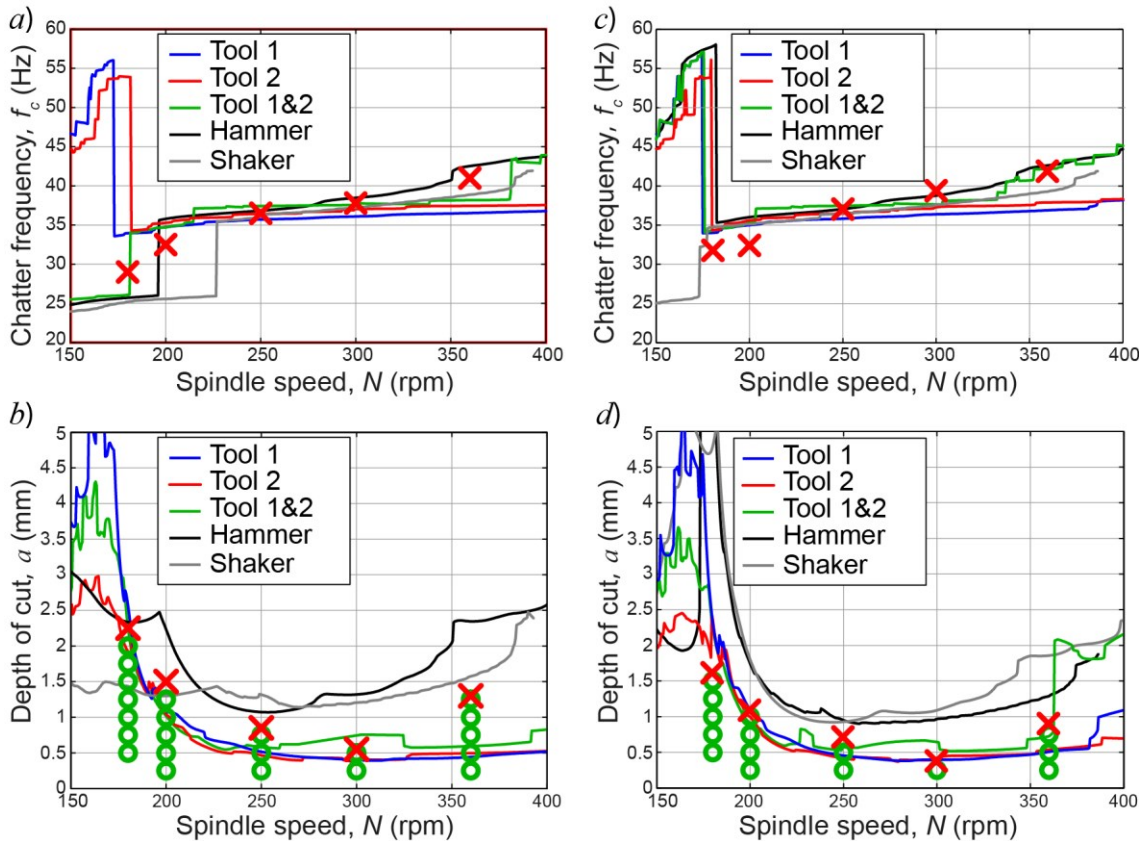
Figure 8.11: Comparison of the lobes obtained from SMFE method FRFs with lobes obtained from standard FRFs. *a*) chatter frequency f_c for down-milling; *b*) depth of cut *a* for down-milling; *c*) chatter frequency f_c for up-milling; *d*) depth of cut *a* for up-milling. Experimental stable tests (green circles) and unstable tests (red crosses) are also shown.

The lobe results may seem incompatible with the FRF graphs shown in section 8.3.4 if only the absolute value of the dynamic stiffness is compared. However, as explained in section 8.3.4, the FRF region close to the chatter critical mode has a higher dynamic stiffness in the SMFE case for *y* axis. On the other hand, the two close modes in the region of 35Hz in *x* direction could affect each other, resulting in an unexpected behavior in terms of stability.

The lobes calculated by means of the traditional FRF estimation procedures (hammer and shaker) overestimate machine's cutting capability, whereas the lobes calculated by means of the SMFE FRF match reasonably well with the experimental tests. The errors incurred by each method are summarized in Table 8.6.

		180 rpm	200 rpm	250 rpm	300 rpm	360 rpm	Average
Down	**Hammer**	4%	48%	26%	140%	80%	**59%**
	Shaker	36%	13%	54%	119%	21%	**43%**
	SMFE Tool 1	14%	28%	39%	29%	66%	**35%**
	SMFE Tool 2	15%	31%	45%	27%	62%	**36%**
	SMFE Tools 1&2	0	33%	32%	35%	54%	**31%**
Up	**Hammer**	200%	64%	32%	173%	118%	**115%**
	Shaker	305%	58%	36%	142%	52%	**118%**
	SMFE Tool 1	14%	28%	39%	29%	66%	**35%**
	SMFE Tool 2	15%	31%	45%	27%	62%	**36%**
	SMFE Tools 1&2	0	33%	32%	35%	54%	**31%**

Table 8.6: Stability prediction error (%) comparing hammer test, shaker test, SMFE with results from Tool 1, SMFE with results from Tool 2 and SMFE with results from Tools 1 & 2.

In conclusion, these experiments validate the expected higher accuracy of the new dynamic characterization method developed in this work (SMFE method).

8.5   CONCLUSIONS

A new methodology for FRF estimation using the milling force itself as input excitation (SMFE method) has been developed. This method provides a closer excitation to the real in-process conditions than traditional FRF estimation methods like hammer or shaker tests. The methodology consists of exciting the structure through several independent interrupted milling cuts, through proportional ascending or descending cutting speed, in order to perform a frequency sweep over the frequency range of interest by means of the cutting harmonics.

It is convenient to carry out simulations as a previous step to the SMFE test performance in order to define the optimum cutting process to excite the structure. The type of tool, cutting parameters, spindle speed range, duration of the sweep and number of cutting tests to perform are among the main parameters to define. The type of tool should have an adequate geometry to excite the structure in the important directions to characterize; the cutting parameters should guarantee the independence of the different excitation tests performed for a single point FRF calculation; the spindle speed range should be wide enough to properly excite the frequency range of interest through the main cutting harmonics; the duration of the sweep must be long enough to achieve a fine resolution of the FRF and the number of tests to perform is important in order to have enough equations to solve the system.

It has been experimentally proven that the excitation magnitude and the type of tool to use do not entail a significant variation in frequency response, as long as the level of the cutting force is kept within the standard cutting force range and the tool geometry allows a minimum excitation in every direction to characterize.

The obtained FRF through SMFE method does not differ dramatically from traditional FRF methods (hammer and shaker). However these slight differences may have a considerable effect on stability lobes. Thus, stability lobes calculated through SMFE FRFs show a more restrictive cutting limit that matches the experimental tests more accurately. The stability prediction through traditional FRFs shows big deviations, with average cutting depth prediction errors higher than 100% and specific errors at certain speeds higher than 300%. On the other hand, prediction through SMFE FRFs shows an average cutting depth prediction error around 30% and specific errors at certain speeds never higher than 70%, therefore improving stability prediction to a large extent.

Contribution 11:

A new simple and fast methodology for FRF estimation using the milling force itself as input excitation (SMFE method) has been developed. This method provides a closer excitation to the real in-process conditions than traditional FRF estimation methods like hammer or shaker tests. The methodology consists of exciting the structure through several independent interrupted milling cuts, through linearly ascending or descending cutting speed, in order to perform a frequency sweep over the frequency range of interest by means of the cutting harmonics.

Contribution 12:

The FRFs obtained by the developed SMFE methodology are fairly more accurate than the FRFs obtained by traditional excitation methods, as it has been demonstrated through the stability lobe validation through real cutting tests performed.

Related Publications:

Aguirre, G., Iglesias, A., Muñoa, J., & Astarloa, A. (2014). Real milling force based dynamic parameter extraction method. *Proceedings of ISMA*. Leuven, Belgium.

Iglesias, A., Munoa, J., Ramírez, C., Ciurana, J., & Dombovari, Z. (2016). FRF Estimation through Sweep Milling Force Excitation (SMFE). *7th HPC 2016 – CIRP Conference on High Performance Cutting*, submitted.

Part III
Novel Chatter Suppression Techniques

The stability modeling improvements described in Part II will be useful to increase accuracy of current stability models. However, there are still several factors affecting stability which are not considered. These missed effects influence, to a greater or lesser extent, stability predictions. Therefore, as it is not feasible to predict chatter accurately in every milling case and, moreover, although the prediction is accurate the conditions might not be modified, developing suppression techniques is essential in order to cope with chatter problems. Thus, in this Thesis, three novel chatter mitigation techniques are proposed. From the machining process point of view, an on-line cutting parameter correction method is developed (Chapter 9); considering the mechanical design approach, a self-tunable passive damper with contactless damping is presented (Chapter 10) and, from a control approach, an active damping strategy through acceleration feedback using machine drives is demonstrated (Chapter 11). The three chatter mitigation techniques are complementary: the on-line cutting parameter correction method is useful for high frequency chatter in high speed machining, the self-tunable passive damper is helpful to cope with fixture related critical modes and the active damping strategy is effective to damp low frequency structural modes of the machine.

Chapter 9

On-line and Wireless Process Parameters Correction

In this Chapter the first of the chatter suppression techniques is presented: a wireless device for on-line chatter identification and process parameters correction in milling processes through fast Fourier transform (FFT) and wavelet analyses. The developed device processes the sound from the cutting process and, as the process becomes unstable, it suggests chatter free spindle speeds on-line.

This suppression technique is useful for stability increase in high speed machining, where high frequency modes are involved in stability limitation.

9.1   WIRELESS DEVICE DEVELOPMENT

The wireless on-line chatter identification system is composed of a wireless microphone, a transmitter, a receiver and a computer with the sound analysis program. This system is a step forward from other chatter detection systems for its several advantages. The main advantage is that the microphone is placed close to the sound source without the interference of wires.

The system set-up is presented in Figure 9.1. The microphone is a condenser C-417L (AKG) that allows a high bandwidth and a flat dynamic response. It allows capturing frequencies between 20Hz and 20kHz. The microphone is placed at a distance from the sound source to avoid proximity interferences and is plugged to the transmitter system, which is also attached to the mill head. This system (WMS45 from AKG) transmits the sound captured and provides energy to the microphone with a 1.5V battery. The receiver (SR45) is placed outside the machine. It receives the signal from the transmitter and it is connected to a computer, which receives and records the samples of noise for its later analysis. The sound captured is analyzed by a program developed in LABVIEW®. The information is processed with this software, the generation of chatter detected and the optimum spindle speeds suggested.
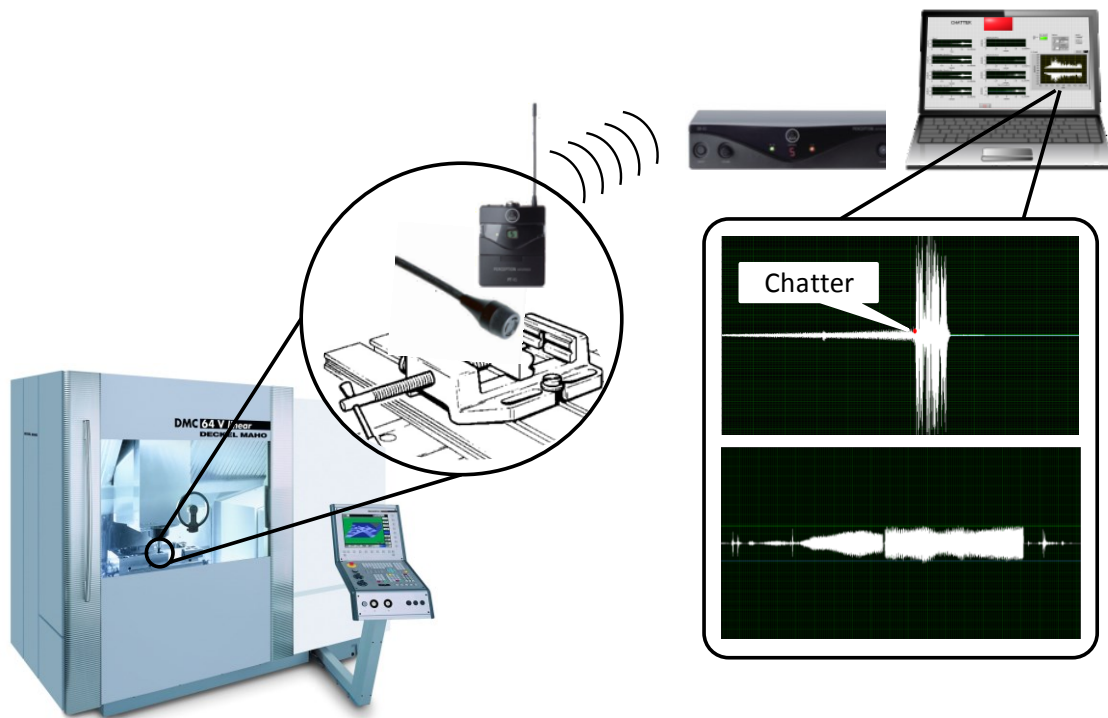
Figure 9.1: Wireless device setup.

9.2   EXPERIMENTAL SETUP

While the wireless device for on-line chatter detection was developed, parallel experimental work was carried out in order to tune up and test the developed system.

The work of Tönshoff cited by Dornfeld (2007) used a workpiece with an inclined plane to illustrate the sensitivity of forced and self-excited vibrations to machining conditions. Tönshoff showed that at a certain depth of cut along the tool path, forced vibrations

turn into self-excited vibrations and the milling process becomes unstable. In this work several experiments were carried out following the inclined plane methodology. First of all, sound samples were captured during the milling process. These samples were analyzed to see how this phenomenon behaved over time, with the purpose of determining the dominant frequencies of the system composed of the machine tool, the cutting tool, the toolholder and the workpiece. After preliminary results were obtained, an on-line chatter identification system was developed, tested and validated.

Experiments were carried out in a Deckel Maho 64V linear 3 axes vertical machine. The cutting tool used was a Mitsubishi flat end mill, 20mm of diameter, with 4 cutting edges installed in a collet chuck ER32 tool holder with 88.5mm cantilever. The geometry and the dimensions of the cutting tool are shown in Figure 9.2 and Table 9.1. The workpiece material was aluminum 7076 T6, its properties are presented in Table 9.2. No coolant was used.
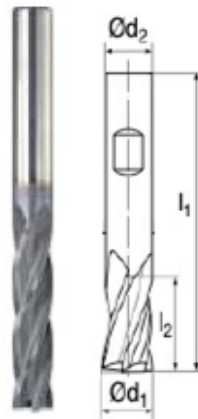
Figure 9.2: Mitsubishi V05066120 cutter schematically represented.

l1	Overall length (mm)	150
l2	Length of cut (mm)	75
Ød1	Diameter (mm)	20
Ød2	Shank diameter	20
Z	Number of teeth	4

Table 9.1: Geometrical characteristics of the Mitsubishi V05066120 cutter.

Density	2,81 g/cm3
Hardness	150 HB
Ultimate Tensile Strength	572 MPa
Tensile Yield Strength	503 MPa
Modulus of Elasticity	159 MPa

Table 9.2: Physical and mechanical properties of the Aluminum 7076 T6.

The stability lobe diagram (SLD) was calculated using the ZOA method (Altintas and Budak, 1995) developed in section 2.3.5. Thus, cutting speeds (V_c) and axial depths-of-cut (a) of the stability limit were determined. From the SLD, seven points on the limit of the stable zone were selected. These points determined the cutting speed and the axial depth of cut where the chatter was estimated to start. Two sets of experiments were performed for the selected points, according to the cutting conditions presented in Table 9.3.

Test	Cutting speed N (rpm)	Feed rate f_{min} (mm/min)	Theoretical a (mm)
1	5175	2070	1.63
2	5500	2200	0.35
3	6000	2400	0.18
4	6500	2600	0.19
5	7000	2800	0.42
6	7500	3000	1.39
7	7750	3100	2.36

Table 9.3: Design of experiments.

The first set of experiments consisted of cutting slots along the y axis of the machine tool while increasing the axial depth of cut (from 0 to 1.5mm), thanks to the inclined plane. The second set performed the same experiments decreasing the axial depth of cut (from 1.5 to 0mm). Both sets are performed offline and online, therefore it resulted in a total of 28 experiments.

9.3   CHATTER IDENTIFICATION PROCESS

9.3.1   Off-line chatter detection

The 14 cutting tests (7 increasing and 7 decreasing axial depth of cut) previously obtained were analyzed off-line using the LABVIEW® software. A signal analysis using wavelet decomposition wave was carried out in order to accurately determine the chatter onset. A frequency analysis using Fourier Transform FFT was also performed in order to find the chatter frequency.

FFT Analysis

The fast Fourier transform analysis (FFT) provides information of peak signal frequency and its harmonics. If the frequency peaks correspond to the frequency of the spindle speed or the tooth passing frequency (TPF), the signal is stable, whereas if there are

frequency peaks outside these harmonics, it indicates the presence of chatter. The analyses of the sound signal were performed using the methodology and algorithms developed in previous works (Quintana and Ciurana, 2011; Quintana et al., 2009). A platform was developed in LABVIEW®, where two graphs present the time domain of the signal and the frequency domain calculated with a FFT. Introducing the spindle speed and the number of teeth, the tooth passing frequency (TPF) is automatically calculated.

Wavelet Analysis

Wavelet analysis is based on processing only certain subset of scales and positions of the signal, the so-called dyadic scales and positions, with the purpose of avoiding the Fourier uncertainty principle. The most efficient way to implement this system, developed by Mallat (1988), is using filters. The Mallat algorithm allows filtering the signal and making a quick wavelet transform with the consequent production of coefficients. The original signal is submitted in two complementary filters named high and low frequency, which results in two components: the approximations and the details. The detail coefficients are small and consist mainly of high frequency noise, while the approximation coefficients contain much less noise than the original signal. This decomposition process can be repeated with successive approximations (tree decomposition). In this case, the level where the appearance of chatter can be detected more precisely is the decomposition level 3 (Zhehe et al., 2010).

A LABVIEW® platform was developed in order to perform multilevel wavelet analysis and establish the limits for the signal amplitude. When the signal amplitude increases dramatically and exceeds the limits with a disruptive change indicates that chatter may appear. When this happens, the software warning indicator is set, and the points where the signal contains chatter are presented on a graph. Otherwise, while the limits are not exceeded, the indicator remains deactivated.

9.3.2   On-line chatter detection

The on-line detection becomes a more complicated task, due to the required speed in chatter detection. In FFT detection methods, if short time detection is needed, the frequency resolution obtained is poor, whereas if high frequency resolution is needed, the signal must be long and the detection instant is not accurate. Therefore, the detection methods developed could be combined for efficient chatter detection, using the wavelet transform to detect the chatter onset instant and the FFT analysis in order to define the chatter frequency accurately.

On-line chatter detection through wavelet analyses

Once primary analyses were performed with all the experimental data captured in the first set of experiments, an on-line chatter detection system through wavelet analyses was designed and developed. The idea was to use the same technique as in previous section, but performing the detection in real time at the beginning of the instability. As detailed in the previous section, the sound signals are sent by the transmitter to the receiver connected to the computer. The received signal and the approximations and details of the wavelet decomposition levels are displayed on screen at all times.

The limits for the signal amplitude were set based on the values obtained in the off-line case considering an interval of tolerance. When the signal is received and a drastic change is observed exceeding the limits, the chatter detection is triggered. To correctly locate the boundaries and be able to accurately detect its occurrence, it is important to choose precise values for the limits with previous signal calibration in comparison with a stable cut.

Frequency spectrogram

The frequency spectrogram developed (Figure 9.3) permits to know when chatter arises online, replacing the static FFT. A spectrogram is the representation of the frequencies that occur in a signal in a color map. The warm colors, yellow but mostly red, indicate that the dominant frequencies are in that band, whereas cold colors indicate absence of energy content in the respective frequency bands. The analysis of the signal permits to differentiate the frequencies and observe chatter emergence as soon as it occurs. This allows observing visually which frequencies appear on the milling process.
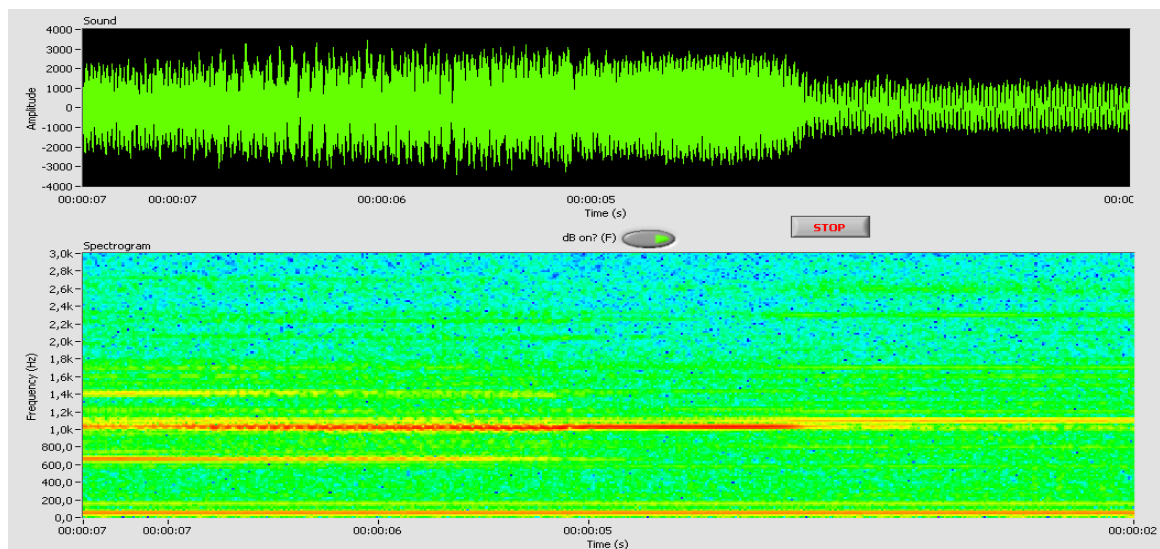

Figure 9.3: Frequency spectrogram.

9.3.3 Process parameters modification to stabilize the milling process

The chatter detection interface developed permits to identify both the occurrence of this phenomenon as well as the moment of its onset and its frequency. This makes possible to identify the chatter appearance during the milling process, and allows the operator to modify the process parameters in order to ensure a stable process varying the spindle speed. Thus, it is possible to seek stable regions between lobes avoiding the unstable regions. In order to be able to modify the process parameters as soon as the chatter onset is detected, an algorithm to determine a proper spindle speed following the methodology proposed in (Delio et al., 1992) was developed, ensuring the process to continue working in stable zone without limiting the productivity.

When the algorithm detects a significant change in the amplitude and, thus, the onset of chatter, the application captures the frequency of the signal at that particular time. At the same time, it identifies the lobe in which it is working and suggests spindle speeds to work in the stable area avoiding chatter. The formula used for the spindle speed suggestion is obtained from equation (2.1-1), neglecting the phase shift term:

$$N = \frac{60 f_c}{l\,Z}.$$

(9.3-1)

9.4 EXPERIMENTAL VALIDATION

9.4.1 Chatter detection algorithm validation

Results after the wavelet decomposition are presented in this section and analyzed off-line. Considering the inclined plane dimensions and the feed rate, the timing and the axial depth at which the signal amplitude changes were calculated.

The SLD of both sets of experiments (increasing and decreasing axial depth of cut) have been obtained and represented in a plot against the theoretical SLD in Figure 9.4. The correlation between the theoretical and experimental lobes is excellent, with the theoretical lobe always inside band defined by the ascending and descending depth of cut tests. This band is the sum of the existing delay in chatter detection and the unsafe zone area.
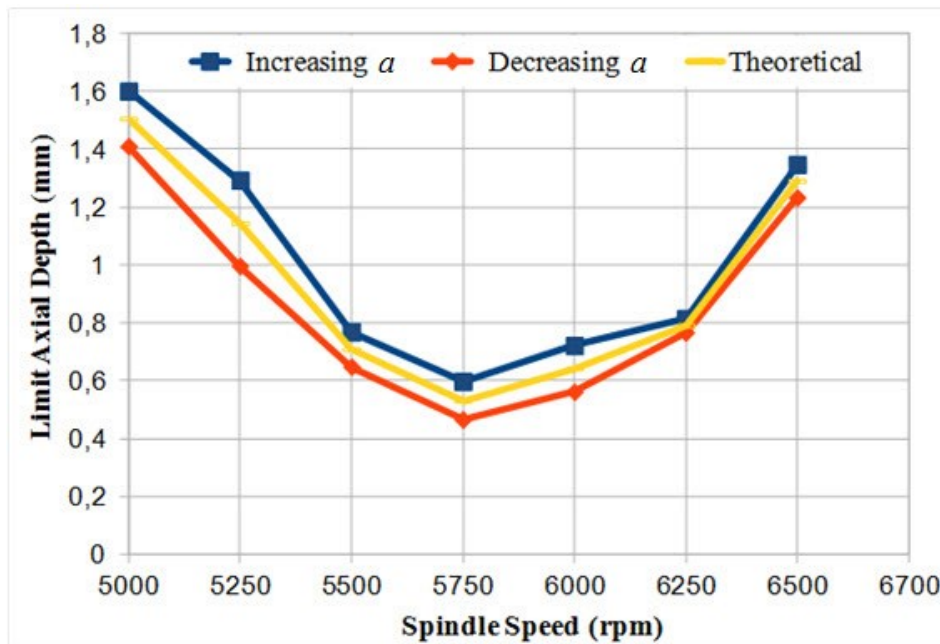
Figure 9.4: Comparison between experimental and theoretical lobes.

9.4.2   Chatter control algorithm validation

The control system to modify process parameters with the purpose of increasing process stability has been validated.

For that purpose, the milling tool represented in Figure 9.5a) has been tested, which has the characteristics listed in Table 9.4. According to the initial cutting tests (Table 9.4), the cutting process was already unstable when cutting a depth of cut a=1mm, with a chatter frequency of 713.3Hz, which corresponds to the first bending mode of the tool. Applying equation (9.3-1), the spindle speed N=10700rpm is proposed. Next cutting test was carried out at this speed and the process became stable, thus verifying the effectiveness of the process parameter selection algorithm.

There are other cases where the algorithm does not reach the maximum stable speed in the first iteration; therefore, several iterations are needed until it converges to a stable condition. If an unstable solution cannot be achieved for a specific depth of cut, a considerable shift in the proposed spindle speed will be produced at some point in the iterative process.
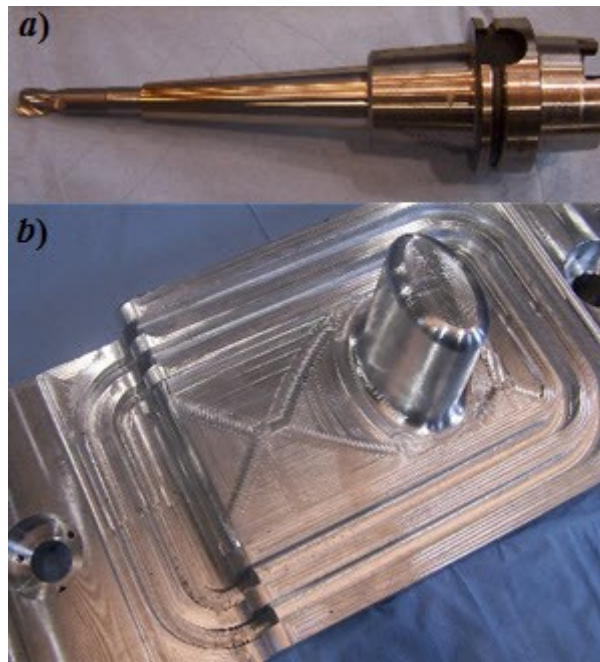
Figure 9.5: Validation experiment for on-line parameter selection algorithm determination. a) Cutting tool and b) machined AL7075 workpiece.

Tool characteristics		Invariant cutting conditions		Initial cutting conditions		After chatter control	
Diameter D	12 mm	Width of cut a_e	12 mm	Depth of cut a	1mm	Depth of cut a	1mm
Number of flutes Z	2	Feed f_z	0.3 mm/Z	Spindle speed N	10070 rpm	Spindle speed N	10700 rpm
Helix angle (º)	25°			Stability	UNSTABLE (713.3Hz)	Stability	STABLE

Table 9.4: Tool characteristics and cutting conditions in the validation experiment of the on-line parameter selection algorithm.

9.5 CONCLUSIONS

This chapter presents the development of a wireless device for on-line chatter identification and process parameters correction in milling processes. The platform performs chatter detection through FFT and wavelet analyses of the machining sound. The wireless system developed is a step forward from other chatter detection systems.

The microphone can be placed close to the sound source without the interference of wires. At the same time, the absence of wires makes possible to close the door of the CNC machine ensuring a safer process. This presents several advantages for industrial environments, where the sound coming from other machines through the whole workshop can negatively affect the sound capture. However, it could be necessary to

implement sound filters in order to mitigate the background noise and collect only the interesting part of the sound that is required to analyze.

In comparison with the analyses that an experienced operator can provide, the wireless device can make objective evaluations of the cutting sound to identify chatter onset.

The WMS45 system and the C417-L microphone have allowed a perfect sound transmission, allowing a linear response throughout its range for both high and low frequencies. The present work demonstrates that the microphone is a proper sensor for the detection of chatter in high speed machining of light alloys.

Several experiments were performed varying the axial depth of cut and the spindle speed, maintaining a constant feed per tooth. The wireless data acquisition platform was implemented to collect the milling process audio signal. The time-based audio signal was analyzed off-line to identify chatter frequencies. Milling sound analyses of frequencies and amplitudes, through FFT and wavelet, have given good results and permitted to obtain an accurate approach to understand the milling process incidences through the recorded vibrations. Once the chatter onset is identified, the appropriate spindle speed is proposed in order to maximize the process stability. The system proposed can be easily implemented by machinists without the need of high investments.

Contribution 13:

A wireless device for on-line chatter identification and process parameters correction in milling processes has been developed. Chatter is detected through a FFT and wavelet analyses of the recorded machining sound. As a wireless microphone is used, the sensor can be placed close to the cutting point, inside the machine enclosure, which increases the reliability of the solution. The chatter detection procedure has been experimentally validated.

Related Publications:

Barnada, F., Teixidor, D., Iglesias, A., Quintana, G., & Ciurana, J. (2015). Wireless device for on-line chatter identification and process parameters correction in milling processes. *Robotics and Computer Integrated Manufacturing*, submitted.

Chapter 10

Tunable Mass Dampers with Variable Stiffness

The second chatter suppression technique developed in this Thesis is a new generation passive damper attached on the machining system, the so called variable stiffness tuned mass damper (VSTMD). The main breakthrough of this VSTMD is the possibility of adjusting the stiffness, enabling the self-tuning of the damper at different frequencies depending on the specific needs at a given machining process. Thus, the damper includes an adaptive capability, which ensures its effectiveness against chatter originated by different vibration modes.

A second optional special feature of the damper is the addition of contactless damping through the eddy current effect. This contactless nature facilitates the tuning process of the damper and avoids unwanted nonlinearities typical of standard passive dampers.

Different tuning strategies are tested, following Den Hartog's theory, Sim's parameters and finally a newly developed self-tuning algorithm for chatter suppression.

This solution is especially interesting for critical mode damping in flexible workpiece fixtures.

10.1 CHARACTERISTICS OF A VSTMD

Tuned mass dampers (TMD) consist of a mass connected to the machine with a certain stiffness and damping, so that its natural frequency is tuned to the frequency of the machine mode leading to chatter, increasing dynamic stiffness and allowing higher cutting depths.

A variable stiffness tunable mass damper (VSTMD) goes one step beyond a simple TMD. Within the same machine, chatter frequency can vary with the position in the workspace (due to the variation in the machine stiffness), with the process parameters and with the workpiece mass. The effectiveness of the damper depends greatly on an accurate tuning of the damper frequency, which can be achieved through the stiffness variability feature in a VSTMD. A sketch of a VSTMD acting in a milling process is depicted in Figure 10.1.
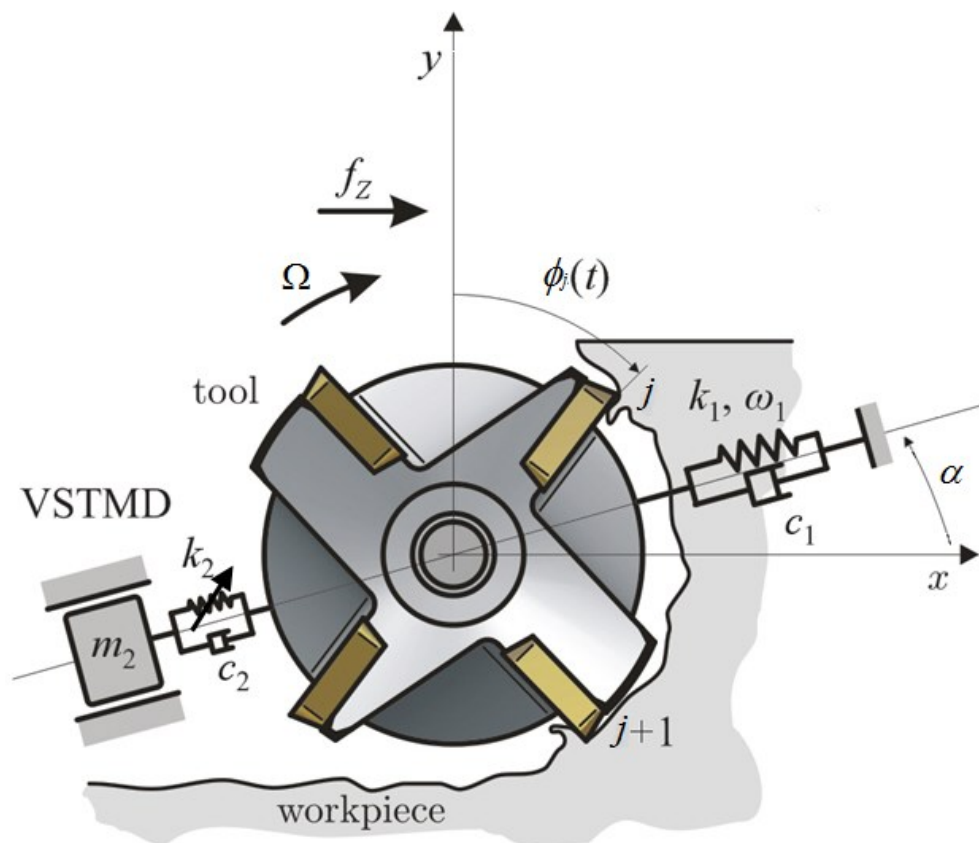

Figure 10.1: Sketch of VSTMD in a milling machine.

Three important characteristics for the optimum design of a self-tuning VSTMD are described next:

- The vibration modes involved in chatter generation must be correctly identified. An experimental modal analysis of the machining is required, which combined with the simulation of the cutting process, leads to stability diagrams that can help in detecting the critical modes. The stiffness tunable range of the VSTMD must cover the range the critical modes are located on.

- The location and mass of the damper on the machine must be carefully chosen. Looking at the mode shape of the damper, the damper should be located at a point, within feasible ones, where the vibration amplitude is maximum, so that the modal mass at this point is minimum, requiring thus less inertial mass on the damper for the same efficiency. The inertial mass is typically set to 5-10% of the equivalent modal mass at the location point.

- The damping of the inertial damper should be approached to the optimal value. The effectiveness in chatter reduction is vaguely sensitive to proper tuning of the damper, whenever a good level of damping is provided. Therefore, even in semi-active solutions, the damping is usually fixed at a value similar to the optimum, and not modified afterwards.

A self-tuning VSTMD is thus of advantage for ensuring optimal damping in a wider range of working conditions. Such damper needs to be upgraded with the following functions:

- Online chatter monitoring and identification of optimal damper tuning frequency.

- Automatic control of the damper resonance frequency to match the monitored chatter frequency.

The classical approach relates the stability of the cutting process to the value of real part of the FRF. According to the ZOA solution described in Altintas (2012), the stability of a one dominant mode system is inversely proportional to the real part of the critical mode.

$$a_{\lim}(\omega) = -\frac{\pi}{Z\,K_t\,\beta_0 G_{11}(\omega)}, \tag{10.1-1}$$

$$\tau(\omega) = \frac{1}{\omega_c}\big((2l+3)\pi + 2\psi(\omega)\big), \tag{10.1-2}$$

$G_{11}(\omega)$ is obtained from $\{\eta\}=[\Phi]\{P\}$ and

$$[\Phi(\omega)] = (-\omega^2[M] + j\omega[C] + [K])^{-1} = [\Phi_{mn}(\omega)], \ if \ m,n = 1,2. \tag{10.1-3}$$

$$[M] = \begin{bmatrix} m_1 & 0 \\ 0 & m_2 \end{bmatrix}, [C] = \begin{bmatrix} c_1 + c_2 & -c_2 \\ -c_2 & c_2 \end{bmatrix}, [K] = \begin{bmatrix} k_1 + k_2 & -k_2 \\ -k_2 & k_2 \end{bmatrix}, [P(t)] = \begin{bmatrix} \{p\}^{\mathrm{T}}\{F(t)\} \\ 0 \end{bmatrix},$$

where the subindex 1 refers to the machine and 2 to the VSTMD.

Therefore, equations (10.1-1) and (10.1-2) open the way for using simple optimization based on the analytical representation of the FRF $\Phi_{11}(\omega)$ supposing $c_1 \approx 0$ (Sims, 2007). The stability of regenerative cutting process requires a special tuning where the real part should be shrunk. The average directional factor β_0 can be positive or negative value depending on the engagement and the cutting characteristics. Therefore, if the directional factor is positive, the negative side of the real part should be maximized creating two equal peaks. On the other hand, if the directional factor is negative the positive side should be minimized.

TMD /VSTMD				Structure	
mass ratio	damping ratio	frequency ratio	natural frequency	dimensionless frequency	natural frequency
$\mu := \dfrac{m_2}{m_1}$	$\upsilon := \dfrac{c_2}{2m_2\omega_1}$	$f := \dfrac{\omega_2}{\omega_1}$	$\omega_2 := \sqrt{\dfrac{k_2}{m_2}}$	$f_d := \dfrac{\omega}{\omega_1}$	$\omega_1 = \sqrt{\dfrac{k_1}{m_1}}$

Table 10.1: Definition of dimensionless dynamic parameters.

The real part of a FRF dominated by a single mode can be calculated by means of several dimensionless parameters (Table 10.1):

$$G_{11}(f_d) = \frac{1}{k_1} \frac{(f^2 - f_d^2)((1 - f_d^2)(f^2 - f_d^2) - \mu f^2 f_d^2) + 4\upsilon^2 f^2 f_d^2(1 - f_d^2 - \mu f_d^2)}{((1 - f_d^2)(f^2 - f_d^2) - \mu f^2 f_d^2) + 4\upsilon^2 f_r^2(1 - f_d^2 - \mu f_d^2)^2} \tag{10.1-4}$$

where f is the tuning of the absorber, μ is the mass ratio, f_d is the dimensionless frequency and $\upsilon = c_2 / c_{cr}$ is the damping ratio relative to $c_{cr} = 2 \ m_2 \ \omega_1$ "critical" damping defined in (Den Hartog, 1947).

10.2 TUNING OF A VSTMD

In the literature, there are two main analytical results for the ideal tuning of passive dampers. On the one hand, the work of (Den Hartog, 1947) uses two invariant analytical points to achieve the decrease of the receptance magnitude in all frequencies. On the other hand, the work of (Sims, 2007) shows three invariant points to achieve the best possible real parts of the corresponding FRF considering $a_{\lim}$ by ZOA, equation (10.1-1) as an objective.

A case study described by (Aguirre et al., 2013) has been used to compare the performance of different strategies. In this case, the moving mass is $m_2 = 7$kg and the mass ratio is $\mu = 4.7$ %.

Figure 10.2 shows the effect a tuned mass damper produces in the frequency response function, dividing the critical modes into two other dynamically stiffer modes (Figure 10.2a) and in stability lobes, increasing the cutting capability (Figure 10.2b).
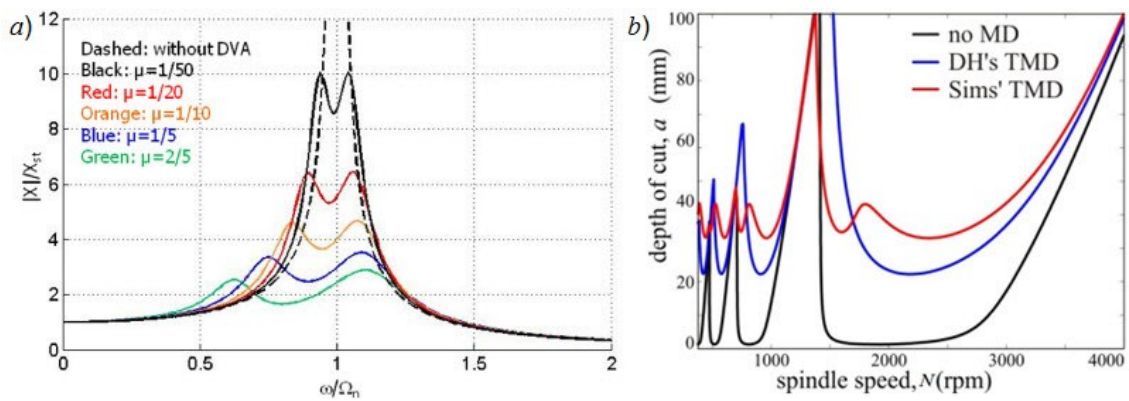
Figure 10.2: Effect of VSTMD on a) frequency response function when different mass ratios are applied and b) stability lobes when tuning with different methods.

The optimal tuning f in equation (10.1-4), the optimal stiffness k_2 and damping c_2 can be determined for both methods by considering initial process parameters presented in Table 10.2 and the optimal parameters described in Table 10.3.

D (mm)	ϕ_{st} (deg)	ϕ_{ex} (deg)	α (deg)
32	20.36	180	0
Material	K_t (MPa)	K_r (MPa)	f_z (mm/Z)
C45	1459	257	0.1
ω_1 (rad/s)	ξ_1 (%)	m_1 (kg)	p_1
2*π*94	0.35	150	[0 1 0]^T

Table 10.2: Milling process parameters.

	Frequency ratio	Damping ratio
(Den Hartog, 1947)	$f_{\mathrm{DH}} = \dfrac{1}{1+\mu}$	$\upsilon \approx \sqrt{\dfrac{3\mu}{8\,(1+\mu)^3}}$
(Sims, 2007) ($\beta_0>0$)	$f_{\mathrm{opt,n}} = \sqrt{\dfrac{\mu+2+\sqrt{2\,\mu+\mu^2}}{2(1+\mu)^2}}$	$\upsilon = \sqrt{\dfrac{3\mu}{8\,(1+\mu)}}$
(Sims, 2007) ($\beta_0<0$)	$f_{\mathrm{opt,p}} = \sqrt{\dfrac{\mu+2-\sqrt{2\,\mu+\mu^2}}{2(1+\mu)^2}}.$	

Table 10.3: Optimal tuning analytical expressions.

Sims's and Den Hartog's theories work with fixed and invariant stiffness of the damper for the different spindle speeds, which is not the case for VSTMD. This tuning procedure and the design of a rotary spring allow setting the stiffness value iteratively or even continuously between a minimum and a maximum stiffness values, which means different optimal tuning can be realized along the stability limits.

10.2.1 Ideal tuning of VSTMD

Regardless of the tuning iteration procedure applied on VSTMD, it can only be successful if the system can be stabilized at all. This means that there is a special stiffness value where the cutting process (stationary cutting) is stable.

This fact is convenient because the ideal tuning can be found by means of the linear theory presented at equation (10.1-1). The ZOA and equation (10.1-4) can be used for the analytical derivation. In order to ease the notation the magnifying function $M_{11}(f_d, f) := \Phi_{11}(f_d)\, k_1$ is introduced.

According to the derivation of ZOA (Altintas et al., 2008b) the arising chatter frequency ω_c can be considered as sampling on the corresponding FRF. Consequently, considering a non-interrupted case, the FRF can be optimized at each dimensionless frequency $f_d = \omega_c/\omega_1$. This means finding an extremum of $\mathrm{Re}(M_{11}(f_d, f))$ by taking $\mathrm{dRe}(M_{11}(f_d, f))/\mathrm{d}f$, which leads to five roots for tuning including one at $f_0 = 0$ and four others symmetrically placed. Thus, these latter four can be considered as two extremums, f_+ and f_-:

$$f_{\pm}(f_d) = \sqrt{\dfrac{f_d^2 + f_d^6(1+\mu) \pm 2\sqrt{f_d^4(f_d^2-1)(f_d^2(1+\mu)-1)^3\,\upsilon^2}}{(f_d^2(1+\mu)-1)^2}} \qquad (10.2\text{-}1)$$

This new formula shows the best tuning of a damper to have the maximum stability for a certain spindle speed represented indirectly by the dimensionless value (f_d). This formula can improve the result of Sims' proposal for a single spindle speed.

In Figure 10.3, Sims' locked frequencies are $f_{d,p}(f)$, $f_{d,n}(f)$ and $f_{d,i}(f) = f$ and their limits are $f_{d,plim}$ and $f_{d,nlim}$. Among the solutions presented at equation (10.2-1), it is always $f_+(f_d)$ that gives the maximum and $f_-(f_d)$ that gives the minimum for $Re(M_{11}(f_d, f))$. Keeping in mind the results of the ZOA depending on the sign of the directional factor $\beta_0 > 0$ ($\beta_0 < 0$), $Re(M_{11}(f_d, f))$ needs to be maximized (minimized). Namely, the best solution for the tuning is always given by $f_+(g)$ ($f_-(f_d)$), except between the values of $f_{d,plim}$ and $f_{d,nlim}$ where the optimum values determined at (10.2-1) are extremes.
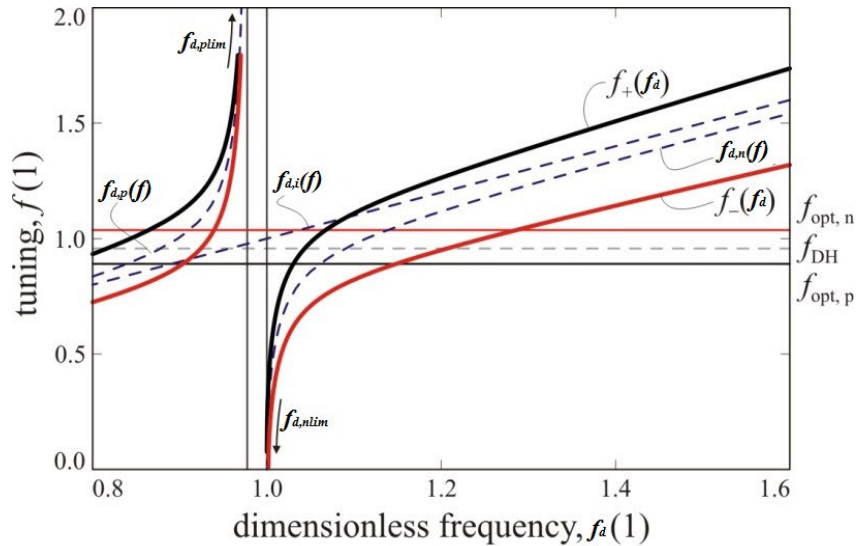
Figure 10.3: Optimal tuning w.r.t. the dimensionless frequency f_d.

In this region, depending on $\beta_0 > 0$ ($\beta_0 < 0$) a minimum f_{min} (maximum f_{max}) tuning is limiting not realizable stiffness values on the rotary spring (equations (10.2-2) and (10.2-3)).

In Figure 10.3, it can be observed that Sims' constant optimal tuning $f_{opt,p}$ ($f_{opt,n}$) for $\beta_0 > 0$ ($\beta_0 < 0$) is only optimal at two dimensionless frequencies f_d, below and above $f_d = 1$. However, limited frequencies are possible along the lobes, usually $f_d > \sim 1$ ($f_d < \sim 1$) if $\beta_0 > 0$ ($\beta_0 < 0$). This means one point along the lobe is optimal for a VSTMD in this simple case (see Figure 10.4).
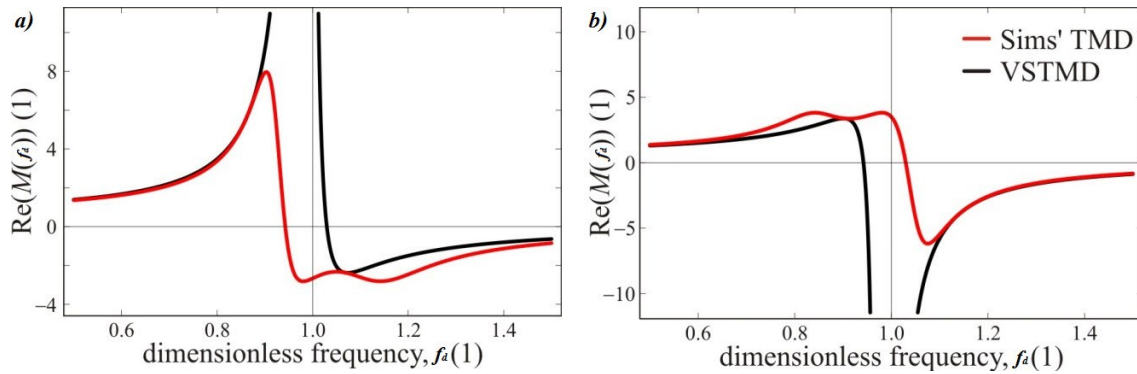
Figure 10.4: Real parts of the optimally tuned magnifying function for positive directional factor ($\beta_0 > 0$) a), and for negative directional factor ($\beta_0 < 0$) b), compared to Sims' optimal tuning (red) (Sims, 2007).

10.2.2   Ideal stability behavior of VSTMD

Based on the calculated optimal tuning function $f_\pm(f_d)$, piecewise smooth function can be defined, which take into account the physical limitation of the rotary spring. The limitations are only active close to the original natural frequency ω_1 of the structure.

When $\beta_0 > 0$, $f_{opt,p}(f_d) = \max\{f_+(f_d), f_{min}\}$,   (10.2-2)

while $\beta_0 < 0$, $f_{opt,n}(f_d) = \min\{f_-(f_d), f_{max}\}$.   (10.2-3)

Using these piecewise smooth definitions, the stability boundaries can be depicted (see Figure 10.5) by simply applying ZOA shown at equation (10.1-1). For both cases of negative and positive directional factors, the stability is improved by using VSTMD solution. In these ideal examples, there is a point in the stability limits where the stability is not improved with respect to the Sims' optimal tuning values (see Figure 10.3). It can be also noticed that in this solution the "double lobe" shape disappears.
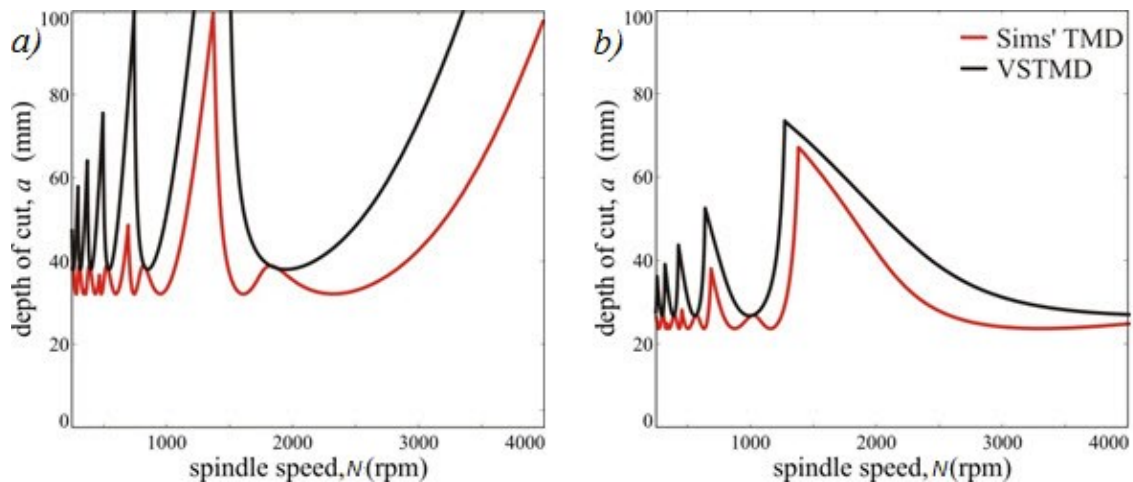

Figure 10.5: ZOA stability limits based on the optimal FRF for positive directional factor ($\beta_0 > 0$) a), and the same for negative directional factor ($\beta_0 < 0$), b) compared with Sims' solutions (red).

10.2.3   Iterative algorithm for optimal tuning VSTMD

It has been demonstrated that if the tuning of the damper is changed for each spindle speed using a VSTMD, the stability of the process can be improved more than an ordinary TMD with the same mass tuned according to Sims' parameter. However, it is a complex procedure to implement it in practice. In this section, an iterative method to approach this optimal solution is going to be proposed.

The first step towards chatter suppression is to detect whether chatter is occurring or not during the machining process. The vibration measured by the accelerometer installed on the structure of the damper is processed in order to find its main frequency components. Here it is important to distinguish between forced vibrations, induced directly by the cutting forces, and chatter, which is due to an unstable regenerative process generated only under certain working conditions.

Forced vibrations appear at harmonics of the tooth passing frequency, but are stable, and thus are usually not a problem for machining, except in finishing operations where surface roughness needs to be improved. Chatter appears at other frequencies than tooth passing frequencies. It is an unstable cutting process, meaning that the cutting forces and vibrations increase with time, leading to unacceptable machining conditions, since they produce very bad surface quality and can lead to damage in the machine.

The chatter detection and suppression algorithm is presented in Figure 10.6.
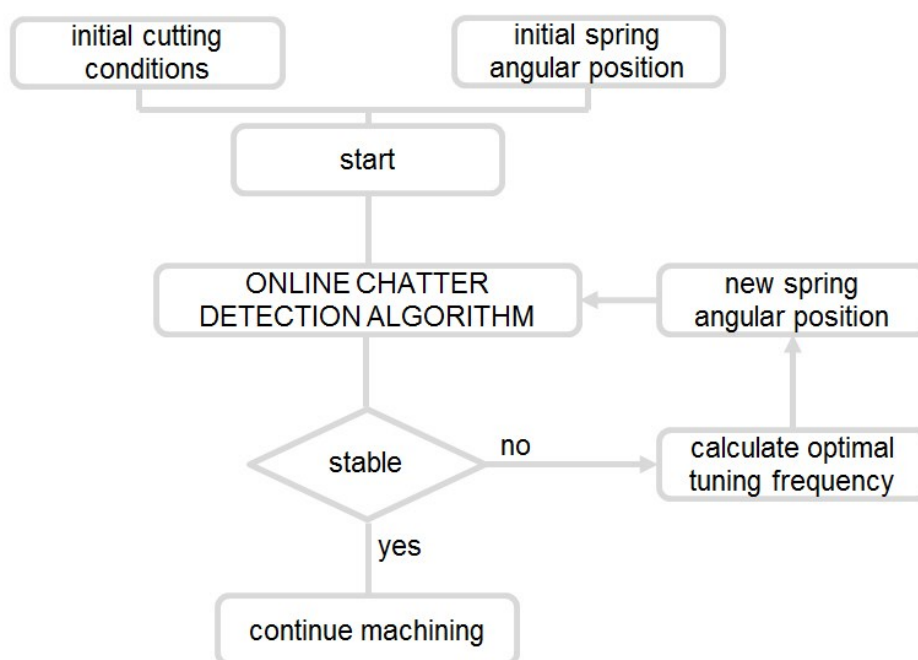

Figure 10.6: Chatter detection and suppression algorithm.

This algorithm is implemented on a real-time controller. It is running continuously during the machining process, calculating the spectrum of the measured vibration of the machine, as shown in Figure 10.7*b*. The algorithm detects the frequency of the maximum vibration peak, and compares it with the tooth passing frequency: if it is an integer multiple of the tooth passing frequency, it is considered to be a forced vibration, and no corrective action is taken. If it is not an integer multiple, it is considered to be chatter, and the angular position in the damper is modified in order to tune it to the chatter frequency.

It is very important to distinguish clearly chatter from forced vibrations, so that the damper is only tuned to chatter frequencies. Otherwise, once the damper is tuned to the chatter frequency, the vibration level at this frequency will drop, and the algorithm will detect a forced vibration as main frequency. If the damper is tuned to this new frequency, chatter generation could start again, which needs to be avoided.

10.3 SIMULATION RESULTS

In this section, real case simulations tuned according to the modeled VSTM solution are presented. Initial value time domain simulations are started from the perturbed stationary solution to reach the threshold when the loss of contact between tool and workpiece is produced (Stepan et al. 2011) in a fast way. Roughly 30-40 periods are simulated and 10-20 period-long signals from the end of the simulation are taken for FFT analysis. With the removal of the DC component, the chatter frequency can be extracted easily since the stationary cutting solution is known and the harmonics of its amplitude can be used as a threshold for chatter. The maximum among the peaks overtaking the limiting amplitude is considered as chatter frequency and the VSTMD is tuned to this main frequency with $k_{2,j} = \omega_c^2 m_2$. This tuning is done subsequently until stability determined by semi-discretization or a preset maximum number of iterations are reached.

Sims' and the ideal tuning solutions are presented in Figure 10.7*a* for milling operation calculated by semi-discretization in this case. Time domain calculations were performed for selected spindle speeds (A, B and C) listed in Table 10.4 in order to see the tuning iterations of the VSTMD. The time domain simulations combined with the loss of contact between tool and workpiece can be performed in order to determine the dominant frequency of the threshold periodic, quasi-periodic or completely chaotic motion (Dombovari et al., 2011).
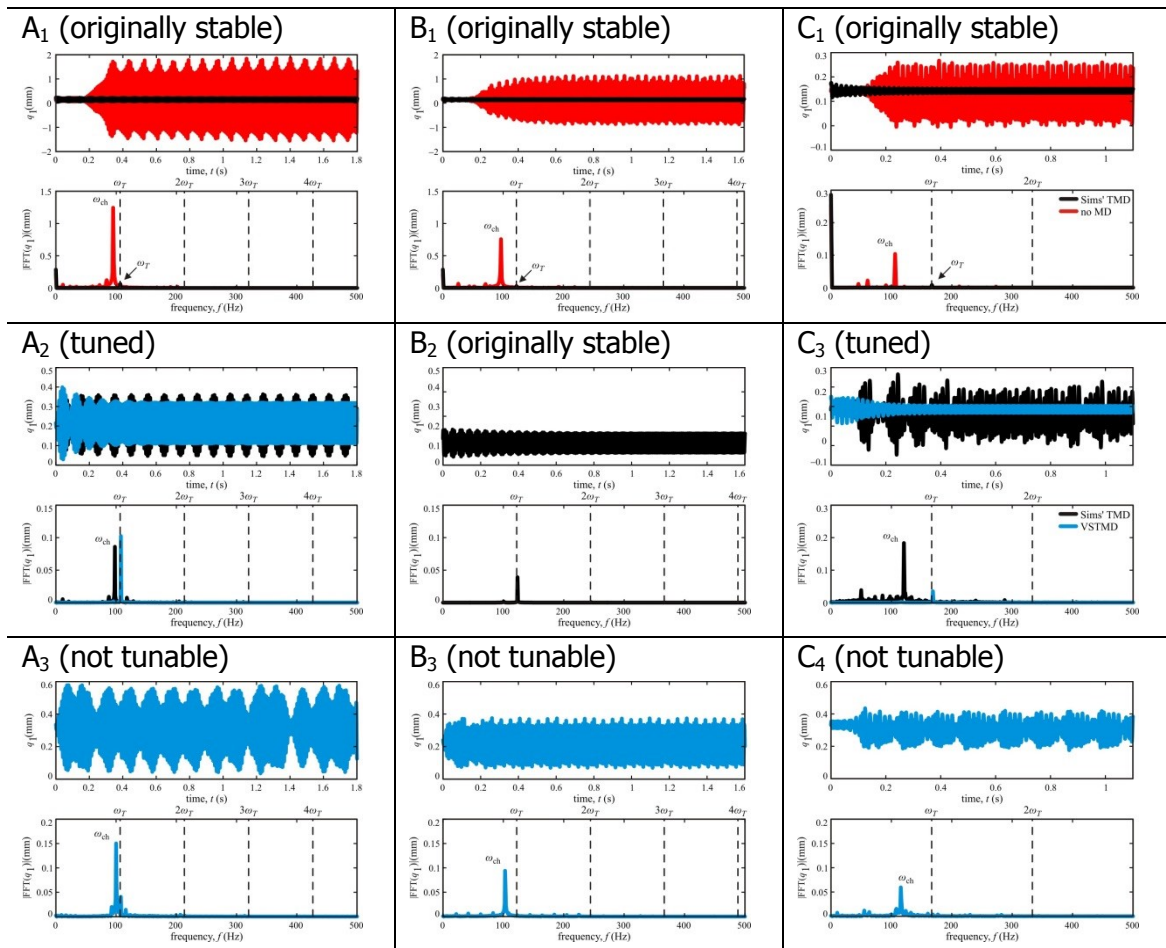
a)
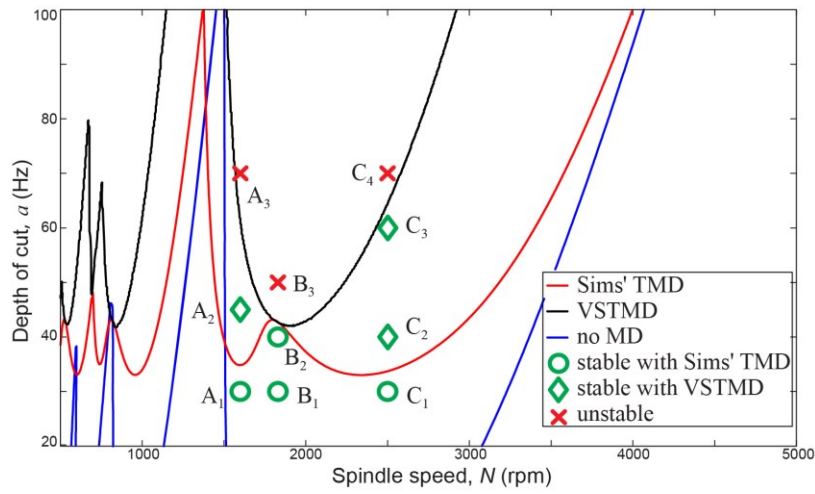
b)

Figure 10.7: *a*) shows ideal tuning solutions for VSTMD performed by SD ($\beta_0 > 0$) compared to Sims' case. *b*) shows time domain solution at selected points.

The 'originally stable' cases in Figure 10.7 and Table 10.4 are stable according to Sims', no tuning is necessary. The 'tuned' cases are parameters, when the tuning was

effective by using the simulated chatter frequencies. The 'not tunable' situations are the cases when even the VSTMD was not effective.

A_1: N_A=1600 rpm, a_1=30 mm	B_1: N_B=1830 rpm, a_1=30 mm	C_1: N_C=2500 rpm, a_1=30 mm
Originally stable	*Originally stable*	*Originally stable*
A_2: N_A=1600 rpm, a_2=45 mm	B_2: N_B=1830 rpm, a_2=40 mm	C_2: N_C=2500 rpm, a_2=40 mm
ω_{cj} = 96.7, 106.7, 94 Hz *Stable in three tuning iterations.*	*Originally stable*	ω_{cj} = 115.6, 111.5 Hz *Stable in two tuning iterations*
A_3: N_A=1600 rpm, a_3=70 mm	B_3: N_B=1830 rpm, a_3=50 mm	C_3: N_C=2500 rpm, a_3=60 mm
ω_{cj} = 98.7, 97.3, 98.7, ... Hz *Unstable*	ω_{cj} = 106.0, 99.1, 99.9, 99.1, 101.4, ... Hz *Unstable*	ω_{cj} =118.8, 113.5, 121.9, 111.5 Hz *Stable in four tuning iterations*
		C_4: N_C=2500 rpm, a_4=70 mm
		ω_{cj} =119.8, 113.5, 124.0, 113.5, 123... Hz *Unstable*

Table 10.4: The detailed results of the time domain simulations of the selected points (see Figure 10.7a).

The specific parameters and tuning data of the simulated cases presented in Figure 10.7 can be followed in Table 10.4.

Summarizing, the time domain simulations confirm that VSTMD can improve the results obtained by a standard TMD tuned according to Den Hartog's and Sims' strategies and the proposed iterative algorithm can approach the optimal solution defined in the previous sections for a VSTMD.

10.4 EXPERIMENTAL REALIZATION

10.4.1 VSTMD prototypes

The VSTMD has been physically developed following two approaches: a preload-type VSTMD (Figure 10.8a) and a spring-type VSTMD (Figure 10.8b) have been built.
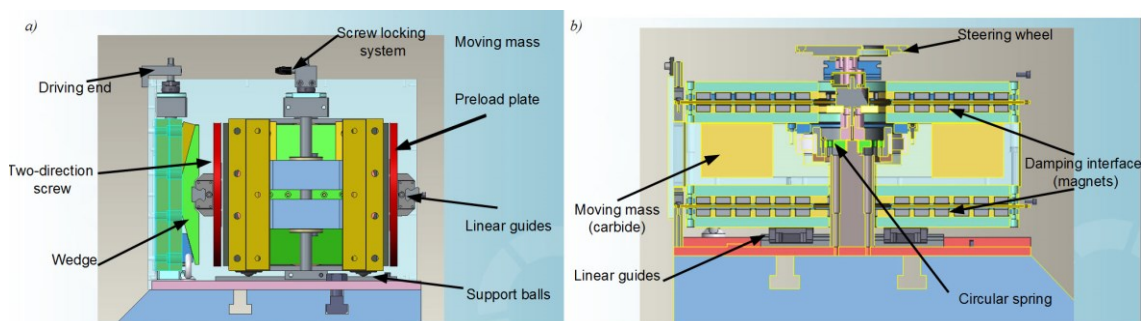
Figure 10.8: a) Preload-type VSTMD and b) Spring-type VSTMD.

The physical characteristics of the dampers are summarized in Table 10.5:

Damper	Total dimensions (mm)	Tuning mass (kg)	Total mass (kg)	Tunable frequency range (Hz)
Preload-type damper	460x460x350	162	333	18-40Hz
Spring-type damper	460x375x250	210	349	20-43Hz

Table 10.5: Physical characteristics of the VSTMD prototypes.

Preload-type VSTMD prototype

The preload-type VSTMD consists of a moving mass confined by two special shaped preload plates in two perpendicular directions x and y (see Figure 10.8a). The preload is applied on a high damping viscoelastic layer (Sylomer SR 220) through the special shaped plate which performs a progressive contact, thus, allowing a wide tunable frequency range. As the preload is increased, the stiffness of the system and, therefore, the tuning frequency, are also increased. The viscoelastic layer of Sylomer also provides the necessary damping to the system.

The preload is provided by two electrical motors (axes x and y) coupled to a reducer gearbox which drives a two-direction screw oriented vertically on the damper box. As the two-direction screw is rotated, a coupled wedge moves back and forth in order to apply the preload (Figure 10.9).
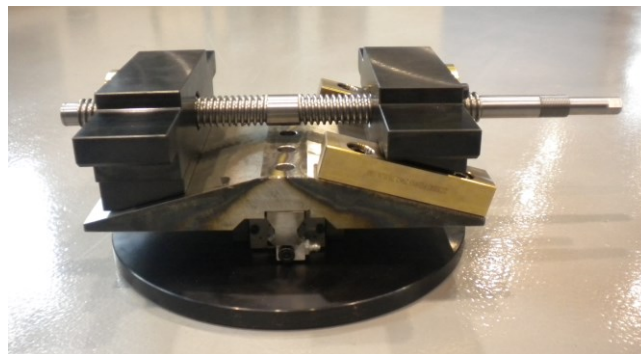
Figure 10.9: Two-direction screw acting on the wedge and preload plate.

A set of linear guides pushing the preload plate allows an independent tuning of both axes x and y. This feature can be used to tune the damper in two perpendicular directions to stabilize two modes which are excited simultaneously, without a cross-effect in the tuning process.

The mass is guided by roller balls inserted on its base. This allows the movement of the mass in any direction. The linear guides used for uncoupling of the tuning axes also guide the mass in the perpendicular directions *x* and *y*.

Spring-type VSTMD prototype

The spring-type VSTMD prototype (Figure 10.8*b*) is a single-axis damper with a rotary spring inserted in the center of the moving mass. This rotary element with variable stiffness as a function of the angular direction is driven by an electric motor, with suitability for automatic control and linearity, predictability and repeatability as main advantages. This rotary spring connects the moving mass to the machine. Automatic stiffness control is implemented by controlling the rotary position of the spring with a motor.

The general design and working principle can be seen in Figure 10.10. The thickness a is used to tune the lower stiffness of the spring, and the thickness b for the higher stiffness of the spring.
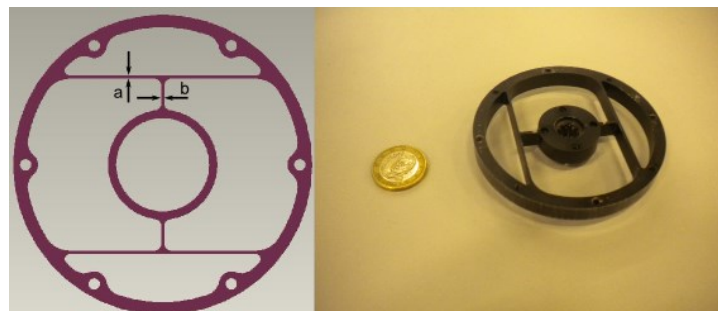
Figure 10.10: Rotary spring with variable stiffness (Aguirre et al., 2012).

Whereas in the preload-type damper damping is provided through the viscoelastic layer itself, in the spring-type damper, damping is created by energy losses related to eddy currents. The damping they produce is very close to ideal viscous behavior and it is generated without contact between parts, avoiding, for example, the non-linear effects produced by friction.

According to Faraday's law, when a time varying magnetic field is applied to a conductor, eddy currents are induced in it. Similarly, if a conductor moves through static but non-uniform magnetic field, eddy currents are induced on it. These eddy currents generate a magnetic field opposed to the variation of the magnetic field seen by the conductor, producing a force that acts against the variation of the magnetic field.

In the second case mentioned above, where a conductor moves through a static and non-uniform field, this force acts as a braking force, trying to slow down the relative motion of the conductor within the field.

Since this force is proportional to the velocity, it can be seen as a damping force. The energy dissipated is converted into heat as Joule's effect losses of the eddy currents on the conductor (Wiederick, 1987).

In order to optimize the damping force, but also the total volume, the configuration shown in Figure 10.11, based on the design by Zuo et al. (2011) was selected. The magnets are attached to the moving mass, whereas a clamped internal conductor layer is placed between the magnet sets. This module design allows fixing the magnets easily, and then handling and mounting each module in the damper independently.
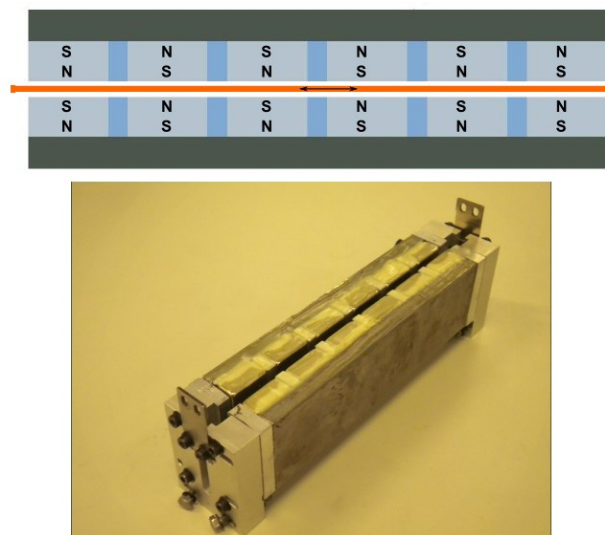
Figure 10.11: Magnet configuration and orientation, design and prototype (Aguirre et al., 2012).

The magnets used are made of Neodymium (magnetic remanence of Br=1.2T) and their size is of 40x20x10mm. An air gap of 0.4 mm between the magnets and the intermediate copper plate layer has been defined.

The damper is oriented in the direction of the critical mode and it is guided through three flexural plates on the bottom of the moving mass.

10.4.2 Communication and control

The VSTMDs are communicated with the accelerometer that monitors the cutting process wireless (see Figure 10.12). The control algorithm developed in section 10.2.3

runs in a PC which receives the signal from the accelerometer and sends back the command for the correct tuning of the VSTMD. The spring-type system is totally wireless, since the motor which drives the circular spring is fed with an electrical battery, whereas the motor driving the preload plates in the preload-type damper is plugged to the electrical supply.
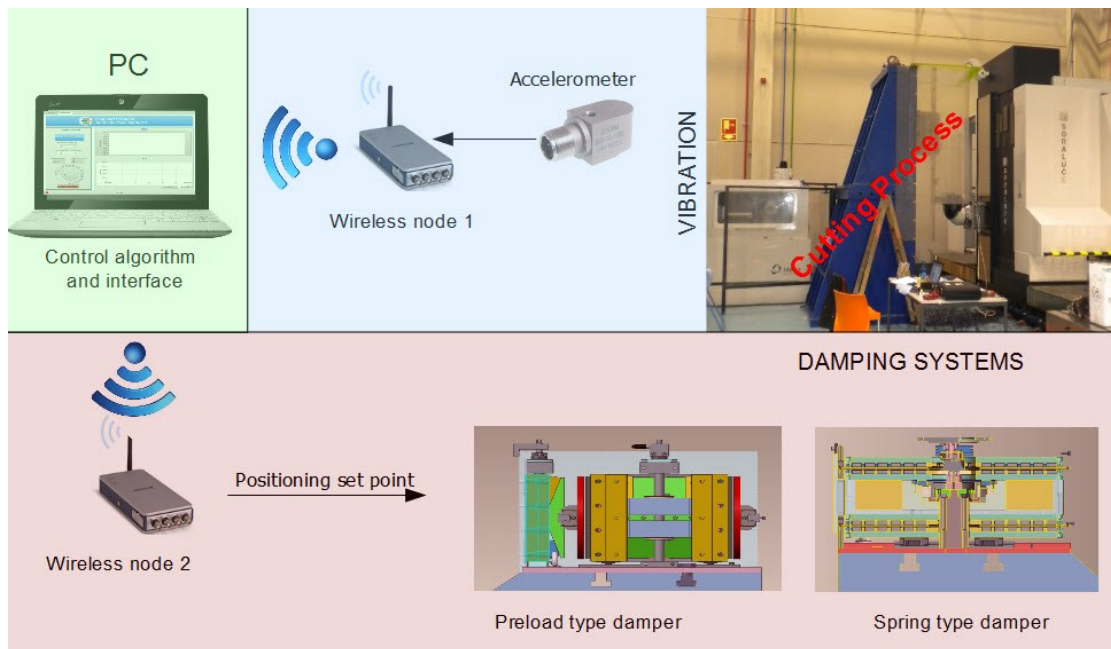
Figure 10.12: Communication loop from the cutting process to the VSTMD

(PoPJIM project. FP7/2007-2013 260048).

10.5 EXPERIMENTAL VALIDATION

10.5.1 Experimental setup

An experimental validation of the system has been carried out by integrating the VSTMDs on a vertical plate supporting the workpiece for a milling operation in a Soraluce's FXR machine (Figure 10.14). Three tests were carried out:

- Cutting tests without VSTM
- Cutting tests with spring-type damper (Figure 10.13a).
- Cutting tests with preload-type damper (Figure 10.13b).
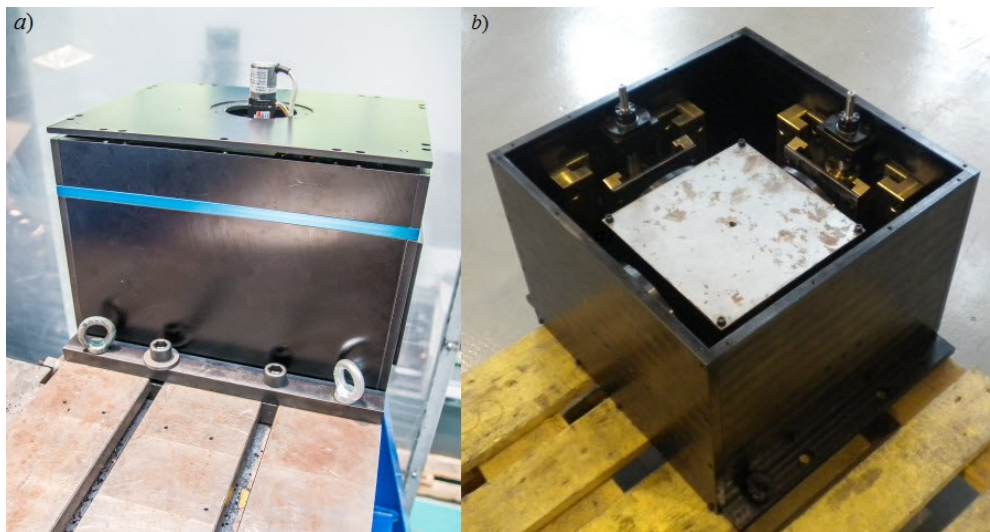
Figure 10.13: VSTMD prototypes: *a*) spring-type, *b*) preload-type.

Figure 10.14: Experimental setup of VSTMD on FXR machine.

The process originally presents a very low stability due to the selected cutting tool geometry, which creates cutting forces mainly oriented in the flexible direction of the cutting plate. The employed cutting conditions are summarized in Table 10.6:

Tool type	Insert type	Tool image	D (mm)	Z	N (rpm)	a_e (mm)	f_z (mm/Z)
HITACHI GFH476 ASF5125RM	SDNW 1505-ZDTN TB6045		125	6	100	87.5	0.3

<p align="center">Table 10.6: Milling cutting conditions for the validation.</p>

10.5.2 Results

The test results are graphically represented in Figure 10.15. Both VSTMD solutions boost the original system cutting capability, with the preload-type damper resulting in slightly higher stability than spring-type damper.
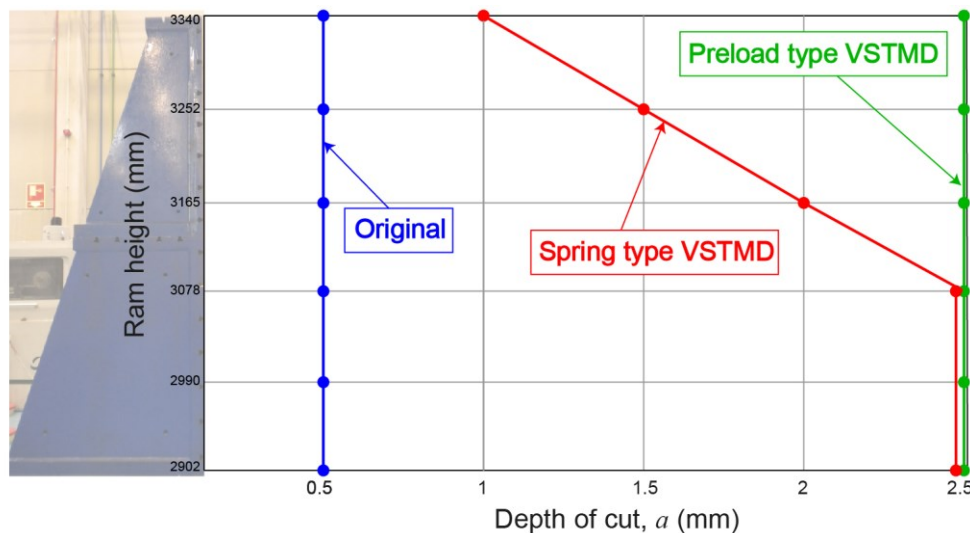
Figure 10.15: Experimental results comparing the cutting capability of a FXR Soraluce machine for an undamped system (original), a spring-type VSTMD integrated workholding system and a preload-type integrated workholding system.

10.6 CONCLUSIONS

In the present work a variable stiffness tunable mass damper concept was investigated. The idealized tuning of this semi-active damper has been investigated. Sims' idea to use the real part of the corresponding frequency response function was used but, in this case, the optimization was performed at each frequency. Thus, a new tuning method has been proposed to maximize the stability in a certain spindle speed. Using this concept, the frequency dependent tuning function was derived analytically and the best possible stability for a VSTMD has been obtained. Later the concept was

confirmed by using the mathematical model of the tuned mass damper performing semi-discretization and initial value time domain simulations.

An iterative method to approach the optimal solution has been proposed and verified by means of initial value time domain simulations. It can be seen that the method together with the VSTMD is able to improve the stability behavior by simply retuning the damper to the best optimal stiffness value in each spindle speed.

Two VSMTD prototypes have been experimentally realized and tested for a low stability milling operation. The developed iterative algorithm has been applied, with significant improvements in cutting capability.

Contribution 14:

A frequency dependent tuning function for a VSTMD has been analytically derived and the best possible stability has been obtained. The method aims to maximize the stability at a certain spindle speed. It has been theoretically demonstrated that the new VSTMD tuning strategy developed improves the stability compared to the tuning methods by Sims and Den Hartog.

Contribution 15:

An iterative algorithm for optimally tuning a VSTMD has been developed. A chatter detection algorithm has been implemented in order to tune the VSTMD according to the measured chatter frequency.

Contribution 16:

A two-axis preload-type variable stiffness tunable mass damper (VSTMD) has been designed, built and investigated. The stiffness and damping are provided by the same viscoelastic layer. The stiffness is varied through the preload of the viscoelastic layer with an especially shaped plate which lengthens the usable frequency range. The tuning in both axes is decoupled by linear guides placed after the preload plates.

Contribution 17:

A spring-type variable stiffness tunable mass damper (VSTMD) has been designed, built and investigated. The stiffness is varied through a circular spring, whereas the damping is provided without physical contact by means of the eddy current effect.

Thus, the stiffness and the damping of the device are decoupled, which allows a simple, accurate and linear tuning capability.

Related Publications:

Munoa, J., Dombovari, Z., Iglesias, A., & Stepan, G. (2015). Tuneable mass dampers with variable stiffness for chatter suppression. *International Conference on Virtual Machining Process Technology*. Vancouver, Canada.

Munoa, J., Iglesias, A., Olarra, A., Dombovari, Z., & Zatarain, M. (2016). Rough milling chatter suppression by self-tunable variable stiffness tuned mass damper, *CIRP Annals-Manufacturing Technology,* submitted.

Chapter 11

Active Damping through Machine Drives

The main drawback of the solution presented in Chapter 9 is that the cutting parameters are modified in order to suppress chatter, which is not always feasible or advisable. The solution in Chapter 10, on the other hand, is adaptable to changing cutting conditions, but it requires the integrating of a device on the machining system, which can be very costly. Moreover, the volume it would require usually makes the solution unfeasible.

In this Chapter, a new chatter suppression solution from a control approach is described. The machine own drives are used to actively mitigate chatter, commanded by an acceleration signal that monitors the cutting process. The measured acceleration is fed back as an additional control loop. Thus, the solution is, at the same time, adaptable to changing cutting conditions and cheap and easy to implement.

The implementation of chatter suppression through the drives requires measuring or estimating the acceleration close to the tool tip As damping is added through machine's drives, the system is non-collocated. Therefore, the design of a robust and stable controller is an important point for a real machine with complex dynamics. Also,

acceleration measurement noise is an important issue. Here, careful design of the control law, and good electrical grounding, is crucial in overcoming this challenge.

11.1 CONTROL ARCHITECTURE AND CHALLENGES

Chen and Tlusty (1995) simulated, for the first time, the possibility of improving chatter stability using acceleration feedback in the servo drive. Since then, active damping of drive vibrations has been studied extensively (Altintas et al., 2011). However, most of the feed drive related vibration damping research has focused either on improving the control bandwidth, or achieving higher positioning accuracy under increasing acceleration and jerk values. Thus, the application of acceleration feedback to increase chatter stability has not been demonstrated yet. Closest to this idea, Kakinuma et al. (2014) applied force control on a test lathe to suppress chatter.

Different additional feedback options have been proposed in the literature to reduce vibrations in different applications (Szabat and Orlowska-Kowalska, 2007). The use of an accelerometer located close to the tool tip to generate additional velocity set points, similar to the approach in (Marushita et al., 2011), has been selected for chatter suppression due to several reasons. First of all, this implementation architecture is very suitable for industrial deployment, as it allows off-the-shelf drives to be used without modification to close the current and velocity control loops. Moreover, it allows having a high value of damping while keeping the proportional velocity loop gain K_p high as well. The CNC kernel, which performs trajectory planning and position control tasks, can thus host the active damping control law; using, for example, compile-cycles which are available on the Siemens 840D CNC. The velocity commands generated by the position and active damping control laws would be superposed and applied directly to the drives.

Figure 11.1a shows the proposed control architecture considering a simple mechanical system with one vibration mode. Figure 11.1b-c shows the damping effect that the acceleration feedback achieves on the vibratory poles, and the resulting load side dynamic compliance.
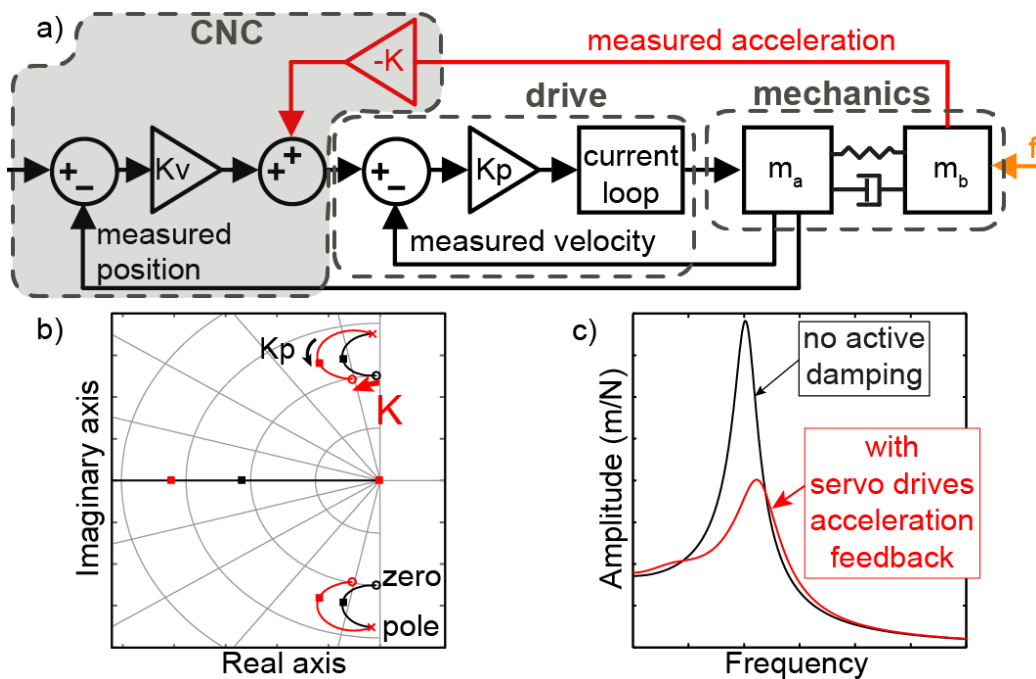
Figure 11.1: Vibration damping by velocity setpoint acceleration feedback: a) Control diagram, b) Velocity loop root locus and c) Tool tip compliance.

While the prospect of increasing a machine tool's dynamic stiffness without adding passive or active dampers is appealing, there are certain requirements for a successful implementation:

- The damping control law should not only damp out the problematic vibration mode(s), but also avoid significantly deteriorating the dynamic stiffness at other frequencies. The destabilization of other modes is an important limitation in non-collocated systems.

- Practical limitations, such as sampling delays or bandwidth and flexibility of the servo system, need to be considered, as well as noise issues which are also of major importance.

- Stability margins need to be retained in the presence of dynamics variations due to machine position change.

- The damping strategy should avoid excessive oscillations in the carriage position. These would lead to early wear and damage of the machine tool drive components.

- Design and commissioning of the damping strategy on industrial machines should be reasonably procedural.

The modeling and controller design presented in section 11.3 was developed to address the requirements above.

11.2 MACHINE DESCRIPTION AND EXPERIMENTAL SETUP

Figure 11.2a shows Soraluce's SV type large milling machine used in this research. Detailed dynamic verification has been carried out, including modal analysis and chatter tests. These tests showed that, depending on the cutting configuration and position in the workspace, either the mode dominant in the x direction with a chatter frequency between 32-44 Hz (Figure 11.2b-c), or a secondary mode dominant in the y direction with 26-29 Hz chatter frequency, were the main contributors to chatter. The proposed active damping architecture has been oriented to damp out both modes.
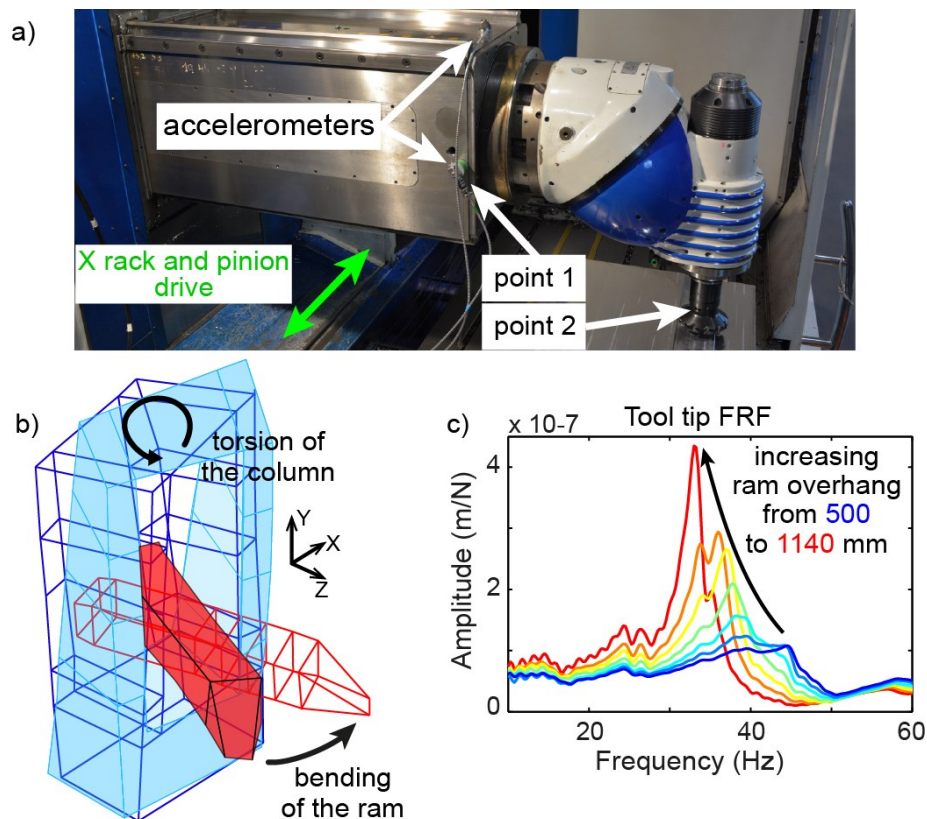
Figure 11.2: a) Large milling machine, b) 36Hz vibration mode shape, c) Variation of tool tip dynamic compliance with ram overhang.

The shape of the targeted mode in the x direction is composed of: torsion of the column, and bending of the ram in the x-z plane. These two elements are vibrating in phase. The presence of a secondary mode at 56 Hz, which is close to the main mode, should also be remarked. This mode is similar to the dominant mode, but the elements are vibrating in counter phase which creates a difficult situation to apply non-collocated active control.

There are other problematic modes as well, around 110 and 180 Hz. However, as these frequencies are beyond the bandwidth of the servo drives, control of these modes was not targeted.

The x axis is driven by a rack and double-pinion mechanism, electronically preloaded to minimize backlash. The y axis is driven by a ball screw drive. The spindle head can change orientation to act in different cutting planes. Therefore, the accelerometers (PCB 602D01) were located at the ram tip in x and y directions to facilitate feedback to handle all possible spindle positions. The motors are driven by drives which, for this study, were configured to operate in torque mode.

An Open CNC was developed to implement the control scheme on the machine tool. The motors' velocity and position loops were closed inside a dSpace controller at 4 and 1 kHz, respectively, imitating their industrial counterparts. The active damping controller was also implemented in dSpace at 4 kHz and injects additional commands into the velocity control loop.

11.3 ACTIVE VIBRATION DAMPING CONTROLLER DESIGN

The active damping is applied both to x and y axes but, to keep the presentation simple, the proceeding analysis on tool tip compliance prediction and loop shaping damping design focuses on the dynamics along the x axis.

11.3.1 MIMO model of the machine tool and damping control law

The machine tool structure, coupled with the servo control system, can be represented as a MIMO plant as shown in Figure 11.3:
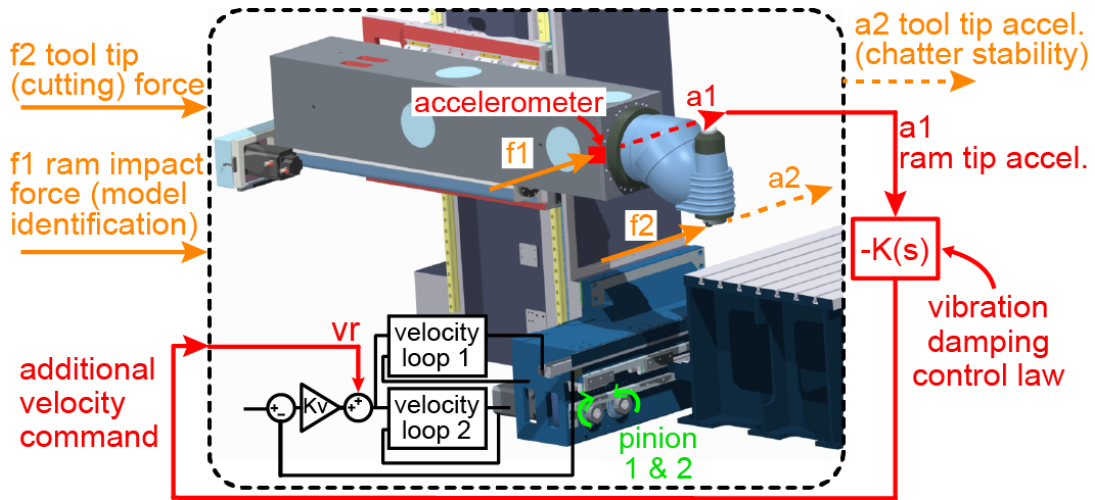
Figure 11.3: Implementation of the proposed active damping strategy.

$$\begin{bmatrix} a_2 \\ a_1 \end{bmatrix} = \begin{bmatrix} \Phi_{a_2 f_2} & \Phi_{a_2 f_1} & \Phi_{a_2 v_r} \\ \Phi_{a_1 f_2} & \Phi_{a_1 f_1} & \Phi_{a_1 v_r} \end{bmatrix} \begin{bmatrix} f_2 \\ f_1 \\ v_r \end{bmatrix},$$

(11.3-1)

where a_2 is the acceleration at the tool tip (i.e., performance point of interest). a_1 is the acceleration at the location of the accelerometer (ram tip). The inputs considered are f_2, f_1 and v_r which are: the cutting force at the tool tip; the measured impact hammer force applied at the ram tip (for model building and compliance prediction); and the additional velocity command injected into the velocity control loop in order to apply active vibration damping.

v_r is computed using the following law:

$$v_r(s) = -K(s)\, a_1(s).$$

(11.3-2)

By combining equations (11.3-1) and (11.3-2), it can be verified that with this control law, the closed-loop (denoted: '*clp*') accelerance functions at the ram tip ($\Phi_{a_1 f_1}^{clp}$) and tool tip ($\Phi_{a_2 f_2}^{clp}$) become:

$$\Phi_{a_1 f_1}^{clp} = \underbrace{\frac{1}{1+\Phi_{a_1 v_r}K}}_{\substack{\text{modifying term}\\\text{due to active}\\\text{vibration damping}}} \underbrace{\Phi_{a_1 f_1}}_{\substack{\text{open}\\\text{loop}}} , \quad \Phi_{a_2 f_2}^{clp} = \underbrace{\Phi_{a_2 f_2}}_{\substack{\text{open}\\\text{loop}}} - \underbrace{\frac{\Phi_{a_2 v_r}K\Phi_{a_1 f_2}}{1+\Phi_{a_1 v_r}K}}_{\substack{\text{modifying term}\\\text{due to active}\\\text{vibration damping}}}.$$

(11.3-3)

The transfer functions in equation (11.3-3) aid in the design of the active vibration damping control law:

- The influence of active damping $K(s)$ on the machining chatter stability can be evaluated by predicting the modified compliance at the tool tip: $\Phi_{x_2f_2}^{clp} = \Phi_{a_2f_2}^{clp} / s^2$.

- The stability implication of active damping on the servo control system can be assessed by inspecting the loop transfer function: $L = \Phi_{a_1v_r} K$ using Nyquist and sensitivity analyses.

Sensitivity and complementary sensitivity functions ($S_f=1/(1+L)$, $T_f=L/(1+L)$) are constructed to inspect robust stability and the closed-loop response to sensor noise (Skogestad and Postlethwaite, 2005). Keeping $|S_f(\omega)|$ low at a given frequency ω allows a higher level of uncertainty to be tolerated in the open loop response of $\Phi_{a_1v_r}(\omega)$; as $1/|S_f(\omega)|$ can be interpreted as the proximity of a point on the Nyquist plot $L(\omega)$ to the critical -1 stability point. Hence, the sensitivity magnitude and its peak are used as a measure of stability margin. $|T_f(\omega)|$, on the other hand, represents how much sensor noise permeates through the control loop and affects the output. While $|T_f(\omega)|\approx1$ is inevitable at frequencies where effective feedback control is needed, it is desirable to keep $|T_f(\omega)|$ as low as possible at other frequencies, to prevent unnecessary oscillations in the actuator torque that would lead to early wear and damage of the feed drive components.

11.3.2 Tool tip compliance and loop transfer function prediction

The required FRF data is obtained following the proceeding steps:

1. While the servo feedback loops (i.e. position, velocity, and current) are closed, without applying any active vibration damping ($K(s)=0$), the ram and tool tip direct and cross acceleration transfer functions are measured using impact hammer testing (i.e., $\Phi_{a_1f_1}, \Phi_{a_2f_2}, \Phi_{a_1f_2}$).

2. The vibration damping controller is set to a constant gain (i.e., $K(s)=K^0$), which is high enough to provide a noticeably different response compared to the non-damping case. The corresponding ram and tool tip acceleration transfer functions are then measured (i.e., $\Phi_{a_1f_1}^{clp0}, \Phi_{a_2f_2}^{clp0}$).

3. The velocity command response functions can be efficiently estimated by re-arranging equation (11.3-3) and using the FRF data gathered in Steps 1 and 2.

$$\Phi_{a_1 v_r} = \frac{\Phi_{a_1 f_1} - \Phi_{a_1 f_1}^{clp0}}{K^0 \, \Phi_{a_1 f_1}^{clp}}, \quad \Phi_{a_2 v_r} = \frac{1 + K^0 \Phi_{a_1 v_r}}{K^0 \Phi_{a_1 f_2}} (\Phi_{a_2 f_2} - \Phi_{a_2 f_2}^{clp0}).$$ (11.3-4)

After completing Steps 1-3, which require only four hammer impact tests for a given machine position, the closed-loop tool tip response ($\Phi_{a_2 f_2}^{clp}$, equation (11.3-3)) and loop transfer function ($L = \Phi_{a_1 v_r} K$) can be evaluated for any linear control law $K(s)$. Figure 11.4 demonstrates the prediction and verification of the tool tip dynamic compliance achieved with the above strategy for the active damping controller design presented in section 11.3.3.
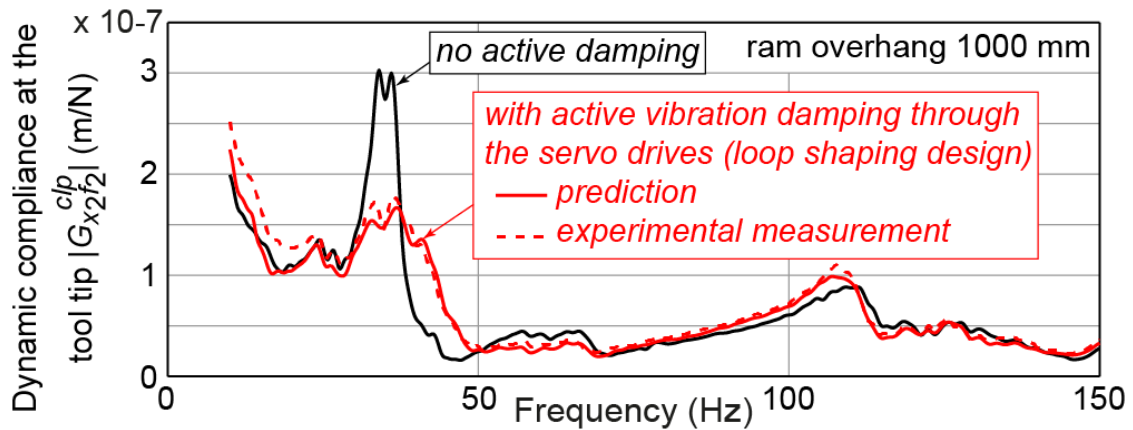
Figure 11.4: Tool tip compliance without and with active vibration damping.

11.3.3 Loop shaping based active damping controller design

The proposed active damping controller design follows the loop shaping methodology, which selectively amplifies the feedback gain in frequencies of interest for performance, attenuates it in other ranges for robustness and sensor noise rejection, and corrects the phase to retain robust stability margins (Skogestad and Postlethwaite, 2005). The graphical nature of this method allows the active damping controller to be designed while considering an envelope of FRFs taken from different positions of the machine tool, without having to curve-fit individual modal models for each of them. This approach has been demonstrated by designing the active damping controller to accommodate several ram overhangs. The resulting control law has the following form:

$$K(s) = \underbrace{K_d}_{\substack{\text{Gain} \\ \text{Adjustment}}} \underbrace{K_{hpf}}_{\substack{\text{High-pass} \\ \text{filter} \\ \text{1st order} \\ f=2.5\,\text{Hz}}} \underbrace{K_{res}}_{\substack{\text{Resonance} \\ \text{filter} \\ \omega=30\,\text{Hz} \\ \zeta_N=0.707 \\ \zeta_D=0.3}} \underbrace{K_{lead}}_{\substack{\text{Lead} \\ \text{filter} \\ z=50\,\text{Hz} \\ p=800\,\text{Hz}}} \underbrace{K_{lpf}}_{\substack{\text{Low-pass} \\ \text{filter} \\ \text{1st order} \\ f=100\,\text{Hz}}}.$$ (11.3-5)

The accelerometer instrumentation has a 2nd order analogue Butterworth high- and low-pass filters set at 1 and 500 Hz. The control law in equation (11.3-5) further restricts the active band by imposing additional high- and low-pass filters, which limit the injection of low-frequency accelerometer drift and high frequency measurement noise into the servo loop. The resonance filter selectively amplifies the gain around the vibration mode which has to be damped out. The lead filter adds positive phase, which in the Nyquist diagram can be observed to have the effect of 'rotating' the loop transfer function in the counter clockwise direction such that the circular lobes point furthest away from the critical -1 point. The gain adjustment sets the trade-off between performance and stability. The terms in equation (11.3-5) were designed while monitoring the aforementioned closed-loop tool tip compliance, loop sensitivity, and co-sensitivity transfer functions.

The proposed loop shaping control law has been compared to applying only proportional acceleration feedback with a gain adjusted experimentally to obtain the highest chatter stability at a spindle speed of 250 rpm. Tool tip compliance and sensitivity/co-sensitivity predictions for the envelope of given ram overhangs, as well as the control law FRFs and sample Nyquist plots for a single ram overhang, are shown in Figure 11.5. While both control laws seem capable of achieving similar improvements in the dynamic compliance (Figure 11.5a), the loop shaping controller is able to maintain significantly lower sensitivity and complementary sensitivity values (i.e., better stability margin and superior noise immunity) over proportional feedback (Figure 11.5b). Indeed, as shown by the highest sensitivity peak, the proportional feedback is destabilizing the 56 Hz mode which is in counter phase with the 36 Hz mode. This does not happen with the loop shaping design, because, except for its targeted frequency range of ~30 Hz, this controller is much less aggressive at other frequencies (Figure 11.5c).

(a) Tool tip compliance for an envelope of ram overhangs: 500-1140 mm

(b) Robust stability (S) and sensor noise injection (T) for posture envelope

(c) Control law frequency response

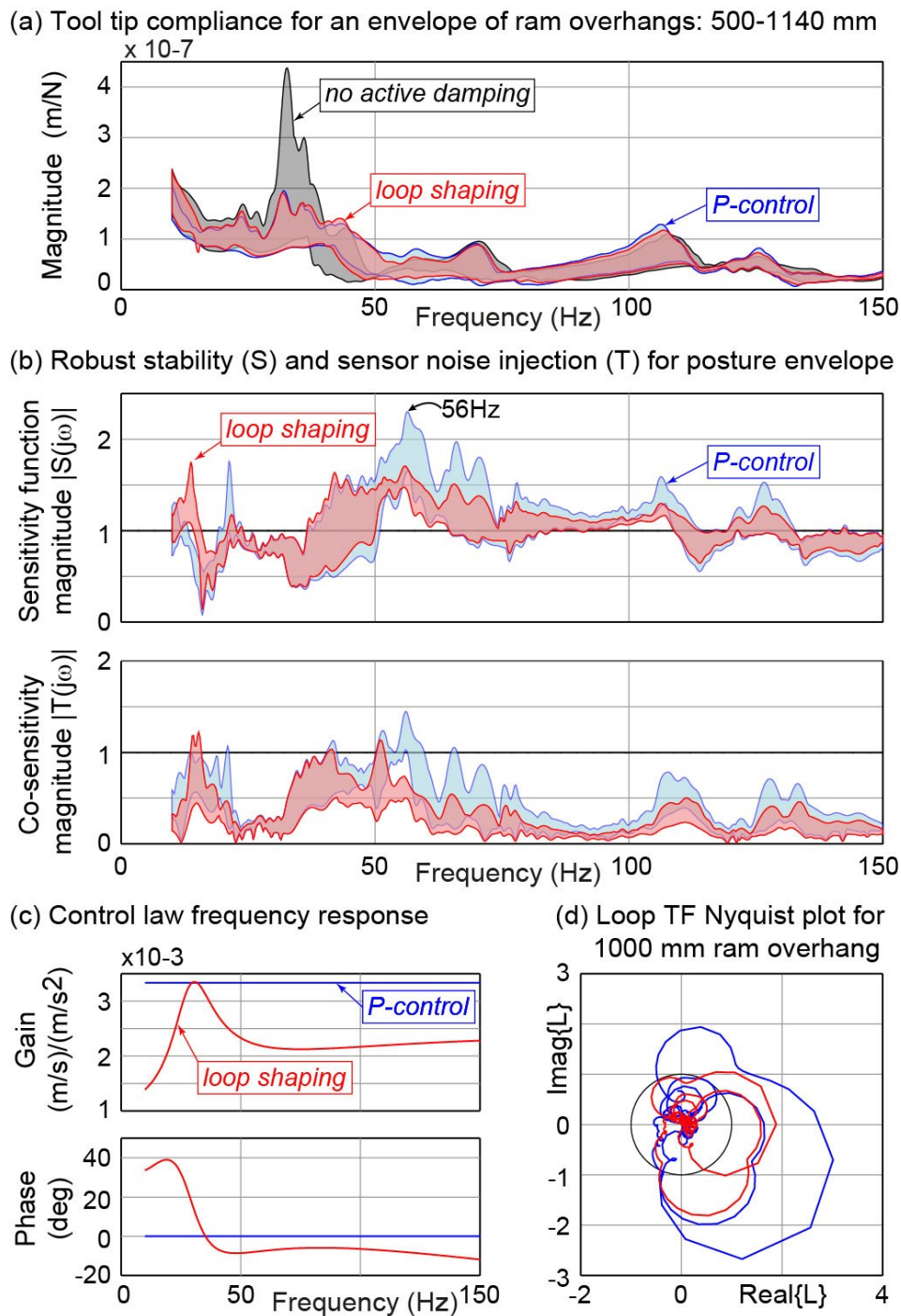(d) Loop TF Nyquist plot for 1000 mm ram overhang

Figure 11.5: Comparison of loop shaping and proportional acceleration feedback strategies for active vibration damping through the servos.

Overall, the developed MIMO modeling strategy, based on the use of practical FRF measurements, allows accurate assessment of the contribution of acceleration feedback, and the design of a robust vibration damping control law.

11.4 STABILITY PREDICTION AND EXPERIMENTAL VALIDATION

Chatter stability predictions have been carried out to evaluate the effectiveness of the proposed acceleration feedback strategy. Worst-case stability limits for machining C45 steel with a 125 mm diameter 12 tooth face milling cutter at 0.2mm/tooth up milling with a_e=100mm have been predicted using the zero-order approximation method (Altintas and Budak, 1995). Figure 11.6 shows the stability lobes based on FRFs taken from the tool tip. Proportional control (P-control) improves the stability around 250 rpm (by damping the mode at 36 Hz). However, this is at the expense of reducing the stability due to the 56 Hz mode at other spindle speeds. On the other hand, the loop shaping design recovers a similar amount of depth of cut around 250 rpm, but also avoids significant deterioration in the stability at other spindle speeds. The stability limit deteriorates a bit due to the modes at 110 and 180 Hz, which can perhaps be avoided in the future through further iterations in the loop shaping design.
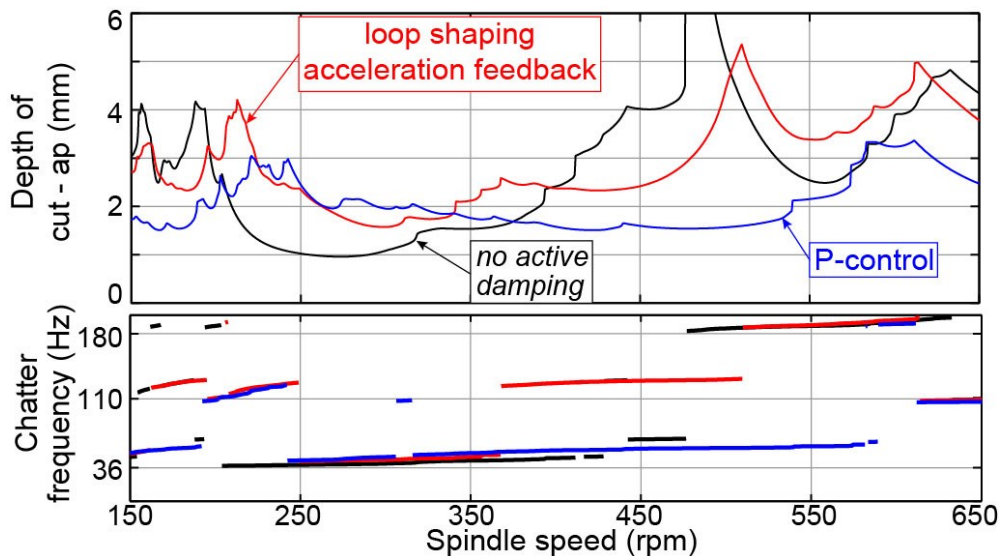
Figure 11.6: Stability lobes for 937mm ram overhang. No active damping, P-control and loop shaping acceleration feedback are compared.

These predictions have been experimentally validated for four different ram overhangs. As seen in Figure 11.7a, the proposed damping strategy significantly improves the stable depth of cut at 250 rpm. The specifically designed P-controller performs slightly better than the loop shaping controller. However, as predicted by the model, the cutting experiments at 550 rpm confirm that the proportional feedback reduces the stability due to the presence of low frequency chatter around 56 Hz. The loop shaping strategy, on the other hand, proves its robustness and reduces considerably this negative effect, thus maintaining good stability at 550 rpm. Moreover, the better noise

immunity and the selective gain amplification leads to less stress on the motor and mechanical components of the drives. Finally, if needed, the modeling approach presented in section 11.3 can also enable a further refined tuning of the controller to open a sweet spot and obtain the highest stability at a given spindle speed. Better results are achieved by the previously developed inertial actuator (Munoa et al., 2013b) but it is at the expense of locating an additional device on the ram tip.
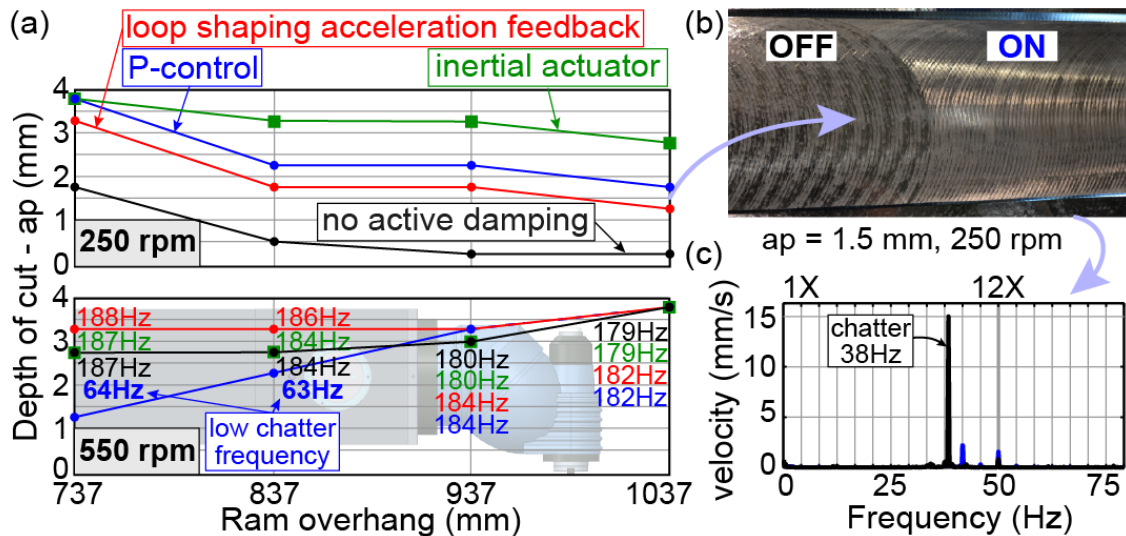
Figure 11.7: (a) Experimental chatter limit. Surface finish (b) and vibration spectra (c) with P-control at 1037 mm ram overhang.

For the spindle speed of 250 rpm, the effect of the machine's drives active damping strategy during a cutting test is shown in Figure 11.7b-c. The surface finish and vibration spectrum show that the chatter vibrations are successfully removed.

11.5   CONCLUSIONS

This chapter has presented a new chatter suppression method, able to actively damp out the structural modes of a large milling machine using only the machine tool's own feed drives and low-cost accelerometers. A MIMO model, based on experimental frequency response measurements, has been developed in order to predict the active damping effect and to design a robust controller. Factors like position dependent dynamics, servo/chatter stability, and sensor noise permeation have been considered. Experimental validation shows that the proposed strategy can increase the productivity between 85-600% by suppressing structural chatter. Future work targets migration of this idea into an industrial CNC platform.

Contribution 18:

A new active damping system for chatter suppression through machine drives has been developed. The acting force is introduced through the machine drives, which are controlled by an acceleration signal of the cutting process that is regarded as an additional acceleration feedback loop in the machine control system. A minimum investment is needed to implement the system and it is adaptable to changing cutting conditions. A significant chatter stability increase in a roughing operation in a large milling machine has been achieved.

Contribution 19:

A new vibration damping control procedure based on a loop shaping strategy has been proposed. The loop shaping attenuates or amplifies the feedback gains and corrects the phase in order to increase the immunity to noise and improve the stability margin avoiding the destabilization of adjacent modes.

Contribution 20:

A new MIMO modeling strategy, based on the use of practical FRF measurements, has been posed. This strategy allows accurate assessment of the contribution of acceleration feedback and the design of a robust vibration damping control law.

Related Publications:

Munoa, J., Beudaert, X., Erkorkmaz, K., Iglesias, A., Barrios, A., & Zatarain, M. (2015). Active suppression of structural chatter vibrations using machine drives and accelerometers. CIRP Annals-Manufacturing Technology, 64, 385-388.

Part IV
Conclusions

Part IV contains the main conclusions and contributions obtained in this research, as well as the proposed future work related to the field (Chapter 12). Finally, the references cited in this work are listed (Chapter 13).

Chapter 12

Conclusions and Outlook

In this Chapter, the conclusions of the work are summarized. The new findings and developments generated by this research and the future working lines arising from the results of the Thesis are also detailed.

12.1 CONCLUSIONS

This research has focused on milling chatter prediction and mitigation. Chatter is a complex phenomenon that jeopardizes machine and workpiece integrity and cause severe productivity losses. A huge effort has been done in recent years for chatter understanding and modeling, but there are still many unknown factors and conditions that play a role in its onset.

From this reason, several weaknesses of current stability models and chatter mitigation techniques have been highlighted in this Thesis. A suitable chatter prediction is essential for a correct process planning, however, many inaccurate prediction scenarios have been reported by the scientific community. This assertion is confirmed in this work, through the experimental correlation of a heavy-duty milling process stability lobe diagram.

Among the sources of error in current stability prediction models, the double period type stability lobes, also called flip lobes, are not taken into account by some of the most popular stability models like ZOA. For this reason, a new combined stability model based on ZOA has been developed in order to consider the presence of these lobes. This new model maintains the main advantages of ZOA: short time calculation and possibility to handle experimental FRFs directly. Experimental results show a significant improvement of the prediction by this combined model with respect to ZOA under the presence of flip lobes.

Although the usual thinking is that flip lobes can affect stability only when very low immersion milling processes are present, it has been demonstrated that a process can be very interrupted and therefore, have a very low flip limit, even if the cutting immersion is high. Interesting expressions to assess when the cutting process can be subject to flip and how this instability will affect the cutting speed range have been obtained. Analytical expressions of systems in which a dominant mode limits stability have been obtained, acquiring a wider knowledge about this type of instability. This new formulae are useful to reduce calculation time of current time consuming stability models. The experimental results show that the analytical formulae provide a good approximation when low damping and fairly continuous milling processes are analyzed.

Flip lobe omission can be an important source of errors in stability prediction, but there are many other minor factors influencing the overall stability limit that are not considered in the stability models. Experimental approaches are the most appropriate techniques for an accurate determination of the stability lobes without a mathematical description of those minor effects that affect stability. The main drawback of these methods is that they require cutting tests in advance. Two different experimental techniques have been implemented.

On the one hand, a one dominant mode and two equal orthogonal modes inverse method have been developed for straightforward chatter limit identification. A lobe type curve is fitted around the experimental chatter limit, obtaining inversely the dynamic parameters of the system, which can later be extrapolated to any cutting test. This method is highly effective and precise, but cannot be applied if more than one mode or two equal orthogonal modes are involved in stability limitation, as it is the usual case. Moreover, it requires setting the system into chatter vibrations, which is not always advisable.

On the other hand, a new experimental method for FRF extraction named sweep milling force excitation (SMFE) has been developed. This method consists of obtaining the FRF response of the system using the cutting force itself as the excitation input

force. The FRFs obtained through this method lead to much more accurate stability lobe prediction that FRFs obtained through standard FRF extraction methods like hammer or shaker.

Stability prediction is a useful but, at the same time, very complex task. There will be always specific cases in which the stability prediction fails or operations where the cutting conditions fall in an unstable area and cannot be modified, and this is why chatter suppression techniques are also needed. Chatter can be tackled from different approaches and, in this Thesis, three solutions to mitigate chatter from different approaches have been proposed.

First, an online wireless system for automatic parameter selection has been proposed. The cutting process is monitored through a wireless microphone. The acquired signal is sent to a receiver and a simple algorithm selects the most nearby stable cutting speed that provides the higher stability.

Two variable stiffness damper (VSTMD) prototypes have also been developed: a preload-type damper and a spring-type damper. The two prototypes present enhanced properties with respect to a standard passive damper. The preload-type damper allows a progressive and uncoupled tuning in two directions due to its special shape preload plate and the linear guides placed after the preload plate respectively. On the other hand, the spring-type damper can be tuned through a circular spring and the damping is applied by eddy current effect in a contactless way. For this reason, stiffness and damping are uncoupled and the damper can self-tune in a fast an accurate way, providing a semi-active solution. Moreover, a new iterative tuning strategy which outperforms the currently used tuning method by Sims has been developed.

Finally, an active damping method through machine tool's own drives has been developed. This approach goes one step further than classical active damping systems, since no external device is needed as an actuator. The use of machine drives as actuators simplifies the solution and makes it easy and affordable. Furthermore, a new control strategy named loop shaping has been developed, which outperforms current proportional controls, increasing the stability margin of the actuator and increasing immunity to input noise.

The three developed chatter suppression techniques are complementary, since they present different application fields. The on-line parameter modification algorithm is aimed at high speed machining processes, where tool or spindle high frequency modes are involved in chatter onset. The main application of the variable stiffness tuned mass damper is the workpiece fixture, where the location of a considerable damper besides

the machined workpiece is a feasible solution. Finally, the active damping technique is focused on machine tool structural mode chatter dampening. All these chatter suppression solutions have been satisfactorily validated through intensive experimentation.

12.2 CONTRIBUTIONS

The specific contributions of this research are classified below. From the original 20 contributions, the most relevant are set up in brief:

Contributions related to stability prediction improvement:

- **Contribution 1:**
  A new procedure for tool selection in heavy-duty milling process planning through the use of dedicated stability lobes has been proposed.

- **Contribution 2:**
  It has been demonstrated that there is no universal tool that holds the higher cutting capability. A specific tool can be a good choice for a particular machine but the worst choice for another machine with a different dynamic behavior.

- **Contribution 4:**
  Analytical expressions for flip minimum analytical expression a_{Bf} and absolute minimum determination (considering Hopf and flip limits) for one dominant mode systems have been defined and correlated with SD method.

- **Contribution 5:**
  The importance of the directional factor harmonic ratio r_β has been highlighted. Thus, flip dominates over Hopf for r_β values bigger than 0.5 roughly and, when r_β turns bigger than 1, flip lobes become different from the currently known in terms of shape and features.

- **Contribution 7:**
  A new combined frequency domain analytical method has been developed and experimentally validated. This method calculates the standard ZOA solution combined with the double period chatter limit in a single frequency scanning loop.

Contributions related to experimental techniques for model input data quality improvement:

- **Contributions 8 & 9:**

  An inverse modal parameter estimation method from chatter tests has been described for the case of two equal and orthogonal modes. The employed mathematical model is too simple to describe the real behavior of the system.

- **Contribution 10:**

  The effect of tool wear on cutting coefficients or dynamic parameters is negligible for the conventional cutting condition range, therefore, tool wear can be neglected for stability analysis.

- **Contributions 11 & 12:**

  A new simple and fast methodology for FRF estimation using the milling force itself as input excitation (SMFE method) has been developed. It has been experimentally demonstrated that the FRFs obtained by the developed SMFE methodology are fairly more accurate than the FRFs obtained by traditional excitation methods.

Contributions related to chatter mitigation techniques:

- **Contributions 14 & 15:**

  It has been theoretically demonstrated that the optimal tuning of the VSTMD improves the stability compared to the tuning methods by Sims and Den Hartog for a standard TMD. An iterative algorithm for optimally tuning a VSTMD has been developed.

- **Contributions 16 & 17:**

  Two VSTMD prototypes have been built and experimentally validated. A two-axis preload-type with stiffness and damping provided through a viscoelastic layer and a one-axis spring-type with the stiffness varied through a circular spring and damping provided by means of the eddy current effect.

- **Contribution 18:**

  A new active damping system for chatter suppression through machine drives has been developed and experimentally validated.

- **Contribution 19:**

  A new vibration damping control procedure based on loop shaping has been proposed in order to increase the immunity to noise and improve the stability margin avoiding the destabilization of adjacent modes.

12.3 FURTHER WORK

The work developed in this Thesis poses a step forward in chatter understanding, prediction and mitigation capabilities. A deeper investigation in the concepts addressed in this Thesis will lead to a further refinement of stability models, including more currently ignored factors that affect cutting stability in today's well known stability models. Furthermore, higher capacities in chatter removal techniques should be also addressed. The pursued objective is to industrialize and standardize optimal solutions for intensive industrial use.

Future work related to stability prediction improvement:

1. Although ZOA model has been improved with the inclusion of double period lobe calculation, there are still other effects, which are not currently taken into account by the ZOA method and should be progressively included. One of these additional effects is the helix angle influence. It has been demonstrated that the helix angle can affect higher order harmonics and therefore affect the flip lobe area (Zatarain et al., 2006).

2. The torsional stiffness, which is already considered by current drilling and plunge milling models, is a factor that has been omitted in milling stability models. However, its effect in certain applications has been demonstrated (Rivin and Kang, 1992). Therefore, a research on its quantitative influence on milling stability and the methodology to model it should be subject of research in the near future.

3. Another non-modeled factor affecting milling stability is the effect of the unsafe zone (Dombovari et al., 2011a), whose influence has been observed experimentally but, however, it is not considered by any current theoretical stability model. A deeper research for understanding this nonlinear phenomenon should be conducted.

Future work related to experimental techniques for model input data quality improvement:

4. The inverse method developed in this Thesis has a limited applicability, since it is only valid for cases of one dominant mode and two equal and orthogonal modes. Moreover, the mathematical approach used is too simple to describe the mathematical complexity of milling chatter and, therefore, the method sometimes results in unrealistic modal parameters. These problems could be overcome by a new approach consisting of obtaining the dynamic parameters from experimental data, using a singular value decomposition (SVD) of the experimental FRF instead of fitting the curves as it is traditionally done.

5. The sweep milling force excitation method (SMFE) has provided excellent improvement in milling stability prediction. However, considering that the method is newly developed, further testing is needed in order to completely validate the outperformance of this method with respect to standard FRF extraction methods. For that purpose, milling machines in which current stability prediction results are unsatisfactory should be analyzed. It is also interesting to apply the methodology to machines with clear dynamics (one dominant mode in each direction, for instance) with the purpose of comparing the extracted dynamic parameters with those obtained by standard methods. This will be useful to acquire knowledge about the physical reasons of the inaccuracies of standard FRF extraction methodologies, analyzing which are the dynamic parameters more subject to deviations.

Future work related to chatter mitigation techniques:

6. The on-line parameter selection tool is already in a high technology readiness level. The system could be boosted by combining it with the continuous spindle speed variation, in order to complement the current system and increase the capability to tackle chatter at different areas in the stability lobe diagram.

7. The variable stiffness tuned mass damper (VSTMD) is ready to be implemented in machine tool industry, with a huge cutting capability increasing potential. A new working line is the addition of an extra working axis, in order to achieve a biaxial system together with eddy current damping, thus increasing the capability to act on different critical modes of the fixture.

8. Also connected with VSTM technology, the application of this solution to the dynamic behavior improvement of rotating parts of the machine tools is also of

great interest. The wireless capability allows the use of this solution for rotating parts, although the space and weight issues should also be managed. The use of a coupled electrical circuit for damping purposes could be a good approach to solve space and weight related constraints. On the other hand, its application in different sectors from the machine tool industry should also be addressed.

9. The active damping strategy through the control drives, however, is still in an earlier phase of development and should be further refined before taking it to real production sites. The next step for this technology would be to substitute the current external controller by the own CNC of the machine. This would mean a further step in the integration of this technique. It must be taken into account that there could be different integration procedures, depending on the CNC brand. Furthermore, more intensive chatter suppression testing must be done under different milling conditions and using different control laws for the acceleration feedback. Finally, the research on techniques to avoid the destabilization of other originally non-critical modes is also needed.

Chatter prediction and suppression is in the spotlight of the manufacturing industry as a key factor to increase productivity and competiveness. The manufacturing industry is constantly evolving and the new emerging processes and machine types and architectures entail new technological challenges that will have to be addressed in the future.

Rapid manufacturing is an increasingly used technique for small and medium size workpiece manufacturing by means of the addition of layers on top of each other until the final shape is achieved. With the increasing use of this technique, cutting processes will be progressively reduced. However, rapid manufacturing often requires finishing operations which can still cause chatter vibrations when dealing with slender parts. This fact, together with the remaining need of large-size workpiece roughing processes, will keep chatter vibrations in the spotlight in the following decades.

Another emerging manufacturing trend is the use of robots for assisting machine tools in machining operations. The robot can be used for smooth machining, deburring or side operations in collaborative work with the machine tool. Robots are highly versatile and can be adapted to many different tasks, but their specific architecture makes them usually very flexible and prone to vibration problems. Several techniques developed in this project, such as the VSTM and the active vibration control through drives can be effectively applied to this kind of structures for mitigation of vibrations.

Therefore, despite the fast evolution of manufacturing concepts, vibration mitigation and specifically chatter prediction and suppression will remain as a main subject of study in order to improve productivity of the manufacturing processes in the future.

Chapter 13

References

Abele, E., Bauer, J., Pischan, M., Friedmann, M., Hemker, T., & von Stryk, O. (2010). *Industrial Robot and a Removal Process. CIRP 2nd International Conference on Process Machine Interactions*. Vancouver, Canada.

Abele, E., & Fiedler, U. (2004). Creating Stability Lobe Diagrams during Milling. *CIRP Annals*, 53(1), 309-312.

Abele, E., Kreis, M., & Roth, M. (2006). Electromagnetic actuator for in process non-contact identification on spindle-tool frequency response functions. *Proceedings of the 2nd International Conference on High Performance Cutting*. Vancouver, British Columbia, Canada.

Abele, E., Sielaff, T., & Schiffler, A. (2012). Method for chatter detection with standard PLC systems. *Prod. Eng. Res. Devel.*, 6, 611-619.

Agneni, A., Coppotelli, G., & Grappasonni C. (2012). A method for the harmonic removal in operational modal analysis of rotating blades. *International Journal of Machine Tools and Manufacture*, 27, 604-618.

Aguirre, G., Gorostiaga, M., Porchez, T., & Munoa, J. (2012). Self-tuning semi-active tuned-mass damper for machine tool chatter suppression. *ISMA2012-USD2012*, 109-124. Leuven, Belgium.

Aguirre, G., Gorostiaga, M., Porchez, T., & Munoa, J. (2013). Self-tuning dynamic vibration absorber for machine tool chatter suppression. *In 28th Annual Meeting of the American Society for Precission Engineering (ASPE)*.

Aguirre, G., Iglesias, A., Munoa, J., & Astarloa, A. (2014). Real milling force based dynamic parameter extraction method. *Proceedings of ISMA*, Leuven, Belgium.

Ahmadi, K., & Ismail, F. (2011). Analytical stability lobes including process damping effect on machining chatter. *International Journal of Machine Tools and Manufacture*, 51(4), 296-308.

Al-Regib, E., Ni, J., & Lee, S. H. (2003). Programming spindle speed variation for machine tool chatter suppression. *International Journal of Machine Tools and Manufacture*, 43(12), 1229-1240.

Alter, D. M., & Tsao, T. C. (1994). Stability of turning processes with actively controlled linear motor feed drives. *Journal of Manufacturing Science and Engineering*, 116(3), 298-307.

Altintas, Y. (2001). Analytical prediction of three dimensional chatter stability in milling. *Japan Society of Mechanical Engineers, International Journal Series C: Mechanical Systems, Machine Elements and Manufacturing*, 44(3).

Altintas, Y. (2012). Manufacturing automation: metal cutting mechanics, machine tool vibrations, and CNC design. *Cambridge university press*.

Altintas, Y., Brecher, C., Beck, M., & Witt, S. (2005). Virtual machine tool. *CIRP Annals*, 54(2), 115-138.

Altintas Y., & Budak, E. (1995). Analytical prediction of stability lobes in milling. *CIRP Annals*, 44(1), 357-362.

Altintas, Y., & Chan, P. K. (1992). In-process detection and suppression of chatter in milling. *International Journal of Machine Tools and Manufacture*, 32(3), 329-347.

Altıntaş, Y., Engin, S., & Budak, E. (1999). Analytical stability prediction and design of variable pitch cutters. *Journal of Manufacturing Science and Engineering*, 121(2), 173-178

Altintas, Y., Eynian, M., & Onozuka, H. (2008a). Identification of dynamic cutting force coefficients and chatter stability with process damping. *CIRP Annals*, 57(1), 371-374.

Altintas, Y., & Lee, P. (1996). A general mechanics and dynamics model for helical end mills. *CIRP Annals*, 45(1), 59-64.

Altintas, Y., & Spence, A. (1991). End milling force algorithms for CAD systems, *CIRP Annals*, 40(1), 31-34.

Altintas, Y., Stepan, G., Merdol, D., & Dombovari, Z. (2008b). Chatter stability of milling in frequency and discrete time domain. *CIRP Journal of Manufacturing Science and Technology*, 1(1), 35-44.

Altintas, Y., Verl, A., Brecher, C., Uriarte, L., & Pritschow, G. (2011). Machine Tool Feed Drives. *CIRP Annals*, 60(2), 779-796.

Altintas, Y., & Weck, M. (2004). Stability of dynamic cutting and grinding. *CIRP Annals*, 53(2), 619-684.

Archenti, A., & Nicolescu, C.M. (2010). Recursive estimation of operational dynamic parameters in milling using acoustic signals. *CIRP 2nd International Conference on Process Machine Interactions*. Vancouver, Canada.

Armarego, E. J. A., & Epp, C. J. (1970). An investigation of zero helix peripheral up-milling. *International Journal of Machine Tool Design and Research*, 10(2), 273-291.

Arnold, R.N. (1946). The mechanism of tool vibration in the cutting of steel. *Proceeding of Institution of Mechanical Engineering*, 154, 261-276.

Astarloa, A. (2011). Estudio de la linealidad de sistemas mecánicos en máquina herramienta. *End Course Project*, University of Mondragon, Mondragon, Spain.

Bachrathy, D., & Stépán G. (2010). Time-periodic velocity-dependent process damping in milling processes. *CIRP 2nd International Conference on Process Machine Interactions*. Vancouver, Canada.

Bachrathy, D., Stépán, G., & Turi, J. (2011). State dependent regenerative effect in milling processes. *Journal of Computational and Nonlinear Dynamics*, 6(4), 041002.

Bailey, T., Ruget, Y., Spence, A., & Elbestawi, M.A. (1995). Open-architecture controller for die and mould machining. *Proceedings of the American Control Conference*, 1, 194-199.

Barnada, F., Teixidor, D., Iglesias, A., Quintana, G., & Ciurana, J. (2015). Wireless device for on-line chatter identification and process parameters correction in milling processes. *Robotics and Computer Integrated Manufacturing*, submitted.

Bayly, P.V., Halley, J.E., Mann, B.P., & Davies, M.A. (2003). Stability of interrupted cutting by temporal finite element analysis. *Journal of Manufacturing Science and Engineering*. *Transactions of the ASME*, 125(2), 220-225.

Bediaga, I. (2009). Supresión de chatter regenerativo mediante variación en proceso de la velocidad de giro. *Doctoral Thesis*. University of Basque Country, Bilbao, Spain.

Bediaga, I., Egaña, I., & Muñoa, J. (2006). Reducción de la inestabilidad en cortes interrumpidos en fresado a alta velocidad mediante variación de la velocidad del husillo. *In XVI Congreso de Máquinas-Herramienta y Tecnologías de Fabricación*, San Sebastián, Spain.

Bediaga, I., Hernández, J., Munoa, J., & Uribe-Etxeberria, R. (2004). Comparative analysis of spindle speed variation techniques in milling. *In The 15th INTERNATIONAL DAAAM SYMPOSIUM "Intelligent Manufacturing & Automation: Focus on Reconstruction and Development"*, 1-2.

Bediaga, I., Munoa, J., & Egaña, I. (2005). Computer model for simulating and optimizing milling process. *Proceedings of the IEEE EUROCON 2005, The International Conference on "Computer as a tool"*, 1714-1717. Belgrade, Serbia.

Bediaga, I., Munoa, J., Hernández, J., & López de Lacalle, L.N. (2009). An automatic spindle speed selection strategy to obtain stability in high-speed milling. *International Journal of Machine Tools and Manufacture*, 49, 384-394.

Biermann, D., Kersting, P., & Surmann, T. (2010). A general approach to simulating workpiece vibrations during five-axis milling of turbine blades, *CIRP Annals*, 59(1), 125-128.

Brecher, C., & Esser, M. (2007). Stability prediction: advances and current restrictions. *6th International Conference on High Speed Machining*. San Sebastian, Spain.

Brecher, C., & Esser, M. (2008). The consideration of dynamic cutting forces in the stability simulation of HPC-milling processes. *1st CIRP International Conference on Process Machine Interactions*. Hannover, Germany.

Budak, E. (1994). Mechanics and dynamics of milling thin walled structures. *Doctoral Thesis*. University of British Columbia, Vancouver, Canada.

Budak, E., & Altintas, Y. (1998). Analytical Prediction of Chatter Stability in Milling - Part 1: General Formulation. *Journal of Dynamic Systems, Measurement and Control. ASME*, 120(1), 22-30.

Budak, E., Ozturk, E., & Tunc, L.T. (2009). Modeling and simulation of 5-axis milling processes, *CIRP Annals*, 58(1), 347-350.

Burney, F.A., Pandit, S.M., & Wu S.M. (1976). Stochastic approach to characterization of machine tool system dynamics under actual working conditions. *Journal of Engineering for Industry. Transactions of the ASME*, 98(2), 614-619.

Burney, F.A., Pandit, S.M., & Wu, S.M. (1977). New approach to analysis of machine-tool system stability under working conditions. *Journal of Engineering f or Industry - Transactions of the ASME*, 99(3), 585–589.

Cai, H., Mao, X., Li, B., & Luo, B. (2014). Estimation of FRFs of machine tools in output-only modal analysis. *The International Journal of Advanced Manufacturing Technology*, 77, 117-130.

Cai, H., Luo, B., Mao, X., Gui, L., Song, B., Li, B., & Peng, F. (2015). A Method for Identification of Machine-tool Dynamics under Machining. *Procedia CIRP*, 31, 502-507.

Cao, H., Altintas, Y., & Holkup, T. (2010). Modeling and comparison of high speed spindle systems with different bearing preload mechanisms. *CIRP 2nd International Conference on Process Machine Interactions*. Vancouver, Canada.

Cao, H., Li, B., & He, Z. (2012). Chatter stability of milling with speed-varying dynamics of spindles. *International Journal of Machine Tools and Manufacture*, 52, 50-58.

Chen, J.S., & Hwang, Y.W. (2006). Centrifugal force induced dynamics of a motorized high-speed spindle. *International Journal of Advanced Manufacturing Technologies*, 30, 10-19.

Chen, Y.C., & Tlusty, J. (1995) Effect of Low-Friction Guideways and Lead-Screw Flexibility on Dynamics of High-Speed Machines. *CIRP Annals*, 44(1), 353-356.

Cheng, C.H., Schmitz, T.L., & Duncan, G.S. (2007). Rotating tool point response prediction using RCSA. *Machining Science and Technology*, 11(3), 433-446.

Choi, T., & Shin, Y.C. (2003). On-Line Chatter Detection Using Wavelet-Based Parameter Estimation. *Journal of Manufacturing Science and Engineering, Transactions of the ASME*, 125, 21-28.

Comstock, T. R., Tse, F. S., & Lemon, J. R. (1969). Application of controlled mechanical impedance for reducing machine tool vibrations. *Journal of Manufacturing Science and Engineering*, 91(4), 1057-1062.

Cooley, J.W., & Tukey, J.W. (1965). An algorithm for the machine calculation of complex Fourier series. *Mathematics of Computation* 19, 297-301.

Corpus, W. T., & Endres, W. J. (2000). A high-order solution for the added stability lobes in intermittent machining. *In Proceedings of the Symposium on Machining Processes*, 871-878.

Cowley, A., & Boyle, A. (1970). Active dampers for machine tools. *CIRP Annals*, 18(1), 213-222.

Davies, M.A., Pratt, J.R., Dutterer, B.S., & Burns, T.J. (2000). The stability of low radial immersion milling. *CIRP Annals*, 49, 37-40.

Davies, M.A., Pratt, J.R., Dutterer, B.S., & Burns, T.J. (2002). Stability Prediction for Low Radial Immersion Milling. *Journal of Manufacturing Science and Engineering, Transactions of the ASME*, 124(2), 217-225.

Delio, T. (1992). Method of controlling chatter in a machine tool. *Patent No. US005170358A*.

Delio, T., Tlusty, J., & Smith, S. (1992). Use of audio signals for chatter detection and control. *Journal of Manufacturing Science and Engineering*, 114(2), 146-157.

Den Hartog, J. P. (1947). Mechanical vibrations. *McGraw-Hill*, New York.

Dion J.L., Tawfiq, G., & Chevallier, G. (2012). Harmonic component detection: Optimized Spectral Kurtosis for operational modal analysis. *International Journal of Machine Tools and Manufacture*, 26, 24-33.

Dombovari, Z., Altintas, Y., & Stépán, G. (2010). The effect of serration on mechanics and stability of milling cutters. *International Journal of Machine Tools and Manufacture*, 50, 511-520.

Dombovari, Z., Barton, D.A.W., Wilson, R.E., & Stépán, G. (2011a). On the global dynamics of chatter in the orthogonal cutting model. *International Journal of Nonlinear Mechanics*, 46(1), 330-338.

Dombovari, Z., Iglesias, A., Zatarain, M., & Insperger, T. (2011b). Prediction of multiple dominant chatter frequencies in milling processes. *International Journal of Machine Tools and Manufacture*, 51(6), 457-464.

Dombovari, Z., & Stepan, G. (2010). Experimental and Theoretical Study of Distributed Delay in Machining. *In Proceedings of 9th IFAC Workshop on Time Delay Systems*, Prague, 1-5.

Dombovari, Z., & Stepan, G. (2015). On the bistable zone of milling processes. *Phil. Trans. R. Soc. A*, 373(2051), 20140409.

Dornfeld D. (2007). Precision manufacturing. *1st ed. New York, NY: Springer*.

Du Bois, J. L., Lieven, N., & Adhikari, S. (2012). A tensioned cable as an adaptive tuned vibration absorber for response suppression in rotorcraft. *In ISMA 2012 International Conference on Noise and Vibration Engineering*, 385-393.

Endres, W. J., & Loo, M. (2002). Modeling Cutting Process Nonlinearity for Stability Analysis - Application to Tooling Selection for Valve-Seat Machining. *Proc. 5th CIRP Workshop*, West Lafayette, USA.

Ehmann, K. F., Kapoor, S. G., DeVor, R. E., & Lazoglu, I. (1997). Machining process modeling: a review. *Journal of Manufacturing Science and Engineering*, 119(4B), 655-663.

Engin, S., & Altintas, Y. (2001a). Mechanics and Dynamics of General Milling Cutters. Part I: Helical End Mills. *International Journal of Machine tools & Manufacture*, 41(15), 2195-2212.

Engin, S., & Altintas, Y. (2001b). Mechanics and Dynamics of General Milling Cutters. Part I: Inserted Cutters. *International Journal of Machine tools & Manufacture*, 41(15), 2213-2231.

Esser, M., Brecher, C., & Paepenmüller, F. (2006). Motor Spindles for HPC: Testing and Chatter Simulation. *CIRP 2nd International Conference on High Performance Cutting*, Vancouver, Canada.

Eynian, M. (2010). Chatter stability of turning and milling with process damping. *Doctoral Thesis*. University of British Columbia, Vancouver, Canada.

Faassen, R.P.H., van de Vouw, N., Oosterling, J.A.J., & Nijmeijer, H. (2003). Prediction of regenerative chatter by modeling and analysis of high-speed milling. *International Journal of Machine Tools & Manufacture* 43(14), 1437-1446.

Farkas, M. (1994). Periodic motions. *Applied Mathematical Sciences*, 104.

Ferry, W.B., & Altintas, Y. (2008a). Virtual five-axis flank milling of jet engine impellers - Part I: Mechanics of five-axis flank milling. *Journal of Manufacturing Science and Engineering*, 130(1).

Ferry, W.B., & Altintas, Y. (2008b). Virtual Five-Axis Flank Milling of Jet Engine Impellers – Part II: Feed Rate Optimization of Five-Axis Flank Milling. *Journal of Manufacturing Science and Engineering*, 130(1).

Gagnol, V., Bouzgarrou, V.C., Ray, P., & Barra, C. (2007). Model-based chatter stability prediction for high-speed spindles. *International Journal of Machine Tools and Manufacture*, 47(9), 1176-1186.

Gimenez, J.G., & Iriondo, A. (1997). Diseño y Control de Máquina Herramienta. *EUNSA Ediciones*, Universidad de Navarra, San Sebastián, Spain.

Gonzalo, O., Beristain, J., Jauregi, H., & Sanz, C. (2010). A method for the identification of the specific force coefficients for mechanistic milling simulation. *International Journal of Machine Tools and Manufacture*, 50(9), 765-794.

Gradišek, J., Baus, A., Govekar, E., Klocke, F., & Grabec, I. (2003). Automatic chatter detection in grinding. *International Journal of Machine Tools and Manufacture*, 43(14), 1397-1403.

Gradišek, J., Govekar, E., & Grabec, I. (1998a). Using coarse-grained entropy rate to detect chatter in cutting. *Journal of Sound and Vibration*, 214(5), 941-952.

Gradišek, J., Govekar, E., & Grabec, I. (1998b). Time series analysis in metal cutting: Chatter versus chatter-free cutting. *Mechanical systems and signal processing*, 12(6), 839-854.

Gradišek, J., Kalveram, M., Insperger, T., Weinert, K., Stépán, G., Govekar, E., & Grabec, I. (2005). On stability prediction for milling. *International Journal of Machine tools & Manufacture*, 45(1), 769-781.

Hahn, R. S. (1951). Design of Lanchester damper for elimination of metal-cutting chatter. *Trans. ASME*, 73(3).

Heisel, U., Storchak, M., Krivoruchko, V., & Braun, S. (2010). Modeling of Interaction Processes in Cutting. *CIRP 2nd International Conference on Process Machine Interactions*. Vancouver, Canada.

Henninger, C., & Eberhard, P. (2008). Improving the computational efficiency and accuracy of the semi-discretization method for periodic delay-differential equations. *European Journal of Mechanics-A/Solids*, 27(6), 975-985.

Hongqi, L., & Yung, C.S. (2004). Analysis of bearing configuration effects on high speed spindles using an integrated dynamic thermo-mechanical spindle model. *International Journal of Machine Tools and Manufacture*, 44(1), 347-364.

Hoshi, T., Sakisaka, N., Moriyama, I., Sato, M., Higashimoto, A., & Tokunaga, T. (1977). Study for practical application of fluctuating speed cutting for regenerative chatter control. *CIRP Annals*, 25(1), 175-179.

Hosseini, A., Moetakef-Imani, B., Kishawy, H.A., & El-Mounayri, H. (2011). Simulation of Serrated End Milling Using Solid Modeling Techniques. *Advanced Materials Research*, 223, 900-910.

Ibrahim, R.A., & Pettit, C.L. (2005). Uncertainties and dynamic problems of bolted joint and other fasteners. *Journal of Sound and Vibration*, 279, 857-936.

Iglesias, A., Munoa, J., & Ciurana, J. (2014). Optimisation of face milling operations with structural chatter using a stability model based process planning methodology. *The International Journal of Advanced Manufacturing Technology*, 70(1-4), 559-571.

Iglesias, A., Munoa, J., Ciurana, J., & Dombovari, Z. (2015). Analytical expressions for chatter analysis in milling operations with one dominant mode. *Journal of Sound and Vibration*, submitted.

Iglesias, A., Munoa, J., Ciurana, J., & Dombovari, Z. (2015). Analytical model for interrupted milling: ZOA method enhancement including double period instability. *International Journal of Machine Tools and Manufacture*, submitted.

Iglesias, A., Munoa, J., Ciurana, J., & Dombovari, Z. (2015). Analytical stability model for interrupted milling processes. *International Journal of Advanced Manufacturing Technology*, submitted.

Iglesias, A., Munoa, J., Ramírez, C., Ciurana, J., & Dombovari, Z. (2016). FRF Estimation through Sweep Milling Force Excitation (SMFE). *7th HPC 2016 – CIRP Conference on High Performance Cutting*, submitted.

Insperger, T., Munoa, J., Zatarain, M., & Peigné, G. (2006). Unstable islands in the stability chart of milling processes due to helix angle. *CIRP 2nd International Conference High Performance Cutting*. Vancouver.

Insperger, T., & Stépán, G. (2000). Stability of the milling process. Periodica Polytechnica, *Ser. Mech. Eng.*, 44(1), 45-57.

Insperger, T., & Stépán, G. (2001). Semidiscretization of delayed dynamical systems. *Proceedings of ASME Design Engineering Technical Conferences and Computers and Information in Engineering Conference*. Pittsburg.

Insperger, T., & Stépán, G. (2011). Semi-discretization for time-delay systems: stability and engineering applications. *Springer Science & Business Media*, 178.

Ismail F., & Soliman, E. (1997). A new method for the identification of stability lobes in machining. *International Journal of Machine Tools and Manufacture*, 37(6), 763-774.

Jayaram, S., Kapoor, S. G., & DeVor, R. E. (2000). Analytical stability analysis of variable spindle speed machining. *Journal of Manufacturing Science and Engineering*, 122(3), 391-397.

Jensen, S.A., & Shin Y.C. (1999a). Stability analysis in face milling operations. Part I: Theory of stability lobe prediction. *Journal of Manufacturing Science and Engineering, Transactions of ASME*, 121(4), 600-605.

Jensen, S.A., & Shin Y.C. (1999b). Stability analysis in face milling operations. Part 2: Experimental validation and influencing factors. *Transactions of ASME, Journal of Manufacturing Science and Engineering*, 121(4), 606-610.

Kakinuma, Y., Enomoto, K., Hirano, T., & Ohnishi, K. (2014). Active Chatter Suppression in Turning by Band-Limited Force Control. *CIRP Annals*, 63(2), 365-368.

Karandikar, J., & Schmitz, T. L. (2010). An investigation of stability dependence on tool wear. *CIRP 2nd International Conference on Process Machine Interactions*. Vancouver, Canada.

Khraisheh, M.K., Pezeshki, C., & Bayoumi, A.E. (1995) Time series based analysis for primary chatter in metal cutting. *Journal of Sound and Vibration*, 180(1), 67-87.

Kilic, Z. M. (2015). Generalized modelling of flexible machining system with arbitrary tool geometry.

Kilic, Z. M., Iglesias, A., Munoa, J., & Altintas, Y. (2010). Investigation of tool wear on the stability of milling process using an inverse method. *CIRP 2nd International Conference on Process Machine Interactions*, Vancouver, Canada.

Ko, J.H., & Altintas, Y. (2005). Mechanics and Dynamics of Plunge Milling Process. Part 1- Time Domain Model. *Trans. of the ASME, J. of Manufacturing Science and Engineering*.

Koenigsberger, F., & Tlusty, J. (1970). Machine tool structures. Volume 1. *Pergamon Press*

Kruth, J.P., Liu, A.M., Vanherck, P., & Lauwers, B. A strategy for selecting optimal cutting parameter in high-speed milling to avoid chatter vibration. *International Journal of Production Engineering and Computers*, 4(5), 35-42.

Kurata, Y., Suzuki, N., Hino, R., & Shamoto, E. (2010) Prediction of Chatter-Free Cutting Conditions for High Performance Boring Operations. *CIRP 2nd International Conference on Process Machine Interactions*. Vancouver, Canada.

Lamraoui, M., Thomas, M., El Badaoui, M., & Girardin, F. (2014). Indicators for monitoring chatter in milling based on instantaneous angular speeds. *Mechanical Systems and Signal Processing*, 44(1), 72-85.

Lamraoui, M., El Badaoui, M., & Guillet, F. (2015). Chatter Detection in CNC Milling Processes Based on Wiener-SVM Approach and Using Only Motor Current Signals. *In Vibration Engineering and Technology of Machinery*, 567-578.

Lazoglu, I., Vogler, M., Kapoor, S.G., DeVor, R.E. (1998). Dynamics of the simultaneous turning process, *Transactions North American Manufacturing Research Institution of SME*.

Li, B., Cai, H., Mao, X., Huang, J., & Luo, B. (2013b). Estimation of CNC machine–tool dynamic parameters based on random cutting excitation through operational modal analysis. *International Journal of Machine Tools and Manufacture*, 71, 26-40.

Li, B., Luo, B., Mao, X., Cai, H., Peng, F., & Liu, H. (2013a). A new approach to identifying the dynamic behavior of CNC machine tools with respect to different worktable feed speeds. *International Journal of Machine Tools and Manufacture*, 72, 73-84.

Lin, C.W., Tu, J.F., & Kamman, J. (2003). An integrated thermo-mechanical model to characterize motorized machine tool spindles during very high speed rotation. *International Journal of Machine Tools and Manufacture*, 43, 1035-1050.

Liu, X., Cheng, K., & Webb, D. (2002) Prediction and simulation on the machining dynamics and instability in peripheral milling. *ASPE Annual Meeting*, 581-584. St. Louis, USA.

Liu, H.Q., Chen, Q.H., Li, B., Mao X.Y., Mao, K.M., & Peng, F.Y. (2012). On-line chatter detection using servo motor current signal in turning. *Sci China Tech Sci*, 54, 3119-3129.

Lourens, E., Reynders, E., Lombaert, G., De Roeck, G., & Degrande, G. (2010) Dynamic force identification by means of state augmentation: a combined deterministic-stochastic approach. *ISMA 2010, International Conference on Advanced Acoustics and Vibration Engineering*, 2069-2080. Leuven, Belgium.

Magnevall, M., Liljerehn, A., Lundblad, M., & Ahlin, K. (2010). Improved cutting force measurements in high speed milling using inverse structural filtering. *CIRP 2nd International Conference on Process Machine Interactions*. Vancouver, Canada.

Mallat, S. G. (1988). Multiresolution representations and wavelets.

Mancisidor, I. (2009). Correlación analítico experimental de la duplicadora X-CODE de JMA. *End Course Project*. University of Mondragon, Spain.

Mancisidor, I. (2014). Active chatter suppression by means of computer-controlled inertial actuators. *Doctoral Thesis*. University of Basque Country, Bilbao, Spain.

Mancisidor, I., Munoa, J., Barcena, R., Beudaert, X., & Zatarain, M. (2015). Coupled model for simulating active inertial actuators in milling processes. *The International Journal of Advanced Manufacturing Technology*, 77(1-4), 581-595.

Mann, B.P., Bayly, P.V., Davies, M.A., & Halley, J.E. (2004). Limit cycles, bifurcations, and accuracy of the milling process. *Journal of Sound and Vibration*, 277(1), 31-48.

Mann, B.P., Insperger, T., Bayly, P.V., & Stépán, G. (2003). Stability of up-milling and down-milling. Part 2: Experimental verification. *International Journal of Machine tools & Manufacture*, 43(1), 35-40.

Mao, X., Luo, B., Li, B., Cai, H., Liu, H., & Pen, F. (2014). An approach for measuring the FRF of machine tool structure without knowing any input force. *International Journal of Machine Tools and Manufacture*, 86, 62-67.

Marushita, Y., Ideka, H., & Matsumoto, K. (2011). Electric Motor Control Apparatus. *US Patent* 7,868,577 B2.

Matsubara, A., Tsujimoto, S., & Kono, D. (2015). Evaluation of dynamic stiffness of machine tool spindle by non-contact excitation tests. *CIRP Annals-Manufacturing Technology*, 64, 365-368.

Merdol, D. S (2008). Virtual three-axis milling process simulation and optimization.

Merdol, D., & Altintas, Y. (2004). Multi frequency solution of chatter stability for low immersion milling. *Journal of Manufacturing Science and Engineering. Transactions of the ASME*, 126, 459-466.

Merdol, S. D., & Altintas, Y. (2008). Virtual cutting and optimization of three-axis milling processes. *International Journal of Machine Tools and Manufacture*, 48(10), 1063-1071.

Merritt, H.E. (1965). Theory of self-excited machine-tool chatter. Contribution to machine-tool chatter. Research 1. *Journal of Engineering for Industry, ASME*, 87(4), 447-453.

Minis, I.E., Magrab E.B. & Pandelidis, I.O. (1990). Improved Methods for the Prediction of Chatter in Turning. Part 1: Determination of Structural Response Parameters. *Transactions of the ASME*, 112, 12-20.

Minis, I., & Yanushevski, R.A. (1993). A new theoretical approach for the prediction of machine tool chatter in milling. *Journal of Engineering for Industry. ASME*, 115, 1-8.

Montgomery, D. & Altintas, Y. (1991). Mechanism of Cutting Force and Surface Generation in Dynamic Milling. *Journal of Engineering for Industry, ASME*, 113, 160-168.

Mori, T., Hiramatsu, T., & Shamoto, E. (2011). Simultaneous double-sided milling of flexible plates with high accuracy and high efficiency—Suppression of forced chatter vibration with synchronized single-tooth cutters. *Precision Engineering*, 35(3), 416-423.

Movahhedy, M.R., & Mosaddegh, P. (2006). Prediction of chatter in high speed milling including gyroscopic effects. *International Journal of Machine Tools and Manufacture*, 46(9), 996-1001.

Munoa, J. (2007). Desarrollo de un modelo general para la predicción de la estabilidad del proceso de fresado. Aplicación al fresado periférico, al planeado convencional y a la caracterización de la estabilidad dinámica de fresadoras universales. *Doctoral Thesis*. University of Mondragon, Spain.

Munoa, J., Beudaert, X., Erkorkmaz, K., Iglesias, A., Barrios, A., & Zatarain, M. (2015). Active suppression of structural chatter vibrations using machine drives and accelerometers. *CIRP Annals-Manufacturing Technology*, 64, 385-388.

Munoa, J., Dombovari, Z., Iglesias, A., & Stépán, G. (2010). Estudio de la estabilidad de las fresas de perfil ondulado. *18 Congreso de Máquinas- Herramienta y Tecnologías de Fabricación*. San Sebastián, Spain.

Munoa, J., Dombovari, Z., Iglesias, A., & Stepan, G. (2015). Tuneable mass dampers with variable stiffness for chatter suppression. *International Conference on Virtual Machining Process Technology*, Vancouver, Canada.

Munoa, J., Dombovari, Z., Mancisidor, I., Yang, Y., & Zatarain, M. (2013a). Interaction between multiple modes in milling processes. *Machining Science and Technology*, 17(2), 165-180.

Munoa, J., Iglesias, A., Olarra, A., Dombovari, Z., & Zatarain, M. (2016). Rough milling chatter suppression by self-tunable variable stiffness tuned mass damper, *CIRP Annals-Manufacturing Technology*, submitted.

Munoa, J., Mancisidor, I., Loix, N., Uriarte, L. G., Barcena, R., & Zatarain, M. (2013b). Chatter suppression in ram type travelling column milling machines using a biaxial inertial actuator. *CIRP Annals-Manufacturing Technology*, 62(1), 407-410.

Munoa, J., Zatarain, M., Bediaga I., & Lizarralde, R. (2005) Optimization of hard material roughing by means of a stability model. *Proceedings of the 8th CIRP International Workshop on Modeling of Machining Operations*, 431-438. Chemnitz, Germany.

Munoa, J., Zatarain, M., Bediaga, I., & Peigné, G. (2006). Stability study of the milling process using an exponential force model in frequency domain. *Proceedings of the 2nd CIRP International Conference on High Performance Cutting*. Vancouver, Canada.

Munoa, J., Zatarain, M., Dombovari, Z., & Yang, Y. (2009). Effect of mode interaction on stability of milling processes. *Proceedings of 12th CIRP Conference on Modeling of Machining Operations*. San Sebastian, Spain.

Nachtigal, C. (1972). Design of a force feedback chatter control system. *Journal of Dynamic Systems, Measurement and Control*, 94(1), 5-10.

Nachtigal, C. L., & Cook, N. H. (1970). Active control of machine-tool chatter. *Journal of Fluids Engineering*, 92(2), 238-244.

Opitz, H., & Bernardi, F. (1970). Investigation and calculation of chatter behaviour of lathes and milling machines. *CIRP Annals*, 18, 335-342.

Opitz, H., & Weck, M.C. (1969). Determination of the transfer function by means of spectral density measurements and its application to the dynamic investigation of machine tools under machining conditions. *10th International MTDR Conference*, 349-378.

Orlando, S., Peeters, B., & Coppotelli, G. (2008, September). Improved FRF estimators for MIMO Sine Sweep data. *In Proceedings of the ISMA 2008 International Conference on Noise and Vibration Engineering*, 229-241. Leuven, Belgium.

Ozdoganlar, O.B., Endres, W.J. (1999). Parallel-Process (Simultaneous) Machining and Its Stability, *Presented at ASME IMECE'99, Nashville, TN. Proc., Symp. On Mach. Sci. and Tech.*, MED-10, 361–368.

Özsahin, O., Budak, E., & Özgüven H.N. (2011). Investigating dynamics of machine tool spindles under operational conditions. *Advanced Materials Research*, 223, 610-621.

Özsahin, O., Budak, E., & Özgüven H.N. (2015). In-process tool point FRF identification under operational conditions using inverse stability solution. *International Journal of Machine Tools and Manufacture*, 89, 64-73.

Ozturk, E., & Budak, E. (2010) Modeling dynamics of parallel milling processes in time-domain. *CIRP 2nd International Conference on Process Machine Interactions*. Vancouver, Canada.

Ozturk, E., Kumar, U., Turner, S., & Schmitz, T. (2012). Investigation of spindle bearing preload on dynamics and stability limit in milling. *CIRP Annals*, 61, 343-346.

Patel, B.R., Mann, B.P., & Young, K.A. (2008). Uncharted islands of chatter instability in milling. *International Journal of Machine Tools and Manufacture*, 48(1), 124-134.

Pedersen, P.T. (1972). On forward and backward precession of rotors. *Archive of applied mechanics*, 46(1), 26-41.

Pérez-Canales, D., Vela-Martínez, L., Jáuregui-Correa, J.C., & Alvarez-Ramirez, J. (2012), Analysis of the entropy randomness index for machining chatter detection. *International Journal of Machine Tools & Manufacture*, 62, 39-45.

Quintana, G. (2010). Stability lobes diagram identification and surface roughness monitoring in milling processes. *Doctoral Thesis*. University of Girona, Spain.

Quintana, G., Campa, F.J., Ciurana, J., López de Lacalle, L. N. (2011). Productivity improvement through chatter-free milling in workshops. Proceedings of the Institution of Mechanical Engineers, Part B, Journal of Engineering Manufacture, 225(7), 1163-1174.

Quintana, G., & Ciurana, J. (2011). Chatter in machining processes: a review. *International Journal of Machine Tools and Manufacture*, 51(5), 363-376.

Quintana, G., Ciurana, J., Ferrer, I., Rodríguez, C.A. (2009). Sound mapping for identification of stability lobe diagrams in milling processes. *International Journal of Machine Tools & Manufacture*, 49(3-4), 203-211.

Quintana, G., Ciurana, J., & Teixidor D. (2008). A new experimental methodology for identification of stability lobes diagram in milling operations. *International Journal of Machine Tools and Manufacture*, 48(15), 1637-1645.

Rantatalo, M., Aidanpaa, J.-O., Goransson, B., & Norman, P. (2007). Milling machine spindle analysis using FEM and non-contact spindle excitation and response measurement. *International Journal of Machine Tools and Manufacture*, 47(7-8), 1034–1045.

Rasper, P., Rott, O., Hömberg, D., & Uhlmann, E. (2010). Analysis of uncertainties in the stability prediction for milling processes. *CIRP 2nd International Conference on Process Machine Interactions*. Vancouver, Canada.

Rivin, E., & Kang, H. (1992). Enhancement of dynamic stability of cantilever tooling structures. *International Journal of Machine Tools and Manufacture*, 32(4), 539-561.

Rock, S. (2010). Real-time Simulation of Process Machine Interactions - A numerical analysis. *CIRP 2nd International Conference on Process Machine Interactions*. Vancouver, Canada.

Roukema, J. C., & Altintas, Y. (2007). Generalized modeling of drilling vibrations. Part I: Time domain model of drilling kinematics, dynamics and hole formation. *International Journal of Machine Tools and Manufacture*, 47(9), 1455-1473.

Sastry, S., Kapoor, S. G., & DeVor, R. E. (2002). Floquet theory based approach for stability analysis of the variable speed face-milling process. *Journal of manufacturing science and engineering*, 124(1), 10-17.

Schedlinski, C., & Lüscher, M. (2002). Application of classical output-only modal analysis to a laser cutting machine. *Proceedings of ISMA*. Leuven, Belgium.

Schedlinski, C., Scharpf P.D., & Weber M. (2010). A strategy for experimental investigation of machine tool dynamics. *ISMA 2010, International Conference on Noise and Vibration Engineering*, 2597-2608. Leuven, Belgium.

Schmitz, T.L. (2003). Chatter recognition by statistical evaluation of the synchronously sampled audio signal. *Journal of Sound and Vibration*, 262(3), 721-730.

Schmitz, T.L., & Davies, M.A. (2002). Method and device for avoiding chatter during machine tool operation. *Patent No. US20020146296A1*.

Schmitz, T.L., Medicus, K., & Dutterer, B. (2002). Exploring one-per-revolution audio signal variance as a chatter indicator. *Machining Science and Technology*, 6(2), 215-233.

Schmitz, T. L., Powell, K., Won, D., Duncan, G. S., Sawyer, W. G., & Ziegert, J. C. (2007). Shrink fit tool holder connection stiffness/damping modeling for frequency response prediction in milling. *International Journal of Machine Tools and Manufacture*, 47(9), 1368-1380.

Seguy, S., Insperger, T., Arnaud, L., Dessein, G., & Peigné, G. (2010). On the stability of high-speed milling with spindle speed variation. *The International Journal of Advanced Manufacturing Technology*, 48(9-12), 883-895.

Sellmeier, V., & Denkena, B. (2011). Stable islands in the stability chart of milling processes due to unequal tooth pitch. *International Journal of Machine Tools and Manufacture*, 51(2), 152-164.

Sexton, J. S., & Stone, B. J. (1978). The stability of machining with continuously varying spindle speed. *CIRP Annals*, 27(1), 321-326.

Shi, H.M., & Tobias, S.A. (1984). Theory of finite amplitude machine tool instability. *International Journal of Machine Tool Design and Research*, 24(1), 45-69.

Siddhpura, M., & Paurobally, R. (2012). A review of chatter vibration in turning. *International Journal of Machine Tools and Manufacture*, 61, 27-47.

Sims, N.D. (2007). Vibration absorbers for chatter suppression: a new analytical tuning methodology. *Journal of Sound and Vibration*, 301(3), 592-607.

Sims, N.D., Bayly, P.V., & Young, K.A. (2005). Piezoelectric sensors and actuators for milling tool stability lobes. *Journal of Sound and Vibration*, 281(3-5), 743-762.

Skogestad, S., Postlethwaite, I. (2005). Multivariable Feedback Control: Analysis and Design. *2nd ed, Wiley*.

Slavicek, J. (1965). The effect of irregular tooth pitch on stability of milling. *In Proceedings of the 6th MTDR Conference,* 15-22.

Soliman, E., & Ismail, F. (1997). Chatter Detection by Monitoring Spindle Drive Current. *The International Journal of Advanced Manufacturing Technology*, 13, 27-34.

Sims, N. D., Manson, G., & Mann, B. (2010). Fuzzy stability analysis of regenerative chatter in milling. *Journal of Sound and Vibration*, 329(8), 1025-1041.

Sridhar, R., Hohn, R.E., & Long, G.W. (1968) A general formulation of the milling process equation. Contribution to machine tool chatter. Research-5. *Journal of Engineering for Industry, ASME*, 90, 317-324.

Stein, G. J., Darula, R., & Sorokin, S. (2012). Control of forced vibrations of mechanical structures by an electromagnetic controller with a permanent magnet. *In Proc. Intl. Conference on Noise and Vibration Engineering, ISMA*, 385-393. Leuven, Belgium.

Stepan, G. (1989). Retarded dynamical systems: stability and characteristic functions. *Longman Scientific & Technical*.

Stepan G., Dombovari, Z., & Munoa, J. (2011). Identification of cutting force characteristics based on chatter experiments. *CIRP Annals – Manufacturing Technology*, 60, 113-116.

Stepan, G., Munoa, J., Insperger, T., Surico, M., Bachrathy, D., Dombovari, Z. (2014). Cylindrical milling tools: Comparative real case study for process stability, *CIRP Annals – Manufacturing Technology*, 63(1), 385-388.

Stern, E., (1999). A device and method for recommending dynamically preferred speeds for machining. *Patent No. WO/1999/015310*.

Sun, Y., Zhuang, C., & Xiong, Z. (2014). Real-time chatter detection using the weighted wavelet packet entropy. *In Advanced Intelligent Mechatronics (AIM), 2014 IEEE/ASME International Conference*, 1652-1657. Besançon, France.

Surmann, T., & Enk, D. (2007). Simulation of milling tool vibration trajectories along changing engagement conditions. *International Journal of Machine Tools & Manufacture*, 47, 1444-1448.

Suzuki, N., Kurata, Y., Hino, R., & Shamoto, E. (2008). Identification of transfer function of mechanical structure by inverse analysis of regenerative chatter vibration and in end milling. *CIRP 3rd International Conference on High Performance Cutting*, 455-463. Dublin, Ireland.

Szabat, K., & Orlowska-Kowalska, T. (2007). Vibration Suppression in a Two-Mass Drive System using PI Speed Controller and Additional Feedbacks- Comparative Study. *IEEE Transactions on Industrial Electronics*, 54(2):1193-1206.

Tangjitsitcharoen, S., & Pongsathornwiwat, N. (2012). Development of chatter detection in milling processes. The International Journal of Advanced Manufacturing Technology, 65(5-8), 919-927.

Tansel, I.N., Li, M., Demetgul, M., Bickraj, K., Kaya, B., & Ozcelik, B. (2010). Detecting chatter and estimating wear from the torque of end milling signals by using Index Based Reasoner (IBR). *International Journal of Advanced Manufacturing Technology*, 1-10.

Taylor, F.W. (1907). On the Art of Cutting Metals. *Transactions of ASME*, 28, 231-248.

Tian, J., & Hutton, S.G. (2001). Chatter Instability in Milling Systems with Flexible Rotating Spindles – A New Theoretical Approach. *Journal of Manufacturing Science and Engineering-Transactions of the ASME*, 123 (1) 1-9.

Tlusty, J. (1978). Analysis of the state of research in cutting dynamics. *CIRP Annals*, 27(2), 583-589.

Tlusty, J., & Ismail, F. (1981). Basic nonlinearity in machining chatter. *CIRP Annals*, 30(1), 299-304.

Tlusty, J., Ismail, F.; & Zaton, W. (1983). Use of Special Milling Cutters against Chatter, *NAMRC 11 Conference*, 408-415. University of Wisconsin – Madison, USA.

Tlusty, J., & Polacek, M. (1957). Besipiele der behandlung der selbsterregten Schwingung der Werkzeugmaschinen FoKoMa, *Hanser Verlag*. Munich, Germany.

Tlusty, J., & Polacek, M. (1963). The stability of the machine tool against self-excited vibration in machining. *International Research in Production Engineering, ASME*, 465-474.

Tlusty, J., Smith, S., & Winfough, W. R. (1996). Techniques for the use of long slender end mills in high-speed milling. *CIRP Annals-Manufacturing Technology*, 45(1), 393-396.

Tobias, S.A. (1965). Machine Tool Vibrations. *Blackie & Sons Limited*. Glasgow, UK.

Tobias, S.A., & Fishwick, W. (1958). Theory of regenerative machine tool chatter. *The Engineer*, 205.

Tukora, B., & Szalay, T. (2011). Real-time Cutting Force Prediction and Cutting Force Coefficient Determination during Machining Processes. *Advanced Materials Research*, 223, 85-92.

Tunç, L.T., & Budak, E. (2012). Effect of cutting conditions and tool geometry on process damping in machining. *International Journal of Machine Tools and Manufacture*, 57, 10-19.

Turner, S. (2010). Tool tuning for enhanced process damping performance. *CIRP 2nd International Conference on Process Machine Interactions*. Vancouver, Canada.

Vanherck, P. (1967). Increasing Milling Machine Productivity by Use of Cutter with Non-Constant Edge Pitch, *Proceedings of the 8th MTDR Conference*, 9, 947-960, Manchester, UK.

Varma, S., & Baras, J. (2002). Tool wear estimation from acoustic emissions: A model incorporating wear rate. *International Conference on Pattern Recognition*, 1, 492-495. Québec, Canada.

Vela-Martínez, L., Jáuregui-Correa, J.C., & Álvarez-Ramírez, J. (2009). Characterization of machining chattering dynamics: An R/S scaling analysis approach. *International Journal of Machine Tools and Manufacture*, 49(11), 832-842.

Weck, M. (1984). Handbook of machine tools. Volume 4. Metrological Analysis and Performance Test. *John Wiley & Sons*. Chichester, UK.

Wiederick, H. D., Gauthier, N., Campbell, D. A., & Rochon, P. (1987). Magnetic braking: Simple theory and experiment. *American Journal of Physics*, 55(6), 500-503.

Wiercigroch, M., & Budak, E. (2001). Sources of nonlinearities, chatter generation and suppression in metal cutting. *Phil. Trans. R. Soc. Lond. A.*, 359, 663-693.

Xiong, G.L., Yi, J.M., Zeng, C., Guo, H.K., & Li, L.X. (2003). Study of the gyroscopic effect of the spindle on the stability characteristics of the milling system. *Journal of Materials Processing Technology*, 138, 379-384.

Yang, Y., Munoa, J., & Altintas, Y. (2010). Optimization of multiple tuned mass dampers to suppress machine tool chatter. *International Journal of Machine Tools and Manufacture*, 50(9), 834-842.

Yang, F., Zhang, B., & Yu, J. (2003). Chatter suppression with multiple time-varying parameters in turning. *Journal of Materials Processing Technology*, 141(3), 431-438.

Yao, Z., Mei, D., & Chen, Z. (2010). On-line chatter detection and identification based on wavelet and support vector machine. *Journal of Materials Processing Technology*, 210(5), 713-719.

Yilmaz, A., Emad, A. R., & Ni, J. (2002). Machine tool chatter suppression by multi-level random spindle speed variation. *Journal of manufacturing science and engineering*, 124(2), 208-216.

Yusoff, A.R.; & Sims; N.D. (2011). Optimisation of variable helix tool geometry for regenerative chatter mitigation. *International Journal of Machine Tools & Manufacture*, 51(2), 133-141.

Zaghbani, I., & Songmene, V. (2009). Estimation of machine-tool dynamic parameters during machining operation through operational modal analysis. *International Journal of Machine Tools & Manufacture*, 49(12), 947- 957.

Zatarain, M., Bediaga, I., Munoa, J., & Insperger, T. (2010). Analysis of directional factors in milling: importance of multi-frequency calculation and of the inclusion of the effect of the helix angle. *The International Journal of Advanced Manufacturing Technology*, 47(5-8), 535-542.

Zatarain, M., Bediaga, I., Munoa, J., & Lizarralde, R. (2008). Stability of milling processes with continuous spindle speed variation: analysis in the frequency and time domains, and experimental correlation. *CIRP Annals*, 57(1), 379-384.

Zatarain, M., & Dombovari, Z. (2014). Stability analysis of milling with irregular pitch tools by the implicit subspace iteration method. *International Journal of Dynamics and Control*, 2(1), 26-34.

Zatarain, M., Munoa, J., Peigné, G., & Insperger, T. (2006). Analysis of the Influence of mill helix angle on chatter stability. *CIRP Annals*, 55(1), 365-368.

Zatarain, M., Munoa, J., Villasante, C., & Sedano, A. (2004). Estudio comparativo de los modelos matemáticos de chatter en fresado: Monofrecuencia, multi-frecuencia y simulación en el tiempo. *XV Congreso de Máquinas-Herramienta y Tecnologías de Fabricación*. San Sebastian, Spain.

Zhang, C., Yue, X., Jiang Y., & Zheng, W. (2010). A hybrid approach of ANN and HMM for cutting chatter monitoring. *Advanced Materials Research*, 97-101, 3225.

Zhehe Y., Deqing M., Zichen C. (2010). On-line chatter detection and identification based on wavelet and support vector machine. *Journal of Materials Processing Technology*, 210, 713–719.

Zuo, L., Chen, X., & Nayfeh, S. (2011). Design and analysis of a new type of electromagnetic damper with increased energy density. *Journal of vibration and acoustics*, 133(4), 041006.

Zuo, L., & Nayfeh, S. A. (2006). The two-degree-of-freedom tuned-mass damper for suppression of single-mode vibration under random and harmonic excitation. *Journal of vibration and acoustics*, 128(1), 56-65.